THE UNIVERSITY OF QUEENSLAND

AUSTRALIA

Catalytic conversion of biorenewable-carbohydrate sources to 5-Hydroxymethylfurfural: a platform molecule for future chemical and energy

Luqman Abiola Atanda

A thesis submitted for the degree of Doctor of Philosophy at

The University of Queensland in 2016

Australian Institute for Bioengineering and Nanotechnology

Abstract

Cellulosic biomass provides renewable alternatives to fossil-fuel resources for the sustainable production of liquid fuels and valuable chemicals. The challenge for the effective utilization of biomass resources is to develop cost-effective processing methods for the transformation of carbohydrates into value-added chemicals. Carbohydrates, predominantly cellulose, represent the largest fraction of biomass, and various strategies for their efficient use as a commercial chemical feedstock are currently being established with the aim to supplement and ultimately replace fossil fuels. To achieve this goal, it is pivotal to develop more efficient and environmental-friendly methods to convert cellulose into useful chemicals. One possible conversion route of cellulose is through the synthesis of 5-hydroxymethyfurfural (HMF), which the US Department of Energy has classified as one of the most promising renewable molecules.

This thesis is aimed at advancing the potential application of heterogeneous catalysis and water-organic biphase system for the synthesis of HMF directly from solid biomass. Firstly, we undertook a literature survey of the current strategies employed for HMF production with more attention on solid catalysis.

Secondly, we explored the catalytic potential of non-toxic TiO_2 nanoparticle prepared by sol-gel technique on glucose conversion into HMF in an aqueous reaction system. Catalytic performance of TiO_2 was modified by introducing a second metal oxide (ZrO_2) to form binary oxides. Compared to pure TiO_2, the binary oxide displayed better activity in terms of HMF yield, which was attributed to optimum balance of basic and acid sites for the tandem isomerization-dehydration reactions. Solvent effect was also studied in order to promote the reaction preferentially towards target product. Consequently, a biphase system of water-organic solvent mix was utilized and in combination with TiO_2-ZrO_2/Amberlyst 70 catalyst system, a remarkable yield of HMF can be produced from glucose

Thirdly, catalytic properties of TiO_2 nanoparticle were fine-tuned to develop a single solid acid bifunctional (Lewis and Brønsted acidity) catalyst. To achieve this goal, TiO_2 was modified with phosphate anion and evaluated as catalysts for the conversion of glucose to HMF in a water-butanol biphasic system. Catalyst synthesis protocol was optimized by varying loading amount of phosphate anion and calcination temperature. X-ray spectroscopic analysis confirmed phosphorus incorporation into the TiO_2 framework giving rise to small-sized nanocrystals with high surface acidity. Pyridine-infrared (Py-IR) spectroscopy on the TiO_2 catalyst confirmed the presence of bifunctional Lewis and Brønsted acid sites as compared to pure TiO_2 with only Lewis acidity. The

phosphate modified TiO_2 demonstrated excellent catalytic performance in terms of both activity and selectivity, as well as good recyclability.

Fourthly, the robustness of phosphated TiO_2 catalyst to transform a variety of sugar moieties ranging from simple to complex ones was evaluated in a water-THF biphasic system. Addition of N-methyl-2-pyrrolidone (NMP) to the biphasic medium enhanced the overall effectiveness of the reaction process to selectively produce HMF through: a) suppressing humin formation and b) preventing rehydration of HMF. The sugar moieties were successfully transformed giving ≥ 80% HMF yield. In the case of cellulose, its crystalline structure strongly inhibited its reactivity. Because of its poor reactivity, structural deconstruction of cellulose was carried out by acid catalyzed solid state depolymerization using a ball milling system (mechanocatalysis). Subsequently, conversion of the highly reactive water soluble oligomers that resulted from the mechanocatalytic deconstructed cellulose, gave improved yield of HMF. To simulate an industrial production of HMF under a continuous process, a bench scale biphasic flow reactor was designed and utilized for the conversion of solubilized cello-oligomers into HMF under which a reasonable yield of HMF (53%) can be produced.

Lastly, the potential realization of an efficient eco-friendly catalytic process for converting cheap source of renewable biomass-derived carbohydrates into 5-hydroxymethylfurfural was explored. A more facile synthesis of the highly active phosphated–TiO_2 nanomaterial was designed by combining the previously two-stage technique to a one-pot route. Acid-catalyzed dehydration of cellulosic biomass (sugarcane bagasse and rice husk) into HMF was carried out in the presence of water–methyltetrahydrofuran (water–MeTHF) biphasic system modified with N-methyl-pyrrolidone (NMP). Chemical transformation of biomass to HMF was facilitated by solid state depolymerization. Eventually, sugarcane bagasse and rice husk were effectively converted to produce 72% and 65% yields of HMF, respectively. Even though production of HMF in a biphasic system is well documented, kinetic study of this reaction over a solid acid in a biphasic reaction system has never been reported. Therefore, kinetics study of cellulose–to–HMF reaction was conducted and a simplified kinetic model comprising of two reaction steps was developed: (a) hydrolysis of cello-oligomers to glucose; and (b) glucose dehydration to HMF. Finally, the obtained reaction rate parameters from the kinetic analysis could potentially serve as a valuable analogy in developing models for a scale-up biphasic process of HMF production.

Declaration by author

This thesis is composed of my original work, and contains no material previously published or written by another person except where due reference has been made in the text. I have clearly stated the contribution by others to jointly-authored works that I have included in my thesis.

I have clearly stated the contribution of others to my thesis as a whole, including statistical assistance, survey design, data analysis, significant technical procedures, professional editorial advice, and any other original research work used or reported in my thesis. The content of my thesis is the result of work I have carried out since the commencement of my research higher degree candidature and does not include a substantial part of work that has been submitted to qualify for the award of any other degree or diploma in any university or other tertiary institution. I have clearly stated which parts of my thesis, if any, have been submitted to qualify for another award.

I acknowledge that an electronic copy of my thesis must be lodged with the University Library and, subject to the policy and procedures of The University of Queensland, the thesis be made available for research and study in accordance with the Copyright Act 1968 unless a period of embargo has been approved by the Dean of the Graduate School.

I acknowledge that copyright of all material contained in my thesis resides with the copyright holder(s) of that material. Where appropriate I have obtained copyright permission from the copyright holder to reproduce material in this thesis.

Publications during candidature

Journal publications

a) **Catalytic behaviour of TiO_2–ZrO_2 binary oxide synthesized by sol-gel process for glucose conversion to 5-Hydroxymethylfurfural**
Luqman Atanda, Adib Silahua, Swathi Mukundan, Abhijit Shrotri, Gilberto Torres-Torres and Jorge Beltramini, RSC Advances, 2015, 5, 80346-80352.

b) **Catalytic conversion of glucose to 5-Hydroxymethylfurfural with a phsophated–TiO_2 catalyst**
Luqman Atanda, Swathi Mukundan, Abhijit Shrotri, Qing Ma and Jorge Beltramini, ChemCatChem, 2015, 7, 781-790.

c) **Direct production of 5-Hydroxymethylfurfural via catalytic conversion of simple and complex sugars over phosphated–TiO_2**
Luqman Atanda, Abhijit Shrotri, Swathi Mukundan, Qing Ma, Muxina Konarova and Jorge Beltramini, ChemSusChem, 2015, 8, 2970-2916.

d) **High yield conversion of cellulosic biomass into 5-Hydroxymethylfurfural: a study of reaction kinetics of cellulose–to–HMF in a biphasic system**
Luqman Atanda, Muxina Konarova, Qing Ma, Swathi Mukundan, Abhijit Shrotri and Jorge Beltramini, Catalysis Science & Technology, DOI: 10.1039/c6cy00820h.

Conference presentations

a) **Catalytic dehydrogenation of glucose to HMF using TiO_2–ZrO_2 mixed oxides**
Luqman Atanda and Jorge Beltramini, TOCAT7, Kyoto2014, Kyoto, Japan, June 1-6, 2014.

b) **Phosphated titania catalyst for acid catalyzed transformation of sugars to 5-Hydroxymethylfurfural in a biphasic system**
Luqman Atanda, Abhijit Shrotri, Qing Ma and Jorge Beltramini, Future Energy Conference, Sydney, Australia, November 3-5, 2014.

c) **5-Hydroxymethylfurfural production from catalytic transformation of carbohydrates in a biphasic system**
Luqman Atanda, Abhijit Shrotri, Qing Ma and Jorge Beltramini, 24th North American Catalysis Society Meeting, Philadelphia, Pittsburgh, USA, June 14-19, 2015.

d) **Direct utilization of lignocellulosic biomass waste for the production of 5-Hydroxymethylfurfural**
Luqman Atanda, Muxina Konarova and Jorge Beltramini, 16th International Congress on Catalysis, Beijing, China, July, 3-8, 2016.

Publications included in this thesis

a) **Catalytic behaviour of TiO_2–ZrO_2 binary oxide synthesized by sol-gel process for glucose conversion to 5-Hydroxymethylfurfural**

Luqman Atanda, Adib Silahua, Swathi Mukundan, Abhijit Shrotri, Gilberto Torres-Torres and Jorge Beltramini, RSC Advances, 2015, 5, 80346-80352

Incorporated as Chapter 4.

Contributor	Statement of contribution
Luqman Atanda	Concept and experimental design (60%) Conduct experiment and data analysis (70%) Wrote the paper (100%)
Adib Silahua	Conduct experiment and data analysis (10%)
Swathi Mukundan	Conduct experiment and data analysis (15%)
Abhijit Shrotri	Conduct experiment and data analysis (5%)
Gilberto Torres-Torres	Concept and experimental design (10%)
Jorge Beltramini	Concept and experimental design (30%) Edited the paper (100%)

b) **Catalytic conversion of glucose to 5-Hydroxymethylfurfural with a phsophated–TiO_2 catalyst**

Luqman Atanda, Swathi Mukundan, Abhijit Shrotri, Qing Ma and Jorge Beltramini, ChemCatChem, 2015, 7, 781-790.

Incorporated as Chapter 5.

Contributor	Statement of contribution
Luqman Atanda	Concept and experimental design (70%) Conduct experiment and data analysis (80%) Wrote the paper (90%)
Swathi Mukundan	Conduct experiment and data analysis (10%)
Abhijit Shrotri	Wrote the paper (10%)
Qing Ma	Conduct experiment and data analysis (10%)
Jorge Beltramini	Concept and experimental design (30%) Edited the paper (100%)

c) Direct production of 5-Hydroxymethylfurfural via catalytic conversion of simple and complex sugars over phosphated–TiO_2

Luqman Atanda, Abhijit Shrotri, Swathi Mukundan, Qing Ma, Muxina Konarova and Jorge Beltramini, ChemSusChem, 2015, 8, 2970-2916.

Incorporated as Chapter 6.

Contributor	Statement of contribution
Luqman Atanda	Concept and experimental design (70%) Conduct experiment and data analysis (80%) Wrote the paper (100%)
Abhijit Shrotri	Concept and experimental design (5%)
Swathi Mukundan	Conduct experiment and data analysis (10%)
Qing Ma	Conduct experiment and data analysis (10%)
Muxina Konarova	Concept and experimental design (5%)
Jorge Beltramini	Concept and experimental design (20%) Edited the paper (100%)

d) High yield conversion of cellulosic biomass into 5-Hydroxymethylfurfural and a study of the reaction kinetics of cellulose to HMF conversion in a biphasic system

Luqman Atanda, Muxina Konarova, Qing Ma, Swathi Mukundan, Abhijit Shrotri and Jorge Beltramini, Catalysis Science & Technology, DOI: 10.1039/c6cy00820h.

Incorporated as Chapter 7.

Contributor	Statement of contribution
Luqman Atanda	Concept and experimental design (75%) Conduct experiment and data analysis (90%) Wrote the paper (100%)
Muxina Konarova	Edited the paper (10%)
Qing Ma	Conduct experiment (5%)
Swathi Mukundan	Conduct experiment (5%)
Abhijit Shrotri	Concept and experimental design (5%)
Jorge Beltramini	Concept and experimental design (20%) Edited the paper (90%)

Contributions by others to the thesis

No contributions by others

Statement of parts of the thesis submitted to qualify for the award of another degree

None

Acknowledgements

My foremost gratitude is due to ALLAH for His Mercies and Grace, to have spared my life in good health and sound mind to be able to undertake this research.

I would like to thank Dr Jorge Beltramini for giving me the opportunity to work on such a challenging yet amazing research topic. I am grateful for his compassionateness, guidance and wealth of experience. I also appreciate the invaluable suggestions provided by Dr Muxina Konarova, Professor Lianzhou Wang and Professor Gordon Zhu.

I acknowledge the technical assistance provided by the staff members of The Centre for Microscopy and Microanalysis. I appreciated and benefited immensely from the expertise of Dr. Kim Sewell, Dr. Graeme Auchterlonie, Dr. Barry Wood and Ying Yu.

In addition, I appreciate the financial support from the International Postgraduate Research Scholarship (IPRS) and University of Queensland Centennial Scholarship (UQ Cent). I also acknowledge the top-up scholarships provided by Australian Institute for Bioengineering and Nanotechnology.

I am grateful to all the staff members of Nanomaterials Centre. Thanks to Cheryl Berquist, Chaoqing Lu and Celestien Warnaar-Notschaele for their administrative support during my research. I would also like to thank Dr. Qing Ma and Dr. Helen Tang for their technical support.

Special thanks also go to my colleagues for their friendship and selfless assistances in and out of the laboratory. Abhijit Shrotri, Swathi Mukundan, Yusilawati Ahmad Nor, to mention a few, thank you all.

I would also like to acknowledge the unwavering support from my friends. Most importantly, I wish to express my heartfelt appreciation to my family for their unalloyed contributions through thick and thin of my academic sojourn. I would not have been able to achieve this feat without your mentorship, love and care.

Keywords

Cellulosic biomass, 5-hydroxymethylfurfural, biphasic catalytic dehydration, heterogeneous catalysis, bifunctional solid acids, mechanocatalysis, kinetics

Australian and New Zealand Standard Research Classifications (ANZSRC)

ANZSRC code: 090402, Catalytic Process Engineering, 60%

ANZSRC code: 030601, Catalysis and Mechanisms of Reactions, 40%

Fields of Research (FoR) Classification

FoR code: 0904, Chemical Engineering, 60%

FoR code: 0305, Organic Chemistry, 20%

FoR code: 0306, Physical Chemistry, 20%

Table of Contents

Abstract i
Declaration by author iii
Acknowledgements viii
List of Figures xv
List of Tables xxii
List of Schemes xxiii
List of Abbreviations xxiv
Chapter 1 Introduction 1
1.1 Background 2
1.2 HMF synthesis 5
1.2.1 Solvent system 5
1.2.2 Catalysts 7
1.3 Aim and Scope 8
1.4 Thesis Outline 9
References 10
Chapter 2 Literature Review: Advances in the conversion of biomass-derived carbohydrates into 5-Hydroxymethylfurfural over heterogeneous catalysts 12
Abstract 13
2.1 Introduction 14
2.1.1 Ionic liquid-mediated HMF synthesis 16
2.1.2 Water/organic biphasic system-mediated HMF synthesis 17
2.2 Scope 18
2.3 Overview of heterogeneously catalyzed dehydration of carbohydrates into HMF 19
2.3.1 Metal oxides and phosphates 19
2.3.2 Ionic resins 29
2.3.3 Heteropolyacid based 31
2.3.4 Carbon based 35
2.3.5 Immobilized IL on solid support 38
2.3.6 Zeolites 40
2.3.7 Silica based 45
2.3.8 Other catalyst systems 47
2.4 Conclusion and outlook 50
References 52

Chapter 3 Experimental Methodology **57**
3.1 Introduction 58
3.2 Material Synthesis 58
3.2.1 Titania–Zirconia binary oxide synthesis 58
3.2.2 Heteropolyacid salt synthesis 59
3.2.3 Phosphated titania synthesis 59
3.3 Materials characterization 60
3.3.1 X-ray diffraction (XRD) 60
3.3.2 Nitrogen sorption measurement 60
3.3.3 High resolution transmission electron microscopy (HR-TEM) 60
3.3.4 Field emission scanning electron microscopy (FE-SEM) 60
3.3.5 Raman spectroscopy 60
3.3.6 Temperature programmed desorption of ammonia and CO_2 61
3.3.7 Pyridine adsorption with fourier transform infrared spectroscopy (FT-IR) 61
3.3.8 X-ray photoelectron spectroscopy (XPS) 61
3.3.9 Elemental microanalysis for C, H, N, S, O 62
3.3.10 Inductively coupled plasma atomic emission spectroscopy (ICPAES) 62
3.4 Biomass pretreatment 62
3.4.1 Biomass crushing 62
3.4.2 Biomass fractionation 62
3.4.3 Mechanocatalytic depolymerization of cellulose/biomass 63
3.5 Catalyst Evaluation 63
3.5.1 Batch reactor 63
3.5.2 Flow reactor 64
3.6 Product analysis 65
References 66
Chapter 4 Catalytic behaviour of TiO_2–ZrO_2 binary oxide synthesized by sol-gel process for glucose conversion to 5-Hydroxymethylfurfural **67**
Abstract 68
4.1 Introduction 69
4.2 Experimental 70
4.2.1 Chemicals and materials 70
4.2.2 Preparation of TiO_2–ZrO_2 binary oxides 70
4.2.3 Preparation of heteropolyacid salts - $Cs_{2.5}PW$ and $Cs_{3.5}SiW$ 70
4.2.4 Catalyst characterization 70

4.2.5 Catalytic activity procedure and product analysis 71
4.3 Results and discussion 72
4.3.1 Characterization of TiO_2–ZrO_2 binary oxides 72
4.3.2 Activity tests 76
4.4 Conclusion 81
Acknowledgements 81
References 82
Supplementary Material 85
Chapter 5 Catalytic conversion of glucose to 5-Hydroxymethylfurfural with a phosphated-TiO_2 catalyst 92
Abstract 93
5.1 Introduction 94
5.2 Experimental 96
5.2.1 Materials and catalyst synthesis 96
5.2.2 Catalyst characterisation 96
5.2.3 Catalytic evaluation 97
5.3 Results and Discussion 98
5.3.1 Powder X-ray diffraction 98
5.3.2 N_2 adsorption-desorption 99
5.3.3 Compositional and surface analysis 100
5.3.4 Transmission electron microscopy (TEM) 102
5.3.5 Acidity measurement 102
5.3.6 Catalyst activity 103
5.3.6.1 Influence of reaction parameters 106
5.3.6.2 Plausible reaction pathway 109
5.3.6.3 Catalyst reusability 109
5.4 Conclusion 111
Acknowledgements 111
References 112
Supplementary Material 116
Chapter 6 Direct production of 5-Hydroxymethylfurfural via catalytic conversion of simple and complex sugars over phosphated–TiO_2 129
Abstract 130
6.1 Introduction 131
6.2 Experimental 133

6.2.1 Materials and catalyst preparation 133
6.2.2 Catalyst characterisation 134
6.2.3 Mechanocatalytic depolymerization of cellulose 135
6.2.4 Catalytic reactions 135
6.3 Results and Discussion 136
6.3.1 Catalyst characterization 137
6.3.2 Catalyst evaluation 140
6.3.2.1 Simple sugars to HMF 140
6.3.2.2 Complex sugars to HMF 144
6.3.3 Catalyst recyclability 145
6.3.4 HMF production under a continuous flow condition 146
6.4 Conclusion 148
Acknowledgements 149
References 150
Supplementary Material 154
Chapter 7 High yield conversion of cellulosic biomass into 5-Hydroxymethylfurfural and a study of the reaction kinetics of cellulose to HMF conversion in a biphasic system 158
Abstract 159
7.1 Introduction 160
7.2 Experimental 161
7.2.1 Chemicals and materials 161
7.2.2 Catalyst preparation 162
7.2.3 Catalyst characterization 162
7.2.4 Two-stage biomass fractionation 162
7.2.5 Mechanocatalytic depolymerization 162
7.2.6 Catalytic test and product analysis 163
7.3 Results and Discussion 164
7.3.1 Catalyst characterization 164
7.3.2 Activity tests 166
7.3.3 Reaction pathway and kinetics of cellulose to HMF reaction 171
7.4 Conclusions 175
Acknowledgements 176
References 177
Supplementary Material 180

Chapter 8 Conclusions and Recommendations 187
8.1 Conclusions 188
8.2 Recommendations 189

List of Figures

Figure 1.1 Molecular structure of cellulose showing hydrogen bonding between sugar units (left) and β (1→4) glycoside bonding (right)[10] 2

Figure 1.2 Structure of xylan, glucomannan as hemicellulose model[17] 3

Figure 1.3 Structure of lignin model 4

Figure 1.4 HMF production and its utilization routes for chemicals and fuels[20] 5

Figure 2.1 Chemical structure of HMF 14

Figure 2.2 Chemistry and applications of 5-HMF and its derivatives (solid arrow, direct transformation; broken arrow, multistep reaction; 5-HMF, 5-hydroxymethylfurfuran; LEVA, levulinic acid; LEVE, levulinic ester; FA, formic acid; HFCA, 5-hydroxymethylfuroic acid; FDC, 2,5-furandicarboxyaldehyde; FDCA, 2,5-furandicarboxylic acid; DHMF, 2,5-di(hydroxymethyl)furan; DHM-THF, 2,5-di(hydroxymethyl)tetrahydrofuran; HMTHFA, 5-(hydroxymethyl)tetrahydrofuran-2-carbaldehyde; **1**, 2-(hydroxy(5-(hydroxymethyl)tetrahydrofuran-2-yl)methyl)-5-(hydroxymethyl)tetrahydrofuran-2-carbaldehyde; **2**, (E)-4-(5-(hydroxymethyl)furan-2-yl)but-3-en-2-one; **3**, (1E,4E)-1,5-bis(5- (hydroxymethyl)furan-2-yl)penta-1,4-dien-3-one; **4**, tetrahydrofurfuryl alcohol; **5**, 2,5-dimethyltetrahydrofuran; **6**, furan; **7**, 2-hydroxymethyl- 5-vinylfuran; **8**, furfuryl alcohol; **9**, 2,5-di(aminomethyl)furan; **10**, 2-methyl tetrahydrofuran; **11**, 2,5-dimethylfuran; **12**, 2-methylfuran)[6] 15

Figure 2.3 Bi-functional surface catalyzed mechanism for a) isomerization of glucose to fructose over basic O^{2-} sites of monoclinic ZrO_2 (Lewis acidic Zr^{4+} may help stabilize the enolate intermediate) and b) dehydration of fructose to HMF over Brønsted acid sites present in submonolayer SO_4/ZrO_2 catalysts 20

Figure 2.4 SEM images (left) and TEM images with electron diffraction patterns (right) of $CuHPO_4.H_2O$ (a, b); α-$Cu_2P_2O_7$-600 (c, d); α-$Cu_2P_2O_7$-900 (e) 22

Figure 2.5 Reaction network for fructose dehydration to HMF catalyzed by cupric phosphate under hot compressed water 22

Figure 2.6 Yield of liquid products from the reaction of sugarcane bagasse at 250 °C and 5 min with and without the present of catalysts 24

Figure 2.7 Plot of glucose conversion (■), fructose yield (▲) and 5-hydroxymethylfurfural (HMF) yield (●) for the transformation of glucose as a function of reaction time. Amberlyst-15 added after 2.5 h. *Reaction conditions:* glucose (0.1 g), hydrotalcite (0.2 g), Amberlyst-15 (0.1 g), *N*,*N*-DMF (3 mL), 373K.[55, 56] 25

Figure 2.8 Diagram of a continuous flow system including a "solubilization" chamber for the production of HMF from cellulose (MIBK: methyl isobutyl ketone)[57] 26

Figure 2.9 Dehydration of sugar by different catalysts. Reaction conditions: 2400 mg of sugar in a Parr reactor (size, 50 mL), the total volume of biphasic system 26 mL, 0.025 mmol of catalyst, 120 °C, 60 min for fructose and 0.1 mmol of catalyst, 130 °C, 4 h for glucose, respectively.....32
Figure 2.10 Selective conversion of fructose and glucose to HMF catalyzed by poly(VMPS)-PW[72] 33
Figure 2.11 Proposed mechanisms of the dehydration of glucose to HMF catalyzed by nano-POM/ nano-ZrO_2/nano-γ-Al_2O_3 catalysts.....34
Figure 2.12 Dehydration of fructose to HMF in the presence of acidic catalysts.....38
Figure 2.13 Schematic representation of 1-(tri-ethoxy silyl-propyl)-3-methyl-imidazolium hydrogen sulphate (IL-HSO_4) immobilization on silica nanoparticles 39
Figure 2.14 Synthetic process for preparing the bi-functionalized MSN 40
Figure 2.15The plausible mechanism for the conversion of glucose into HMF in the presence of Hβ-zeolite and [BMIM]Cl.[87] 43
Figure 2.16 One-pot biphasic water/tetrahydrofuran (THF) reactor system[92] 44
Figure 2.17 Continuous fructose dehydration in a ¼ inch packed bed reactor.....46
Figure 2.18 Plausible reaction mechanism for tandem isomerisation-dehydration of glucose to HMF over Sn-Mont catalyst.[102] 48
Figure 2.19 The synthesis of Cr^{3+}-HPFs-1-H^+ and the conversion of carbohydrate into HMF in [Emim]Cl under atmospheric pressure[103] 49
Figure 3.1 Experimental set up for titania–zirconia binary oxide synthesis 59
Figure 3.2 Schematic diagram of the batch reactor set-up for carbohydrates conversion reaction to HMF. 1 – Ar cylinder; 2 – magnetic drive; 3 – heating mantle; 4 – thermocouple; 5 – pressure guage; 6 – depressurization valve; 7 – vial for sample collection; 8 – pressure and temperature PID controller. 64
Figure 3.3 Schematic diagram of a biphasic flow reactor set-up. 65
Figure 4.1 XRD patterns of: a) TiO_2, b) TiO_2–ZrO_2 (3/1), c) TiO_2–ZrO_2 (1/1), d) TiO_2–ZrO_2 (1/3) and e) ZrO_2. A: anatase; M: monoclinic; T: tetragonal 72
Figure 4.2 Infrared spectra of pyridine adsorbed on: a) TiO_2, b) TiO_2–ZrO_2 (1/1) and c) ZrO_2 74
Figure 4.3 Raman spectra of: a) TiO_2, b) TiO_2–ZrO_2 (3/1), c) TiO_2–ZrO_2 (1/1), d) TiO_2–ZrO_2 (1/3) and e) ZrO_2 75
Figure 4.4 Glucose conversion to HMF over TiO_2–ZrO_2 binary oxides in an aqueous medium. Reaction conditions: 2 g glucose, 0.8 g catalyst wt., 3 h reaction time, 175 °C reaction temperature, 100 ml water. (●), glucose conversion and product yields: (●) fructose, (●) HMF, (●) levulinic acid.....76

Figure 4.5 Catalytic conversion of glucose over TiO_2–ZrO_2 with solid acid co-catalysts. Reaction conditions: 2 g glucose, 0.8 g catalyst wt. (TiO_2–ZrO_2(1/1)/co-catalyst ratio = 1/1 w/w), 100 ml solvent (THF/water = 4/1 v/v), 4 g NaCl, 3 h reaction time, 175 °C reaction temperature 78

Figure 4.6 Influence of organic solvent in the biphase system on selective HMF yield with TiO_2–ZrO_2 (1/1) and Amberlyst 70 catalysts. Reaction conditions: 5 g glucose, 2 g catalyst weight (TiO_2-ZrO_2/Amberlyst = 1/1 w/w), 100 ml solvent (THF/water = 4/1 v/v), 4 g NaCl, 3 h reaction time, 175 °C reaction temperature. (●) Glucose conversion, (■) HMF_{org} and (■) HMF_{aq} 79

Figure S4.1 a) CO_2 and b) Ammonia temperature programmed desorption profiles of the metal oxides 86

Figure S4.2 Role of reaction medium on glucose conversion to HMF catalyzed by TiO_2–ZrO_2 (1/1). Reaction conditions: 2 g glucose, 0.8 g catalyst wt., 100 ml solvent, 4 g NaCl, 3 h reaction time, reaction temperature 175 °C 87

Figure S4.3 HPLC analytical profile measured using RID detector for glucose to HMF reaction using TiO_2–ZrO_2 (1/1) in aqueous reaction medium. Reaction conditions: 2 g glucose, 0.8 g catalyst wt., 100 ml solvent, 3 h reaction time, reaction temperature 175 °C. 1) glucose, 2) fructose, 3) formic acid, 4) levulinic acid and 5) 5-hydroxymethyfurfural 88

Figure S4.4 HPLC analytical profile measured using RID detector for glucose to HMF reaction using TiO_2–ZrO_2 (1/1) in water/THF monophase reaction medium. Reaction conditions: 2 g glucose, 0.8 g catalyst wt., 100 ml solvent (water/THF = 1/4 v/v), 3 h reaction time, reaction temperature 175 °C. 1) glucose, 2) fructose, 3) formic acid, 4) levulinic acid, 5) 5-hydroxymethyfurfural and 6) tetrahydrofuran 89

Figure S4.5 HPLC analytical profile measured using RID detector for glucose to HMF reaction using TiO_2–ZrO_2 (1/1) in water/THF biphase reaction medium. Reaction conditions: 2 g glucose, 0.8 g catalyst wt., 100 ml solvent (THF/water = 4/1 v/v), 4 g NaCl, 3 h reaction time, reaction temperature 175 °C. a) aqueous phase and b) organic phase 90

Figure S4.6 Influence of initial glucose concentration on HMF yield. Reaction conditions: glucose/catalyst = 2.5 w/w, catalysts = TiO_2–ZrO_2 (1/1) and Amberlyst 70 (1/1 w/w), 100 ml solvent (THF/water = 4/1 v/v), 4 g NaCl, 3 h reaction time, 175 °C reaction temperature 91

Figure 5.1 XRD patterns of: a) TiO_2, b) 5P-TiO_2, c) 10P-TiO_2, d) 15P-TiO_2, e) 20P-TiO_2, and f) 25P-TiO_2 nanoparticles 99

Figure 5.2 (i) BET isotherm and (ii) pore size distribution of: a) TiO_2, b) 5P-TiO_2, c) 10P-TiO_2, d) 15P-TiO_2, e) 20P-TiO_2, and f) 25P-TiO_2 nanoparticles 100
Figure 5.3 High resolution XP spectra of: a) O 1s, b) Ti 2p, c) P 2p, and d) wide scan survey 101
Figure 5.4 TEM images of: TiO_2 (a & b) and 15P-TiO_2 (c & d). Images (b) & (d) represent HRTEM of TiO_2 and 15P-TiO_2 showing lattice fringes of plane (101) 102
Figure 5.5 Infrared spectra of pyridine adsorbed on: a) TiO_2 and b) 15P-TiO_2 after evacuation at 150 °C 103
Figure 5.6 Influence of phosphate content on catalytic activity of TiO_2 NP. (●) Glucose conversion and (○) HMF yield. Reaction conditions: 2 g glucose, catalyst wt. = 0.4 g, temperature = 160 °C, time = 5 h, water = 30 mL, n-butanol = 70 mL 104
Figure 5.7 Effect of calcination temperature on crystal size and catalytic activity of TiO_2 NP: a) pure and b) phosphated (15 wt%). Reaction conditions: 2 g glucose, catalyst wt. = 0.4 g, temperature = 160 °C, time = 5 h, water = 30 mL, n-butanol = 70 mL. (○) Glucose conversion, (Δ) HMF yield and (■) crystal size 105
Figure 5.8 Glucose dehydration to HMF as a function of catalyst loading in a water/butanol biphasic solvent using 15P-TiO_2 catalyst. Reaction conditions: 2 g glucose, temperature = 160 °C, time = 5 h, water = 30 mL, n-butanol = 70 mL. (●) Glucose conversion and (○) HMF yield 107
Figure 5.9 Influence of reaction time and temperature on glucose dehydration on 15P-TiO_2 catalyst. (—■—) 160 °C, (—●—) 170 °C, (—▲—) 175 °C and (—▼—) 180 °C. Reaction conditions: 2 g glucose, catalyst wt. = 0.6 g, water = 30 mL, n-butanol = 70 mL 108
Figure 5.10 Influence of initial glucoe concentration on HMF yield over 15P-TiO_2 catalyst. (■) Glucose conversion and (■) HMF yield. Reaction conditions: glucose/catalyst wt. ratio = 10:3, temperature = 175 °C, time = 3 h, water = 30 mL, n-butanol = 70 mL 108
Figure 5.11 Reusability test of 15P-TiO_2 catalyst for the conversion of glucose to HMF. Reaction conditions: 2 g glucose, catalyst wt. = 0.6 g, temperature = 175 °C, time = 3 h, water = 30 mL, n-butanol = 70 mL. (●) Glucose conversion, (■) HMF yield 110
Figure S5.1 TEM images along with particle size distribution of TiO_2 NP 117
Figure S5.2 NH_3-TPD spectra of: a) TiO_2, b) 5P-TiO_2, c) 10P-TiO_2, d) 15P-TiO_2, e) 20P-TiO_2 and f) 25P-TiO_2 118
Figure S5.3 X-ray diffraction pattern of: A) pure TiO_2 and B) 15P-TiO_2 calcined at various temperatures 119
Figure S5.4 HPLC analytical profile measured using RID detector of the organic layer obtained from glucose-to-HMF reaction with 15P-TiO_2 catalyst. Reaction conditions: 2 g glucose, catalyst wt. = 0.6 g, temperature = 175 °C, time = 3 h, water = 30 mL, n-

butanol = 70 mL. 1) glucose, 2) fructose, 3) levoglucosan, 4) formaldehyde, 5) formic acid, 6) levulinic acid, 7) 5-hydroxymethylfurfural, 8) furfural.....120
Figure S5.5 Typical representative of HPLC UV analytical profile of HMF in the organic layer. (Same reaction conditions as Figure S5.4).....121
Figure S5.6 Mass spectrum of: a) 5-hydroxymethylfurfural in the reaction product, and b) standard 5-hydroxymethylfurfural.....122
Figure S5.7 Mass spectrum of: a) furfural in the reaction product, and b) standard furfural 123
Figure S5.8 Mass spectrum of: a) levulinic acid in the reaction product, and b) standard levulinic acid 124
Figure S5.9 Product yield as a function of time in the conversion of glucose to HMF on 15P-TiO_2 catalyst. Reaction conditions: 2 g glucose, catalyst wt. = 0.6 g, temperature = 175 °C, water = 30 mL, n-butanol = 70 mL. (●) HMF, (●) Fructose, (●) Levoglucosan, (●) Levulinic acid, (●) Furfural.....125
Figure S5.10 Product distribution of glucose conversion over 15P-TiO_2 catalyst. Reaction conditions: 2 g glucose, 0.6 g catalyst wt., temperature = 175 °C, time = 3 h, water = 30 mL, n-butanol = 70 mL. (■) HMF, (■) fructose, (■) levulinic acid, (■) levoglucosan, (■)furfural 126
Figure S5.11 X-ray diffraction of fresh and spent 15P-TiO_2 catalyst.....127
Figure S5.12 HR-TEM image showing lattice fringes of 15P-TiO_2 catalyst: a) fresh and b) spent.....128
Figure 6.1 XRD measurement of: a) TiO_2, b) V-TiO_2, c) P-TiO_2, d) W-TiO_2 and e) Mo-TiO_2. * vanadium oxide, • rutile-TiO_2.....137
Figure 6.2 TEM micrographs of: a) TiO_2, b) P-TiO_2, c) W-TiO_2, d) Mo-TiO_2 and e) V-TiO_2.....139
Figure 6.3 FT-IR spectra of adsorbed pyridine on: a) TiO_2, b) P-TiO_2, c) W-TiO_2, d) Mo-TiO_2 and e) V-TiO_2 140
Figure 6.4 a) Influence of organic co-solvents on the selective conversion of glucose to HMF; 10 mL organic co-solvent, 70 mL THF. b) Volume ratio effect of THF/NMP on glucose-to-HMF reaction. Reaction conditions: 4:1 glucose/cat. wt. ratio, 1.25 g P-TiO_2 catalyst, 100 mL solvent (water:organic = 1:4 v/v), 4 g NaCl, 105 mins reaction time, 175 °C reaction temperature, 20 bar Ar gas. (o) Glucose conversion and (●) HMF yield 142
Figure S6.1 Nitrogen adsorption-desorption isotherms for: a) TiO_2, b) P-TiO_2, c) W-TiO_2, d) Mo-TiO_2 and e) V-TiO_2.....155
Figure S6.2 Colour change of P-TiO_2 catalyst: a) before reaction and after reaction. Reaction conditions: 4:1 glucose/cat. wt. ratio, 100 mL solvent (water:THF = 1:4 v/v), 4 g NaCl, 105 mins reaction time, 175 °C reaction temperature, 20 bar Ar gas 156

Figure S6.3 Colour change of P-TiO_2 catalyst after reaction: a) without NMP and b) with NMP. Reaction conditions: 4:1 glucose/cat. wt. ratio, 100 mL solvent (water:organic = 1:4 v/v), 4 g NaCl, 105 mins reaction time, 175 °C reaction temperature, 20 bar Ar gas 157
Figure 7.1 Structural and textural properties of phosphated–TiO_2 nanoparticle: a) XRD pattern and b) N_2 adsorption-desorption isotherm 164
Figure 7.2 XPS analysis of phosphated–TiO_2 nanoparticle. a) wide survey scan and high resolution spectra of: b) Ti 2p, c) P 2p, d) O 1s 165
Figure 7.3 Microscopic analysis of phosphated–TiO_2 showing micrographs obtained by: a) FE-SEM and b) HR-TEM 166
Figure 7.4 Glucose conversion to HMF in unmodified and modified water–MeTHF biphasic system. Reaction conditions: 10 g glucose, 1.25 g catalyst, 175 °C, 80 min, 100 mL solvent volume (water–organic solvent 3:7 v/v). MeTHF:NMP 6:1 v/v for the modified reaction system. Glucose conversion (●) and HMF yield in: organic phase (■) and aqueous phase (■) 167
Figure 7.5 Effect of residual acid on the conversion of cello-oligomers into HMF. Reaction conditions: 10 g substrate, 1.25 g catalyst, 175 °C, 80 min, 100 mL solvent volume (water–MeTHF/NMP 3:7 v/v). ■ before neutralization, ■ after neutralization 169
Figure 7.6 Cellulosic biomass conversion to furans on phosphated–TiO_2 catalyst in water–MeTHF/NMP biphasic system. Reaction conditions: 7.5 g substrate, 1.25 g catalyst, 180 °C, 80 min, 100 mL solvent volume (water–MeTHF/NMP 3:7 v/v).■ HMF, ■ furfural 170
Figure 7.7 a) Arrhenius plot of cello-oligomers conversion to HMF: cello-oligomers hydrolysis to glucose (blue), glucose dehydration to HMF (olive green). b) parity plot of experimental data and model prediction ○ glucose yield ● HMF yield. Reaction conditions: 428 – 448 K, 10% (w/v) initial substrate concentration, 8:1 substrate/cat wt. ratio, 100 mL solvent (water–MeTHF/NMP 3:7 v/v) 175
Figure S7.1 EDS analysis of phosphated–TiO_2 nanoparticle 181
Figure S7.2 Product distribution of glucose conversion on phosphated-TiO_2 catalyst. Reaction conditions: 10 g glucose, 1.25 g catalyst, 175 °C, 80 min, 100 mL solvent volume (water–organic solvent 3:7 v/v). MeTHF:NMP 6:1 v/v for the modified reaction system 182
Figure S7.3 XRD pattern of microcrystalline cellulose (black), ball-milled cellulose (red), mechanocatalytically depolymerized cellulose (blue) 183
Figure S7.4 XRD pattern of biomass substrates: a) sugarcane bagasse and b) rice husk. untreated (black), alkali-treated (red), organocat-alkali treated (blue) 184
Figure S7.5 HMF production per quantity of biomass source 185

Figure S7.6 HPLC analytical profile of carbohydrates conversion measured using RID detector. a) cellulose, b) cellobiose, c) glucose.[a] Reaction conditions: 1 g substrate, 0.4 g cat. wt. (0.2 g)[a], 180 °C (160 °C)[a], 100 mL water. d) comparison of carbohydrates conversion at 60 min reaction time. Reaction time: 0 min (black), 10 min (red), 20 min (blue), 30 min (orange), 45 min (green) and 60 min (cyan). Products: cellobiose – 2, glucose – 4, fructose – 5, HMF – 8, unknowns – 1, 3, 6 and 7. 186

List of Tables

Table 1.1 Strength/weakness analysis of various processes for HMF production[a].[31] 7
Table 2.1 Formation of HMF from fructose in aqueous solution by different catalysts (conditions: 2wt% fructose aqueous solution (5 g), catalyst 0.02 g, *T* = 200 °C, reaction time 5 min) 19
Table 2.2 Ferrite-CNTs catalyzed dehydration of fructose and glucose 37
Table 2.3 Transformation of glucose to HMF over Beta zeolites[a] 41
Table 2.4 Conversion of glucose into HMF over a variety of zeolite catalysts[a] 42
Table 2.5 Catalytic data in dehydration of fructose to HMF over various catalysts.[a] 47
Table 4.1 Textural and acid-base properties of the mixed oxides 73
Table 4.2 Binding energies and surface composition of TiO_2–ZrO_2 mixed oxides from XPS 75
Table 4.3 Catalytic transformation of sugars to HMF[*a*] 80
Table S4.1 Comparison of fructose and glucose conversion to HMF[*a*] 85
Table 5.1 Physical, compositional and acid properties of TiO_2 NPs 99
Table S5.1 Effect of Lewis and Bronsted acidity on HMF formation[a] 116
Table 6.1 Physical and acid properties of pure and modified TiO_2 nanoparticles 138
Table 6.2 Catalytic conversion of glucose to HMF using TiO_2 and modified TiO_2 nanoparticles[a] 141
Table 6.3 Catalytic conversion of a variant of sugars to HMF over P-TiO_2 catalyst[a] 144
Table S6.1 Catalytic conversion of glucose to HMF using TiO_2 and modified TiO_2 nanoparticles[a] 154
Table 7.1 Influence of cellulose depolymerization on HMF production[*a*] 168
Table 7.2 Estimated kinetic parameters for cello-oligomers and glucose conversion to HMF in water–MeTHF/NMP biphasic system 174
Table S7.1 Furan yield calculation from biomass feedstock 180

List of Schemes

Scheme 5.1 Glucose conversion to HMF in a water-butanol (30:70 v/v) biphasic system on 15P-TiO_2 NP 109

Scheme 7.1 Proposed reaction scheme of cellulose conversion to HMF catalyzed by phosphated–TiO_2 172

List of Abbreviations

2-MF – 2-methylfuran

AA – Acetic acid

BET – Brunauer-Emmett-Teller

BHJ – Barrett-Joyner-Halenda

DP – Degree of polymerization

DMA – Dimethylacetamide

DMF - Dimethylfuran

DMSO – Dimethylsulfoxide

EDX – Energy dispersive x-ray

GC-MS – Gas chromatography-mass spectrometer

HMF – 5-hydroxymethylfurfural

HPLC – High performance liquid chromatography

HR-TEM – High resolution transmission electron microscopy

HT – Hydrotalcite

FID – Flame ionization detector

FTIR – Fourier transform infrared

IL – Ionic liquid

LA – Levulinic acid

LHSV – Liquid hourly space velocity

MeTHF – 2-methyltetrahydrofuran

MIBK – methylisobutylketone

MOF – Metal organic framework

n-BuOH – Butan-1-ol

N,*N*-DMF – Dimethylformamide

NMP – N-methyl-2-pyrrolidone

SEM – Scanning electron microscopy

TCD – Thermal conductivity detector

THF – Tetrahydrofuran

XRD – X-ray diffraction

XPS – X-ray photoelectron spectroscopy

Chapter 1

Introduction

1.1 Background

The current volatility of oil prices and high level greenhouse gas emissions coupled with the propensity of futuristic energy crisis amidst soaring global energy consumption has driven the necessity to seek for alternative energy sources. Lignocellulosic biomass is promising as both carbon-based energy source and sustainable feedstock for the chemical industry. One of the main challenges in converting lignocellulosic biomass is producing chemicals or fuels at high selectivities and yields at economical costs. This happens because of the recalcitrance of lignocellulosics, thus requiring both physical and chemical pretreatments, which is still one of the most expensive stages of biomass conversion strategy. Typically, two-step processing methods are employed to control the reactivity of lignocellulosics and improve product selectivity.[1] These methods first fractionate the lignocellulosics into its main components, hemicellulose, cellulose, and lignin, which allows for processing each fraction at different conditions to achieve high yields of target products.[2]

Cellulose accounts for 30–50 wt% of lignocellulosic biomass and is a linear homopolymer made up of anhydro-D-glucopyranose units linked via β-glycosidic bonds.[3] Cellulose has a degree of polymerization (DP) up to 15000 glucopyranose units[4] with a network of intra- and inter-molecular hydrogen bonding. The formation of intramolecular hydrogen bonding within cellulose structure is responsible for its crystallinity, rigidity and chemical inertness.[5] Cellulose can be converted into glucose by chemical or enzymatic hydrolysis[6 7] and can be used to produce ethanol, platform chemicals, such as levulinic acid (LA) and 5-hydroxymethylfurfural (HMF), and liquid fuels.[8, 9]

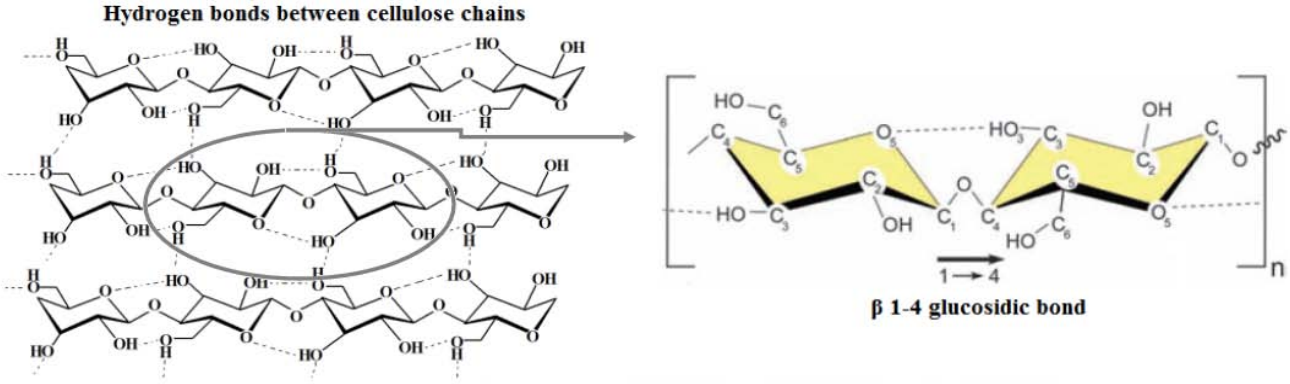

Figure 1.1 Molecular structure of cellulose showing hydrogen bonding between sugar units (left) and β (1→4) glycoside bonding (right)[10]

Hemicellulose accounts for 15–30 wt% of lignocellulosic biomass and is an amorphous polymer consisting of C_5 (such as xylose and arabinose) and C_6 sugars (such as glucose, galactose and mannose); the ratio of which depends on the type of biomass.[11] Xylan and glucomannan are the

main representative hemicelullose components in grasses and hardwood, and softwood, respectively, and their structures are shown in Figure 1.2.[12, 13] Hemicellulose is more reactive than cellulose, easier to remove from lignocellulosic biomass, and is typically associated with the production of xylitol, furfural, and furfural derivatives.[14-16]

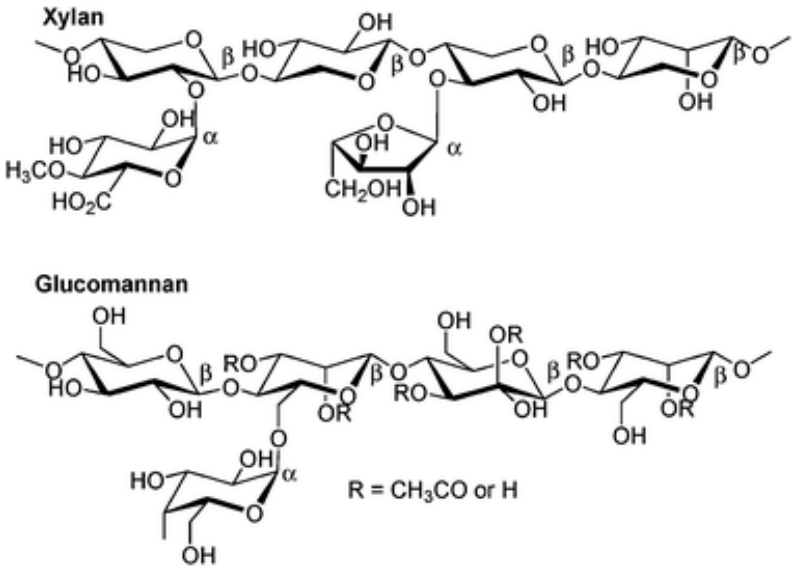

Figure 1.2 Structure of xylan, glucomannan as hemicellulose model[17]

Lignin is an amorphous polymer rich in aromatic monomers that accounts for 15–30 wt% of the lignocellulosic biomass. The structure of lignin depends on many factors and in particular the source of biomass, mainly if it is hardwood or softwood. In general, lignin is composed of three main precursors:[12] *p*-coumaryl, coniferyl, and sinapyl alcohols as shown in Figure 1.3. Lignin also has the potential to be converted into fuels and high value chemicals,[18] but the complexity of its structure and the non-uniformity of its composition makes it more difficult to process than the other fractions.

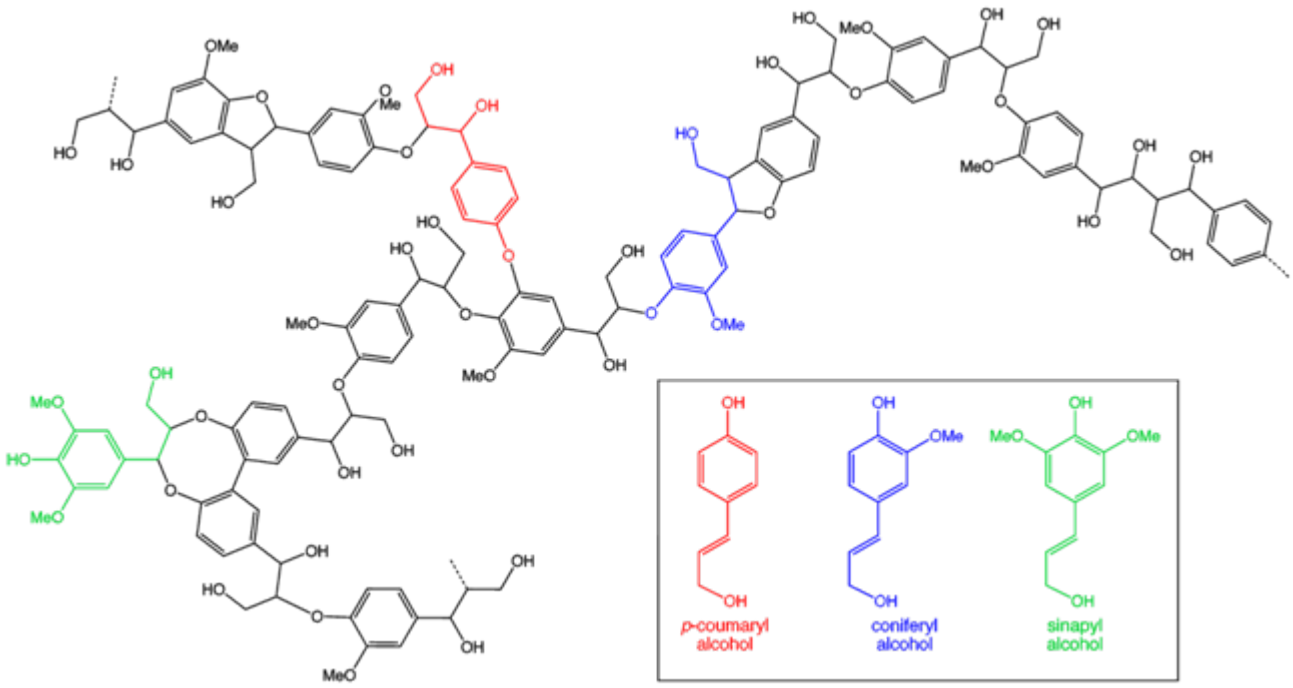

Figure 1.3 Structure of lignin model

Amongst the numerous routes of lignocellulosic biomass valorization, catalytic dehydration of cellulose to produce 5-hydroxymethylfurfural (HMF) represents an attractive strategy.[19, 20] This is because of the versatility of using HMF as an important platform molecule to synthesize an array of intermediate chemicals, from which a diverse range of biofuels as well as commodity and fine chemicals can be generated as shown in Figure 1.4. For example, HMF can be selectively oxidized to furan-2,5-dicarboxylic acid (FDCA) which may be a replacement for terephthalic acid in the production of polyethyleneterephthalate.[21] Alternatively, HMF can be reduced to 2,5-bis(hydroxymethyl)furan (BHMF) and 2,5-bis(hydroxymethyl)tetrahydrofuran (BHMTF) wherein both can serve as alcohol components in the production of polyesters, providing completely biomass-derived polymers when combined with FDCA.[22] HMF may also be rehydrated to levulinic acid from which gamma valerolactone can be produced, which can be utilized as a solvent and fuel additives.[1, 23, 24]

Another important derivative of HMF is 2,5-dimethylfuran (DMF) and 2-methylfuran (2-MF), and both are potential liquid transportation fuels.[25-27] Moreover, HMF can serve as a precursor in the synthesis of liquid alkanes for use as diesel fuel.[28]

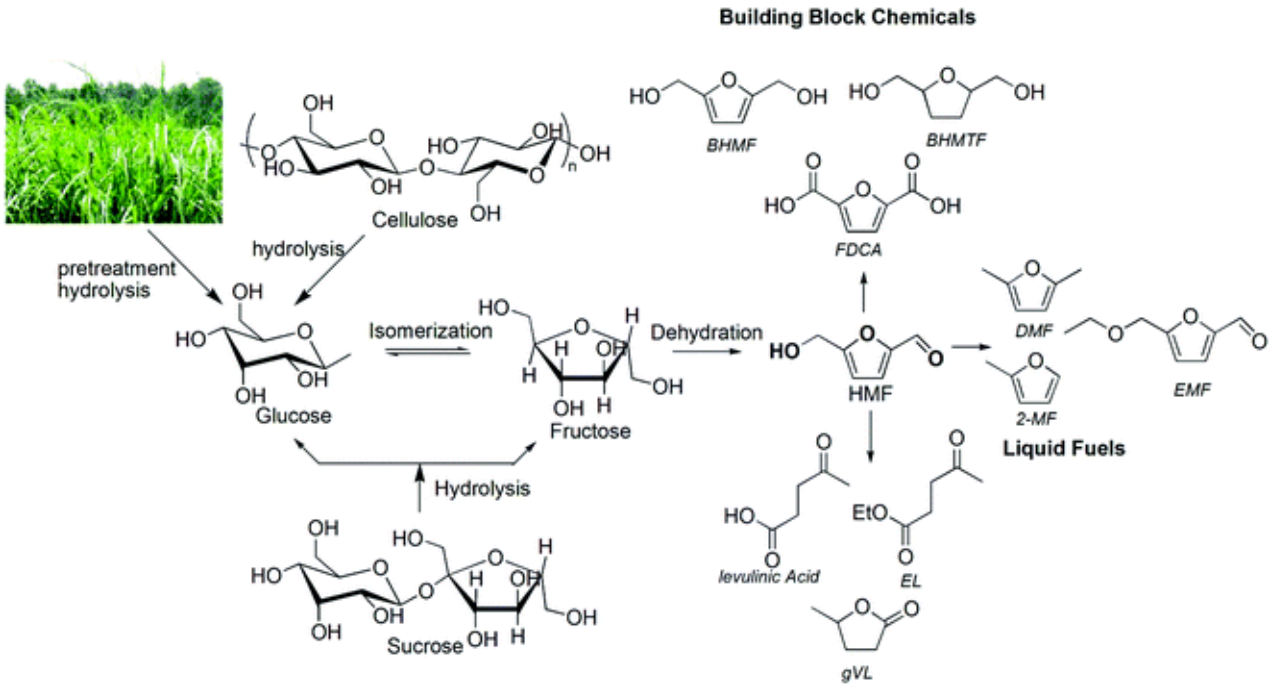

Figure 1.4 HMF production and its utilization routes for chemicals and fuels[20]

1.2 HMF synthesis

HMF is preferentially obtained by acid-catalyzed dehydration of C_6 carbohydrates, such as fructose and glucose. Glucose-based polymers, especially those derived from lignocellulosic sources are favoured feedstocks due to their availability and presence in agricultural side streams and other wastes. Of particular interest to utilize biorenewable feedstock for the sustainable production of HMF is to develop catalytic strategies that can efficiently integrate the complex multi-step transformation reactions involved. To this effect, great research efforts have so far focused on screening various solvents and catalysts to improve reaction rate and selectivity.

1.2.1 Solvent system

Solvents used can be broadly classified into three groups: single phase system (aqueous solvent, organic solvents), ionic liquid and biphasic system (organic-ionic liquid or organic-water).[29]

Water based processes for carbohydrates dehydration is more advantageous in terms of green chemistry principles. So also, water dissolves the majority of carbohydrate substrates in high concentrations. Nevertheless, as the synthesis of HMF in aqueous medium is non-selective often results in low yield because of subsequent reactions to levulinic acid and insoluble polymeric compounds (humins). To improve the selectivity of HMF and prevent its consecutive degradation reactions, HMF may either be:[29]

a) stabilized with some specific solvents or

b) continuously removed from the reaction mixture.

Carbohydrate dehydration in organic solvents especially the polar aprotic ones (dimethylsulfoxide (DMSO), *N*,*N*-dimethylformide (*N*,*N*-DMF), dimethylacetamide (DMA)) generally give higher HMF yields by inhibiting the rate of HMF decomposition, rehydration or condensation.[29] Carbohydrates have very low solubility in organic solvents, with the exception of polar coordinating solvents such as DMSO and DMF. DMSO is the most popular for HMF production as it has the highest solubility for carbohydrates and high stability for HMF. However, high solubility of HMF in these solvents makes it difficult to separate HMF because of their high boiling point, thus requiring high energy intensive processes for product recovery. Moreover, toxic sulfur compounds formed during high temperature distillation of DMSO makes product separation more problematic and costly.[30]

Alternative to high boiling point aprotic solvents are alcohols. Alcohols are another interesting type of solvents as they can be synthesized from biomass, possess better dissolving capacity for sugars and have a variety of boiling points. Alcohols are also environmental friendly, cost efficient and easily operated reaction media. HMF could react with alcohols under acidic condition to form HMF-ether that would possibly prevent HMF from further decomposition or oligomerization. However, it may also be problematic for the conversion of HMF to other downstream chemicals.[31]

Another class of solvent systems are ionic liquids (ILs) which have reportedly been used as both a solvent and a catalyst for producing HMF from carbohydrates due to comparatively higher catalytic activity and adjustable composition.[32, 33] More so, ILs has exceptional capacity to dissolve polymeric carbohydrates and as a result, they may potentially be used for the pretreatment of lignocellulosic biomass.[34-36] Toxicity, cost, corrosiveness and recyclability are some of the drawbacks that reduce applicability of ILs in industrial processes. High cost of ILs commands efficient recycling, though limited success has been achieved in this regard since they have low volatility. Relatively low solubility of carbohydrates due to viscosity of ILs is another challenge that limits the extent of feedstock concentration that can be converted into HMF.

Biphasic system comprises of a reactive phase and an extractive phase. A biphasic system consisting of imidazolium based IL ([BMIM]Cl) as the reactive phase and organic solvent as the extractive phase (THF) has the added advantage of lowering energy requirement by minimizing operational cost.[37] However, a major challenge of this system is the poor mixing between the reactive and organic phases, which hinders HMF extraction and can often lead to lower HMF yield in addition to the inherent problem of product isolation. Water-organic biphasic system appears to be much more suitable in terms of solubility and reaction efficiency. By using this strategy, the aqueous phase serves as the reactive phase whereas the organic phase of the biphasic system affords

in situ extraction and accumulation of HMF immediately after its formation. Consequently, this method allows easy separation and reusability of the reactive aqueous phase. Moreover, because low concentration of HMF remains in the aqueous phase due to continuous extraction, this limits the rate of side reactions and thereby improves HMF yield.[20] In spite of the attractiveness of water-organic biphasic system, a considerably large amount of extracting solvent may be required to isolate HMF.

Summarily, Table 1.1 highlights the strength and weaknesses of the various solvent systems as it relates to economics, environmental impact, etc. on the overall catalytic process of HMF production.

Table 1.1 Strength/weakness analysis of various processes for HMF production[a].[31]

Processes		Selec.	Isolation	Efficiency	Environ. impact	Cost	Processability
Single phase	Aqueous	-	-	-	+	++	-
	DMSO	+++	-	++	-	+	-
	Ionic liquid	+++	-	++	-	-	-
	LBP solvent[b]	++	++	++	++	++	++
Biphasic	Organic/aqueous	+	+	+	+	+	+
	Organic/ionic liquid	++	+	+	-	-	-

[a] Including HMF isolation
[b] Low boiling point green solvents

1.2.2 Catalysts

Besides the effectiveness of the solvent to provide enabling environment for the selective production of HMF, catalysts also play a crucial role in enhancing the formation rate of HMF as well as the overall competitiveness of the process both economically and environmentally. Different catalytic systems have been explored for the synthesis of HMF, which may be classified them into five categories:[38] organic acids, mineral acids, salts, lewis acids and solid catalysts. The first four categories can be grouped as homogeneous catalysts while solid catalysts are also referred to as heterogeneous catalysts. Generally, employing these groups of homogeneous catalyst either as single entity or in combination is favourable for the acid dehydration of carbohydrates due to fast reaction rates, thus producing high yields and selectivities of HMF. In practice, a tandem combination of homogeneous Lewis and Brønsted acids are required to efficiently catalyze one-pot

conversion of polysaccharides and biomass feedstocks. On this basis, a major advantage of heterogeneous catalyst is the possibility of developing a single solid catalyst system with tuneable and diverse acidic sites on the surface. In contrast to acid waste streams generated in homogeneous catalysis, recyclable solid catalysts can mitigate corrosion and risk of environmental hazards. Other advantages of solid acid catalysts over homogeneous catalysts are the ease of product separation and purification, and reusability of the catalysts. Despite these encouraging benefits, heterogeneous catalysts usually suffer from deactivation, leaching and production contamination, mass transfer diffusion limitation and high temperature requirement that remain issues of concern during their use.

Therefore, given the current status, challenges and prospects of HMF production process mentioned above, catalytic strategy of water-organic biphasic process based on heterogeneous catalysis is promising. It combines the attractive features of biphasic system such as improved product recovery and high product selectivity due to minimized side reactions, with important features of solid catalysts such as reusability, eco-friendliness and versatility due to adjustable surface acidity.

1.3 Aim and Scope

The overall objective of the thesis is the conceptual development and optimization of environmentally-friendly and cost efficient strategy that will enable the conversion of biomass-derived carbohydrates into 5-hydroxymethylfurfural. Because of abovementioned benefits of both biphasic media and solid catalysts, emphasis is directed towards the design and implementation of more effective biphasic solvents (exploiting low boiling point organic solvents that are biorenewable) as well as a single bifunctional catalyst system.

To this end, specific aims are:

a) Catalyst design: rational development of a simple synthesis technique to prepare solid acid catalyst that possesses both Lewis and Brønsted acidity.
b) Careful selection of organic co-solvents based on extraction efficiency. Investigate role of volume ratio of organic:aqueous, presence of inorganic salt and phase modifiers on partitioning coefficient of HMF, which is a measure of overall effectiveness of biphasic media.
c) Solid state depolymerization of cellulose and biomass to release water soluble oligosaccharides prior to catalytic dehydration reaction. In the case of raw biomass, fractionation pretreatment will be carried out to obtain cellulose-rich fibres. For the current

study, agricultural residues such as sugarcane bagasse and rice husk are considered as cheap sources of cellulosic biomass.

d) Catalyst characterization and parametric study of reaction conditions in order to understand structure-property-reactivity relationships for the optimization of the carbohydrates dehydration reaction.
e) Kinetic study and reaction pathway elucidation of HMF production in the water-organic biphasic reaction utilizing cellulose as the feedstock.

1.4 Thesis Outline

There are a total of 8 chapters in the thesis. Chapters 2, 4-7 comprise of journal papers that have been published and a manuscript under preparation for journal publication. Each chapter is outlined as follows:

Chapter 1 introduces the background and objectives of the current research.

Chapter 2 presents an overview of the current advancement in the production of 5-hydroxymethylfurfural with emphasis on solid acid transformation of biomass-derived carbohydrates.

Chapter 3 describes the entire experimental methodology used to conduct the outlined research including material synthesis and characterization, feedstock preparation, catalytic conversion reactions, data collection and analysis.

Chapter 4 explores the catalytic potential of TiO_2–ZrO_2 binary oxide for the synthesis of 5-hydroxymethylfurufral from glucose. Solvent effect on product selectivity was also examined.

Chapter 5 illustrates the design of acid bifunctionality (Lewis and Brønsted) on TiO_2 nanoparticle for glucose dehydration reaction in water-butanol biphasic system. Catalyst synthesis and reaction conditions were studied to achieve an optimum design process.

Chapter 6 presents the robustness of the TiO_2 catalyst to produce HMF from a variety of carbohydrate sources utilizing water-THF biphasic system. Role of phase modifiers on HMF selectivity was studied.

Chapter 7 describes the transformation of intact cellulosic biomass to HMF and the fractionation process of biomass to unlock the cellulose component. Reaction kinetics of cellulose conversion to HMF was also investigated.

Chapter 8 presents the overall conclusions and recommendations for future studies.

References

1. D. M. Alonso, S. G. Wettstein and J. A. Dumesic, *Green Chemistry*, 2013, **15**, 584-595.
2. S. G. Wettstein, D. M. Alonso, E. I. Gürbüz and J. A. Dumesic, *Current Opinion in Chemical Engineering*, 2012, **1**, 218-224.
3. C. E. Wyman, B. E. Dale, R. T. Elander, M. Holtzapple, M. R. Ladisch and Y. Lee, *Bioresource technology*, 2005, **96**, 1959-1966.
4. R. Bodirlau, I. Spiridon and C. A. Teaca, *BioResources*, 2007, **2**, 41-57.
5. T. Kondo, *Journal of Polymer Science Part B: Polymer Physics*, 1997, **35**, 717-723.
6. R. Rinaldi and F. Schüth, *ChemSusChem*, 2009, **2**, 1096-1107.
7. M. Galbe and G. Zacchi, in *Biofuels*, Springer, 2007, pp. 41-65.
8. J. C. Serrano-Ruiz, R. Luque and A. Sepulveda-Escribano, *Chemical Society Reviews*, 2011, **40**, 5266-5281.
9. D. M. Alonso, J. Q. Bond and J. A. Dumesic, *Green Chemistry*, 2010, **12**, 1493-1513.
10. M. Poletto, A. J. Zattera and V. Pistor, *Structural Characteristics and Thermal Properties of Native Cellulose*, 2013.
11. J. Cheng, *Biomass to renewable energy processes*, CRC press, 2009.
12. D. Fengel and G. Wegener, *Walter de Gruyter*, 1984, **613**, 1960-1982.
13. A. Hendriks and G. Zeeman, *Bioresource technology*, 2009, **100**, 10-18.
14. A. S. Mamman, J. M. Lee, Y. C. Kim, I. T. Hwang, N. J. Park, Y. K. Hwang, J. S. Chang and J. S. Hwang, *Biofuels, Bioproducts and Biorefining*, 2008, **2**, 438-454.
15. J. P. Lange, E. van der Heide, J. van Buijtenen and R. Price, *ChemSusChem*, 2012, **5**, 150-166.
16. G. Yi and Y. Zhang, *ChemSusChem*, 2012, **5**, 1383-1387.
17. S. Dutta, S. De, B. Saha and M. I. Alam, *Catalysis Science & Technology*, 2012, **2**, 2025-2036.
18. J. Zakzeski, P. C. Bruijnincx, A. L. Jongerius and B. M. Weckhuysen, *Chemical reviews*, 2010, **110**, 3552-3599.
19. T. Wang, M. W. Nolte and B. H. Shanks, *Green Chemistry*, 2014, **16**, 548-572.
20. B. Saha and M. M. Abu-Omar, *Green Chemistry*, 2014, **16**, 24-38.
21. A. Gandini, A. J. Silvestre, C. P. Neto, A. F. Sousa and M. Gomes, *Journal of Polymer Science Part A: Polymer Chemistry*, 2009, **47**, 295-298.
22. B. Kamm, *Angewandte Chemie International Edition*, 2007, **46**, 5056-5058.

23. I. T. Horváth, H. Mehdi, V. Fábos, L. Boda and L. T. Mika, *Green Chemistry*, 2008, **10**, 238-242.
24. Á. Bereczky, K. Lukács, M. Farkas and S. Dóbé, *Natural Resources*, 2014, **2014**.
25. S. Zhong, R. Daniel, H. Xu, J. Zhang, D. Turner, M. L. Wyszynski and P. Richards, *Energy & Fuels*, 2010, **24**, 2891-2899.
26. G. Tian, R. Daniel, H. Li, H. Xu, S. Shuai and P. Richards, *Energy & Fuels*, 2010, **24**, 3898-3905.
27. R. Daniel, G. Tian, H. Xu, M. L. Wyszynski, X. Wu and Z. Huang, *Fuel*, 2011, **90**, 449-458.
28. J. O. Metzger, *Angewandte Chemie International Edition*, 2006, **45**, 696-698.
29. R.-J. van Putten, J. C. van der Waal, E. De Jong, C. B. Rasrendra, H. J. Heeres and J. G. de Vries, *Chemical reviews*, 2013, **113**, 1499-1597.
30. C. Moreau, M. N. Belgacem and A. Gandini, *Topics in Catalysis*, 2004, **27**, 11-30.
31. S. P. Teong, G. Yi and Y. Zhang, *Green Chemistry*, 2014, **16**, 2015-2026.
32. C. Moreau, A. Finiels and L. Vanoye, *Journal of Molecular Catalysis A: Chemical*, 2006, **253**, 165-169.
33. J. Long, B. Guo, J. Teng, Y. Yu, L. Wang and X. Li, *Bioresource technology*, 2011, **102**, 10114-10123.
34. R. P. Swatloski, S. K. Spear, J. D. Holbrey and R. D. Rogers, *Journal of the American Chemical Society*, 2002, **124**, 4974-4975.
35. D. A. Fort, R. C. Remsing, R. P. Swatloski, P. Moyna, G. Moyna and R. D. Rogers, *Green Chemistry*, 2007, **9**, 63-69.
36. H. Wang, G. Gurau and R. D. Rogers, *Chemical Society Reviews*, 2012, **41**, 1519-1537.
37. J. Y. G. Chan and Y. Zhang, *ChemSusChem*, 2009, **2**, 731-734.
38. A. A. Rosatella, S. P. Simeonov, R. F. Frade and C. A. Afonso, *Green Chemistry*, 2011, **13**, 754-793.

Chapter 2

Literature Review: Advances in the conversion of biomass-derived carbohydrates into 5-Hydroxymethylfurfural over heterogeneous catalysts

A paper to be submitted to Bioresource Technology

Advances in the conversion of biomass-derived carbohydrates into 5-Hydroxymethylfurfural over heterogeneous catalysts: An overview

Luqman Atanda,[a] Muxina Konarova[a] and Jorge Beltramini[a]

[a] *Nanomaterials Centre, Australian Institute for Bioengineering & Nanotechnology and School of Chemical Engineering, The University of Queensland, Brisbane, St. Lucia 4072, Australia*

Abstract

Biomass conversion to chemicals and fuels is proposed as a sustainable means to meet the increasing global energy requirement with minimum environmental impact. Cellulose, which is the most abundant component of plant biomass, is a biopolymer consisting of glucose units. As such, potential strategies to selectively convert cellulose to valuable chemical feedstocks will significantly improve the economic feasibility and sustainability of lignocellulosic biomass valorization. Acid dehydration of cellulose to 5-hydroxymethylfurfual (HMF) will play a pivotal role in the emerging biorefinery industry as HMF serves as a building block for biofuels and fine chemicals production. Homogeneous acid catalysts have been widely favoured owing to their fast reaction rates and high product yield. Like most chemical processes, replacement of homogeneous catalysts with heterogeneous ones is of practical economic benefits. Improved recovery efficiency, eco-friendly and cost effectiveness make heterogeneous catalytic processes of economical viable proposition for the commercial development of biorefinery processes. Thus, this review provides with an overview of recent advances in the catalytic conversion of biomass into HMF over solid catalysts.

2.1 Introduction

5-hydroxymethylfurfural (5-hydroxymethyl-2-furaldehyde, 5-hydroxymethyl-2-furancarboxaldehyde), usually referred to as HMF, is a common product generated by thermal treatment of carbohydrate-containing food in the presence of amino acids (Maillard reaction).[1] It is a natural component of dried fruits, coffees, cereals and baking products.[2] It has a molecular mass of 126.11 $gmol^{-1}$ and a boiling point of 114 °C. HMF can be used as a flavouring substance in food or as food additives.[3] Its chemical structure (Figure 2.1) is that of a heterocyclic furanic molecule with an alcohol and aldehyde functionalities, thus making it very reactive which Wang et al.[4] has attributed to three molecular attributes:

a) HMF is an α,ω-bifunctional molecule with substituents in both the 2 and 5 positions
b) HMF is a relatively unsaturated aromatic compound and
c) Heterocyclic structure of furans can be found in an array of biologically active molecules with pharmaceutical applications

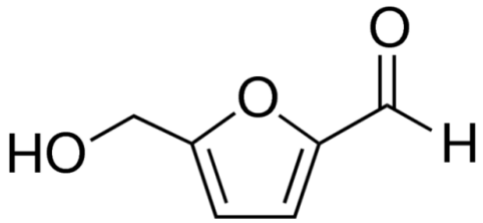

Figure 2.1 Chemical structure of HMF

Due to these unique and attractive properties of HMF, it can be widely utilized as a building block for the synthesis of fine chemicals, production of fuel additives, hydrocarbons and value added chemicals as summarized in Figure 2.2. As a result, the U.S. Department of Energy (DOE) listed HMF among the Top 10 + 4 more important biobased chemicals for the 21st century.[5]

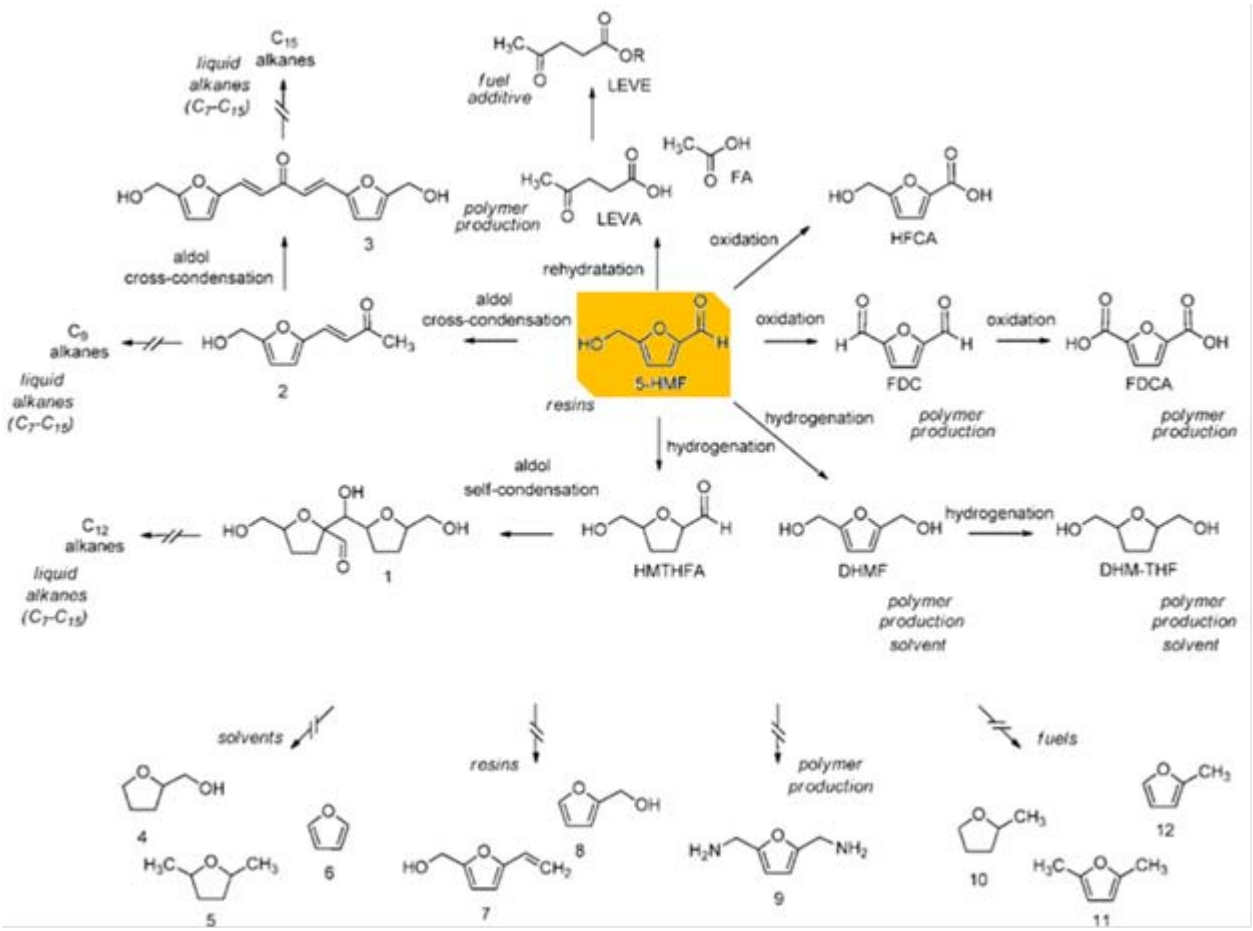

Figure 2.2 Chemistry and applications of 5-HMF and its derivatives (solid arrow, direct transformation; broken arrow, multistep reaction; 5-HMF, 5-hydroxymethylfurfuran; LEVA, levulinic acid; LEVE, levulinic ester; FA, formic acid; HFCA, 5-hydroxymethylfuroic acid; FDC, 2,5-furandicarboxyaldehyde; FDCA, 2,5-furandicarboxylic acid; DHMF, 2,5-di(hydroxymethyl)furan; DHM-THF, 2,5-di(hydroxymethyl)tetrahydrofuran; HMTHFA, 5-(hydroxymethyl)tetrahydrofuran-2-carbaldehyde; **1**, 2-(hydroxy(5-(hydroxymethyl)tetrahydrofuran-2-yl)methyl)-5-(hydroxymethyl)tetrahydrofuran-2-carbaldehyde; **2**, (E)-4-(5-(hydroxymethyl)furan-2-yl)but-3-en-2-one; **3**, (1E,4E)-1,5-bis(5- (hydroxymethyl)furan-2-yl)penta-1,4-dien-3-one; **4**, tetrahydrofurfuryl alcohol; **5**, 2,5-dimethyltetrahydrofuran; **6**, furan; **7**, 2-hydroxymethyl- 5-vinylfuran; **8**, furfuryl alcohol; **9**, 2,5-di(aminomethyl)furan; **10**, 2-methyl tetrahydrofuran; **11**, 2,5-dimethylfuran; **12**, 2-methylfuran)[6]

HMF is commonly synthesized by acid dehydration of carbohydrates, especially fructose and glucose. HMF synthesis has gained a lot interest since it was first reported by Grote et al.[7] in 1875. Renewed interest in the compound dates back to the mid-19th century following the review by Newth et al.[8] As a result of the growing interest in HMF, there have been comprehensive reviews on the development of the chemistry of this furanic compound, synthesis and production processes from bioresources.[2, 4, 6, 9-26]

Recent work has shown that HMF synthesis processes involving ionic liquid and biphasic reaction systems have been well demonstrated. A brief highlight of these processes is presented below:

2.1.1 Ionic liquid-mediated HMF synthesis

Significant progress in HMF production by metal chloride-ionic liquid process was pioneered by Zhao et al.[27] in 2007. In this process, $CrCl_2$ effectively catalyze the dehydration of fructose and glucose in 1-ethyl-3-methylimidazolium chloride [EMIM]Cl to give 65% and 68% HMF yield, respectively, at 100 °C for 3 h. As this was the first time such a high yield of HMF can be produced from glucose, it was proposed that effective dehydration of glucose was assisted by the interaction of $CrCl_3^-$ with glucose, which promoted its isomerization to fructose. In a similar work in the presence of ionic liquids (ILs), Yong et al.,[28] used N-heterocyclic carbene (NHC) as ligands for chromium chlorides in order to improve its catalytic activity to dehydrate fructose and glucose. HMF yields of 95% and 81% were obtained from fructose and glucose, respectively over the NHC/Cr catalyst at 100 °C for 6 h. It was concluded that the ligand prevented the metal centre from binding to the IL (steric crowding), thereby, affording a better catalytic performance. Subsequently, impressive results were achieved by applying the metal chloride-IL system to polymeric carbohydrates like cellulose. Zhang et al.[29] reported a direct conversion of cellulose with a pair of $CuCl_2$–$CrCl_2$ catalyst system that gave 55% HMF yield in [EMIM]Cl. Separation of HMF by extracting with methylisobutylketone (MIBK) improved the performance of the recovered IL and the activity of the catalyst was maintained for three repeated reaction cycles. Moreover, a similar result (55% HMF yield) was reported by Qi et al.[30] by a single-step conversion of cellulose in $CrCl_3$/[BMIM]Cl system whereas Wang et al.[31] reported 60% HMF yield with $CrCl_3$/$LaCl_3$(LiCl) catalyst in [BMIM]Cl. A remarkably high yield of HMF directly from cellulose was reported by Zhang et al.[32] in a [EMIM]Cl–water mixture using $CrCl_2$ under a relatively mild reaction conditions (≤140 °C, 0.1 MP pressure). Cellulose could be converted into water-soluble reducing sugars up to 97% yield in the absence of an added acid catalyst, but when $CrCl_2$ was added to catalyze the aldose–ketose isomerisation reaction, 89% yield of HMF could be obtained in a single step conversion of cellulose. The authors have shown that enhanced water dissociation constant (K_w) of the IL-water mixture is responsible for the efficient conversion of cellulosic biomass. Nikitin and Mascal[33] proposed a different route of cellulose conversion to HMF via solvolysis of 5-Chlorimethylfurfural (CMF). Since CMF can be derived in high yield (70-90%) from cellulose in IL with aqueous HCl at 80-100 °C in 3 h,[34] conversion of cellulose and corn stover via intermediate

CMF formation and its subsequent rapid hydrolysis in boiling water resulted in 72% and 69% yields of HMF, respectively.

2.1.2 Water/organic biphasic system-mediated HMF synthesis

Biphasic dehydration of carbohydrates using mineral acid catalysts was also another major breakthrough in HMF production processes. Dumesic's group[35, 36] advanced the concept of water-organic system after it was first invented by Peniston et al.[37] This process is based on the continuous extraction of HMF from the reactive aqueous phase in order to suppress undesired side reactions as this is a major challenge that causes low selectivity of HMF in aqueous acidic media. Dumesic's group introduced a modified biphasic system[35, 36, 38, 39] that allowed highly selective HMF synthesis at high fructose concentration (10–50 wt%). Partitioning of HMF into the immiscible organic phase, methylisobutylketone (MIBK), was enhanced by adding 2-butanol as a cosolvent. Whereas, the aqueous phase was modified with polar aprotic solvents (DMSO or 1-methyl-2-pyrrolidinone (NMP)) and a hydrophilic polymer (poly(1-vinyl-2-pyrrolidinone (PVP)) to suppress undesired side reactions. An impressive outcome of 83% HMF selectivity at 82% fructose conversion was successfully achieved when this biphasic reaction system was applied to 30 wt% fructose feed concentration.[35] In an effort to further improve partitioning efficiency of several organic solvents, Dumesic and co workers examined the role of saturating the aqueous phase with mineral salts.[39] The authors reported that saturation of the aqueous phase with chlorides of sodium, potassium and cesium improved partitioning and was more beneficial for HMF yield and selectivity when compared to bromides and sulphates. As for the solvents and focus on primary and secondary alcohols (C_3-C_6), ketones (C_3-C_6) and cyclic ethers, C_4 solvents gave the highest yields of HMF as compared with the C_3, C_5, and C_6 compounds. With the desire to improve the economic viability of biphasic dehydration of carbohydrates, Dumesic and co-workers developed a catalytic system of Lewis acidic metal salts (e.g., $AlCl_3$, $SnCl_4$, $GaCl_3$, $YbCl_3$, $LaCl_3$) and HCl for glucose dehydration in a biphasic solvent system consisting 2-*sec*-butylphenol (an alkylphenol) and water.[40] Amongst the metal salts examined, $AlCl_3$ was the most active for the conversion of glucose into 62% yield of HMF. The authors attributed the different activities of the MCl_3 catalysts to two intrinsic properties: Lewis acid softness and ionic radius, and aluminium being the hardest Lewis acid was surmised to interact strongly with the oxygen atoms of the hydroxyl groups in glucose, which are hard Lewis base. Alkyphenol as organic solvent of the biphasic system enhanced the overall performance of the reaction system because of its selective partitioning for HMF without extracting the acid catalysts, thereby allowing effective recycling of the catalysts and high recovery of target product. The authors also found out that Lanthanide-based Lewis acids ($YbCl_3$, $DyCl_3$, $LaCl_3$) were also effective

catalysts for glucose conversion reaction at solution pH values of ~5 in water/sec-butylphenol solvent mixture.[41] Biphasic dehydration could also be extended to other carbohydrates such as cellobiose, starch and cellulose to achieve moderate yields of HMF. Yang et al.[42] achieved 61 mol% HMF yield from glucose using a similar combined Lewis acid, $AlCl_3$, and Brønsted acid, HCl, after 10 min of microwave heating at 160 °C in a water–THF biphasic system. It was observed that higher yield of the target product could be achieved at a much shorter time under microwave-assisted heating as compared to conventional heating. The potential of the combined $AlCl_3$/water–NaCl–THF biphasic system was further demonstrated for the conversion of intact lignocellulosic biomass (corn stover, pinewood, switchgrass, and poplar) resulting in coproduction of both furfural and HMF.[43] Shi et al.[44] reported that a high HMF yield of 53% is achievable by the direct degradation of cellulose in a biphasic system with concentrated $NaHSO_4$ and $ZnSO_4$ as the co-catalysts. Unlike ionic liquid, cellulose cannot be solubilised in the biphasic system. Recently, Rinaldi and coworkers[45] reported a novel approach of converting real lignocellulosic biomass into high yields of HMF as well as furfural in water/4-propylguaiacol biphasic reaction system. The attractiveness of this approach is the solid state depolymerization of biomass to produce water soluble oligomers (WSOs), thus overcoming the problem of lignocellulose recalcitrance. Coupled with energy efficiency of microwave heating, processing of the highly reactive WSOs obtained from α-cellulose, sugarcane bagasse and beechwood in the presence of HCl-$AlCl_3$ catalyst system resulted into high yields of HMF (60-69%) and furfural (74-86%) in short reaction times, and thus minimized the propensity of extensive degradation reactions.

2.2 Scope

Catalytic strategies involving both ionic liquid and biphasic reaction systems are certainly promising for HMF production. In terms of catalyst development, pertinent to both processes is the use of homogeneous Lewis and Brønsted acid catalysts. Despite the efficiency of homogeneous catalysis to transform carbohydrates to high yields of HMF, reutilization of the catalysts is difficult and they also lead to corrosion problems, thus requiring expensive materials for construction. Associated toxic waste that may arise from scaling up remains a concern as well. Not until recently have solid catalysts attracted significant attention for biomass conversion in order to overcome these challenges. Solid catalysts can be easily separated from product solution. Moreover, catalytic properties of solid catalyst can be easily fine-tuned to obtain better activity and selectivity towards targeted product. Yet, more efforts are still required to achieve much more efficient, cheap and eco-friendly processes that are sustainable and suitable for large scale transformation of glucose-based carbohydrate to HMF. Therefore, this review will focus specifically on the recent advances in the

conversion of biomass derived carbohydrates into HMF over heterogeneous catalysts. Under this section, the solid catalysts will be grouped as metal oxides and phosphates, ionic resins, heteropolyacid based, carbon based, immobilized IL on solid support, zeolites, silica based and other catalyst systems.

2.3 Overview of heterogeneously catalyzed dehydration of carbohydrates into HMF

2.3.1 Metal oxides and phosphates

Watanabe et al.[46] studied the dehydration of glucose and fructose in hot compressed water over TiO_2 and ZrO_2 catalysts. They observed that ZrO_2 acts as a base catalyst that promotes glucose isomerisation to fructose whereas anatase–TiO_2 behaves like an acid catalyst that facilitates dehydration of fructose to HMF. Furthermore, the author reported the synthesis of HMF using TiO_2 and ZrO_2 as catalysts in (HCW) water but under microwave irradiation as the heating source.[47] With this technique improved conversion and product yields were achieved in contrast to traditional sand bath heating due to improved heating and cooling efficiency. With anatase–TiO_2 for example, 27.4% yield of HMF at 73.1% fructose conversion was obtained under microwave irradiation as compared to 12% yield of HMF at a fructose conversion of 35.3% under conventional heating when the reaction was performed at 200 °C for 3 min. In continuation of their work to improve the catalytic performance of the solid catalyst, the authors prepared SO_4^{2-}/ZrO_2 catalyst for the dehydration of fructose taking advantage of microwave irradiation.[48] Calcination temperature strongly influences the catalytic performance of SO_4^{2-}/ZrO_2. Increasing calcination temperature caused a corresponding reduction in HMF yield (Table 2.1).

Table 2.1 Formation of HMF from fructose in aqueous solution by different catalysts (conditions: 2wt% fructose aqueous solution (5 g), catalyst 0.02 g, T = 200 °C, reaction time 5 min)

Calcination temperature (°C)	Catalyst	Fructose conversion (%)	HMF yield (%)	HMF selectivity (%)
500	ZrO_2	59.3	20.7	34.9
	SO_4^{2-}/ZrO_2	88.7	33.2	37.4
600	ZrO_2	79.9	36.0	45.1
	SO_4^{2-}/ZrO_2	79.9	29.9	37.4
700	ZrO_2	44.6	18.1	40.6
	SO_4^{2-}/ZrO_2	58.5	25.5	43.6

When the activity of pristine ZrO_2 and SO_4^{2-}/ZrO_2 were compared at similar fructose conversion, HMF selectivity on SO_4^{2-}/ZrO_2, 37.4%, was found lesser than 45.1% observed on ZrO_2 which was

attributed to deactivation of the active acid sites by water. Given that SO_4^{2-}/ZrO_2 deactivated rapidly in water, the authors replaced the reaction system with acetone-DMSO mixture and found that catalytic performance of SO_4^{2-}/ZrO_2 to dehydrate fructose was significantly enhanced. Fructose conversion of 91.3% and 71.9% HMF selectivity were achieved in this non-aqueous reaction medium over SO_4^{2-}/ZrO_2 as compared to 75.1% and 60.9% conversion and selectivity respectively, on ZrO_2 at a reaction condition of 180 °C for 5 min.

In order to understand the influence of sulfate treatment on the catalytic property of zirconia for one-pot conversion of glucose to HMF in an aqueous medium, Osatiashtiani et al.[49] reported the synthesis of a series of SO_4/ZrO_2 by systematically controlling the sulfur loading content. Characterization by acid–base titration, XPS, XRD and Raman revealed that saturation with sulfate monolayers resulted in material with only Brønsted acid character that are least efficient for HMF formation. On the contrary, unsulfated zirconia possessed mixed Lewis acid and base surface sites that effectively isomerized glucose to fructose but poor towards fructose dehydration to HMF. Thus, careful tuning of the degree of zirconia surface sulfation to achieve submonolayer sulfate coverages enabled the successful generation of bi-functional catalyst that possessed optimum dual solid acid–base character which facilitated the conversion of glucose to HMF under mild reaction conditions. As a result, the authors postulated a bi-functional catalytic surface mechanism for glucose conversion to HMF consisting of two steps as shown in Figure 2.3: i) initial Lewis base catalyzed proton abstraction from glucose on surface O^{2-} sites of monoclinic ZrO_2 followed by hydrogen transfer to form fructose and ii) subsequent dehydration of spilled over fructose onto neighbouring Brønsted acid sulfate moieties to HMF.

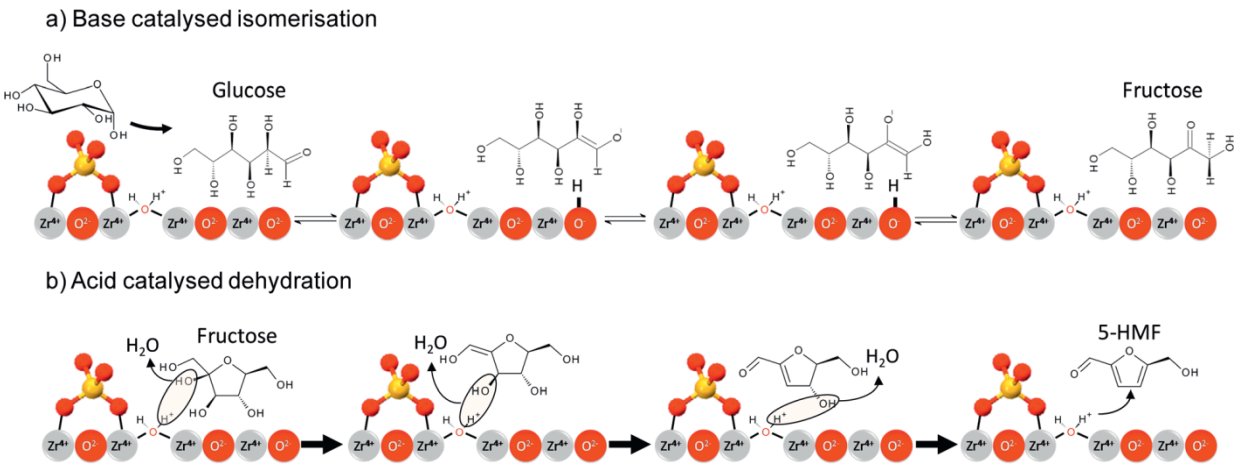

Figure 2.3 Bi-functional surface catalyzed mechanism for a) isomerization of glucose to fructose over basic O^{2-} sites of monoclinic ZrO_2 (Lewis acidic Zr^{4+} may help stabilize the enolate intermediate) and b) dehydration of fructose to HMF over Brønsted acid sites present in submonolayer SO_4/ZrO_2 catalysts

At the same time, Benvenuti et al.[50] reported the dehydration of fructose using zirconium and titanium phosphates and pyrophosphates as catalysts. Among the catalysts investigated, cubic zirconium pyrophosphate (c-ZrP_2O_7) has the highest activity. The presence of both surface Brønsted and Lewis acid sites may be involved in the catalytic process. However, HMF yield is proportional to Lewis acid strength which is superior in c-ZrP_2O_7 whereas cubic titanium pyrophosphate (c-TiP_2O_7) displayed lower catalytic activity because of the presence of lower strength of Lewis acid sites on its external crystal surface. In addition, gamma titanium phosphate (γ-TiP) displayed high activity which was also influenced by Lewis acid strength and thus confirming the role played by Lewis acid strength in their catalytic process. More so, under this acidic aqueous condition, HMF remains stable under as there were no appreciable rehydration products (levulinic and formic acids).

Working under subcritical water condition (240 °C and 33.5 bar), Asghari et al.[51] examined the dehydration of both fructose and glucose with zirconium phosphate (ZrP) catalyst. Highest conversion of fructose (80%) and selectivity to HMF (61%) was achieved with amorphous ZrP after 120 s of reaction. Interestingly, rehydration products such as levulinic and formic acids were not identified in the side reaction products. Nonetheless, soluble polymers and furaldehyde were the only major and minor side products found, respectively. This phenomenon was explained by two plausible explanations suggesting that the catalyst either possesses: a) moderate acidity or b) low availability of macroporous structures. The catalytic activity of ZrP for glucose dehydration under identical conditions as that of fructose gave 38.7% conversion and 31.7% selectivity to HMF. Under the present subcritical water condition, ZrP was found to be stable and can easily be recovered without any changes in the catalytic properties.

Khemthong et al.[52] applied nanostructured copper phosphate catalysts in hot compressed water to dehydrate fructose. As-synthesized $CuHPO_4.H_2O$ calcined at 900 °C (α-$Cu_2P_2O_7$-900) exhibited superior catalytic activity with 35.8% yield of HMF at 82.2% fructose conversion and a turnover number of 34.0 mmol HMF/ h·g of catalyst. The catalytic activities of these copper phosphates nanoparticles are related to surface properties in terms of Brønsted and Lewis acid sites which are strongly dependent on morphology and influenced by heat treatment. With copper species being distributed throughout the phosphate network, $CuHPO_4.H_2O$ (copper hydrogen phosphate monohydrate) exhibits needle-like nanocrystals while calcination at 600 and 900 °C gave α-$Cu_2P_2O_7$ (copper pyrophosphate) of rod-like nanostructure and irregularly shaped microcrystal (Figure 2.4).

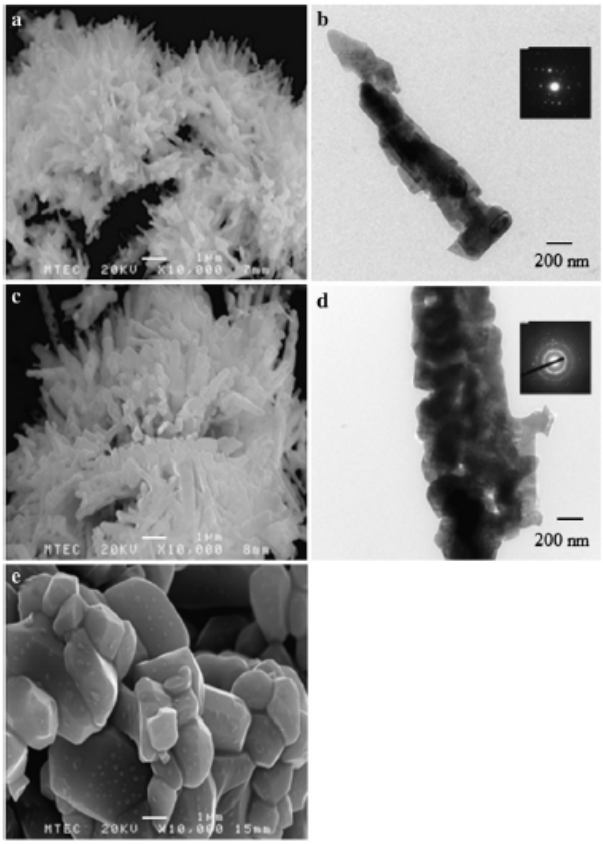

Figure 2.4 SEM images (left) and TEM images with electron diffraction patterns (right) of $CuHPO_4.H_2O$ (a, b); α-$Cu_2P_2O_7$-600 (c, d); α-$Cu_2P_2O_7$-900 (e)

A plausible reaction pathway proposed for fructose dehydration over copper phosphate proceeds with protonation of the hydroxyl group of fructose into H_2O^+ followed by release of three water molecules to produce HMF with the possibility of furfural as a side product (Figure 2.5). Dehydration and polymeric products of various side reactions may also occur in tandem with HMF formation.

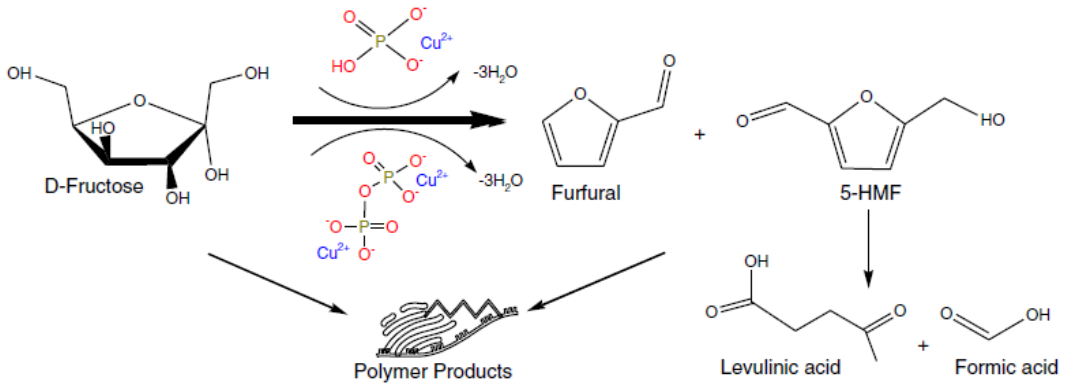

Figure 2.5 Reaction network for fructose dehydration to HMF catalyzed by cupric phosphate under hot compressed water

Glucose was dehydrated to HMF in the presence of TiO_2 and ZrO_2 catalysts in hot compressed water at 250 °C for 5 min.[53] Chareonlimkun and co workers found out that calcination temperature and salt precursor used during metal oxide synthesis strongly affected catalytic performance. Catalysts prepared from chloride precursor had higher reactivity than those prepared from nitrate precursor. The authors explained this in terms of acid site density which was observed to be higher in oxides obtained from chloride precursor than those from nitrate. For example, yield of HMF obtained over TiO_2 prepared from chloride precursor at each calcination temperature is approximately 5% more than that obtainable with TiO_2 from nitrate precursor. Also, relatively lower calcination temperature favoured better catalytic activity as highest yield of 27% HMF was obtained on TiO_2 calcined at 500 °C. Gradual decline of HMF yield to 25% and then 20% was observed at 600 °C and 700 °C calcination temperatures, respectively. This effect was attributed to phase change as the predominant and active anatase phase at 500 °C gradually transforms into the less active rutile phase with increasing calcinations temperature. ZrO_2 showed similar trends in terms of precursor and calcination temperature just like TiO_2. A maximum HMF yield of 17% was obtained for ZrO_2 prepared from its chloride precursor and calcined at 500 °C. A comparison of the activity of TiO_2 and ZrO_2 showed that TiO_2 was more active under these reaction conditions and resulted in superior HMF yield, which was attributed to higher acid density of TiO_2 as determined by temperature programmed desorption. Another factor that greatly influenced catalyst reactivity was sulfur doping, especially on ZrO_2. Even though sulfate treatment of ZrO_2 (SO_4–ZrO_2; with 1.8% sulfur content) showed the greatest dehydration reactivity, nevertheless, its reactivity was relatively less than TiO_2 but better than ZrO_2. Subsequently, TiO_2, ZrO_2 and SO_4–ZrO_2 from chloride precursors were demonstrated for the conversion of cellulose and sugarcane bagasse under similiar reaction conditions. HMF, glucose, fructose, furfural and anhydroglucose were observed as the main products of cellulose conversion and xylose was an additional product when sugarcane bagasse was used as the feed substrate. As a result, higher portion of furfural was produced from sugarcane in comparison to cellulose which was because of the hydrolysis and dehydration of hemicellulose present in the former. TiO_2 and SO_4–ZrO_2 were found to be more active for hydrolysis and dehydration reactions producing high furfural and HMF yields as compared to ZrO_2, which was more active for isomerization reaction; thus significant amount of fructose was observed in the liquid product (Figure 2.6). Reusability of the catalysts for the sugarcane conversion reaction showed that TiO_2 and ZrO_2 maintained almost identical reactivities throughout the repetitive runs for five times. In contrast, there was a significant decline in activity of SO_4–ZrO_2 which could be attributed to leached sulphur from the catalyst.

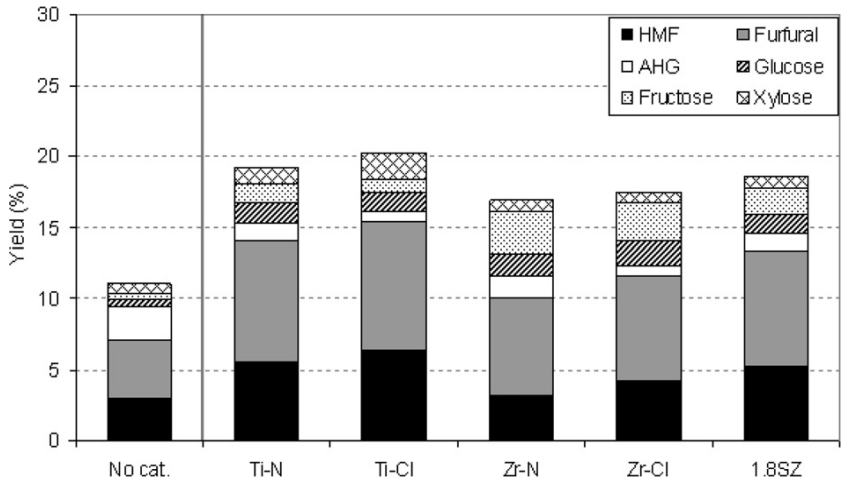

Figure 2.6 Yield of liquid products from the reaction of sugarcane bagasse at 250 °C and 5 min with and without the present of catalysts

In the same year, Chareonlimkun and coworkers[54] further extended their work to transforming other biomass sources such as rice husk and corncob alongside sugarcane bagasse. Hot water compressed conversion of the biomass sources was carried out in the presence of TiO_2, ZrO_2 and TiO_2–ZrO_2 mixed oxides (Ti/Zr molar ratio of 1/3, 1/1 and 3/1). It was observed that catalyst reactivity, phase formation and acidity–basicity properties are closely related, yet, dependent on catalyst preparation procedure and calcination temperature. Therefore, highest HMF and furfural productions could be achieved from TiO_2–ZrO_2 (prepared by co-precipitation method with Ti/Zr molar ratio of 1/1 and calcination temperature of 600 °C) as a result of its bifunctionality for both acidity and basicity properties. With this catalyst, the simultaneous hydrolysis/dehydration of corncob provided the highest yields of HMF (8.6%) and furfural (10.3%).

Takagaki et al.[55, 56] reported a one-pot synthesis of HMF from glucose using a combination of solid acid and base catalysts. Glucose conversion to HMF was discerned as a two-step reaction of base catalyzed isomerisation and acid dehydration of isomerisation product into HMF. For each step of the reaction, the authors investigated different catalysts. Among the catalysts tested, the combination of moderate basicity of hydrotalcite (HT) with acidity of Amberlyst-15 was considered optimum for selective HMF production. Under mild reaction condition (80 °C and 9 h) in a *N*,*N*-dimethylformide solvent, the HT-Amberlyst catalyst system afforded 73% glucose conversion and 58% HMF selectivity. This catalyst also effectively catalyzed fructose dehydration to obtain 76% HMF selectivity at >99% conversion at a shorter reaction time but higher temperature (100 °C and 9 h). With the intent of minimizing anhydroglucose formation, which is a product of acid dehydration of glucose, the author decided to introduce the acid catalyst after a considerable isomerization of glucose had occurred with the base catalyst. Also confirming the mechanism of

sequential reaction, addition of Amberlyst-15 into a solution containing fructose formed from glucose in the presence of HT after 2.5 h of reaction, resulted in disappearance of fructose and simultaneous formation of HMF within 1 h. 76% of HMF selectivity was obtained after 4.5 h and other side products including anhydroglucoses were not detected as shown in Figure 2.7.

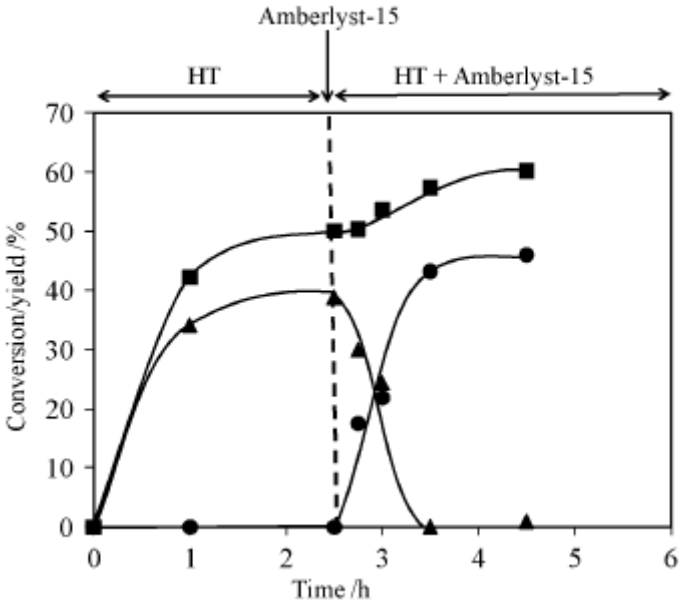

Figure 2.7 Plot of glucose conversion (■), fructose yield (▲) and 5-hydroxymethylfurfural (HMF) yield (●) for the transformation of glucose as a function of reaction time. Amberlyst-15 added after 2.5 h. *Reaction conditions:* glucose (0.1 g), hydrotalcite (0.2 g), Amberlyst-15 (0.1 g), *N*,*N*-DMF (3 mL), 373K.[55, 56]

Analogous to the sequential glucose reaction, one pot conversion of cellobiose and sucrose were initiated by acid hydrolysis, followed by base isomerization of glucose and then fructose dehydration by acid. Since the reaction was carried out in *N*,*N*-DMF, adsorbed water on the unpretreated catalyst system was considered as the initial source of water that triggered the hydrolytic reaction, which was then sustained by the three water molecules produced along with HMF during dehydration. At 120 °C and 3 h reaction condition, conversion of cellobiose gave 67% selectivity to HMF at 52% conversion, while sucrose conversion resulted in 93% HMF selectivity at 58% conversion.

A continuous production of HMF from a variety of carbohydrate sources using a fixed bed porous metal oxide catalytic process was explored by McNeff et al.[57] Under a biphasic continuous flow system with MIBK as the extracting organic cosolvent, TiO_2 catalyst was found to catalyze aqueous sugar solutions with yields up to 29% within short contact time. More importantly, the process could be applied to cellulose after a simple retrofit of the process configuration. By installing a solubilization chamber and placing cellulose inside it, cellulose dissolution was

achieved by feeding the chamber with a preheated water–organic mixture. The cascade process of a preheater–solubilization chamber–catalytic reactor shown in Figure 2.8 enabled continuous depolymerization of cellulose and subsequent conversion to produce 35% yield of HMF and cellulose conversion of 87%. The catalyst showed good stability over a variety of operating conditions and can be easily regenerated via pyrolysis.

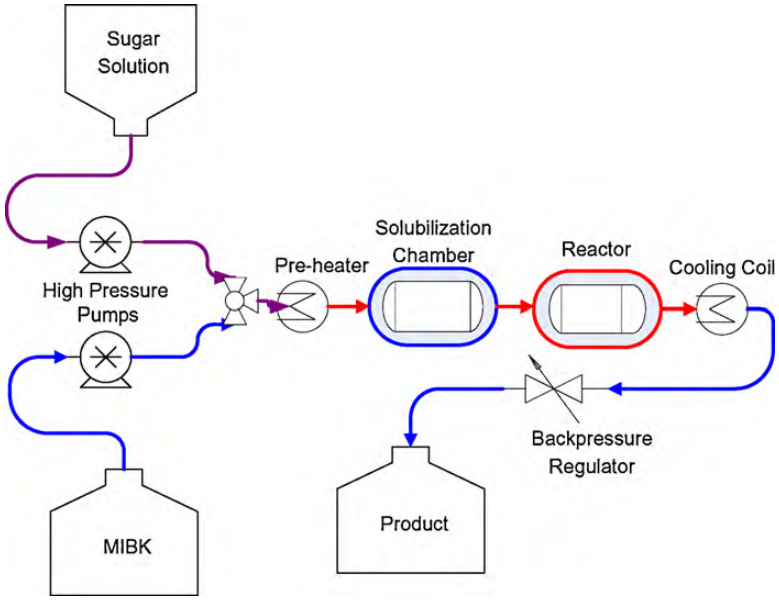

Figure 2.8 Diagram of a continuous flow system including a "solubilization" chamber for the production of HMF from cellulose (MIBK: methyl isobutyl ketone)[57]

Nakajima et al.[58] reported a highly effective titania Lewis acid catalyst for selective conversion of glucose to HMF. In a THF–water mixture, the activity of pure anatase TiO_2 and phosphate/TiO_2 (prepared by phosphate immobilization of anatase TiO_2) was examined. After 2 h of reaction at 120 °C, it was observed that a small fraction of the reacted glucose (99% conversion) was converted to 8.5% yield of HMF. This was ascribed to complex intermolecular side reactions leading to formation of complex polymeric species. These intermolecular side reactions, which include aldol condensation among reducing saccharides, are promoted preferentially on the Lewis acid sites than the HMF formation reaction pathway i.e. isomerization of glucose to fructose and the intramolecular dehydration of fructose. Phosphoric acid modification on anatase TiO_2 (phosphate/TiO_2) caused a significant improvement in HMF production by decreasing side reactions. Under comparable reaction conditions 81.2% yield of HMF and 98% glucose conversion were attained on phosphate/TiO_2. Since the Lewis acid sites of TiO_2 were not covered with phosphate ions after phosphate immobilization, esterification of –OH groups on TiO_2 into –O-

$PO(OH)_2$ could be responsible for the minimized side reactions. Hence, a synergistic effect between Lewis acid sites and phosphate ions was suggested to be responsible for selective conversion of glucose to HMF. Moreover, phosphate/TiO_2 was demonstrated to be a stable and reusable catalyst as there was no decline in activity after multiple (five) reaction cycles.

De et al.[59] explored Lewis acid mesoporous TiO_2 nanoparticle for the conversion of fructose and glucose to HMF in DMA–LiCl (10%). DL-aspartic acid was used as a template which aided self-assembly of uniformly sized and shape-controlled TiO_2 nanoparticle with high surface area. The material displayed excellent catalytic activity due to its high surface acidity, affording 74.8% yield of HMF from fructose under microwave irradiation at 130 °C for 2 min. Addition of 20 wt% [BMIM]Cl to the solvent system led to formation of higher concentration of weakly ion-paired chloride ions which further improved the yield of HMF to 82.3%. However, significantly lower yield of HMF (30.2%) could be produced from glucose. Recyclability of the spent catalyst was done and reused for five catalytic cycles without significant loss of activity. The authors also reported the conversion of mannose, galactose and lactose over porous TiO_2 nanocatalyst templated by biopolymer sodium alginate.[60] Highest yield of HMF (44%) could be produced from mannose, under microwave irradiation for 5 min in DMA–LiCl medium at 140 °C. Surface area, small particle size and strong acidic sites generated through biopolymer templating were considered crucial for the activity of the catalyst.

Dutta et al.[61] developed a hierarchically porous titanium phosphate through a slow evaporation method using orthophosphoric acid as the phosphorous precursor and pluronic P123 as the structure directing agent. The as-prepared self-aggregating mesoscopic nanoparticle (MTiP-1) has a surface area of 193 m^2g^{-1} together with 7 nm average pore diameter. MTiP-1 was demonstrated as an active catalyst for dehydrating biomass derived carbohydrates under microwave assisted heating. Fructose dehydration in DMA–LiCl solvent gave 44% HMF yield at 140°C for 5 min. As inferior yields of HMF could be obtained when the solvent was changed to water, MIBK or water–MIBK, it was concluded that the formation of Cl^- ions associated with $DMA{\cdot}Li^+$ macrocation facilitated the dehydration of fructose to HMF in DMA–LiCl solvent. Subsequently, glucose and mannose were dehydrated in DMA–LiCl solvent over MTiP-1 catalyst. In comparison to fructose, lower yields of HMF (22-23%) could be obtained which was ascribed to the additional isomerization step in the reaction sequence. Catalytic activity of the catalyst could be relatively maintained for successive catalytic cycles without significant deactivation as only ~8% loss of HMF was observed by the end of five reaction cycles. The effectiveness of MTiP-1 to catalyze sucrose, cellulose and sugarcane bagasse conversion into HMF was also evaluated. The dehydration of sucrose in DMA-LiCl solvent gave 27% HMF yield under microwave assisted heating at 140 °C

for 5 min. The catalyst also displayed good activity for the direct conversion of cellulose and sugarcane bagasse under similar reaction conditions. Interestingly, 26% yield of HMF from sugarcane bagasse was found to be much higher than 17% HMF produced from cellulose. This was attributed to the degree of hydrolysis in both substrates which depends on the microcrystalline structure involving the H-bonded 3D network of polymeric sugar units. Sugarcane bagasse can be easily hydrolyzed due to the presence of hemicellulose of weaker H-bond interaction and some percentage of amorphous cellulose within the total cellulose content as compared to pure microcrystalline cellulose of strong H-bond network of sugar units.

Templated mesoporous niobium phosphates with tunable acidity were prepared and evaluated as catalysts for the direct conversion of glucose and its polymers into HMF.[62] It was observed that selectivity to HMF was dependent on the ratio of Brønsted to Lewis acid sites (B/L). Excess of either acid sites was detrimental: Lewis acid sites promoted formation of humins whereas Brønsted acid sites impeded the isomerization reaction step. As pH controls the acidity of the catalyst, niobium phosphate prepared at pH of 7 had optimum catalytic performance corresponding to B/L ratio of 0.72. In water, glucose conversion and HMF yield were 68.1% and 33.6%, respectively, after 60 min at 140 °C in the presence of NbPO-pH7. The catalyst is highly stable and tolerant in the aqueous system, although, it deactivated after repeated usage due to active sites coverage by by-products. Nonetheless, catalytic activity can be recovered fully simply by calcination treatment. Glucose conversion to HMF was further improved by adding an immiscible organic solvent to the aqueous system to form a biphase system. As MIBK was utilized as the organic extracting phase, HMF yield improved to 39.4% due to the fact that consecutive side reactions were minimized since HMF was continuously extracted as it was generated. Direct production of HMF from other biomass-derived carbohydrates was also investigated in the MIBK/H_2O system using the NbPO-pH7 as catalyst. Without coupling the catalyst with other acid or enzyme catalysts, the yields of HMF from sucrose and cellobiose were 30.7% and 39.9%, respectively. Moreover, consecutive hydrolysis-isomerization-dehydration of starch and cellulose proceeded over the catalyst in one-pot to give yields of 30.9% and 16.2% HMF, respectively.

Zhang et al.[63] had explored the potential of a series of amorphous metal oxides as catalyst for the conversion of glucose to HMF in [EMIM]Br at 140 °C. High yields of HMF between 81–99% could be obtained over amorphous Cr_2O_3, SnO_2 and SrO. On the contrary, the catalytic activity of these oxides after calcination was almost completely lost. Additionally, graphene oxide-metal oxide (GO-MO) was examined for glucose conversion to HMF. Out of these GO-MO based catalysts, GO-Fe_2O_3 catalyzed reaction produced highest HMF yield (86%) despite the very poor catalytic activity exhibited by pure Fe_2O_3. The major advantage of GO is that it allowed for well

dispersed 3-5nm sized Fe_2O_3 nanoparticles on its 2D layered surfaces. Surprisingly, yield of HMF declined to 77% when fructose was dehydrated over GO-Fe_2O_3. It was suggested that direct formation of HMF from glucose without intermediate isomerisation step to fructose was responsible for the difference of catalytic performance of GO-Fe_2O_3 in glucose and fructose dehydration. The authors also surmised that hydration of HMF to levulinic acid and formic acid could also play a role for the declined yield of HMF from fructose.

Working with a water/THF (1:3 v/v) biphasic solvent mixture, Xu et al.[64] tested the influence of a number of variables including reaction temperature, time, catalyst dosage and solvent on the formation of HMF from fructose catalyzed by bi-functional $CrPO_4$. A maximum HMF yield of up to 83% at a complete fructose conversion was obtained at 140 °C for 15 min of reaction time. With glucose as a starting material, increasing the reaction time from 15 to 30 min at 140 °C resulted in a corresponding increased HMF yield from 51.7% to 63%. Direct conversion of microcrystalline cellulose was also attempted to give a reasonable yield of HMF (37%) from cellulose and this was attributed to the Lewis-Brønsted bifunctional acid sites generated by hydrolysis of partially dissolved $CrPO_4$ to $[Cr(H_2O)_5OH]^{2+}$- and H^+ species. Thus, they proposed a mechanism for cellulose conversion over the catalyst that comprise of cascade reaction sequence that was initiated by homogeneous acid-catalyzed depolymerization of cellulose to glucose, and $[Cr(H_2O)_5OH]^{2+}$- served as the Lewis acid site for subsequent isomerization of glucose to fructose and then dehydration of fructose to HMF by homogeneous acid (H^+).

2.3.2 Ionic resins

Nakamura and Morikawa[65] conducted fructose dehydration in DMSO over porous (Diaion PK-208, Diaion PK-216, and Diaion PK-228) and gel (Amberlite IR-118, Amberlite IR-120, and Lewatit SC-108) types of strongly acidic ion-exchange resin catalysts. Then they investigated the influence of divinylbenzene (DVB) content of the ion-exchange resins on the rate of fructose dehydration to HMF at 80 °C. Modelling the rate of HMF formation by a first-order reaction model, dehydration rate was found to be dependent on DVB content in the resin. At the same DVB content, porous resins exhibited higher reaction rates, hence, more effective than the gel type resins. With Diaion PK-216, the maximum yield of HMF was 90% for a reaction time of 500 min. Catalyst stability for fructose dehydration was evaluated under a continuous reaction condition over Amberlite IR-118 at 60 °C. After about 100 h of reaction, 0.45 M concentration of HMF was reached and this was maintained even up to 900 h indicating no activity loss.

To enhance the production of HMF and minimize side-reactions, Shimizu et al.[66] developed a reaction protocol under mild evacuation for continuous removal of water. Demonstrating the

effectiveness of this technique for fructose dehydration with various solid acid catalysts, it was found that removal of water suppressed: a) hydrolysis of HMF to levulinic acid and b) reaction of partially dehydrated intermediates to condensation products. It was also observed that decreasing the particle size of Amberlyst 15, by crushing and sieving to 0.15–0.053 nm (Amberlyst-15 powder), increased HMF selectivity. This behaviour was related to improved removal of adsorbed water from the surface and near-surface of the catalyst. The conversion of fructose dehydration in DMSO at 120 ° for 2 h under mild evacuation at 0.97 x 10^5 Pa, gave 100% HMF yield at high fructose concentration (50 wt%) in the presence of Amberlyst-15 powder.

Microwave-assisted dehydration of fructose into 5-HMF using a strong acid cation exchange resin (DOWEX 50wx8) as catalyst in aqueous acetone mixtures was also investigated by Qi et al.[67] It was observed that fructose conversion rate improved with an increase in acetone concentration in the acetone–water mixtures as well as increased yield of HMF yield due to the suppression of HMF rehydration. The use of acetone–water reaction (70:30 w/w) media and 2wt% initial fructose concentration resulted in yields of HMF as high as 73.4% for 95.1% conversion at 150 °C under microwave irradiation for 15 min. High initial fructose concentration (20 wt%) could also be processed but accompanied with increased rate of soluble polymer formation, yet, 54.3% HMF yield was obtainable at 89.3% fructose conversion. The resin displayed good stability as it could be reused for five times with negligible decline in catalytic activity. Compared with conventional heating, it was found that microwave irradiation heating had a remarkable accelerating effect, not only on the rate of fructose conversion, but also on the formation rate of HMF. Under similar reaction conditions (5 ml of 2 wt% fructose solution, 0.1 g of resin, 150 °C and 10 min), fructose conversion and HMF yields by microwave heating (91.7% and 70.3%, respectively) were higher than those by conventional heating (22.1% and 13.9% respectively). Subsequently, Qi et al.[68] observed that acetone-DMSO solvent mixture was an effective solvent for the dehydration of fructose to HMF owing to improved separation efficiency and highly selective product formation. Under microwave heating and in the presence of ion-exchange resin catalyst (DOWEX 50WX8–100), they reported a 91.7% HMF selectivity at a fructose conversion of 97.9% for a 20 min reaction time in 70:30 (w/w) acetone/DMSO solvent mixtures.

Maqueda et al.[69] developed a work-up process of sequential conversion of sucrose to HMF catalyzed by cation- and anion-exchange resins that comprises of four (4) steps: hydrolysis of sucrose, dehydration of fructose, glucose-to-fructose isomerization and second dehydration. Hydrolytic and dehydration steps were carried out in the presence of an acid catalyst in form of Amberlite IR-120 (H^+) while isomerization proceeded over Amberlite IRA-400 (OH^-), a base catalyst. Inter-stage extraction of HMF after the second step gave 21% yield which increased to

50% on completion of all reaction steps. Attempts to accomplish the hydrolysis, dehydration and isomerisation steps in a one-pot fashion, by combining both, acidic and basic resins in H_2O, DMF or 1:1 H_2O-DMF failed, as no HMF was detected in the reaction mixture.

2.3.3 Heteropolyacid based

A sulfonated organic heteropolyacid salt ($[MIMPS]_3PW_{12}O_{40}$) was reported to efficiently catalyze the dehydration of fructose into HMF.[70] Highest selectivity of 98.8% to HMF was observed in sec-butanol solvent at 120°C for 2 h. The catalyst can be easily recycled because of its reaction-induced self-separation property, i.e. it precipitates out at the end of the reaction. The catalyst was reused six times without no appreciable loss of activity, as HMF yield dropped to 96.5% from 99.1% after the sixth reaction cycle.

Dehydration of fructose and glucose to HMF studied in two-phase reactor system by using solid heteropolyacid salt of $Ag_3PW_{12}O_{40}$ was reported by Fan et al.[71] The experimental results demonstrated $Ag_3PW_{12}O_{40}$ to be an efficient solid catalyst for the conversion of the hexoses into HMF with high selectivity. A yield of 77.7% HMF and fructose conversion of 82.8% could be achieved at 120 °C within 60 min. In addition, $Ag_3PW_{12}O_{40}$ was active for the conversion of glucose into HMF with high yield of 76.3% but at higher reaction temperature and time (130 °C for 4 h). Selective dehydration of the hexoses into HMF over $Ag_3PW_{12}O_{40}$ could be attributed to its moderate acid strength. Because of the mild Lewis acidity introduced by exchanging H^+ of $H_3PW_{12}O_{40}$ with Ag^+, rehydration of HMF could be minimized which was otherwise favored on Brønsted catalysts (HCl and $H_3PW_{12}O_{40}$) due to strong acidity. Comparison with other catalysts as shown in Figure 2.9 indicated that pure Lewis acid catalyst like $AgNO_3$ displayed low conversion and low yield whereas low catalytic activity of $Cs_3PW_{12}O_{40}$ was due to the absence of both Brønsted and Lewis acidity. Therefore, it was concluded that higher catalytic activity of $Ag_3PW_{12}O_{40}$ was as a result of the synergistic effect of Lewis and Bronsted acid sites as well as accumulation of substrate on the catalyst. Moreover, the catalyst displayed high tolerance to high concentration feedstock and could be recycled for six times with stable catalytic performance.

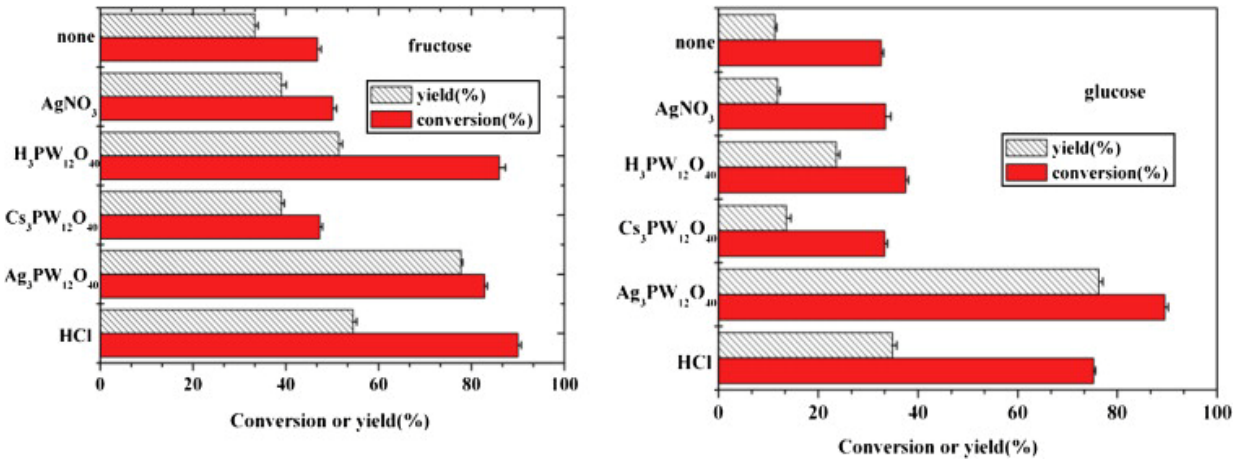

Figure 2.9 Dehydration of sugar by different catalysts. Reaction conditions: 2400 mg of sugar in a Parr reactor (size, 50 mL), the total volume of biphasic system 26 mL, 0.025 mmol of catalyst, 120 °C, 60 min for fructose and 0.1 mmol of catalyst, 130 °C, 4 h for glucose, respectively

Li et al.[72] successfully employed Brønsted acidic heteropolyanion-based polymeric hybrid catalyst (FPIL) in DMSO for the dehydration of fructose, producing good yields of HMF (up to 83%); however, low yields of HMF were obtained when glucose was used as the substrate (26%). As an extension of their ongoing efforts to improve the performance of FPIL to transform glucose, SO_3H-functionalized polymeric ionic liquids previously reported was coupled with $CrCl_3.6H_2O$ to produce bi-functional FPILs of Brønsted and Lewis acidic groups.[73] The bi-functional FPILs catalysts displayed improved performance for fructose-to-HMF conversion in DMSO for reaction conditions of 120 °C and 60 min. HMF yields around 90% could be produced which were relatively higher than those on mono-functional Brønsted FPILs. Besides, moderate yields of glucose (34.2-39.4%) could be achieved on the bi-functional FPILs, though requiring higher reaction temperature and longer reaction time. It was suggested that the presence of Cr^{3+} as active centers was responsible for the remarkably improved catalytic performance due to higher affinity towards substrate. More so, Lewis acid centers of Cr^{3+} could isomerize glucose to fructose which readily dehydrates to HMF, thus increasing reaction rate by altering the reaction pathway which could have proceeded via 3-deoxy-D-erythro-hex-2-ulose (primary route of glucose-to-HMF conversion on mono-functional FPILs) as shown in Figure 2.10.

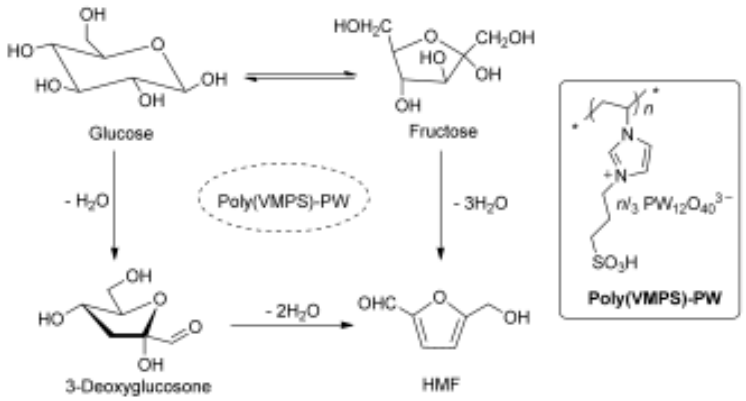

Figure 2.10 Selective conversion of fructose and glucose to HMF catalyzed by poly(VMPS)-PW[72]

Furthermore, catalytic conversion of glucose to HMF on the bi-functional FPILs could be improved to 48.7% yield by changing the reaction medium to a mixture of aqueous/organic solvent (1:1), comprising of H_2O:DMSO (1:4)/MIBK:*n*-BuOH (3:7). Better stability of the bi-functional FPILs in H_2O:DMSO (1:4)/MIBK:*n*-BuOH (3:7) contributed to its higher catalytic performance and afforded reusability of the spent catalyst without significant loss of activity. Satisfactory yield of HMF by direct conversion of cellulose in [BMIM]Cl with DMSO as co-solvent could also be achieved. Evaluation of the catalytic performance of the bi-functional FPILs catalyst at 160 °C for 5 h reaction time gave a maximum 30.8% yield of HMF. Nevertheless, lower HMF yield of 16.3% was obtained when $CrCl_3 \cdot 6H_2O$ was used for the same catalytic process. This showed that conversion of cellulose to HMF could take place on Lewis acid sites but the coexistence of Lewis and Brønsted acidity on FPILs remarkably enhanced activity due to the synergistic effect between Cr^{3+} and SO_3H groups.

The application of phosphotungstic acid encapsulated in Metal-Organic Framework (MOF) as catalysts for carbohydrate dehydration to HMF was first reported by Zhang et al.[74] Employing a metal−organic framework with a chromium carboxylate cubic structure, MIL-101, phosphotungstic acid (PTA) of varying amount was encapsulated (PTA(*x*)/MIL-101 where *x* = amount of PTA added in grams). The catalysts were evaluated for fructose dehydration in ionic liquid at 80 °C. The results showed that activity of the catalysts depended on PTA loading. PTA(3.0)/MIL-101 exhibited the best catalytic performance with a yield of 79% HMF from fructose after 2.5 h of reaction time. However, the catalyst is not stable in ionic liquid due to proton release from the PTA entities in the MOF into the ionic liquid. Alternatively, DMSO was used as the solvent for the dehydration reaction and 63% yield of HMF could be obtained at 130 °C and 30 min with PTA(3.0)/MIL-101 catalyst.

In another interesting work, a series of nano-sized polyoxometalates supported on zirconia-alumia (Nano-POM/nano- ZrO_2/nano-γ-Al_2O_3) were prepared and evaluated as catalysts for the conversion of glucose into HMF by Teimouri et al.[75] They found that HMF production was strongly dependent on catalyst concentration of POM and the reaction solvent. Then, 20% POM content and acetone/DMSO solvent mixture were confirmed to be an excellent combination for the production of HMF. At 190 °C and 4 h reaction conditions, selectivity of HMF reaches a maximum corresponding to 60.1% yield of HMF at 91.2% glucose conversion. Reaction mechanism of glucose to HMF transformation over the catalyst was understood to involve a bond between the moiety of the nano-ZrO_2/nano-γ-Al_2O_3 and the metal centre of POM. Coordination of glucose to the active metal species allowed mutarotation of the α-glucopyranose anomer to the β-glucopyranose. This was followed by isomerization to fructose and subsequent dehydration into HMF (Figure 2.11).

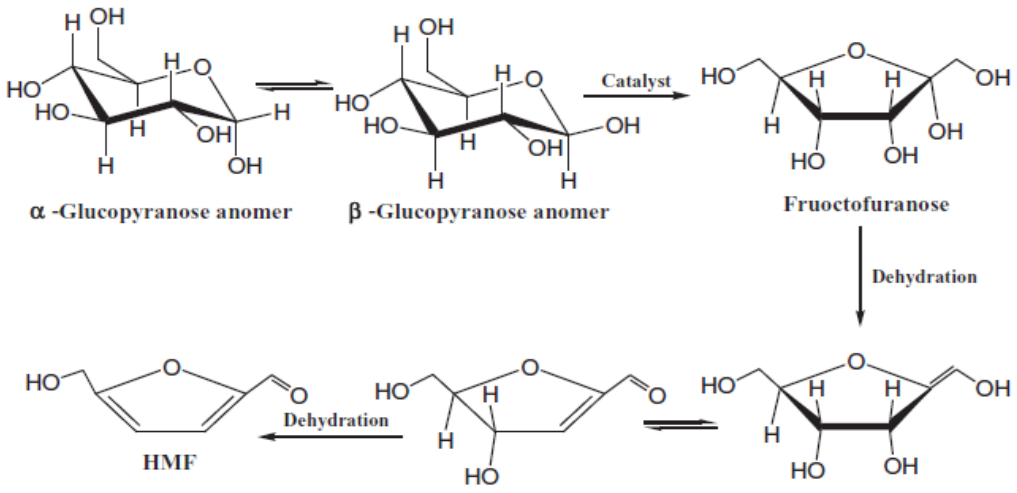

Figure 2.11 Proposed mechanisms of the dehydration of glucose to HMF catalyzed by nano-POM/ nano-ZrO_2/nano-γ-Al_2O_3 catalysts

A Brønsted-Lewis-surfactant-combined heteropoly acid catalyst $Cr[(DS)H_2PW_{12}O_{40}]_3$ (DS represents $OSO_3C_{12}H_{25}$ dodecyl sulphate) was developed by Zhao et al.[76], wherein the Lewis acidity of the catalyst originates from the metal cation as an electron pair acceptor, and Brønsted acidity is generated from some protons of HPA molecules. $Cr[(DS)H_2PW_{12}O_{40}]_3$ is an amphiphilic molecule consisting of a hydrophilic head group, $CrH_2PW_{12}O_{40}$, and a hydrophobic tail, $OSO_3C_{12}H_{25}$ and this enabled the catalyst to assemble micelles in water. The material displayed excellent catalytic activity for the tandem cellulose depolymerization and glucose conversion to HMF in a one pot aqueous process under mild conditions (150 °C and 2 h), which enabled 52.7% yield of HMF and

77.1% conversion cellulose. The effectiveness of the catalyst for the reaction was attributed to: a) the adsorption of cellulose onto the micellar HPA catalyst, thus overcoming diffusion problem in the solid-solid reaction, b) synergistic effect of the Brønsted acid conversion of cellulose into glucose and Lewis acid dehydration of glucose into HMF and c) hydrophobic environment arising from the micellar droplets dispersed in water that sufficiently protected HMF from further decomposition and decreased by-products formation. Stability of the catalyst was evaluated and it was confirmed that $Cr[(DS)H_2PW_{12}O_{40}]_3$ could be recycled by a simple process and reused approximately six times with excellent stability. The catalyst was also effective for the production of HMF and furfural in one step from untreated lignocellulosic biomass such as corn stover and husk of Xanthoceras sorbifolia Bunge (XSB). Under the same reaction conditions as cellulose, 57.3 and 62.5% of dry weight of corn stover and husk of XSB were transformed into 30.8% and 35.5% HMF, respectively. Notably, furfural was also formed from these biomasses in yields of 28.9% and 30.7%, respectively.

2.3.4 Carbon based

Wang et al.[77] reported the synthesis of a novel carbon-based solid material to be applied as a solid acid catalyst for the conversion of fructose into HMF. The carbonaceous material (Glu-TsOH) was prepared via a one-setp carbonization of glucose and p-toluenesulfonic acid under mild conditions. Sulfonation of Glu-TsOH was confirmed by acid titration in which $–SO_3H$ group was detected with a measured acid density of 1.3 mmol/g. Other identified surface functional groups were –COOH and –OH with corresponding acid densities of 0.6 mmol/g and 0.1 mmol/g, respectively. Thus, the total acid density of Glu-TsOH is 2 mmol/g, which comprised of a few strong acid sites and large quantity of weak to moderate acid sites. For fructose dehydration reaction at 130 °C in DMSO solvent, Glu-TsOH displayed an excellent catalytic performance with an HMF yield as high as 91.2% after 1.5 h, higher than that for $AC–SO_3H$, H-BEA zeolite and Amberlyst-15. Remarkable catalytic performance of Glu-TsOH was attributed to its preferential and better affinity to fructose as well as the synergic effect between surface carboxylic acid and sulfonic acid groups. Glu-TsOH also showed a good reusability under the reaction conditions with the catalytic activity nearly constant after being reused five times.

On the basis of overcoming the major challenge of HMF extraction and purification from DMSO, the same research group proposed THF/DMSO mixtures as solvent for fructose dehydration using sulfonated carbonaceous material (GTS).[78] GTS was prepared in a similar manner like Glu-TsOH but with a slight modification by adding an inorganic salt, sodium sulfate. An advantage of the inorganic salt was to serve as a porogen (crystal nucleus in an anhydrous

environment) thereby facilitating dramatic increase in surface area. Thus, GTS has a surface area of 188.9 m^2g^{-1}, much greater than that of Glu-TsOH (<1 m^2g^{-1}). Another benefit of sodium sulfate was to enhance hydrophobicity of the material. Catalytic activity of GTS for fructose dehydration was examined. Operating at reaction conditions 160 °C and 60 min reaction time, high fructose conversion of 99.0% with HMF yield of 98.0% was in a 70:30 (v/v) THF/DMSO mixture. More importantly, HMF from the reaction solution could be isolated through simple extraction method. With the addition of diethyl ether (DEE) and H_2O into the reaction system to extract HMF, high purity of HMF (ca.96.4%) could be obtained. Compared with 91% HMF previously achieved in pure DMSO by the group[77], it was established that combination of low boiling point THF with DMSO not only gives higher yield of HMF, but also improves separation efficiency.

Mazzotta et al.[79] described the synthesis of a sulfonated carbonaceous material that contains Brønsted acidic sulfonic acid groups and Lewis acidic TiO_2 sites. Glu-TsOH-Ti was prepared by the thermal treatment of glucose, p-toluenesulfonic acid and titanium IV propoxide at 180 °C. The self-assembled Glu-TsOH-Ti nanoparticle is characterized by mesoporosity, with a surface area of 42.5 m^2g^{-1} and an average pore size of 4.5 nm. With a total acid density of 1.03 mmol g^{-1} and 0.56 mmol g^{-1} Brønsted acidity corresponding to $–HSO_3$ group, the nanoparticle has a Brønsted to Lewis acid density ratio of 1.2. As a catalyst, the effectiveness of Glu-TsOH-Ti to catalyze the conversion of fructose into HMF was demonstrated using a biphasic system of water and methyltetrahydrofuran under a microwave-assisted heating. Fructose dehydration produced 59% HMF in 60 min at 180 °C. Under comparable conditions, the dehydration of fructose catalyzed by anatase TiO_2 and Glu-TsOH produced 14 and 44% HMF, respectively. These results confirmed that the Glu-TsOH-Ti catalyst, which contains Brønsted and Lewis acid sites, is more effective for HMF production than the individual Lewis (TiO_2) and Brønsted (Glu-TsOH) acid sites. Other factors contributing to the catalytic activity of Glu-TsOH-Ti includes accessibility of acid sites as a result of porosity, the higher surface area and pore volume. The effectiveness of the Glu-TsOH-Ti catalyst was further tested for glucose dehydration. At the same reaction temperature but increased time to 2 h, 46% HMF could be produced. The involvement of an additional isomerization step in the glucose dehydration reaction was concluded to be the reason for the lower HMF yield from glucose than that obtained from fructose. The catalyst was also effective for producing HMF from cellobiose. A reaction between 0.22 mmol of cellobiose and 23 mg of catalyst in the biphasic reactor produced 26% HMF in 10 min at 180 °C. The yield of HMF increased from 26 to 36% when the reaction was left to proceed from 10 until 20 min. Comparing the activity of the Glu-TsOH-Ti catalyst for the conversion of cellobiose (a dimer of two glucose units) and glucose under comparable reaction conditions (180 °C, 60 min reaction time, and a similar amount of catalyst), HMF yields from

cellobiose and glucose were recorded as 39 and 31%, respectively. Because of a slightly higher HMF yield from cellobiose than from glucose, the authors suggested that the overall HMF yield from cellobiose was limited by the glucose isomerization step. The recyclability experiments showed that the catalyst could be reused for four reaction cycles with negligible loss of catalytic activity in terms of HMF yield.

Recently, Ranganath et al.[80] prepared a multi-walled carbon nanotubes decorated with ferrites for the dehydration of glucose and fructose. The structure and morphology of cobalt ferrite ($CoFe_2O_4$) and magnetite (Fe_3O_4) are inverse spinel which is different to the normal spinel of zinc ferrite ($ZnFe_2O_4$). Inverse spinel ferrites were more active for the dehydration of fructose in DMF at 80 °C than normal spinel ferrite. The activity of the ferrites descended in the order: $CoFe_2O_4$ > Fe_3O_4 > $ZnFe_2O_4$. $CoFe_2O_4$ afforded 34% conversion of fructose with 78% selectivity to HMF (Table 2.2, entry 6). Contrarily, $ZnFe_2O_4$ (Table 2.2, entry 8) showed no catalytic activity for the reaction while less conversion (10%) of fructose was observed on Fe_3O_4 but without production of HMF (Table 2.2, entry 4).

Table 2.2 Ferrite-CNTs catalyzed dehydration of fructose and glucose

Entry	Catalyst	Reactant	Time (h)	Conversion (%)	Selectivity (%)
1	CNT	Fructose	24	N.R	-
2	CNT-COOH	Fructose	15	28	-
3	CNT-NH_2	Fructose	15	32	-
4	Fe_3O_4	Fructose	6	10	-
5	Fe_3O_4	Glucose	10	N.R	-
6	$CoFe_2O_4$	Fructose	8	34	78
7	$CoFe_2O_4$	Glucose	12	N.R	-
8	$ZnFe_2O_4$	Fructose	24	N.R	-
9	CNT-Fe_3O_4	Fructose	6	22	98
10	CNT-$CoFe_2O_4$	Fructose	8	75, 74[a], 75[b]	99, 98[a], 99[b]
11	CNT-$CoFe_2O_4$	Glucose	10	64	98
12	CNT-$ZnFe_2O_4$	Fructose	8	N.R	-

Reactions were performed using 20.0 mg of catalyst, 180.0 mg of fructose, DMF: 3.0 mL at 80 °C. The reaction mixture was analyzed by using UV spectroscopy with Carrez solutions. [b]II[nd] cycle, [c]III[rd] cycle.

Activity of the ferrites were substantially increased by decorating them on CNTs, nevertheless, $ZnFe_2O_4$-CNT remained inactive to catalyze the dehydration of fructose which was attributed to the

diamagnetic property of the material. Optimum fructose dehydration up to 75% conversion with 99% selectivity to HMF was obtained on $CoFe_2O_4$-CNT (Table 2.2 entry 10) atrributable to its stability towards acidic and environmental conditions. To confirm the role of CNT, unfunctionalized CNT as well as acid and base functionalized CNTs were employed for the reaction. Dehydration of fructose did not occur with unfunctionalized CNT (Table 2.2, entry 1) whereas very little conversion was observed with acid and base functionalized CNTs without HMF formation (Table 2.2, entries 2-3). It was thus concluded that CNT in the $CoFe_2O_4$-CNT system, promoted the dehydration reaction because of its extreme conducting properties, thereby facilitating the redox reaction of Co^{2+} to Co^{3+}. Notably, $CoFe_2O_4$-CNT effectively catalyzed the dehydration of glucose with selectivity towards HMF up to 98% at 64% conversion (Table 2.2, entry 11).

2.3.5 Immobilized IL on solid support

Development of Supported ionic liquid catalysts (SILC) is one of the approaches aimed at solving the serious drawbacks of complex separation and recovery of IL catalysts from the reaction mixture. SILC are potentially more advantageous for catalytic application than bulk IL catalyst as they combine the attractive features of homogeneous catalysis such as the uniform nature of the catalytic centres, high specificity and selectivity of the catalyst, with important features of heterogeneous catalysts, such as high interfacial surface area, high system stability and reusability.[81] Exploiting SILC as a solid acid catalyst for the synthesis of HMF, Bao et al.[82] immobilized Brønsted acidic 3-allyl-1-(4-sulfobutyl)imidazolium trifluromethanesulfonate and Lewis acidic 3-allyl-1-(4-sulfurylchloride butyl) imidazolium trifluromethanesulfonate ILs on silica gel and then evaluated their catalytic activity for fructose dehydration reaction as shown in Figure 2.12.

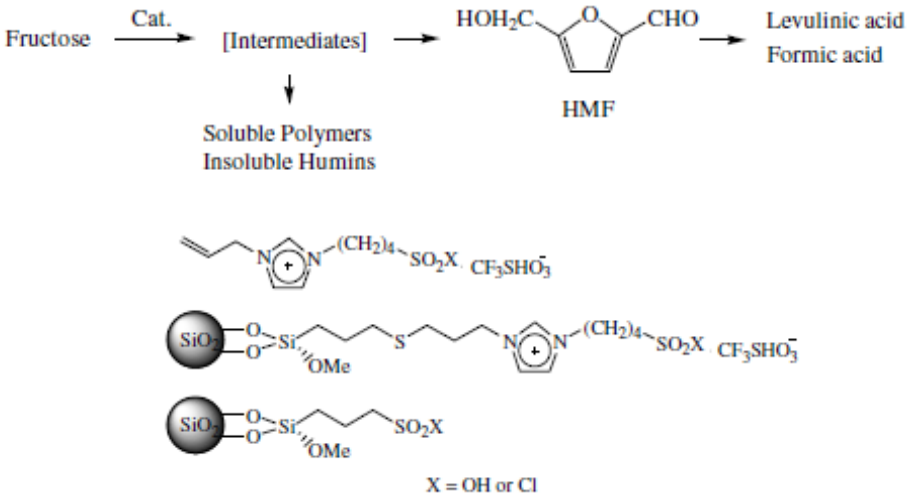

Figure 2.12 Dehydration of fructose to HMF in the presence of acidic catalysts

Under microwave irradiation at 200 W for 4 min in the presence of DMSO, fructose dehydration on ILIS-SO_3H (Brønsted acid catalyst) and ILIS-SO_2Cl (Lewis acid catalyst) gave 70% and 67% yield of HMF, respectively, with fructose conversion on both catalysts at 100%. Compared to sulfuric acid and sulfonylchloride modified silica gel, better results have been achieved for the dehydration reaction in terms of activity and reusability. Moreover, these catalysts could be effectively recycled multiple times with no significant deactivation and when compared with sulfuric acid and sulfonylchloride modified silica gels, they can afford better activity and reusability for the dehydration of fructose to HMF.

A new class of Supported Ionic Liquid nanoParticles (SILnP) with varying particle size (293–610 nm) were developed via immobilization of ionic liquid, 1-(tri-ethoxy silyl-propyl)-3-methyl-imidazolium hydrogen sulfate (IL-HSO_4) on the surface of silica nanoparticles (Figure 2.13).[83] These SILnPs were evaluated as catalysts for the synthesis of HMF in DMSO via fructose dehydration and the role of particle size on catalytic performance was studied. SILnP of particle size 610 nm (Si-3-IL-HSO_4) showed excellent catalytic activity for the conversion of fructose in DMSO to give 63% HMF yield at 99% conversion when the reaction was carried out at 130 °C for 30 min. Under comparable reaction conditions, similar catalytic activity measurements were observed on both Si-1-IL-HSO_4 and Si-2-IL-HSO_4 (particle sizes of 293 and 471 nm, respectively) as compared to Si-3-IL-HSO_4, thus indicating no effect of particle size. Si-3-IL-HSO_4 could be recycled several times without significantly losing its activity.

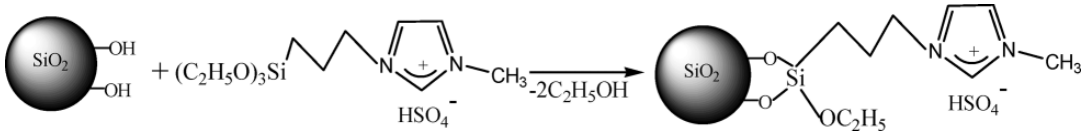

Figure 2.13 Schematic representation of 1-(tri-ethoxy silyl-propyl)-3-methyl-imidazolium hydrogen sulphate (IL-HSO_4) immobilization on silica nanoparticles

Bi-functionalized mesoporous silica nanoparticle with sulfonic acid and ionic liquids [HSO_3 + ($ILs/CrCl_2$)]-MSN shown in Figure 2.14 was synthesized and used as an efficient and recyclable heterogeneous catalyst for fructose dehydration under mild reaction conditions (90 °C and 3 h) in DMSO, producing 72.5% HMF yield at complete conversion.[84] It was proposed that increased reaction sites owing to high surface area and large mesopores of the catalyst contributed to its enhanced performance. Catalytic efficiency of [HSO_3 + ($ILs/CrCl_2$)]-MSN was confirmed through kinetic study as 67.5 kJ mol^{-1} energy barrier was required to be overcome on the catalyst as

compared to 80.05 kJ mol^{-1} energy requirement without catalyst, thus indicating that the bifunctional catalyst could accelerate the fructose dehydration reaction.

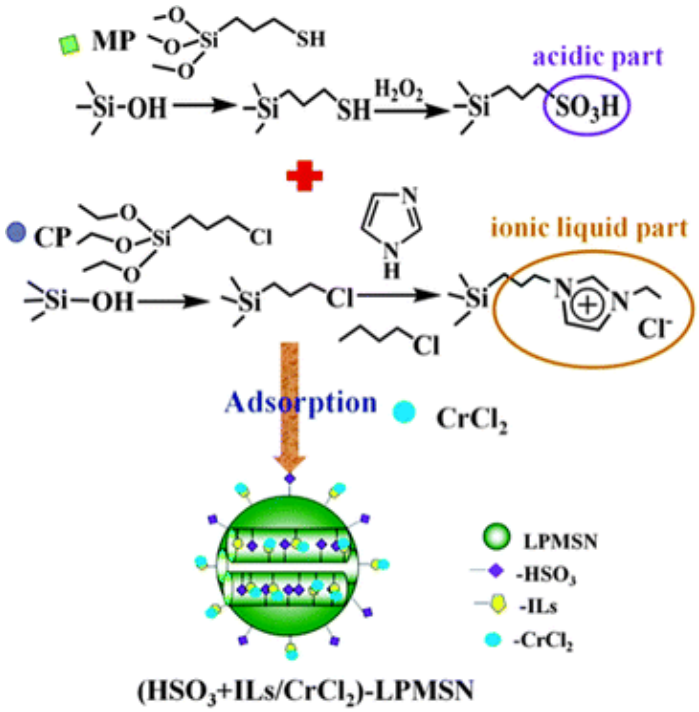

Figure 2.14 Synthetic process for preparing the bi-functionalized MSN

2.3.6 Zeolites

An acid bifunctional Beta zeolite was reported effective for the conversion of glucose to HMF in water-DMSO-THF solvent mixture.[85] Acid property of the zeolite material could be altered by calcination at high temperature or steam treatment, thereby inducing dealumination to form Al species out of the framework. This effect was more pronounced with steam treatment at high temperature due to severity of hydrolysis of Si-O-Al bond by high vapour pressure. Employing pyridine as a probe molecule, dealumination led to reduced Brønsted acid sites due to removal of tetrahedral Al species from the framework. Contrarily, dealuminated Al species act as Lewis acid sites and increased concurrently with the degree of dealumination. Therefore, enhanced Lewis catalyzed isomerization of glucose to fructose through a hydride transfer mechanism in tandem with the dehydration of fructose to HMF was optimum on either zeolite calcined at 750 °C (Beta-Cal750) or steam treated at 600 °C (Beta-ST600). At 180 °C and 3 h of reaction, glucose conversion of 78% was attained with a corresponding 55% selectivity to HMF as shown in Table 2.3.

Table 2.3 Transformation of glucose to HMF over Beta zeolites[a]

Catalyst	Acid (mmol/g)[b]		B/L	Conversion[c] (%)	HMF selectivity (%)
	Brønsted	Lewis			
Beta-SDAcal	0.23	0.14	1.6	57 (91)[d]	38 (68)
Beta-Cal500	0.25	0.13	1.9	57 (96)	36 (70)
Beta-Cal600	0.24	0.14	1.7	61 (93)	37 (70)
Beta-Cal700	0.20	0.17	1.2	69 (97)	50 (68)
Beta-Cal750	0.17	0.18	0.94	78(97)	55 (66)
Beta-ST500	0.11	0.17	0.65	77 (92)	51 (60)
Beta-ST600	0.09	0.15	0.60	78 (91)	55 (55)

[a] Catalyst, 100 mg; glucose, 0.67 mmol; water, 4.5 ml; DMSO 0.5 ml; THF 15 ml; temperature, 180 °C; time, 3 h.
[b] Each acid amount corresponds to the amount of adsorbed pyridine after evacuation at 250 °C.
[c] Conversion of glucose.
[d] Values in bracket correspond to activity result of fructose conversion into HMF

In contrast, the result of fructose dehydration to HMF showed a different trend over the zeolite catalysts. Catalytic runs for 1 h showed that >90% conversion was achieved irrespective of the catalysts but selectivity declined with decreasing Brønsted acidity (i.e. increased dealumination). It was suggested that high Lewis acidity as a result of severe dealumination could promote undesired reactions of fructose. Therefore, the authors conclude that effective conversion of glucose in a one pot reaction to HMF should involve rapid dehydration of fructose to HMF faster than undesired reactions over the Lewis acid sites.

In an effort to improve the environmental suitability of IL process for glucose conversion reaction to HMF, Jadhav et al.[86] investigated the potential replacement of Cr salt with a zeolite catalyst as well using a cheap and less toxic ionic liquid as a replacement for imidazolium based IL. With a preliminary study employing different solvents for the dehydration of glucose using H-ZSM-5 zeolite catalyst, no isolable yield of HMF could be obtained in DMA, DMSO, toluene, alcohols or sulfanone. Only when [BMIM]Cl was used as the solvent was a yield of up to 45% obtained. The performance of [BMIM]Cl was related to its polarity and its ability to dissolve ions and disrupt H-bonds. Nevertheless, when [BMIM]Cl was combined with tetrabutylammonium chlroride (TBAC) which the authors has proposed to serve as a more environmentally friendly reaction system and a replacement for imidazolium based ionic liquid, a lesser yield of HMF (27%) was obtained. In the presence of $CrCl_x$ Lewis acids however, considerable performance of TBAC was observed with HMF yields between 49-56% obtainable.

Zeolite-promoted conversion of glucose into HMF was studied by Liu et al.[87] Various zeolite catalysts including HY-zeolite, H-mordenite, Hβ-zeolite and HZSM-5 were screened for the reaction in [BMIM]Cl. Preliminary activity results showed that catalytic performance of the zeolites is strongly dependent on both the strength and density of acid sites, which are influenced by Si/Al ratio. Hβ-zeolite with Si/Al ratio of 25 exhibited the best catalytic activity as compared to other zeolites (Table 2.4). At optimized reaction conditions (0.6 w/w ratio Hβ-zeolite:glucose, 150 °C and 50min) a glucose conversion of 80.6% and HMF yield of 50.3% were obtained. However, it is of importance to control the water content of the system as it plays a crucial on the effectiveness of [BMIM]Cl, due to its hydroscopic nature, to selectively produce HMF in high yield. Experiments conducted on the effect of addition of water to the reaction system showed that HMF yield peaked at 5 wt% (52.4 %) water content and thereafter, it gradually declined. The authors concluded that an optimum amount of water is necessary to promote dissolution of glucose and reduce viscosity of [BMIM]Cl, wherein both factors could promote HMF production and inhibit the formation of undesired by-products to some extent.

Table 2.4 Conversion of glucose into HMF over a variety of zeolite catalysts[a]

Entry	Zeolite catalyst	Si/Al ratio[b]	Total acidity (mmol g^{-1})[c]	Brønsted/Lewis acidity ratio[d]	HMF yield	Glucose conversion
1	No catalyst	-	-	-	1.5	2.7
2	HY-zeolite	5	1.37	0.46	11.8	24.6
3	H-mordenite	15	1.18	0.79	13.1	27.2
4	Hβ-zeolite	15	1.09	0.82	18.4	37.9
5	Hβ-zeolite	25	0.91	1.03	23.7	48.1
6	HZSM-5	25	0.95	0.98	14.2	31.3
7	HZSM-5	50	0.83	1.25	20.5	42.7
8	HZSM-5	100	0.61	1.81	16.4	35.4
9	HZSM-5	300	0.26	2.34	8.3	14.5

[a] Reaction conditions: 100 mg glucose, 40 mg zeolite catalyst, 1 g [BMIM]Cl, 140 °C, 30 min
[b] The Si/Al ratios were obtained from the supplier
[c] The total acidities of zeolite catalysts were determined by NH_3-TPD method
[d] The Brønsted/Lewis acidity ratios of zeolite catalysts were determined by FT-IR spectroscopy of adsorbed pyridine

Reaction kinetics study of glucose into HMF showed that it could be modelled as a first-ordered rate reaction and the calculated activation energy was 97.4 kJ mol^{-1}. Mechanism of the reaction was proposed to proceed via isomerization of glucose into fructose on the Lewis acid site followed by

dehydration of fructose into HMF on the Brønsted acid sites (Figure 2.15). Hence, a good synergy between the surface Brønsted and Lewis acid sites on Hβ-zeolite were claimed to be essential for good activity. Although the catalyst displayed gradual deactivation after every reuse, its activity can be restored by simple calcination. Fructose could also be converted to a high yield of HMF (86.8%) under similar conditions as that of glucose reaction.

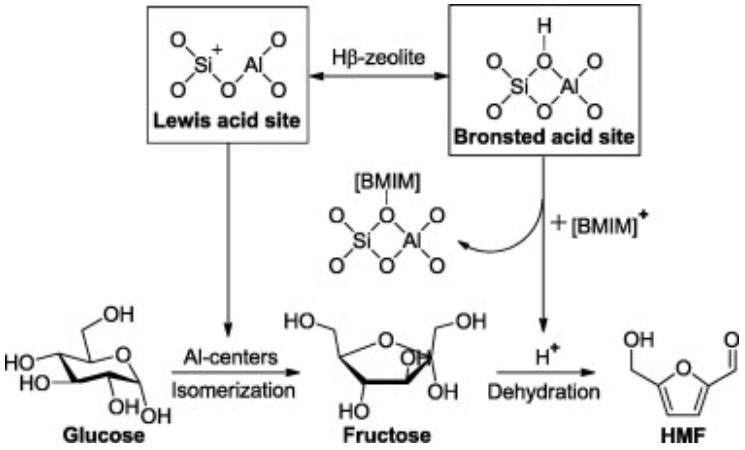

Figure 2.15The plausible mechanism for the conversion of glucose into HMF in the presence of Hβ-zeolite and [BMIM]Cl.[87]

Furthermore, combination of Hβ-zeolite (Si/Al = 25) and [BMIM]Cl was demonstrated to be effective for transforming a variety of carbohydrates into HMF. Conversion of sucrose, maltose and cellobiose resulted in 67.6%, 47.8% and 49.3% yields of HMF, respectively. Starch and cellulose could also be effectively converted into HMF with yields of 45.4% and 46.5%, respectively, which were almost comparable to that from glucose (50.3%).

Moreau et al.[88, 89] employed a water/methyl isobutyl ketone mixture to investigate the dehydration of fructose to HMF in the presence of dealuminated H-form microporous zeolite catalysts. Acidity and pore structure of the zeolites were found to strongly influence fructose conversion and HMF selectivity. In relation to acidity, selectivity tends to decrease by increasing acidity (by increasing Si/Al ratio) of the catalytic sites, thus allowing rehydration of HMF to levulinic and formic acids or condensation to humins. Structurally, mordenite possessing only parallel large elliptical channels preferentially improved HMF selectivity by preventing its rearrangement into higher molecular weight compounds. Hence, among the zeolite catalysts, H-Mordenite with a Si/Al ratio of 11 and a low mesoporous volume provided an optimum balance between selectivity and activity. At 165 °C, selectivity in HMF of 91-92% was obtained up to a fructose conversion of 76%.

Exploiting the fact that Sn-Beta could facilitate the isomerisation of glucose to fructose even at low pH,[90, 91] a pair of Sn-Beta and Brønsted acid catalyst was developed for the conversion of carbohydrates in a water-THF biphasic system depicted in Figure 2.16.[92] The combination of Sn-Beta and aqueous acidic solution of HCl saturated with NaCl gave 57% HMF yield at 79% glucose conversion. High HMF selectivities could also be obtained from more complex carbohydrates in this reactor system. Synthesis of HMF from cellobiose and starch gave HMF selectivities of ~86% and 69% at cellobiose and starch conversion of ~73% and 75%, respectively, when the reaction was performed at 180 °C.

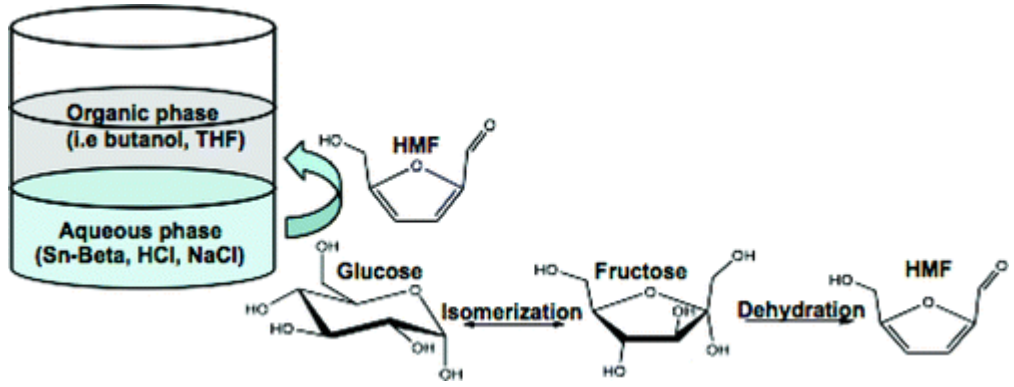

Figure 2.16 One-pot biphasic water/tetrahydrofuran (THF) reactor system[92]

Recently, Yang et al.[93] reported the synthesis of Sn-Beta zeolite by either adding NH_4F as a mineralizing agent (Sn-Beta-F) or steam assisted conversion (Sn-Beta-SAC). Adopting similar acidic environment of THF/H_2O biphasic system as that reported by Nikolla et al.,[92] the catalytic performance of the zeolites was evaluated for one-pot conversion of glucose to HMF. The catalyst system of Sn-Beta-F and HCl was found to be optimal in terms of activity and selectivity to HMF. Working at 190 °C for 70 min, 53% HMF could be produced from glucose. Furthermore, the robustness of Sn-Beta-F to catalyze cellobiose and sucrose was evaluated. Synthesis of HMF at 190 °C for 70 min occurred readily with sucrose (dimer of glucose-fructose) to give 55.2% yield of HMF as compared to 38.3% HMF yield from cellobiose (dimer of glucose-glucose). The authors explained the observed difference in HMF yield on the basis of the monomeric units that make up the disaccharides, as ketose is known to dehydrate more rapidly to HMF than aldose. Under similar reaction conditions, direct conversion of cellulose was attempted and 32.2% yield of HMF could be reached.

Gallo et al.[94] also reported a one-pot synthesis of HMF from glucose whereby Sn-β was utilized to catalyze the isomerisation of glucose to fructose and Amberlyst resin as the source of

Brønsted acidity to dehydrate fructose to HMF. High yields of HMF from glucose were achievable using biomass derived solvents (tetrahydrofuran (THF), γ-valerolactone (GVL), methyltetrahydrofuran (MTHF), γ-hexalactone (GHL)) mixed with water in 9:1 weight ratio. In the presence of Sn-Beta/Amberlyst 70 catalyst system and a monophasic system of water and GVL, GHL, THF:MTHF (1:1) or THF yields of HMF 59, 55, 60 and 63%, respectively, could be achieved at 130 °C.

Cellulose is by far the most abundant carbohydrate biopolymer found in plant biomass. Depolymerization and hydrolysis of lignocellulosics into intermediates that are more susceptible for chemical transformation is a prerequisite for production of biofuels and chemicals. Direct conversion of cellulose into HMF using a combined $CrCl_2$/zeolite/[BMIM]Cl catalytic system was performed by Tan et al.[95] at 120 °C. Zeolite with moderate acidity (Zeolite H-Y, CVB 400) promoted cellulose hydrolysis and in combination with a bulky N-heterocyclic carbine containing $CrCl_2$ (NHC-$CrCl_2$) catalyst, 47.5% HMF yield was obtainable after 12 h of reaction.

2.3.7 Silica based

Jiménez-Morales et al.[96] performed the dehydration of glucose to HMF in water/methyl isobutyl ketone using mesoporous MCM-41 silica containing ZrO_2. Activation of zirconium incorporated into MCM-41 at 550 °C resulted in the most active catalyst, achieving HMF yield of 23% and 82% glucose conversion at 175 °C and 150 min of reaction time. The catalyst was quite selective, since only fructose and HMF were detected. Although the catalyst can be reused for successive reactions, catalytic activity monotonously decreased with number of cycles due to progressive acid site blockage. However, activity of the spent catalyst can be restored by calcination at 500 °C, thus requiring frequent regeneration.

Similarly, Scott et al.[97] reported the dehydration of fructose at 180 °C using acid functionalized SiO_2 as catalysts in a water-methyl isobutyl ketone/2-butanol mixture. A mesoporous (SBA-15) and nonporous (A380) silicas were used and functionalized with propylsulfonic acid (BTPSA, 3-(Butylthio) propane-1-sulfonic acid) to give resultant solid acids labelled as TAA-SBA-15 and TAA-A380, respectively. TAA-SBA-15 was found to be most active with 74% HMF selectivity at 66% fructose conversion. The difference in activity between TAA-SBA-15 and TAA-A380 was explained by the higher acid loading on SBA-15. Although, co-condensation incorporation of functional acidic groups on SBA-15 gave a more robust catalyst than post-grafting technique, the catalyst was unstable at the reaction temperature. This behaviour was related to the collapse of the ordered mesostructure and loss of functionality. An alternative synthetic route was proposed to overcome this problem by using a silane of higher functional group

loadings (TESAS, 3-((3-(trimethoxysilyl)propyl)thio)propane-1-sulfonic acid) to functionalize SBA-15.[98] TESAS-SBA-15 and SSA-SBA-15 were obtained and both possessed a two dimensional ordered hexagonal mesoporous structure with acid loading of 1.25 mmol/g and 0.82mmol/g, respectively. Working at 130 °C in water-MIBK/2-butanol system, selectivity to HMF between 65-71% was achieved at a fructose conversion of 81-84%.

Dumesic and co-workers[99] prepared a series of propylsulfonic acid modified ordered porous silicas including an SBA-15-type (E0) and two ethane-bridged PMOs with SBA-15-type structure (E45, E90). The activity, selectivity and stability of E0, E45 and E90 for the continuous production of HMF were evaluated in a tubular reactor using a single phase solution of THF and water. In comparison to commercially available nonordered pSO_3H-SC, the silicas prepared with ordered structures are more selective and robust. Operating the reactor at 130 °C for 190 h, E0, E45 and E90 showed improved HMF selectivity in the range of 60 to 75% in comparison to 20% selectivity on pSO_3H-SC. The latter also showed the greatest extent of deactivation, losing 94% of its activity over 24 h while all of the ordered mesoporous catalysts showed much higher stabilities. Catalyst deactivation under these flow conditions was ascribed primarily to hydrolytic cleavage of the acid sites. Amongst the ordered silica deactivation rate is in the order of E45 (0.012 h^{-1}) > E90 (0.022 h^{-1}) > E0 (0.027 h^{-1}), indicating that organosilicas are more stable than the inorganic one.

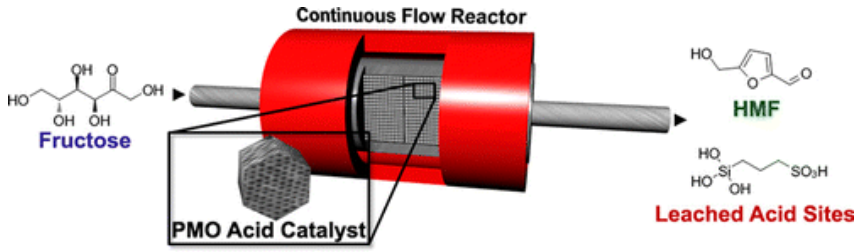

Figure 2.17 Continuous fructose dehydration in a ¼ inch packed bed reactor

Acid-base bi-functionalized large pore mesoporous silica nanoparticles was explored by Peng et al.[100] for cooperative catalysis of one-pot cellulose conversion to HMF in [EMIM]Cl. Large pored mesoporous silica nanoparticles (LPMSN) was synthesized from brij-97 template and dimethyl o-phthalate as the swelling agent. In addition, acid (SO_3H), base (NH_2) and both acid-base functionalized LPMSN denoted as LPMSN-SO_3H, LPMSN-NH_2, and LPMSN-both, respectively were prepared by grafting method. Catalytic results at 120 °C and 3 h show that LPMSN-SO_3H and LPMSN-NH_2 could increase the yield of produced HMF from reactions that need acid and base catalysts, respectively. In addition, LPMSN-SO_3H and LPMSN-both are found to be useful for one-pot cellulose conversion to glucose and HMF in yields of 35.8% and 19.2%, respectively (LPMSN-

SO_3H) and 36.3 and 14.7%, respectively (LPMSN-both). With the goal of understanding the role of each LPMSN-based catalyst in the carbohydrate conversion, cellobiose, glucose, and fructose were also used as reactants. Efficacy of LPMSN-both was confirmed to be as a result of cooperative catalysis of both acid and base functional groups. Carbohydrate conversion to HMF was modelled by three consecutive reactions as follows: (1) cellobiose-to-glucose depolymerization, (2) glucose-to-fructose isomerization, and (3) fructose-to-HMF dehydration, and each reaction need an acid, base, and catalyst, respectively.

2.3.8 Other catalyst systems

Wang et al.[101] designed a series of solid acid and base catalysts with different wettabilities for the selective production of HMF. With the aid of computational simulation, the authors demonstrated that superhydrophobic meosporous polymer acid catalyst (P-SO_3H-154) with strong wettability could prevent rehydration of HMF, and HMF could be solely produced from fructose dehydration reaction. Experimental results with P-SO_3H-154, regardless of the solvent gave similar yield of HMF whereas other solid acids could catalyze the hydration of HMF. It was concluded that P-SO_3H-154 prevented HMF rehydration by favourably isolating water molecules from the acidic site.

Table 2.5 Catalytic data in dehydration of fructose to HMF over various catalysts.[a]

Entry	Catalyst	Solvent	HMF yield (%)
1	P-SO_3H-154	DMSO	99.0
2	P-SO_3H-154	THF–DMSO	> 99.0
3	H_2SO_4[b]	DMSO	53.8
4	H_2SO_4[b]	THF–DMSO	62.0
5	amberlyst-15	DMSO	66.0
6	amberlyst-15	THF–DMSO	45.7
7	C_6H_5-SO_3H[b]	THF–DMSO	53.3
8	P-SO_3H-154	THF–DMSO–water[c]	> 99.0
9	amberlyst-15	THF–DMSO–water[c]	21.0
10	P-SO_3H-154	THF–DMSO	> 99.0

[a] Reaction conditions: 100 mg of fructose, 50 mg of solid catalyst, 5 g of solvent (weight ratio of THF to DMSO in the mixed THF–DMSO solvent at 1.5) for 10 h at 100 °C; the major by-products were LA and FA.
[b] The same number of acidic sites as in P-SO_3H.
[c] 4.5 g of THF–DMSO (weight ratio at 1.5) and 0.5 g of water.
[d] 150 mg of catalyst, 2.5 h reaction time.

Combined catalyst of P-SO_3H-154 with a superhydrophilic base catalyst, P-VI-0, efficiently catalyzed one-pot conversion of glucose in a THF-DMSO solvent mixture to 95.4% yield of HMF and this was attributed to the controlled wettability of the solid acid-base catalyst system. Process development aimed at continuous production of HMF from glucose was attempted by using a fixed bed reactor. At 100 °C in a THF-DMSO solvent, glucose conversion gave a steady yield of HMF between 34.1–38.9% up to 45 h of reaction. Finally, a simple technique of product isolation by means of carbon-black adsorption was also reported with an isolation efficiency of HMF reaching 76% yield.

Wang et al.[102] published promising results on tin-montmorillonite catalyzed dehydration of carbohydrates to HMF. A novel Sn-mont catalyst of bifunctional acidity (Lewis and Brønsted acid sites) was prepared from a natural calcium montmorillonite (Ca-Mont) via ion exchange with an aqueous tin tetrachloride solution ($SnCl_4.5H_2O$). The activity of the catalyst reported for glucose and fructose conversion in THF/H_2O–NaCl biphasic system at 160 °C for 3 h was 59.3% and 78.8%, respectively. The authors concluded that the synergistic effect of the Lewis and Brønsted acid sites is responsible for the successful conversion of glucose to HMF. Sn^{4+} plays a crucial role as the Lewis acid sites in the isomerization of glucose to fructose and Sn-OH acted as the Brønsted site active for the dehydration of generated fructose to HMF as shown in Figure 2.18.

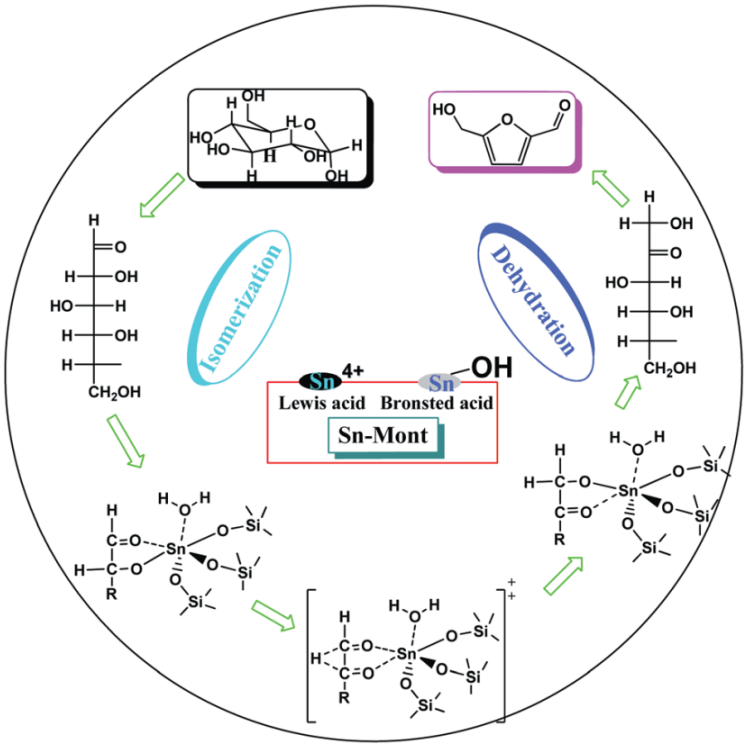

Figure 2.18 Plausible reaction mechanism for tandem isomerisation-dehydration of glucose to HMF over Sn-Mont catalyst.[102]

Interestingly, the catalyst was found to be stable and after 4 repeated reaction cycles, HMF yield from glucose was maintained around 58%. Moreover, robustness of the catalyst to synthesize HMF from complex carbohydrate sources was demonstrated. Without coupling any other acid catalysts with Sn-Mont, one-pot conversion of sucrose, cellobiose, inulin, starch and cellulose in the THF/H_2O–NaCl biphasic system resulted in 43.6%, 40.1%, 42.6%, 44.4% and 39.1% yields of HMF, respectively.

Recently, Pan et al.[103] reported the fabrication of multifunctional polymeric foams as efficient catalysts for one-pot conversion of carbohydrates to HMF. Hydrophobic polymers (Cr^{3+}-HPFs-1-H^+ and HPFs-1-H^+) with hierarchical porous structure, inhomogeneous acidic composition and Lewis-Brønsted acid sites were synthesized through water-in-oil (W/O) high internal phase emulsions (HIPEs) template method and subsequent ion-exchange process as shown in Figure 2.19.

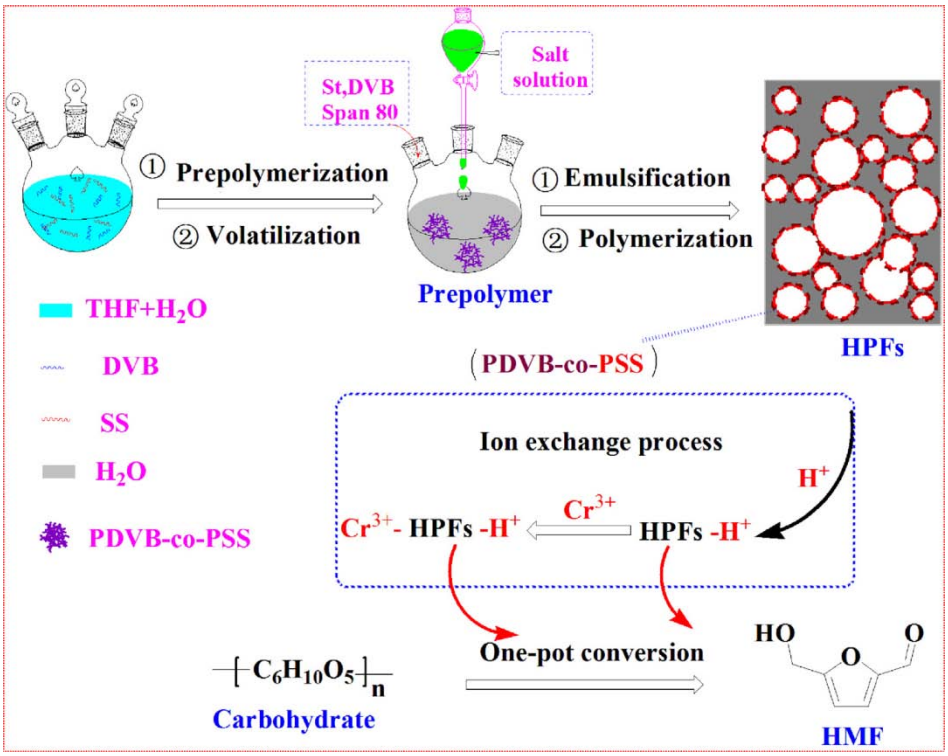

Figure 2.19 The synthesis of Cr^{3+}-HPFs-1-H^+ and the conversion of carbohydrate into HMF in [Emim]Cl under atmospheric pressure[103]

Optimal yield of HMF (42.1%) from cellulose was achieved at 140 °C for 4 h with Cr^{3+}-HPFs-1-H^+ catalyst in the presence of [Emim]Cl solvent. Also, Cr^{3+}-HPFs-1-H^+ effectively catalyzed the dehydration of fructose and glucose. At optimized reaction parameters of 130 °C/2 h for glucose and 110 °C/2h for fructose, remarkable yields of 64% and 91% HMF, respectively, were achieved. Cr^{3+}-HPFs-1-H^+, which contained both isomerization (Lewis acid) and dehydration (Brønsted acid)

catalytic sites showed improved yield of HMF from cellulose and glucose when compared to those obtained (29.2% and 42.5%, respectively) on HPFs-1-H^+ that possessed only Brønsted acidity. Meanwhile, presence of Lewis acid sites on Cr^{3+}-HPFs-1-H^+ resulted only in slight improvement of HMF yield from fructose as compared to HPFs-1-H^+. This confirmed that Brønsted acid sites are mainly responsible for fructose dehydration whereas Lewis acid sites are needed to promote isomerization of glucose based carbohydrates to fructose prior to dehydration.

2.4 Conclusion and outlook

A large number of solid catalysts have been explored and developed for the dehydration of carbohydrates with remarkable success for the production of HMF. Despite these major advancements, several aspects need to be carefully evaluated such as catalysts deactivation and regeneration, solvent system, mass transfer phenomenon and techno-economic analysis in view of industrial implementation of solid catalysis. Further attention needs to be focused on fine-tuning catalytic properties to design much improved catalyst systems as well as optimization of reaction systems and conditions.

In spite of the strategies developed to synthesize multifunctional single catalyst for the multistep conversion of carbohydrates to HMF, longer reaction time and sometimes harsher reaction conditions are required to achieve similar effectiveness like that of homogeneous catalysts. This is because effective utilization ratio of catalytic active sites is low as the active sites on the catalyst surface mostly participate in the catalytic reaction. Hence, facile strategies of synthesizing non hazardous multifunctional catalyst with hierarchical porous structure, binary acid sites and inhomogeneous acidic composition are highly desirable to improve reaction rate. Moreso, the catalyst should be suitable for mass production and commercialization.

Moreover, in terms of feedstock used, many efforts are been focused on catalyzing glucose and fructose due to their simple conversion steps. Conversion of low-cost carbohydrate sources accessible from lignocellulosic biomass would be more desirable to develop an efficient industrial process for the production of HMF. Depolymerization and hydrolysis of lignocellulosics to unlock highly reactive sugar intermediates is a prerequisite to effectively transform cellulose biopolymer found in abundance in biomass resources into HMF. Therefore, extensive research to design multifunctional solid catalyst that can promote this tandem reaction without the need of IL for cellulose deconstruction is desirable. Example of such catalyst is the amphiphilic $Cr[(DS)H_2PW_{12}O_{40}]_3$[76] with micellar structure that could accumulate cellulose through interaction with the micelle surface or by insertion into the micelle itself, thereby overcoming insolubility of cellulose in water. Thus, intensive catalytic processes of simultaneous hydrolysis of cellulose and

subsequent conversion to HMF in water hold outstanding potential of efficiently transforming lignocellulosics to HMF.

Mechanism of HMF over the multifunctional solid catalysts has been proposed that consist of consecutive reaction steps of Brønsted hydrolysis-Lewis acid or base isomerization-Brønsted dehydration. Since reaction mechanism and kinetics is dependent on the type of catalyst and reaction solvent system, detailed investigation of this aspect is very important to be considered in future works. Techniques using computational tools such as density functional theory simulation or experimental analysis involving nuclear magnetic resonance and in situ fluorescence microscopy may be employed to enhance the design of novel solid acid catalysts as well as be able to predict catalysts performance under real reaction conditions.

An issue of concern after successful generation of HMF is to identify a suitable solvent for the liquid-liquid extraction of HMF in the separation unit operation. As HMF is examined as platform chemical for the production of fine chemicals and liquid fuels, direct upgrade to these commodities opens more cost-effective process that might meet the target for scale up. The challenge is to be able to develop a catalytic process favourable for carbohydrates dehydration to HMF and compatible with upgrading processes, which typically involve oxidation, hydrogenation or hydrolysis reactions.

References

1. M. Cuzzoni, G. Stoppini, G. Gazzani and P. Mazza, *Food and chemical toxicology*, 1988, **26**, 815-822.
2. A. A. Rosatella, S. P. Simeonov, R. F. Frade and C. A. Afonso, *Green Chemistry*, 2011, **13**, 754-793.
3. K. Abraham, R. Gürtler, K. Berg, G. Heinemeyer, A. Lampen and K. E. Appel, *Molecular nutrition & food research*, 2011, **55**, 667-678.
4. T. Wang, M. W. Nolte and B. H. Shanks, *Green Chemistry*, 2014, **16**, 548-572.
5. J. J. Bozell and G. R. Petersen, *Green Chemistry*, 2010, **12**, 539-554.
6. M. E. Zakrzewska, E. Bogel-Łukasik and R. Bogel-Łukasik, *Chemical reviews*, 2010, **111**, 397-417.
7. A. F. V. Grote and B. Tollens, *Justus Liebigs Annalen der Chemie*, 1875, **175**, 181-204.
8. F. Newth, *Advances in carbohydrate chemistry*, 1951, **6**, 83.
9. C. Moye and Z. Krzeminski, *Australian Journal of Chemistry*, 1962, **16**, 258-269.
10. M. S. Feather and J. F. Harris, *Advances in carbohydrate chemistry and biochemistry*, 1973, **28**, 161-224.
11. A. Gaset, J. Gorrichon and E. Truchot, *Inf. Chim*, 1981, **212**, 179-184.
12. A. Faury, A. Gaset and J. Gorrichon, *Inf. Chim*, 1981, **214**, 203-209.
13. B. Kuster, *Starch-Stärke*, 1990, **42**, 314-321.
14. L. Cottier and G. Descotes, *ChemInform*, 1994, **25**.
15. J. Lewkowski, 2001.
16. C. Moreau, M. N. Belgacem and A. Gandini, *Topics in Catalysis*, 2004, **27**, 11-30.
17. A. Corma, S. Iborra and A. Velty, *Chemical reviews*, 2007, **107**, 2411-2502.
18. A. Boisen, T. Christensen, W. Fu, Y. Gorbanev, T. Hansen, J. Jensen, S. Klitgaard, S. Pedersen, A. Riisager and T. Ståhlberg, *Chemical engineering research and design*, 2009, **87**, 1318-1327.
19. X. Tong, Y. Ma and Y. Li, *Applied Catalysis A: General*, 2010, **385**, 1-13.
20. Y. Zhang and J. Y. G. Chan, *Energy & Environmental Science*, 2010, **3**, 408-417.
21. T. Ståhlberg, W. Fu, J. M. Woodley and A. Riisager, *ChemSusChem*, 2011, **4**, 451-458.
22. S. Lima, M. M. Antunes, M. Pillinger and A. A. Valente, *ChemCatChem*, 2011, **3**, 1686-1706.
23. R.-J. van Putten, J. C. van der Waal, E. De Jong, C. B. Rasrendra, H. J. Heeres and J. G. de Vries, *Chemical reviews*, 2013, **113**, 1499-1597.

24. S. Dutta, S. De and B. Saha, *biomass and bioenergy*, 2013, **55**, 355-369.
25. S. P. Teong, G. Yi and Y. Zhang, *Green Chemistry*, 2014, **16**, 2015-2026.
26. B. Saha and M. M. Abu-Omar, *Green Chemistry*, 2014, **16**, 24-38.
27. H. Zhao, J. E. Holladay, H. Brown and Z. C. Zhang, *Science*, 2007, **316**, 1597-1600.
28. G. Yong, Y. Zhang and J. Y. Ying, *Angewandte Chemie*, 2008, **120**, 9485-9488.
29. Y. Su, H. M. Brown, X. Huang, X.-d. Zhou, J. E. Amonette and Z. C. Zhang, *Applied Catalysis A: General*, 2009, **361**, 117-122.
30. X. Qi, M. Watanabe, T. M. Aida and R. L. Smith, *ChemSusChem*, 2010, **3**, 1071-1077.
31. P. Wang, H. Yu, S. Zhan and S. Wang, *Bioresource technology*, 2011, **102**, 4179-4183.
32. Y. Zhang, H. Du, X. Qian and E. Y.-X. Chen, *Energy & Fuels*, 2010, **24**, 2410-2417.
33. M. Mascal and E. B. Nikitin, *Green Chemistry*, 2010, **12**, 370-373.
34. M. Mascal and E. B. Nikitin, *ChemSusChem*, 2009, **2**, 859-861.
35. Y. Román-Leshkov, J. N. Chheda and J. A. Dumesic, *Science*, 2006, **312**, 1933-1937.
36. J. N. Chheda, Y. Román-Leshkov and J. A. Dumesic, *Green Chemistry*, 2007, **9**, 342-350.
37. Q. P. Peniston, *Journal*, 1956.
38. J. N. Chheda and J. A. Dumesic, *Catalysis Today*, 2007, **123**, 59-70.
39. Y. Román-Leshkov and J. A. Dumesic, *Topics in Catalysis*, 2009, **52**, 297-303.
40. Y. J. Pagan-Torres, T. Wang, J. M. R. Gallo, B. H. Shanks and J. A. Dumesic, *Acs Catalysis*, 2012, **2**, 930-934.
41. T. Wang, Y. J. Pagán-Torres, E. J. Combs, J. A. Dumesic and B. H. Shanks, *Topics in Catalysis*, 2012, **55**, 657-662.
42. Y. Yang, C.-w. Hu and M. M. Abu-Omar, *Green Chemistry*, 2012, **14**, 509-513.
43. Y. Yang, C. W. Hu and M. M. Abu-Omar, *ChemSusChem*, 2012, **5**, 405-410.
44. N. Shi, Q. Liu, Q. Zhang, T. Wang and L. Ma, *Green Chemistry*, 2013, **15**, 1967-1974.
45. R. Carrasquillo-Flores, M. Käldström, F. Schüth, J. A. Dumesic and R. Rinaldi, *Acs Catalysis*, 2013, **3**, 993-997.
46. M. Watanabe, Y. Aizawa, T. Iida, R. Nishimura and H. Inomata, *Applied Catalysis A: General*, 2005, **295**, 150-156.
47. X. Qi, M. Watanabe, T. M. Aida and R. L. Smith, *Catalysis Communications*, 2008, **9**, 2244-2249.
48. X. Qi, M. Watanabe, T. M. Aida and R. L. Smith, *Catalysis Communications*, 2009, **10**, 1771-1775.
49. A. Osatiashtiani, A. F. Lee, D. R. Brown, J. A. Melero, G. Morales and K. Wilson, *Catalysis Science & Technology*, 2014, **4**, 333-342.

50. F. Benvenuti, C. Carlini, P. Patrono, A. M. R. Galletti, G. Sbrana, M. A. Massucci and P. Galli, *Applied Catalysis A: General*, 2000, **193**, 147-153.
51. F. S. Asghari and H. Yoshida, *Carbohydrate research*, 2006, **341**, 2379-2387.
52. P. Khemthong, P. Daorattanachai, N. Laosiripojana and K. Faungnawakij, *Catalysis Communications*, 2012, **29**, 96-100.
53. A. Chareonlimkun, V. Champreda, A. Shotipruk and N. Laosiripojana, *Fuel*, 2010, **89**, 2873-2880.
54. A. Chareonlimkun, V. Champreda, A. Shotipruk and N. Laosiripojana, *Bioresource technology*, 2010, **101**, 4179-4186.
55. A. Takagaki, M. Ohara, S. Nishimura and K. Ebitani, *Chem. Commun.*, 2009, 6276-6278.
56. M. Ohara, A. Takagaki, S. Nishimura and K. Ebitani, *Applied Catalysis A: General*, 2010, **383**, 149-155.
57. C. V. McNeff, D. T. Nowlan, L. C. McNeff, B. Yan and R. L. Fedie, *Applied Catalysis A: General*, 2010, **384**, 65-69.
58. K. Nakajima, R. Noma, M. Kitano and M. Hara, *Journal of Molecular Catalysis A: Chemical*, 2014, **388**, 100-105.
59. S. De, S. Dutta, A. K. Patra, A. Bhaumik and B. Saha, *Journal of Materials Chemistry*, 2011, **21**, 17505-17510.
60. S. De, S. Dutta, A. K. Patra, B. S. Rana, A. K. Sinha, B. Saha and A. Bhaumik, *Applied Catalysis A: General*, 2012, **435**, 197-203.
61. A. Dutta, A. K. Patra, S. Dutta, B. Saha and A. Bhaumik, *Journal of Materials Chemistry*, 2012, **22**, 14094-14100.
62. Y. Zhang, J. Wang, X. Li, X. Liu, Y. Xia, B. Hu, G. Lu and Y. Wang, *Fuel*, 2015, **139**, 301-307.
63. M. Zhang, K. Su, H. Song, Z. Li and B. Cheng, *Catalysis Communications*, 2015, **69**, 76-80.
64. S. Xu, X. Yan, Q. Bu and H. Xia, *RSC Advances*, 2016, **6**, 8048-8052.
65. Y. Nakamura and S. Morikawa, *Bulletin of the Chemical Society of Japan*, 1980, **53**, 3705-3706.
66. K.-i. Shimizu, R. Uozumi and A. Satsuma, *Catalysis Communications*, 2009, **10**, 1849-1853.
67. X. Qi, M. Watanabe, T. M. Aida and R. L. Smith Jr, *Green Chemistry*, 2008, **10**, 799-805.
68. X. Qi, M. Watanabe, T. M. Aida and R. L. Smith Jr, *Industrial & Engineering Chemistry Research*, 2008, **47**, 9234-9239.

69. J. Pérez-Maqueda, I. Arenas-Ligioiz, Ó. López and J. G. Fernández-Bolaños, *Chemical Engineering Science*, 2014, **109**, 244-250.
70. Y. Qu, C. Huang, J. Zhang and B. Chen, *Bioresource technology*, 2012, **106**, 170-172.
71. C. Fan, H. Guan, H. Zhang, J. Wang, S. Wang and X. Wang, *biomass and bioenergy*, 2011, **35**, 2659-2665.
72. H. Li, X. He, Q. Zhang, F. Chang, W. Xue, Y. Zhang and S. Yang, *Energy Technology*, 2013, **1**, 151-156.
73. H. Li, Q. Zhang, X. Liu, F. Chang, Y. Zhang, W. Xue and S. Yang, *Bioresource technology*, 2013, **144**, 21-27.
74. Y. Zhang, V. Degirmenci, C. Li and E. J. Hensen, *ChemSusChem*, 2011, **4**, 59-64.
75. A. Teimouri, M. Mazaheri, A. N. Chermahini, H. Salavati, F. Momenbeik and M. Fazel-Najafabadi, *Journal of the Taiwan Institute of Chemical Engineers*, 2015, **49**, 40-50.
76. S. Zhao, M. Cheng, J. Li, J. Tian and X. Wang, *Chemical Communications*, 2011, **47**, 2176-2178.
77. J. Wang, W. Xu, J. Ren, X. Liu, G. Lu and Y. Wang, *Green Chemistry*, 2011, **13**, 2678-2681.
78. J. Wang, J. Ren, X. Liu, G. Lu and Y. Wang, *AIChE Journal*, 2013, **59**, 2558-2566.
79. M. G. Mazzotta, D. Gupta, B. Saha, A. K. Patra, A. Bhaumik and M. M. Abu-Omar, *ChemSusChem*, 2014, **7**, 2342-2350.
80. R. V. Kalluri, M. Shaikh, M. Sahu, P. K. Gavel, S. Khilari, K. K. Atyam and P. Das, *New Journal of Chemistry*, 2016.
81. A. Riisagera, R. Fehrmanna, M. Haumannb and P. Wasserscheidb, *Topics in Catalysis*, 2006, **40**, 91-102.
82. Q. Bao, K. Qiao, D. Tomida and C. Yokoyama, *Catalysis Communications*, 2008, **9**, 1383-1388.
83. K. B. Sidhpuria, A. L. Daniel-da-Silva, T. Trindade and J. A. Coutinho, *Green Chemistry*, 2011, **13**, 340-349.
84. Y.-Y. Lee and K. C.-W. Wu, *Physical Chemistry Chemical Physics*, 2012, **14**, 13914-13917.
85. R. Otomo, T. Yokoi, J. N. Kondo and T. Tatsumi, *Applied Catalysis A: General*, 2014, **470**, 318-326.
86. H. Jadhav, E. Taarning, C. M. Pedersen and M. Bols, *Tetrahedron Letters*, 2012, **53**, 983-985.
87. L. Hu, Z. Wu, J. Xu, Y. Sun, L. Lin and S. Liu, *Chemical Engineering Journal*, 2014, **244**, 137-144.

88. C. Moreau, R. Durand, C. Pourcheron and S. Razigade, *Industrial Crops and Products*, 1994, **3**, 85-90.
89. C. Moreau, R. Durand, S. Razigade, J. Duhamet, P. Faugeras, P. Rivalier, P. Ros and G. Avignon, *Applied Catalysis A: General*, 1996, **145**, 211-224.
90. M. Moliner, Y. Román-Leshkov and M. E. Davis, *Proceedings of the National Academy of Sciences*, 2010, **107**, 6164-6168.
91. Y. Román-Leshkov, M. Moliner, J. A. Labinger and M. E. Davis, *Angewandte Chemie International Edition*, 2010, **49**, 8954-8957.
92. E. Nikolla, Y. Román-Leshkov, M. Moliner and M. E. Davis, *Acs Catalysis*, 2011, **1**, 408-410.
93. G. Yang, C. Wang, G. Lyu, L. A. Lucia and J. Chen, *BioResources*, 2015, **10**, 5863-5875.
94. J. M. R. Gallo, D. M. Alonso, M. A. Mellmer and J. A. Dumesic, *Green Chemistry*, 2013, **15**, 85-90.
95. M. Tan, L. Zhao and Y. Zhang, *biomass and bioenergy*, 2011, **35**, 1367-1370.
96. I. Jiménez-Morales, J. Santamaría-González, A. Jiménez-López and P. Maireles-Torres, *Fuel*, 2014, **118**, 265-271.
97. A. J. Crisci, M. H. Tucker, J. A. Dumesic and S. L. Scott, *Topics in Catalysis*, 2010, **53**, 1185-1192.
98. A. J. Crisci, M. H. Tucker, M.-Y. Lee, S. G. Jang, J. A. Dumesic and S. L. Scott, *Acs Catalysis*, 2011, **1**, 719-728.
99. M. H. Tucker, A. J. Crisci, B. N. Wigington, N. Phadke, R. Alamillo, J. Zhang, S. L. Scott and J. A. Dumesic, *Acs Catalysis*, 2012, **2**, 1865-1876.
100. W.-H. Peng, Y.-Y. Lee, C. Wu and K. C.-W. Wu, *Journal of Materials Chemistry*, 2012, **22**, 23181-23185.
101. L. Wang, H. Wang, F. Liu, A. Zheng, J. Zhang, Q. Sun, J. P. Lewis, L. Zhu, X. Meng and F. S. Xiao, *ChemSusChem*, 2014, **7**, 402-406.
102. J. Wang, J. Ren, X. Liu, J. Xi, Q. Xia, Y. Zu, G. Lu and Y. Wang, *Green Chemistry*, 2012, **14**, 2506-2512.
103. J. Pan, Y. Mao, H. Gao, Q. Xiong, F. Qiu, T. Zhang and X. Niu, *Carbohydrate Polymers*, 2016, **143**, 212-222.

Chapter 3

Experimental Methodology

3.1 Introduction

Titania based nanoparticles were synthesized using sol-gel technique that involved coprecipitation with another metal oxide (zirconia) or sequential impregnation with ammonium salts of phosphorus, molybdenum, vanadium and tungsten. A wide range of techniques have been employed to characterize the as-prepared nanoparticles. Structural and textutral properties were investigated using XRD, and N_2 porosimetry analyses, spectroscopic analysis such as Raman and X-ray photoelectron spectroscopies were employed to investigate surface properties and microscopic analysis including field emission scanning electron microscopy (FE-SEM) and high resolution transmission electron microscopy (HR-TEM) were applied to examine the morphology of the samples. Acid-base measurements were carried out using pyridine adsorption coupled with fourier transform infrared spectroscopy as well as temperature programmed desorption of Ammonia/CO_2. Bulk elemental analysis was achieved with inductively couple plasma atomic emission spectroscopy (ICPAES) whereas carbon content on fresh and spent catalyst samples was determined by CHNS-O elemental analyser.

3.2 Material Synthesis

3.2.1 Titania–Zirconia binary oxide synthesis

A series of TiO_2–ZrO_2 binary oxides with varying ratio of TiO_2 to ZrO_2 (w/w) were prepared by sol-gel method. Metal alkoxides were put inside a funnel attached to a three-necked round bottom flask as shown in Figure 3.1. The sol was prepared by the dropwise addition of the alkoxide precursors into an aqueous solution containing *n*-butanol and kept under vigorous stirring. Initial molar ratios of water:alkoxide = 16 and butanol:alkoxide = 8. The pH of the solution was adjusted to 7 by adding ammonium hydroxide solution and the resulting solution was maintained at 70 °C under reflux for 24 h. After gelation, excess solvent was removed using rotary evaporator and followed by vacuum drying at 120 °C for 12 h. Finally, the dried samples were then calcined at 500 °C for 12 h at a ramping rate of 2 °C/min to obtain the metal oxides.

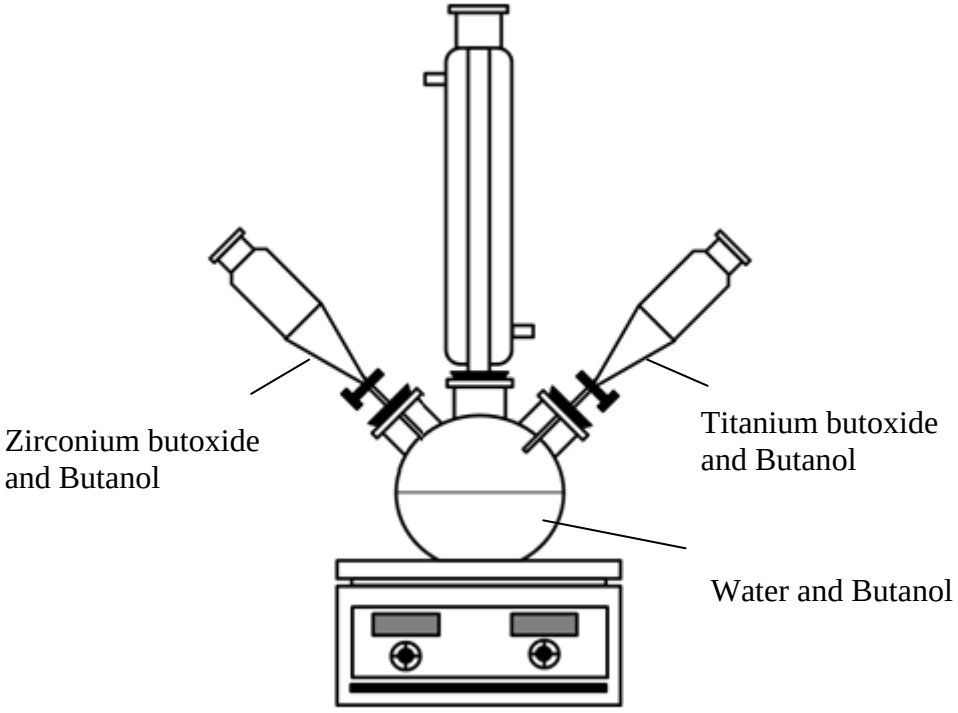

Figure 3.1 Experimental set up for titania–zirconia binary oxide synthesis

3.2.2 Heteropolyacid salt synthesis

Cesium salt of $H_3PW_{12}O_4$ and $H_4SiW_{12}O_4$ were obtained by titrating an aqueous solution of $H_3PW_{12}O_4$ or $H_4SiW_{12}O_4$ (0.08 M) with an aqueous solution of Cs_2CO_3 (0.25 M) while stirring. The resulting precipitate was dried at 110 °C for 12 h in vacuum and then calcined at 300 °C for 3 h.

3.2.3 Phosphated titania synthesis

This is a two stage material synthesis involving initial preparation of titanium hydroxide hydrate ($Ti(OH)_4$) followed by impregnation with ammonium phosphate monobasic ($(NH_4)_3PO_4$). Firstly, $Ti(OH)_4$ was prepared following the procedure described in section 3.2.1 but without the addition of zirconia alkoxide. Typically, titanium IV butoxide was added dropwise into an aqueous solution containing *n*-butanol under stirring. The pH of the solution was adjusted to 7 by adding ammonium hydroxide solution and the resulting solution was maintained under reflux for 24 h. After gelation, excess solvent was removed under reduced pressure in a rotary evaporator followed by vacuum drying at 80 °C overnight. Phosphated TiO_2 was then prepared by impregnating the resulting $Ti(OH)_4$ with an aqueous solution of required amount of $(NH_4)_3PO_4$. $Ti(OH)_4$ was slurred in a minimum amount of ammonium phosphate solution. The mixture was stirred for 4 h before the

removal of excess water by evaporation and then followed by drying at 80 °C overnight. Calcination of the dried sample at 600 °C for 4 h was done to achieve the phosphated TiO_2. Other ammonium salts such as ammonium molybdate, ammonium metavanadate and ammonium metatungstate were used in a similar manner as phosphate treatment of $Ti(OH)_4$ in order to study the effect of different anions on catalytic performance of TiO_2. Samples were designated as x-TiO_2, where x represents P, Mo, V and W heteroatoms.

3.3 Materials characterization

3.3.1 X-ray diffraction (XRD)

Powder XRD measurements were performed on a Rigaku Miniflex with a monochromatic CoKα radiation operated at 30 kV and 15 mA. Data collection was collected in a range of 2θ values between 10 ° and 90 ° using a step size of 0.02 and 1 s step time.

3.3.2 Nitrogen sorption measurement

Nitrogen adsorption data were collected using a Micromeritics TriStar II 3020 surface area and porosity analyzer. Prior to physisorption measurements, all samples were outgassed under vacuum at 200 °C overnight. The specific surface area of the oxides was determined applying the BET method. Total pore volume was estimated from the amount of adsorbed N_2 at relative pressure P/P_o value of 0.99.

3.3.3 High resolution transmission electron microscopy (HR-TEM)

High resolution transmission electron microscopy of the nanoparticles was recorded on a JEOL 2100 microscope operated at 200 kV. Prior to the microscopy analysis, samples were ultrasonically dispersed in ethanol and transferred to carbon-coated copper grids.

3.3.4 Field emission scanning electron microscopy (FE-SEM)

The surface morphology of the nanoparticles was investigated by a field emission-scanning electron microscopy (FE-SEM JEOL JSM 7100F) with an accelerating potential of 20 kV. The instrument was also fitted with energy dispersive x-ray (EDX) as a chemical microanalysis technique to characterize the elemental composition of the nanoparticle.

3.3.5 Raman spectroscopy

Raman spectroscopy was performed on a Reinshaw In-Via Raman microscope equipped with a Leica DM LM Microscope using a 633 nm HPNIR diode laser as an excitation source. An x50

objective lens of 8 mm optical length was used to focus the depolarized laser beam on a spot of approximately 3 μm in diameter, with the laser power at 5 mW. The raman spectra were collected with a CCD array detector in the region of 100–2000 cm^{-1} at 4 cm^{-1} resolution and acquisition time of 1 s.

3.3.6 Temperature programmed desorption of ammonia and CO_2

Temperature-programmed desorption of ammonia and CO_2 was carried out using Micromeritics AutoChemII Chemisorption Analyzer equipped with a thermal conductivity detector to determine the amount and strength of the acid-base sites present on the samples. About 70 mg of each sample was loaded in a quartz U-tube and pretreated at 500 °C in a flow of He (50 ml min^{-1}) for 1 h. This was followed by saturating the sample with ammonia (15 vol.% in He) or CO_2 at 100 °C for 30 min. Physisorbed probe gas on the sample surface was removed by purging the system with He stream for 2 h at 100 °C. The sample was then heated linearly at a heating rate of 10 °C/min from 100 to 800 °C in a flow of He (25 ml/min) while monitoring the ammonia or CO_2 desorption profile using TCD.

3.3.7 Pyridine adsorption with fourier transform infrared spectroscopy (FT-IR)

Pyridine infrared spectroscopy analysis was used to identify the nature of surface acid sites. Prior to pyridine adsorption, the catalysts were activated at 200 °C under vacuum for 1 h, and then cooled to 150 °C. Pyridine is then admitted into the system to saturate the exposed catalyst surface (50 mg, 25 mm thickness). Chemisorption of pyridine was maintained at 150 °C for 30 min. Gaseous and physisorbed pyridine were then evacuated under the flow of N_2 gas at 150 °C for another 30 min. FT-IR spectra of the samples were recorded at room temperature with a Nicolet 6700 (Smart Orbit Accessory). The concentration of Brønsted and Lewis acid sites were estimated using the Lambert-Beer Law in the form $C = A/(\varepsilon\rho)$, where C is the concentration of the vibrating species (μmol g^{-1}), A is the intensity of the band (cm^{-1}), ε is the integration extinction coefficient (cm μmol^{-1}) and ρ is the sample thickness (g cm^{-2}).[1] Values of 1.67 cm μmol^{-1} and 2.22 cm μmol^{-1} were used as the integrated molar extinction coefficients for pyridine bands at 1545 cm^{-1} (PyB) and 1455 cm^{-1} (PyL), respectively.[2]

3.3.8 X-ray photoelectron spectroscopy (XPS)

X-ray photoelectron spectra (XPS) was acquired using a Kratos Axis ULTRA X-ray photoelectron spectrometer equipped with a 165 mm hemispherical electron energy analyser using a monochromatic Al Kα (1486.6 eV) X-ray source at 150 W (15 kV, 10 mA). A survey wide scan

was collected at analyzer pass energy of 160 eV and multiplex (narrow) high resolution scans at 20 eV. Base chamber pressure in the analysis chamber was 1.0 x 10^{-9} Torr and it increased to 1.0 x 10^{-8} Torr during sample analysis. The binding energies were referenced to the C 1s peak of adventitious carbon at 284.8 eV to account for the charging effects. Data analysis was done using Casa-XPS (v 2.3.12) employing a Shirley-background subtraction prior to fitting the spectra using Gaussian–Lorentzian curves.

3.3.9 Elemental microanalysis for C, H, N, S, O

A CHNS-O elemental analyzer (FLASH EA 1112 series, Thermo Electron Corporation) was used to analyze the carbon content of fresh and spent catalyst samples. The technique used is based on a modification of the classical Pregl and Dumas method. Accurately weighed samples of approximately 2 mg (to 3 decimal places in the mg range) in a lightweight tin capsule are dropped at preset intervals of time into a vertical quartz combustion tube maintained at 900 °C, through which a constant flow of helium is run. When the sample is introduced, the helium stream is temporarily enriched with pure oxygen. Flash combustion takes place, primed by the oxidation of the tin container. Quantitative combustion is then achieved by passing the mixture of gases over tungstic oxide. The mixture of gases is then passed over copper to remove the excess of oxygen and reduce oxides of nitrogen to nitrogen. The gaseous products were separated chromatographically and analyzed with a thermal conductivity detector (TCD).

3.3.10 Inductively coupled plasma atomic emission spectroscopy (ICPAES)

Compositional analysis was examined using ICP measurement. The procedure involves sample digestion in 5 mL nitric acid and 4 mL hydrofluoric acid using a Milestone Ethos-1 microwave digester. Digested solid samples were then analyzed using a Varian Vista Pro ICPOES instrument

3.4 Biomass pretreatment

3.4.1 Biomass crushing

Prior to biomass crushing, the samples are washed with hot water to remove dirt and other extractives and dried in oven at 50 °C. The samples were then coarsely pulverized using Culatti Microhammer mill with 1.5 mm screen.

3.4.2 Biomass fractionation

Two-stage fractionation of rice husk and sugarcane bagasse was employed. Firstly, the biomass sources were treated with 2.5% NaOH at 80 °C for 2 h in a solid/liquid ratio (g/mL) of 1:10 for rice husk and 1:15 for sugarcane bagasse. The resultant material was washed with copious amount of

water until neutral, filtered and dried. Subsequently, OrganoCat processing was carried out following the procedure reported by Grande et al.[3] In a one-pot system with two liquid phases (2:1 water:MeTHF) and oxalic acid (0.1 M regarding the aqueous phase), the alkali-treated biomass (i.e rice husk and sugarcane bagasse) was separated into its main components: cellulose, hemicellulose sugars (mostly xylose) and lignin. Under these conditions, hemicellulose is selectively hydrolyzed via acid catalysis, while lignin is partially extracted in situ to the organic phase. The reaction is conducted in a parr reactor with 100 g L^{-1} (referring to the aqueous phase) rice husk or 66.7 g L^{-1} (referring to the aqueous phase) sugarcane bagasse. The temperature was set at 140 °C for 3 h and the reactor pressurized to 20 bar with Ar. After cooling and depressurization of the reactor, the organic phase was separated by decantation, and MeTHF was evaporated to obtain the lignin fraction. The aqueous phase was filtered to isolate the cellulose-rich pulp which was washed with ethanol and dried.

3.4.3 Mechanocatalytic depolymerization of cellulose/biomass

Mechanocatalytic depolymerization of cellulose/biomass was conducted by ball milling of acidulated substrate sample with sulphuric acid as described previously.[4] In a typical method, H_2SO_4 (2.5 mmol) was diluted to a volume of 40 mL. Sigmacell microcrystalline cellulose/biomass (10 g) was then added to this solution, and the solution was stirred for a few minutes. The resultant slurry was dried under a reduced pressure in a rotary evaporator, followed by overnight air drying at 50 °C. The acidulated cellulose/biomass thus obtained was then milled in a planetary ball mill using 5 mm stainless steel balls, with a substrate to ball weight ratio of 1:10. The mill was operated at 400 rpm, with a 15 min pause after every 30 min of continuous milling for a total milling time of 10 h. The milling time reported refers only to the active milling time. The pause allowed dissipation of heat generated during milling, which prevented overheating of reactants.

3.5 Catalyst Evaluation

3.5.1 Batch reactor

A 300 ml stainless steel reactor (series 4840, Parr Instrument Co, Illinois) fitted with gas inlet, outlet valves, a liquid sampling valve, pressure gauge, rupture disc, magnetic drive and a thermocouple was used for the conversion reaction of biomass-derived carbohydrates into HMF. Temperature and stirring speed of the reactor were controlled using a Parr PID controller, model 4844. The reactor was heated with an external mantle while the temperature of the reactor was measured with a J-type thermocouple and maintained at ±2 °C for the set temperature. The pressure

inside the reactor was measured with a pressure gauge. The schematic diagram of the apparatus set-up is shown in Figure 3.2.

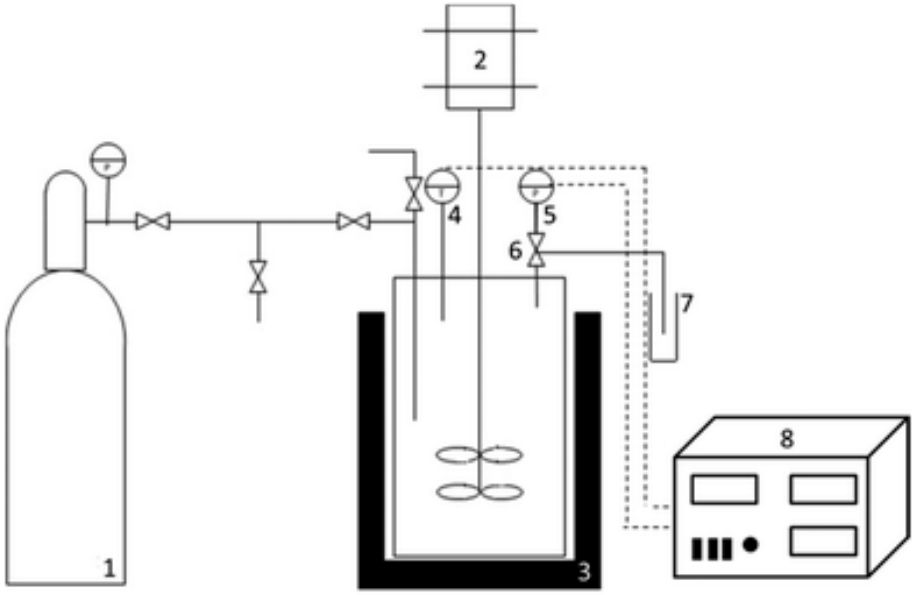

Figure 3.2 Schematic diagram of the batch reactor set-up for carbohydrates conversion reaction to HMF. 1 – Ar cylinder; 2 – magnetic drive; 3 – heating mantle; 4 – thermocouple; 5 – pressure guage; 6 – depressurization valve; 7 – vial for sample collection; 8 – pressure and temperature PID controller.

Catalytic experimental runs were conducted by loading the reaction vessel with the reaction feed, catalyst and solvent. The reactor was sealed, flushed with Ar and then pressurized to 20 bar initial pressure with Ar gas at room temperature. Then, the reactor was heated to the desired temperature and an agitation speed of 500 rpm was maintained constant. During the transformation reaction, liquid samples were withdrawn periodically for analyses. At the end of the reaction, the reactor was rapidly cooled and when the temperature is below 40 °C, the gradual was gradually depressurized.

3.5.2 Flow reactor

Continuous flow reactions were performed on a custom-built packed fixed-bed reactor system as shown in Figure 3.3. A U-shaped fixed-bed reactor was designed by using 1/4 in. OD SS316 Swagelok tubing and tube fittings. Two Alltech HPLC pumps were used to introduce the feedstock: for aqueous sugar solution and organic solvent, into the reactor. The residence time is adjusted by regulating the flow rate of the reaction mixture ranging from 0.2–0.4 mL min^{-1}. The catalyst powder without pelletization was packed inside the reactor and supported by small amounts of quartz wool on both sides of the reactor to hold the catalyst in place. A 7 μm Swagelok inline filter

was connected to the reactor exit, which was followed by a Swagelok back pressure regulator to control the pressure of the reaction system which was maintained at 60 bar. The reactor was heated by means of silicone oil bath set at the reaction temperature. The reaction was started after the feed flow has reached a steady state. Reaction products were collected periodically in sample vials and centrifuged to recover the supernatant prior to analysis.

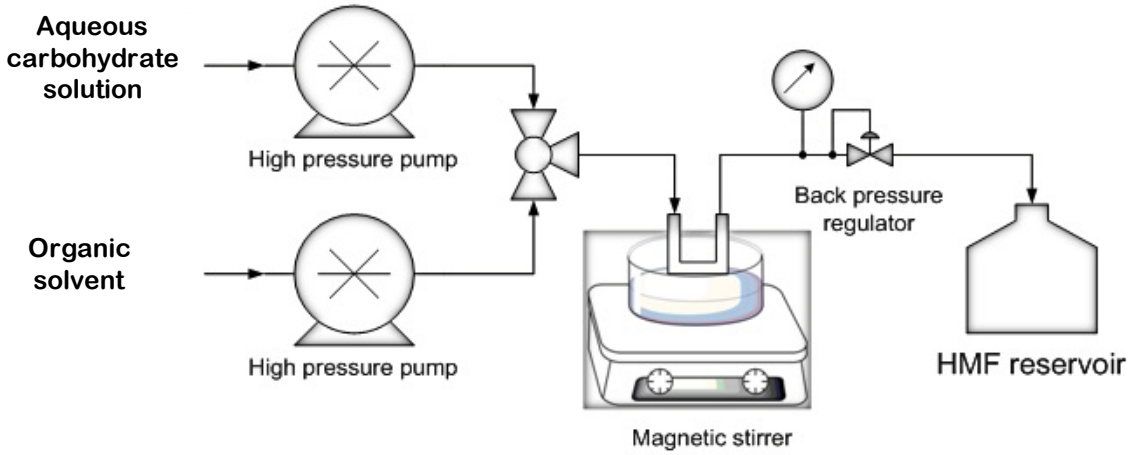

Figure 3.3 Schematic diagram of a biphasic flow reactor set-up.

3.6 Product analysis

Reaction products were analyzed using Shimadzu Prominence HPLC equipped with an analytical column (Bio-Rad Aminex HPX-87H) and both refractive index (RID-10) and UV-Vis (SPD-M20A) as detectors. Prior to analysis, the liquid samples were centrifuged at 13000 rpm for 4 min to recover supernatant which was loaded in a HPLC vial and loaded onto the autosampler. The HPLC was operated under the following conditions: oven temperature – 50 °C, mobile phase – 5 mM H_2SO_4; flow rate – 0.6 mL min^{-1}; injection volume – 10 µL. Commercially available Standard samples were used to establish the calibration curves using external standard method. Product identification was also done using Shimadzu GCMS-QP2010 Ultra equipped with Rxi-5ms column and flame ionization detector (FID).

References

1. A. A. Budneva, E. A. Paukshtis and A. A. Davydov, *React Kinet Catal Lett*, 1987, 34, 63-67.
2. C. A. Emeis, *Journal of Catalysis*, 1993, 141, 347-354.
3. P. M. Grande, J. Viell, N. Theyssen, W. Marquardt, P. Dominguez de Maria and W. Leitner, *Green Chemistry*, 2015, 17, 3533-3539.
4. A. Shrotri, L. K. Lambert, A. Tanksale and J. Beltramini, *Green Chemistry*, 2013, 15, 2761-2768.

Chapter 4

Catalytic behaviour of TiO_2–ZrO_2 binary oxide synthesized by sol-gel process for glucose conversion to 5-Hydroxymethylfurfural

This chapter was published in RSC Advances, 2015, 5, 80346-80352

Catalytic behaviour of TiO_2–ZrO_2 binary oxide synthesized by sol-gel process for glucose conversion to 5-Hydroxymethylfurfural

Luqman Atanda,[a] Adib Silahua,[b] Swathi Mukundan,[a] Abhijit Shrotri,[c] Gilberto Torres-Torres[b] and Jorge Beltramini[a]

[a] *Nanomaterials Centre, Australian Institute for Bioengineering & Nanotechnology and School of Chemical Engineering, The University of Queensland, Brisbane, St. Lucia 4072, Australia*

[b] *Heterogeneous Catalysis Laboratory, Universidad Juárez Autónoma de Tabasco, Cunduacán, Tabasco, México*

[c] *Catalysis Research Center, Hokkaido University, Saporro, Japan.*

Abstract

The catalytic application of as-synthesized TiO_2–ZrO_2 binary oxides was examined for the conversion of glucose to produce 5-hydroxymethylfurfural (HMF). Highest HMF yield (74%) at glucose concentration of 5 wt% was obtained with TiO_2–ZrO_2 (1/1) and Amberlyst 70 catalyst system in a water-THF biphasic reaction system. Notably, a much higher HMF yield (86%) was achieved when the organic phase of the biphasic system was replaced with dioxane. The increased product yield may be ascribed to the role of dioxane as an aqueous phase modifier that stabilizes HMF in the reactive phase as well as promotes partitioning of HMF into the extractive layer. Furthermore, the combined catalyst and biphasic solvent systems were also effective for the conversion of glucose polymers to HMF.

4.1 Introduction

Diversification of energy sources to reduce dependence on fossil fuels has motivated a strong research interest to attain sustainability in biomass conversion to transportation fuels and chemical building blocks.[1-6] For example, 5-hydroxymethylfurfural (HMF), which is a dehydration product of biomass-derived carbohydrates, has been identified as a versatile intermediate for value-added chemicals and biofuels.[7, 8] Conventionally, HMF is produced by triple dehydration of hexoses in an acidic medium.[9] Throughout these studies, it is generally accepted that glucose is less reactive than fructose because of its stable glucopyranose structure.[10, 11] However, glucose is a preferred starting material since it is cheaper and relatively available in abundance.[12, 13] Significant improvement on glucose conversion to HMF can be attained by performing the reaction in the presence of a metal halide, which catalyzes the isomerization of glucose to fructose, in tandem with mineral acids[14, 15] or acidic ionic liquid.[16-19] In spite of these recent achievements, efficient isolation and purification of HMF from the reaction medium remains a challenge.[20] On the other hand, heterogeneous catalysis is a promising cost-effective route for large scale HMF synthesis due to ease of catalyst handling, simple separation and recovery steps.

Several metal oxides, such as titania (TiO_2) and zirconia (ZrO_2) have been reported to possess exceptional redox and acid-base properties, which makes them a good choice as catalysts and catalyst supports.[21] Moreover, catalytic property of these oxides can be improved by mixing them together. This improvement is attributable to the generation of new catalytic sites due to strong interaction between the individual oxides, giving rise to a mixed metal oxide of profound surface acid-base properties and high thermal stability.[21] Thus, the superior properties of TiO_2–ZrO_2 binary oxide make it more suitable for catalytic applications than individual component oxide.[22-25] However, limited reports exist on the catalytic potential of TiO_2–ZrO_2 binary oxide to transform biomass-derived carbohydrates to HMF. Chareonlimkun and co workers[26] explored simultaneous hydrolysis/dehydration of a variety of lignocellulosic biomass under hot compressed water. They found that superior product yield was achieved with TiO_2–ZrO_2 binary oxide in comparison with TiO_2 and ZrO_2, which was ascribed to the synergy between the base sites of ZrO_2 and acid sites of TiO_2. Furthermore, catalyst preparation technique and calcination temperature were two parameters observed to influence the acid-base properties of the oxides, hence their catalytic reactivity.

In this study, we prepared a series of TiO_2–ZrO_2 binary oxides by a neutral amine sol-gel technique. The effect of TiO_2/ZrO_2 weight ratio on the acid-base properties of the binary oxides was examined by temperature programmed desorption of NH_3 and CO_2. Furthermore, the pyhsico-chemical properties of the oxide materials were investigated with N_2 adsorption-desorption, XRD, Raman and XPS techniques. We evaluated their catalytic performance in transforming glucose to

HMF using water as the reaction solvent. In addition, the cooperative role of a co-solvent and a solid Bronsted acid co-catalyst was examined. Thereafter, the robustness of the reaction system was extended to other sugar substrates such as cellobiose, sucrose and cellulose.

4.2 Experimental

4.2.1 Chemicals and materials

Glucose, fructose, sucrose, cellobiose, cellulose, 5-hydroxymethylfurfural (HMF), levoglucosan, titanium IV butoxide, zirconium IV butoxide, ammonium hydroxide solution (28 wt%), phosphotungstic acid ($H_3PW_{12}O_4$), silicotungstic acid ($H_4SiW_{12}O_4$), propan-1-ol, butan-1-ol, Methyl isobutyl ketone (MIBK) and Nafion NR50 were obtained from Sigma-Aldrich. Tetrahydrofuran and 1,4-dioxane were obtained from Merck Millipore. Amberlyst 70 was supplied by Roms and Haas. All the chemicals were used without further purification. Ultrapure water (18.2 $M\Omega\ cm^{-1}$) from Elga distillation system was used for all the experiment.

4.2.2 Preparation of TiO_2–ZrO_2 binary oxides

TiO_2, ZrO_2 and a series of TiO_2–ZrO_2 with varying weight percentage of TiO_2 to ZrO_2 were prepared by sol-gel method. The sol was prepared by the dropwise addition of the alkoxide precursors into an aqueous solution containing butan-1-ol under stirring. The pH of the solution was adjusted to 7 by adding ammonium hydroxide solution and the resulting solution was maintained at 70 °C under reflux for 24 h. After gelation, excess solvent was removed using rotary evaporator and followed by vacuum drying at 120 °C for 12 h. The dried samples were then calcined at 500 °C for 12 h to obtain the corresponding pure or mixed oxides.

4.2.3 Preparation of heteropolyacid salts - $Cs_{2.5}PW$ and $Cs_{3.5}SiW$

Cesium salt of $H_3PW_{12}O_4$ and $H_4SiW_{12}O_4$ were obtained by titrating an aqueous solution of $H_3PW_{12}O_4$ or $H_4SiW_{12}O_4$ (0.08 M) with an aqueous solution of Cs_2CO_3 (0.25 M) while stirring. The resulting precipitate was dried at 110 °C for 12 h in vacuum and then calcined at 300 °C for 3 h.

4.2.4 Catalyst characterization

Powder XRD measurements were performed on a Rigaku Miniflex with a monochromatic CoKα radiation (30 kV, 15 mA) in the 2θ range 10–90 °. Nitrogen adsorption data were collected using a Micromeritics TriStar II 3020 surface area and porosity analyzer. Prior to physisorption measurements, all samples were outgassed under vacuum at 200 °C overnight. The specific surface area of the oxides was determined applying the BET method. Total pore volumes were estimated

from the amount of adsorbed N_2 at p/p_o value of 0.99. Temperature programmed desorption (TPD) of ammonia and CO_2 were performed on a BEL Japan BELCAT-A instrument equipped with a mass spectrometer and thermal conductivity detector (TCD). This was used to determine the amount and strength of the acid-base sites available on the catalyst samples. About 70 mg of sample was saturated with either NH_3 or CO_2 as the probe gas at 100 °C, flushed with He to remove physisorbed gas and then ramped to 800 °C at a heating rate of 10 °C/min under He flow. Pyridine infrared spectroscopy was used to determine the nature of surface acid sites. Pyridine was chemisorbed on the catalyst surface (50 mg) at 150 °C. Excess gaseous and physisorbed pyridine were removed by holding the temperature at 150 °C for 30 min under N_2 flow. FTIR spectra were collected using a Nicolet 6700 (Smart Orbit Accessory) at 128 scans and 4 cm^{-1} resolution. X-ray photoelectron spectra (XPS) of the catalysts was acquired using Kratos Axis ULTRA X-ray photoelectron spectrometer equipped with a 165 mm hemispherical electron energy analyser using a monochromatic Al Kα (1486.6 eV) x-ray source. The binding energies were referenced to C 1s peak at 284.8 eV. Raman spectroscopy was performed on a Reinshaw In-Via Raman microscope equipped with a Leica DM LM Microscope using a 633 nm HPNIR diode laser as an excitation source. The raman spectra were collected with a CCD array detector in the region of 100–2000 cm^{-1} at 4 cm^{-1} resolution and acquisition time of 1 s.

4.2.5 Catalytic activity procedure and product analysis

Glucose conversion to HMF was carried out in a Parr reactor. In a typical experimental run, required amount of glucose, solvent and catalysts were charged into a 300 mL reactor, purged with high purity Ar and then pressurized to 30 bar. The reactor was ramped to its set point temperature which was monitored by a thermocouple inside a thermowell immersed in the reaction mixture. Time zero of the reaction was defined as the time when the reactor reached its set point temperature usually after approx. 9 mins of ramping. Catalytic runs were repeated for data reproducibility. Experimental errors were in the range of ±2%. Liquid samples were taken after reaction and the concentration of the product species were quantified using Shimadzu Prominence HPLC with a Bio-Rad Aminex HPX-87H as the analytical column and both RID–10 (refractive index) and SPD–M20A (UV–Vis) as detectors. The HPLC was operated under the following conditions: oven temperature, 50 °C, mobile phase, 5 mM H_2SO_4; flow rate, 0.6 ml/min; injection volume, 20 µL. The concentrations of glucose, fructose, HMF and other identifiable products were quantified by HPLC analysis through the external standard method and calibration curves of commercially

available standard substrates. Glucose conversion (Conv. mol %) and products yield (mol %) were calculated according to:

$$Conv.(mol\%) = \left(1 - \frac{nC_6}{nC_6^o}\right) \times 100\%$$

$$\text{Pr}oduct\ yield\ (mol\%) = \left(\frac{n_i}{nC_6^o}\right) \times 100\%$$

where nC_6 and nC_6^o denote number of moles of C_6 sugar in the product and feed, respectively, and n_i is the number of moles of identified products (HMF, levulinic acid, levoglucosan etc.).

4.3 Results and discussion

4.3.1 Characterization of TiO_2–ZrO_2 binary oxides

The crystalline phases of TiO_2, ZrO_2, and TiO_2–ZrO_2 binary oxides were investigated using XRD analysis. The XRD pattern of the oxides is shown in Figure 4.1.

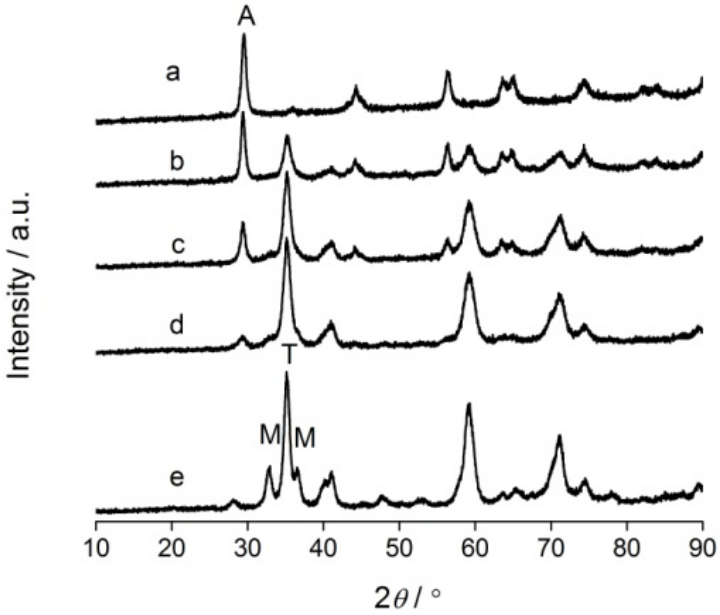

Figure 4.1 XRD patterns of: a) TiO_2, b) TiO_2–ZrO_2 (3/1), c) TiO_2–ZrO_2 (1/1), d) TiO_2–ZrO_2 (1/3) and e) ZrO_2. A: anatase; M: monoclinic; T: tetragonal

The indexed diffraction pattern of TiO_2 revealed that it exists as anatase phase, whereas for ZrO_2, a combination of monoclinic (*m*-ZrO_2) and tetragonal (*t*-ZrO_2) phases were identified, corresponding

to 2θ values of 28.1 ° and 35.1 °, respectively. However, in the case of the binary oxides, regardless of the TiO_2/ZrO_2 ratio, Figure 4.1(b-d) show a composite diffraction pattern that corresponds to the anatase-TiO_2 (2θ = 29.5 °) and *t*-ZrO_2 (2θ = 35.1 °) phases. The *m*-ZrO_2 phase ceases to exist even with the smallest TiO_2/ZrO_2 ratio i.e. 1:3. This indicates that *t*-ZrO_2 phase was stabilized due to the presence of Ti atom in ZrO_2 lattice, which results in dissimilar grain boundaries that prevents the formation and crystal growth of the monoclinic phase.[27] Moreover, no diffraction peaks related to zirconium titanate phase could be detected. It may be that this phase is composed of very small particles below detection limit or could exist in an amorphous state. Surface area and pore volume as determined by N_2-adsorption measurement are summarized in Table 4.1. The surface areas of TiO_2 and ZrO_2 are 79.4 m^2/g and 40.8 m^2/g, respectively. ZrO_2 has the lowest surface area of all the oxides. Surface areas of the binary oxides gradually increase as it becomes enriched with TiO_2.

Table 4.1 Textural and acid-base properties of the mixed oxides

Catalyst	S_{BET}[a] (m^2/g)	Pore vol[b] (cc/g)	Acid site conc.[c] (μmol/g)	Basic site conc.[d] (μmol/g)
TiO_2	79.4	0.33	476.6	12.1
TiO_2–ZrO_2 (3/1)	68.0	0.27	469.8	16.7
TiO_2–ZrO_2 (1/1)	62.0	0.18	452.3	23.7
TiO_2–ZrO_2 (1/3)	60.0	0.13	372.2	27.5
ZrO_2	40.8	0.12	202.1	34.2

[a] Specific surface area calculated by the BET method.
[b] Pore vol calculated at P/P_o = 0.99.
[c] Calculated from ammonia–TPD.
[d] Calculated from CO_2–TPD

Table 4.1 also reports the acid–base property of the oxides measured by temperature programme desorption (TPD). From the table it can be seen that as the ZrO_2 content increases, acidity of the oxides reduces with a corresponding increment in basicity. Furthermore, the distribution and strength of the acid and base sites is shown in Figure S4.1. Acid[28] and base[29] strength is categorized as low, medium and strong, depending on desorption temperature. The CO_2–TPD profile of ZrO_2 (Figure S4.1(a)) shows three peaks centered at 185 °C, 550 °C and 610 °C, which can be attributed to weak and strong basic sites, respectively. Meanwhile, TiO_2 is predominantly characterized with a small broad peak centered at 600 °C corresponding to strong basic site. TiO_2–ZrO_2 (1/1) has a CO_2 desorption profile defined by two well resolved peak signals centered at 170 °C and 550 °C, similar to that of ZrO_2. On the other hand, ammonia desorption profile of the oxides is shown in Figure

S4.1(b). TiO_2 shows a large concentration of weak-to-medium strength acid sites, whereas ZrO_2 is characterized by strong acid sites albeit weak concentration. TiO_2–ZrO_2 (1/1) shows a composite profile of high concentration of weak-to-medium acid sites and low concentration of strong acid sites. The nature of the acid sites available on the oxides was identified through infrared spectra of adsorbed pyridine. As shown in Figure 4.2, the peak intensities observed indicates the oxides are characterized by Lewis acid sites. Pure TiO_2 displays intense bands at 1446 cm^{-1} and 1608 cm^{-1} with moderate bands at 1489 cm^{-1} and 1575 cm^{-1}.

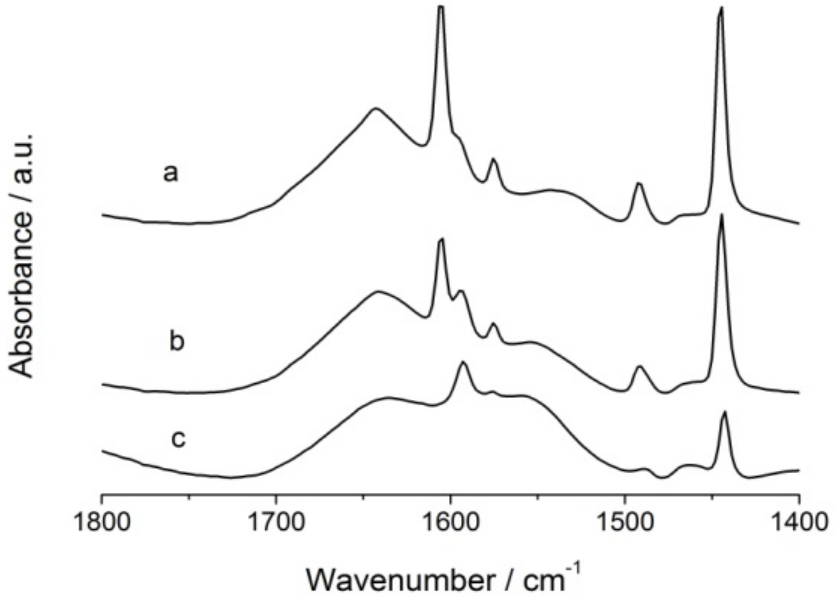

Figure 4.2 Infrared spectra of pyridine adsorbed on: a) TiO_2, b) TiO_2–ZrO_2 (1/1) and c) ZrO_2

Meanwhile, pure ZrO_2 showed fewer and less intense bands, which agrees well with NH_3–TPD result that ZrO_2 has fewer acid sites than TiO_2. TiO_2–ZrO_2 (1/1) mixed oxide has peak reflections similar to TiO_2, though with slightly reduced intensity. Moreover, it has an extra peak at 1590 cm^{-1}, which is a reflection of ZrO_2.

Surface analysis of the oxides was examined by Raman and XPS. Raman spectra of all the oxides are shown in Figure 4.3. Figure 4.3(a) depicts Raman spectrum of TiO_2 is dominated by vibrational bands at 144, 400, 515 and 635 cm^{-1}, which can be attributed to $v_1(E_g)$, $v_2(B_{1g})$, $v_3(A_{1g})$ or $v_3(B_{1g})$ and $v_4(E_g)$, respectively, of anatase-TiO_2 phase.[30] $v_1(E_g)$ and $v_2(B_{1g})$ represent the O–Ti–O bending vibrational mode, whereas $v_3(A_{1g})$ or $v_3(B_{1g})$ and $v_4(E_g)$ represent the Ti–O bond stretching vibrational mode.[31]

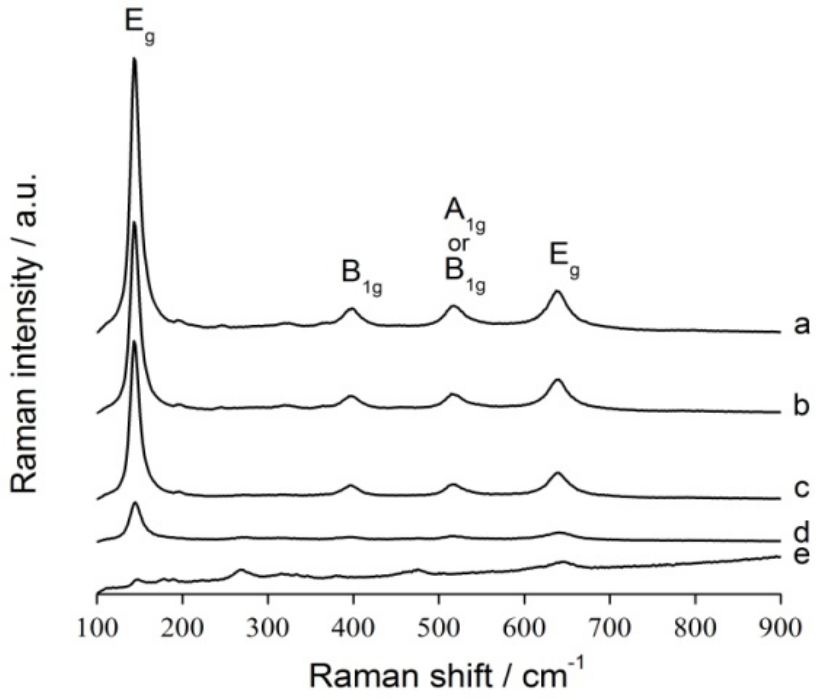

Figure 4.3 Raman spectra of: a) TiO_2, b) TiO_2–ZrO_2 (3/1), c) TiO_2–ZrO_2 (1/1), d) TiO_2–ZrO_2 (1/3) and e) ZrO_2

Figure 4.3(b-d) shows that the intensity of these bands attenuates gradually as the binary oxide becomes enriched with ZrO_2. Elemental surface compositions and binding energies from the XPS analysis are listed in Table 4.2. The changes in the surface composition of Ti and Zr atoms are consistent with the observed pattern in the Raman intensities of the oxides, wherein elemental composition of Ti declines as ZrO_2 content is increased. This indicates mutual interaction between the oxides as a result of Ti^{4+} substitution with Zr^{4+} and vice versa, which is also accompanied by structural changes as depicted by the variations in the Raman signals of the metal oxides.

Table 4.2 Binding energies and surface composition of TiO_2–ZrO_2 mixed oxides from XPS

Sample	Surface atoms (%)			BE (eV)			
	Ti	Zr	C	O/(Ti+Zr)	O 1s	Ti $2p_{3/2}$	Zr $3d_{5/2}$
TiO_2	20.3	-	33.4	2.28	529.9	458.6	-
TiO_2–ZrO_2 (3/1)	17.8	3.3	32.2	2.21	529.9	458.6	182.0
TiO_2–ZrO_2 (1/1)	13.0	7.5	34.5	2.20	529.9	458.6	182.1
TiO_2–ZrO_2 (1/3)	7.1	15.5	29.6	2.12	529.9	458.6	182.2
ZrO_2	-	22.3	29.0	2.18	529.8	-	182.2

Significant carbon atom was also identified on all the oxides. This carbon impurity may be understood to come from the alkoxy groups originating from the sol-gel process. The binding energies associated with Ti $2p_{3/2}$, Zr $3d_{5/2}$ and O 1s are also reported in Table 4.2. Binding energies of 458.6 eV and 182.2 eV corresponds to Ti $2p_{3/2}$ and Zr $3d_{5/2}$ of TiO_2 and ZrO_2 single oxide, respectively. O 1s peak of TiO_2 and ZrO_2 are assigned 529.9 eV and 529.8 eV binding energies, respectively. These values confirm that both Ti and Zr exist in the tetravalent oxidation state.[32] As for the binary oxides, Ti $2p_{3/2}$ has similar binding energy as that of pure TiO_2 while Zr $3d_{5/2}$ is about 0.1–0.2 eV lower than that of pure ZrO_2. This shift towards lower binding energy may indicate the substitution of some Zr^{4+} ions with Ti^{4+}, thereby causing reduction of interatomic potentials due to reduced overall atomic size.[33]

4.3.2 Activity tests

Catalytic application of the metal oxide system was examined for the conversion of biomass-derived sugars into HMF, using glucose as a model compound. Initial reactivity study conducted with water as the reaction medium was used to evaluate catalytic performance of the oxides. Dependence of glucose conversion capacity and products yield in relation to the composition of TiO_2/ZrO_2 binary oxide is shown in Figure 4.4. It can be seen from the Figure that glucose conversion ranges from 72–86%, with HMF as the main product. With increase in ZrO_2 content of the binary oxide, glucose conversion decreases whereas yield of HMF increases and goes through a maximum at TiO_2/ZrO_2 (1:1) followed by a minor decline.

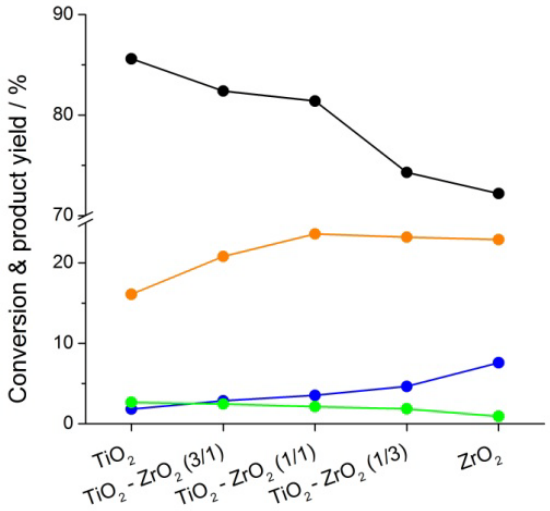

Figure 4.4 Glucose conversion to HMF over TiO_2–ZrO_2 binary oxides in an aqueous medium. Reaction conditions: 2 g glucose, 0.8 g catalyst wt., 3 h reaction time, 175 °C reaction temperature, 100 ml water. (●), glucose conversion and product yields: (●) fructose, (●) HMF, (●) levulinic acid

This occurrence may be interpreted in relation to the acidity of the binary oxides. TiO_2 possesses large concentration of acid sites that can dehydrate fructose, an initial product of glucose isomerization, into HMF. Hence, least concentration of fructose is observed on TiO_2 but the value rises gradually with declining acidity of the binary oxide due to increase in ZrO_2 content. More so, in an aqueous acidic medium, HMF rehydrates to give levulinic acid and may also react with glucose or other reactive intermediates to form humins. Therefore, as TiO_2 content of the binary oxide increases, which correlates to increasing acidity, there is an upward trend of both the yield of levulinic acid and glucose conversion as shown in Figure 4.5. To support this hypothesis, another reaction was conducted at 160 °C for 5 h with fructose as feed but keeping other reaction conditions same. As shown in Table S4.1, fructose conversion of 95.3% and 85.6% was attained on TiO_2 and ZrO_2, respectively. Even though fructose conversion on TiO_2 was superior, a better yield of HMF was achieved on ZrO_2 (29.6 vs 24.1%). Regardless of the pure metal oxide, it is noteworthy that fructose conversion to HMF occurred relatively faster in comparison to glucose. This indicates that glucose proceeds via fructose to produce HMF. From Figure 4.4, an optimum HMF yield of 23.6% is obtained with TiO_2–ZrO_2 (1/1), which can be ascribed to modified acid–base properties of the binary oxide. The mutual interaction of the pure oxides provided a moderate acid–base concentration (Table 4.1) suitable for the glucose-to-HMF reaction. This cooperative interaction between the acid–base sites on TiO_2–ZrO_2 has been reported in literature, wherein glucose is isomerized to fructose preferentially on the basic sites of ZrO_2 and subsequent dehydration of fructose to HMF on the acid sites of TiO_2.[26, 34, 35]

Next, we examined the role of reaction medium on the formation rate of HMF. A water-lean medium was considered since the yield of HMF in a single aqueous medium is relatively low. Tetrahydrofuran (THF) was chosen as a co-solvent. It lacks hydroxyl groups and has the potential to suppress side reactions.[36] In spite of adding THF to water in a ratio of 4:1 (v/v) to make up the reaction medium, glucose conversion and yield of HMF were not significantly enhanced as shown in Figure S4.2. Contrarily, a remarkable increment of HMF yield by almost 3 fold from 23.6% to 71% was observed after the introduction of NaCl (20 wt% of the aqueous phase) into the THF/water solvent mix. The addition of NaCl promoted solvent partitioning into two phases: a reactive aqueous phase and an extractive organic phase. This allowed in situ extraction of HMF from the aqueous phase into the organic phase, thereby preventing undesired side reactions. Moreover, the continuous extraction shifts the reaction equilibrium to produce more HMF. Furthermore, we investigate the role of solid Brønsted acid supports such as Amberlyst 70, Nafion NR50, $Cs_{2.5}PW$ and $Cs_{3.5}SiW$

as co-catalysts, as it has been observed that co-existence of Lewis and Brønsted bifunctional acidity promote glucose conversion to HMF.[37, 38] Herein, co-catalysts refer to physical mixture of TiO_2–ZrO_2 (1/1) and the solid Brønsted acid supports. Under comparable reaction conditions, Figure 4.5 clearly demonstrates that the choice of Amberlyst 70 as co-catalyst is the most beneficial, resulting in HMF yield of about 85.6 % at a near-complete glucose conversion. Meanwhile, using the solid Brønsted acid supports without the binary oxide gave lesser HMF yields. For instance, approximately 10% yield HMF was achieved with $Cs_{3.5}SiW$ at complete glucose conversion. This indicates that the dominant route for glucose conversion to HMF is via intermediate fructose formation, which is otherwise promoted by Lewis acid or base isomerisation of glucose.

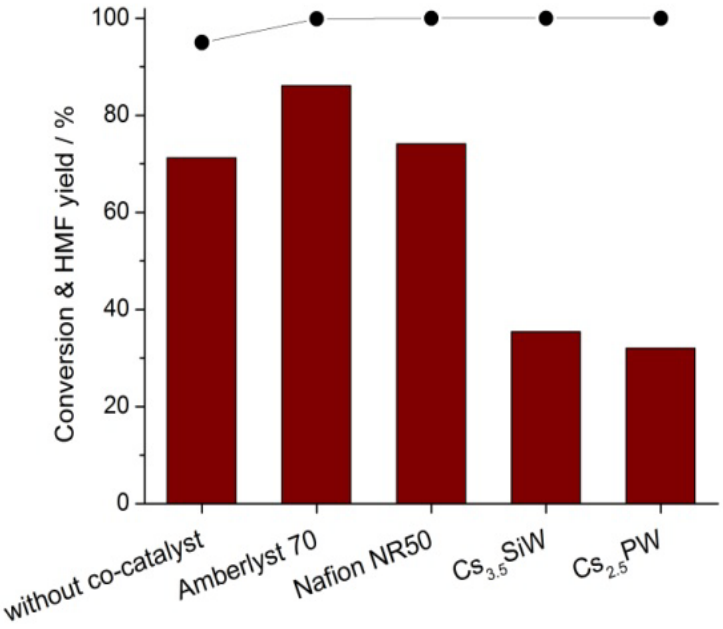

Figure 4.5 Catalytic conversion of glucose over TiO_2–ZrO_2 with solid acid co-catalysts. Reaction conditions: 2 g glucose, 0.8 g catalyst wt. (TiO_2–ZrO_2(1/1)/co-catalyst ratio = 1/1 w/w), 100 ml solvent (THF/water = 4/1 v/v), 4 g NaCl, 3 h reaction time, 175 °C reaction temperature

HMF yield varies with the co-catalysts as follows: Amberlyst 70 (85.6%) > Nafion NR50 (73.4%) > $Cs_{3.5}SiW$ (35.2%) > $Cs_{2.5}PW$ (31.8%). The observed variation can be related to the acid strength of the co-catalysts. $H_3PW_{12}O_{40}$ and $H_4SiW_{12}O_{40}$ are superacids of very strong acid strength (H_0 = –13.6).[39] Nevertheless, $H_3PW_{12}O_{40}$ is slightly more acidic than $H_4SiW_{12}O_{40}$.[40] $Cs_{2.5}PW$ has acid strength similar to the parent phosphotungstic acid[41] and correspondingly, $Cs_{3.5}SiW$ is anticipated to possesses weaker acid strength compared to $Cs_{2.5}PW$. Hammett acidity function, H_0, of Nafion NR50 is –12,[42] whereas Amberlyst 70 has

a similar measure of acidity as Amberlyst 35 with a H_0 value of –5.6.[43] From the H_0 values, Amberlyst 70 possesses the lowest Brønsted acidity. We may infer that there is a linear correlation between Brønsted acid strength and yield of HMF. The stronger the Brønsted acidity, the greater the propensity of HMF to degrade to huminic compounds because of the strong affinity of HMF onto the Brønsted acid sites.[44, 45] For this reason, the pair of TiO_2–ZrO_2 (1/1) and Amberlyst 70 appears to be the optimum catalytic system for the transformation of glucose to HMF. Effectiveness of the catalytic system was further evaluated for HMF synthesis at a higher initial glucose concentration. As shown in Figure S4.6, we observed a reduction in HMF yield as the initial glucose concentration was increased from 2 to 5 wt%, which can be ascribed to polymerization and cross-polymerization of HMF to humins.[46-48] Visually, we observed fine dark-brown powder deposit on the reactor wall, which was more prominent at high glucose concentration. We speculate that the choice of organic solvent of the biphasic system may help reduce the severity of humin compounds formation. Hence, we decided to replace THF with other organic solvents such as 1-butanol, 1-propanol, methyl-isobutyl-ketone (MIBK) and 1,4-dioxane. As shown in Figure 4.6, dioxane was the most effective, selectively producing approximately 86% yield of HMF.

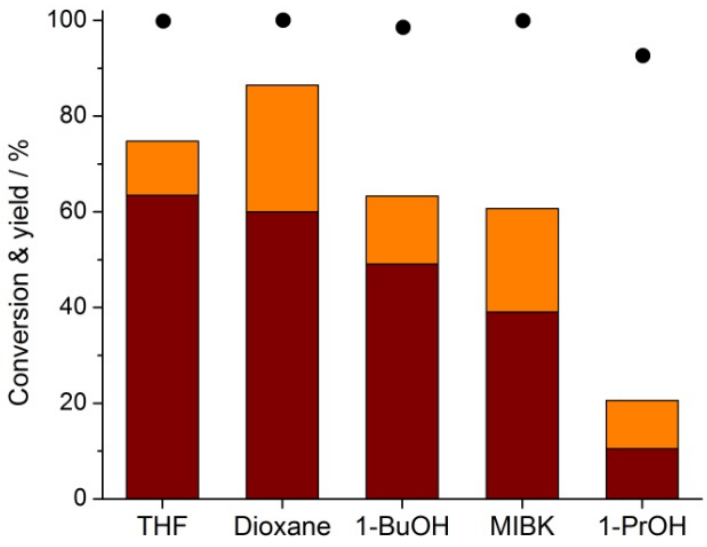

Figure 4.6 Influence of organic solvent in the biphase system on selective HMF yield with TiO_2–ZrO_2 (1/1) and Amberlyst 70 catalysts. Reaction conditions: 5 g glucose, 2 g catalyst weight (TiO_2-ZrO_2/Amberlyst = 1/1 w/w), 100 ml solvent (THF/water = 4/1 v/v), 4 g NaCl, 3 h reaction time, 175 °C reaction temperature. (●) Glucose conversion, (■) HMF_{org} and (■) HMF_{aq}

Not only does dioxane enables good partitioning of HMF into the organic phase, but HMF concentration in the reactive aqueous phase is also highest, suggesting HMF is more stable in the water-dioxane biphase system. Although the cause of this phenomenon is unclear, we consider that the reactive phase was modified by dioxane thereby minimizing degradation of HMF into humins. The outcome of HMF production using water-dioxane biphasic reaction system is promising and provides a step further towards achieving an efficient reaction medium for scaling-up. But dioxane poses a degree of health risk due to its carcinogenic activity,[49] which must be taken into consideration. More so, replacing homogeneous catalysts with solid ones facilitate product separation and solvent recovery, which further improves the attractiveness of biphasic system for industrial application. For instance, we contrasted the catalytic performance of our catalyst system with those reported in literature. Gallo et al.[36] reported HMF yields of 59%, 55% and 63% using a combination of Amberlyst 70 and Sn-Beta with γ-valerolactone, γ-hexalactone and tetrahydrofuran, respectively, as organic solvents of a water-organic biphasic system. Yang et al.[50] demonstrated the conversion of glucose with $AlCl_3$ and HCl using THF as a co-solvent with water to give up to 62% HMF yield. Yang et al.[51] reported 53% yield of HMF using a combination of Sn-Beta and HCl to catalyze glucose dehydration in water with THF as extracting solvent.

Lastly, the catalytic system of TiO_2–ZrO_2 mixed oxide and Amberlyst 70 was examined for the synthesis of HMF using cellobiose, sucrose and cellulose. The result of HMF synthesis from these various sugar substrates is given in Table 4.3.

Table 4.3 Catalytic transformation of sugars to HMF[a]

Entry	Substrate	Temp. (°C)	Conversion (%)	HMF yield (%)
1	Glucose	175	99.9	85.9
2	Sucrose	180	>99	86.5
3	Cellobiose	180	>99	80.8
4	Cellulose	180	42.1	25.5

[a] Reaction conditions: 2 g substrate, solvent volume 100 mL (THF/water = 4/1), 0.8 g catalyst wt. (TiO_2–ZrO_2/Amberlyst 70 = 1), 3 h reaction time, 30 bar Ar pressure.

As observed in Table 4.3, HMF yield from cellobiose and sucrose is above 80%, nevertheless, sucrose gave a better yield. This is because sucrose is a dimer of glucose-fructose molecules, which makes it more reactive than cellobiose, a dimer of glucose-glucose molecules. As anticipated, cellulose was found to be the least reactive with HMF

yield of 25.5%. This is attributable to the strong intermolecular hydrogen bonding of cellulose. A higher temperature such as 200 °C or greater is required for reactivity of cellulose to improve due to increased hydrothermolysis.[52] However, Amberlyst 70 has relatively poor thermal stability at such high temperature, thereby restricting its usage to typically 190 °C.[53]

4.4 Conclusion

We demonstrated that TiO_2–ZrO_2 (1/1) binary oxide is an effective catalyst for the production of HMF from glucose. A water–THF biphasic system remarkably enhanced HMF formation rate. Furthermore, co-addition of Amberlyst 70 to the reaction system selectively improved the formation of HMF. We also show that at relatively high glucose loading (5 wt%), good yield of HMF is achievable. This was further improved by replacing the organic solvent of the biphase system with dioxane, due to its added advantage of modifying the aqueous phase to minimize degradation of HMF to humins. HMF was also obtained in high yields via the transformation of cellobiose and sucrose. Meanwhile, direct conversion of cellulose to HMF was more difficult due to its poor reactivity. Lastly, we conclude that a single multi-functional solid catalytic system and an organic solvent of high partitioning coefficient that can also serve as a phase modifier advance the realization of biphasic reaction system for large scale HMF synthesis.

Acknowledgements

The authors gratefully acknowledge the funding from the Sugar Research Australia (SRA) and ARC Centre of Excellence for Functional Nanomaterials at The University of Queensland, Australia. We also acknowledge the facilities and the scientific and technical assistance of the Australian Microscopy & Microanalysis Research Facility at The University of Queensland.

References

1. G. W. Huber, S. Iborra and A. Corma, *Chemical Reviews*, 2006, **106**, 4044-4098.
2. G. W. Huber and A. Corma, *Angewandte Chemie International Edition*, 2007, **46**, 7184-7201.
3. J. N. Chheda, G. W. Huber and J. A. Dumesic, *Angewandte Chemie International Edition*, 2007, **46**, 7164-7183.
4. F. Cherubini, *Energy Conversion and Management*, 2010, **51**, 1412-1421.
5. J. C. Serrano-Ruiz, R. Luque and A. Sepulveda-Escribano, *Chemical Society Reviews*, 2011, **40**, 5266-5281.
6. R. A. Sheldon, *Green Chemistry*, 2014, **16**, 950-963.
7. J. J. Bozell and G. R. Petersen, *Green Chemistry*, 2010, **12**, 539-554.
8. Y. Román-Leshkov, C. J. Barrett, Z. Y. Liu and J. A. Dumesic, *Nature*, 2007, **447**, 982-985.
9. R.-J. van Putten, J. C. van der Waal, E. de Jong, C. B. Rasrendra, H. J. Heeres and J. G. de Vries, *Chemical Reviews*, 2013, **113**, 1499-1597.
10. J. N. Chheda, Y. Roman-Leshkov and J. A. Dumesic, *Green Chemistry*, 2007, **9**, 342-350.
11. A. Osatiashtiani, A. F. Lee, D. R. Brown, J. A. Melero, G. Morales and K. Wilson, *Catalysis Science & Technology*, 2014, **4**, 333-342.
12. F. W. Lichtenthaler, *Accounts of Chemical Research*, 2002, **35**, 728-737.
13. A. I. Torres, P. Daoutidis and M. Tsapatsis, *Energy & Environmental Science*, 2010, **3**, 1560-1572.
14. Y. J. Pagán-Torres, T. Wang, J. M. R. Gallo, B. H. Shanks and J. A. Dumesic, *ACS Catalysis*, 2012, **2**, 930-934.
15. V. Choudhary, S. H. Mushrif, C. Ho, A. Anderko, V. Nikolakis, N. S. Marinkovic, A. I. Frenkel, S. I. Sandler and D. G. Vlachos, *Journal of the American Chemical Society*, 2013, **135**, 3997-4006.
16. H. Zhao, J. E. Holladay, H. Brown and Z. C. Zhang, *Science*, 2007, **316**, 1597-1600.
17. G. Yong, Y. Zhang and J. Y. Ying, *Angewandte Chemie International Edition*, 2008, **47**, 9345-9348.
18. J. B. Binder and R. T. Raines, *Journal of the American Chemical Society*, 2009, **131**, 1979-1985.
19. M. E. Zakrzewska, E. Bogel-Łukasik and R. Bogel-Łukasik, *Chemical Reviews*, 2011, **111**, 397-417.
20. S. P. Teong, G. Yi and Y. Zhang, *Green Chemistry*, 2014, **16**, 2015-2026.

21. B. M. Reddy and A. Khan, *Catalysis Reviews*, 2005, **47**, 257-296.
22. A. Kitiyanan, S. Ngamsinlapasathian, S. Pavasupree and S. Yoshikawa, *Journal of Solid State Chemistry*, 2005, **178**, 1044-1048.
23. W. Zhou, K. Liu, H. Fu, K. Pan, L. Zhang, L. Wang and C.-c. Sun, *Nanotechnology*, 2008, **19**, 035610.
24. J.-Y. Kim, C.-S. Kim, H.-K. Chang and T.-O. Kim, *Advanced Powder Technology*, 2010, **21**, 141-144.
25. K.-T. Li, I. Wang and J.-C. Wu, *Catalysis Surveys from Asia*, 2012, **16**, 240-248.
26. A. Chareonlimkun, V. Champreda, A. Shotipruk and N. Laosiripojana, *Bioresource Technology*, 2010, **101**, 4179-4186.
27. X. Fu, L. A. Clark, Q. Yang and M. A. Anderson, *Environmental Science & Technology*, 1996, **30**, 647-653.
28. M. Paul, N. Pal, P. R. Rajamohanan, B. S. Rana, A. K. Sinha and A. Bhaumik, *Physical Chemistry Chemical Physics*, 2010, **12**, 9389-9394.
29. G. V. Sagar, P. V. R. Rao, C. S. Srikanth and K. V. Chary, *The Journal of Physical Chemistry B*, 2006, **110**, 13881-13888.
30. W. F. Zhang, Y. L. He, M. S. Zhang, Z. Yin and Q. Chen, *J Phys D Appl Phys*, 2000, **33**, 912-916.
31. T. Ohsaka, F. Izumi and Y. Fujiki, *Journal of Raman Spectroscopy*, 1978, **7**, 321-324.
32. S. Polisetti, P. A. Deshpande and G. Madras, *Industrial & Engineering Chemistry Research*, 2011, **50**, 12915-12924.
33. H.-R. Chen, J.-L. Shi, W.-H. Zhang, M.-L. Ruan and D.-S. Yan, *Chemistry of Materials*, 2001, **13**, 1035-1040.
34. M. Watanabe, Y. Aizawa, T. Iida, R. Nishimura and H. Inomata, *Applied Catalysis A: General*, 2005, **295**, 150-156.
35. M. Watanabe, Y. Aizawa, T. Iida, T. M. Aida, C. Levy, K. Sue and H. Inomata, *Carbohydrate Research*, 2005, **340**, 1925-1930.
36. J. M. R. Gallo, D. M. Alonso, M. A. Mellmer and J. A. Dumesic, *Green Chemistry*, 2013, **15**, 85-90.
37. E. Nikolla, Y. Román-Leshkov, M. Moliner and M. E. Davis, *ACS Catalysis*, 2011, **1**, 408-410.
38. L. Atanda, S. Mukundan, A. Shrotri, Q. Ma and J. Beltramini, *ChemCatChem*, 2015, **7**, 781-790.

39. R. Palkovits, K. Tajvidi, A. M. Ruppert and J. Procelewska, *Chemical Communications*, 2011, **47**, 576-578.
40. F. Lefebvre, F. X. Liu-Cai and A. Auroux, *Journal of Materials Chemistry*, 1994, **4**, 125-131.
41. T. Okuhara, T. Nishimura, H. Watanabe and M. Misono, *Journal of Molecular Catalysis*, 1992, **74**, 247-256.
42. M. A. Harmer and Q. Sun, *Applied Catalysis A: General*, 2001, **221**, 45-62.
43. E. Medina, R. Bringué, J. Tejero, M. Iborra and C. Fité, *Applied Catalysis A: General*, 2010, **374**, 41-47.
44. V. V. Ordomsky, J. van der Schaaf, J. C. Schouten and T. A. Nijhuis, *Journal of Catalysis*, 2012, **287**, 68-75.
45. J. S. Kruger, V. Choudhary, V. Nikolakis and D. G. Vlachos, *ACS Catalysis*, 2013, **3**, 1279-1291.
46. B. F. M. Kuster, *Starch - Stärke*, 1990, **42**, 314-321.
47. S. De, S. Dutta and B. Saha, *Green Chemistry*, 2011, **13**, 2859-2868.
48. S. J. Dee and A. T. Bell, *ChemSusChem*, 2011, **4**, 1166-1173.
49. M. Dourson, J. Reichard, P. Nance, H. Burleigh-Flayer, A. Parker, M. Vincent and E. E. McConnell, *Regulatory Toxicology and Pharmacology*, 2014, **68**, 387-401.
50. Y. Yang, C. Hu and M. M. Abu-Omar, *Journal of Molecular Catalysis A: Chemical*, 2013, **376**, 98-102.
51. G. Yang, C. Wang, G. Lyu, L. A. Lucia and J. Chen, *BioResources*, 2015, **10**, 5863-5875.
52. W. Schwald and O. Bobleter, *Journal of Carbohydrate Chemistry*, 1989, **8**, 565-578.
53. P. F. Siril, H. E. Cross and D. R. Brown, *Journal of Molecular Catalysis A: Chemical*, 2008, **279**, 63-68.

Supplementary Material

Table S4.1 Comparison of fructose and glucose conversion to HMF[a]

Samples	Substrate	Conv. (%)	Yield (%)	
			HMF	Levulinic acid
TiO_2	Fructose[b]	95.3	24.1	1.24
	Glucose	86.0	16.1	2.46
ZrO_2	Fructose[b]	85.6	29.6	0.31
	Glucose	72.2	22.9	0.93

[a]Reaction conditions: 2 g substrate, 100 ml water, 0.8 g catalyst wt., 3 h reaction time, 175 °C temperature.
[b]160 °C temperature, 5 h reaction time.

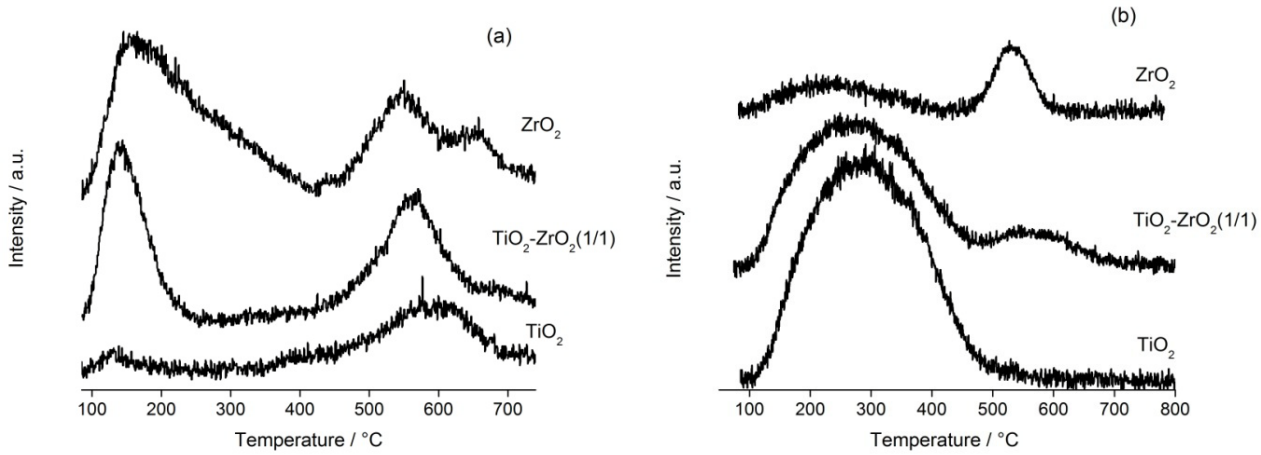

Figure S4.1 a) CO_2 and b) Ammonia temperature programmed desorption profiles of the metal oxides

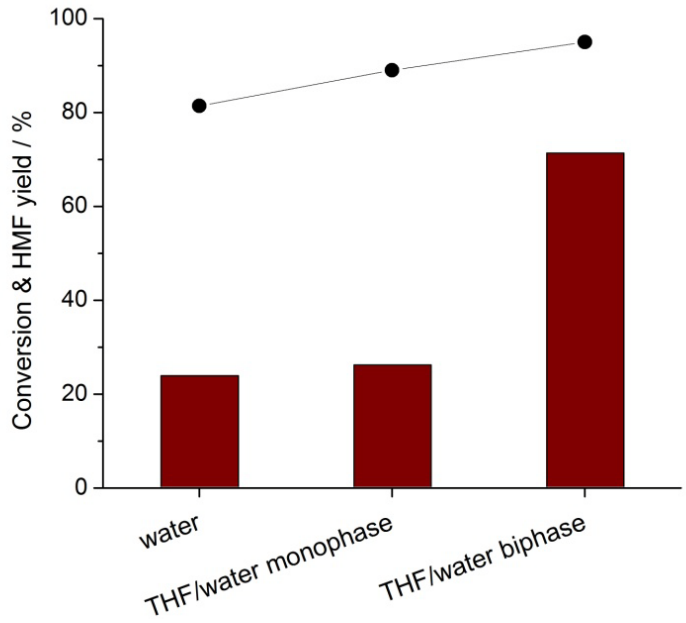

Figure S4.2 Role of reaction medium on glucose conversion to HMF catalyzed by TiO_2–ZrO_2 (1/1). Reaction conditions: 2 g glucose, 0.8 g catalyst wt., 100 ml solvent, 4 g NaCl, 3 h reaction time, reaction temperature 175 °C

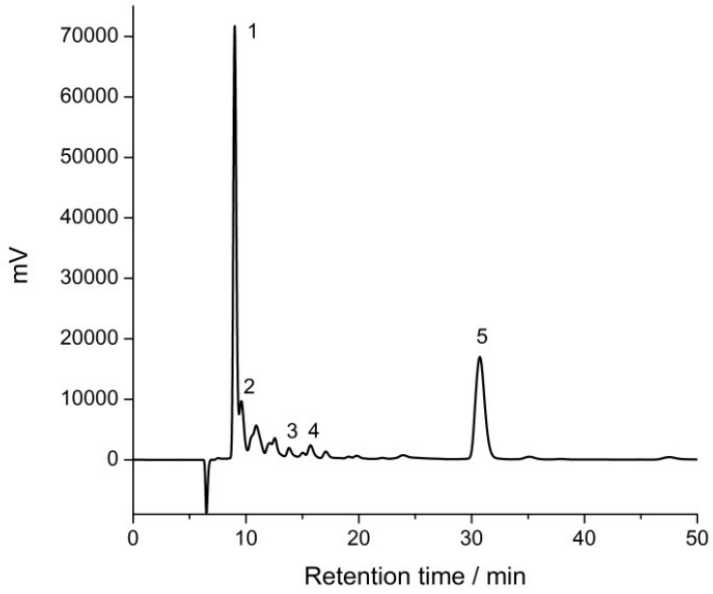

Figure S4.3 HPLC analytical profile measured using RID detector for glucose to HMF reaction using TiO_2–ZrO_2 (1/1) in aqueous reaction medium. Reaction conditions: 2 g glucose, 0.8 g catalyst wt., 100 ml solvent, 3 h reaction time, reaction temperature 175 °C. 1) glucose, 2) fructose, 3) formic acid, 4) levulinic acid and 5) 5-hydroxymethyfurfural

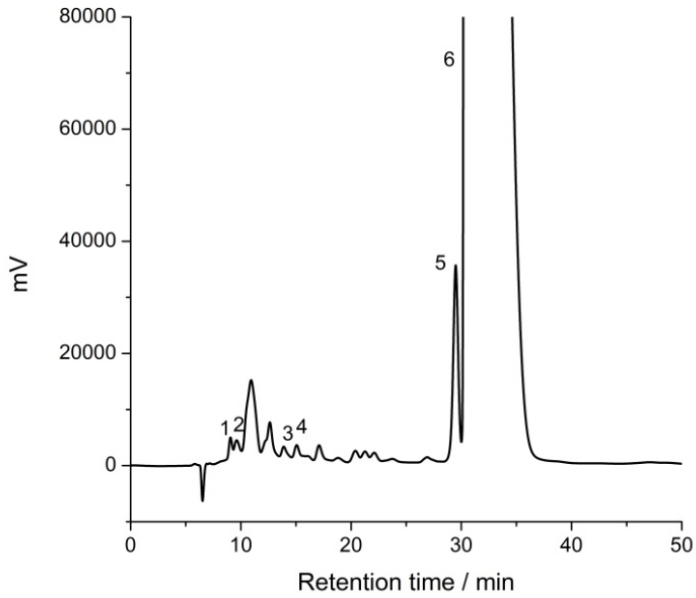

Figure S4.4 HPLC analytical profile measured using RID detector for glucose to HMF reaction using TiO_2–ZrO_2 (1/1) in water/THF monophase reaction medium. Reaction conditions: 2 g glucose, 0.8 g catalyst wt., 100 ml solvent (water/THF = 1/4 v/v), 3 h reaction time, reaction temperature 175 °C. 1) glucose, 2) fructose, 3) formic acid, 4) levulinic acid, 5) 5-hydroxymethyfurfural and 6) tetrahydrofuran

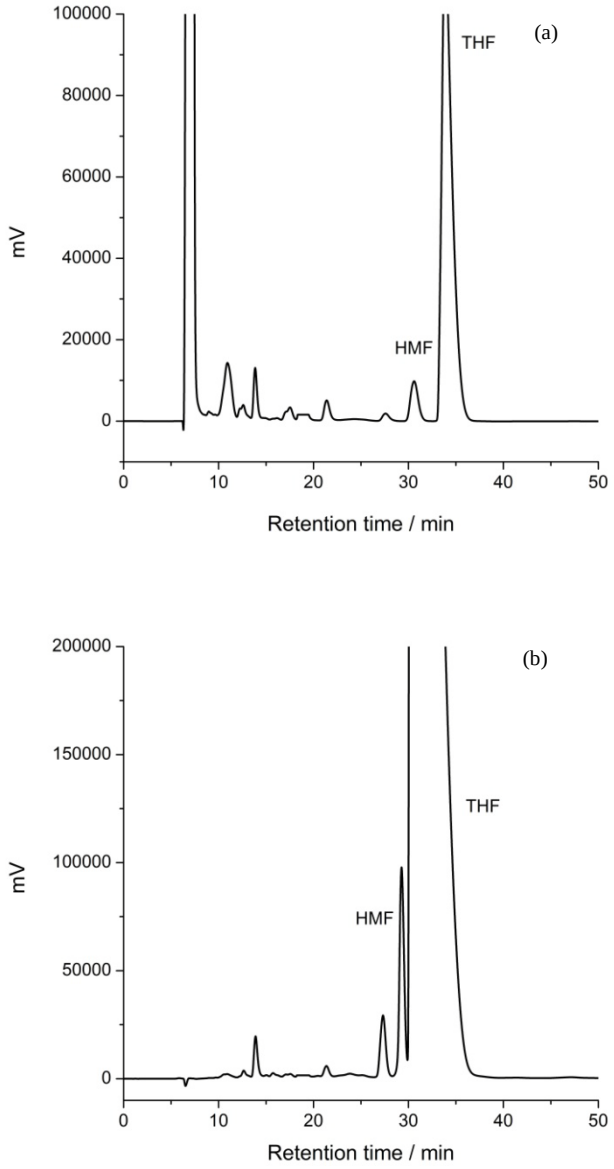

Figure S4.5 HPLC analytical profile measured using RID detector for glucose to HMF reaction using TiO_2–ZrO_2 (1/1) in water/THF biphase reaction medium. Reaction conditions: 2 g glucose, 0.8 g catalyst wt., 100 ml solvent (THF/water = 4/1 v/v), 4 g NaCl, 3 h reaction time, reaction temperature 175 °C. a) aqueous phase and b) organic phase

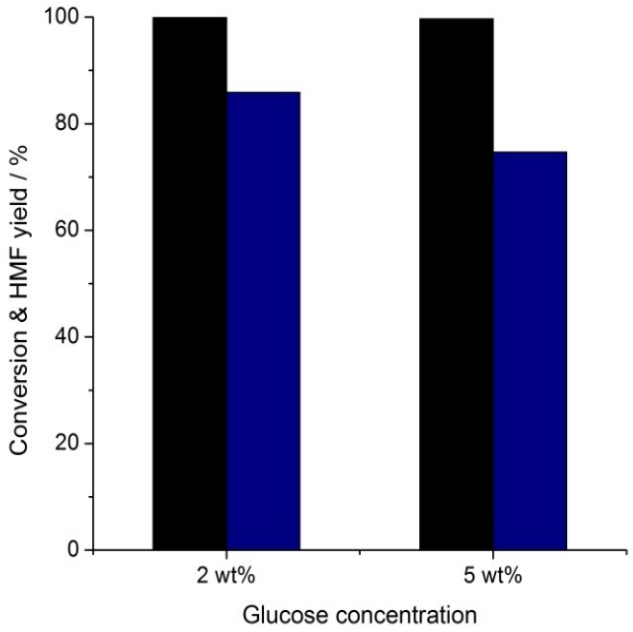

Figure S4.6 Influence of initial glucose concentration on HMF yield. Reaction conditions: glucose/catalyst = 2.5 w/w, catalysts = TiO_2–ZrO_2 (1/1) and Amberlyst 70 (1/1 w/w), 100 ml solvent (THF/water = 4/1 v/v), 4 g NaCl, 3 h reaction time, 175 °C reaction temperature

Chapter 5

Catalytic conversion of glucose to 5-Hydroxymethylfurfural with a phosphated-TiO_2 catalyst

This chapter was published in ChemCatChem, 2015, 7, 781-790

Catalytic conversion of glucose to 5-Hydroxymethylfurfural with a phosphated-TiO_2 catalyst

Luqman Atanda,[a] Swathi Mukundan,[a] Abhijit Shrotri,[a,b] Qing Ma[a] and Jorge Beltramini[a]

[a] *Nanomaterials Centre, Australian Institute for Bioengineering & Nanotechnology and School of Chemical Engineering, The University of Queensland, Brisbane, QLD 4072, Australia*

[b] *Catalysis Research Center, Hokkaido University, Kita 21 Nishi 10, Kita-Ku, Saporro 001-0021, Japan*

Abstract

Nano-sized phosphated TiO_2 catalysts of varying phosphate contents were synthesized and tested for the conversion of glucose to 5-hydroxymethylfurfural. The resulting materials were characterized by N_2-adsorption, XRD, ICPAES, XPS, TEM, NH_3-TPD and pyridine-IR techniques to determine their structural, bulk, surface and acid properties. We found that TiO_2 nanoparticles catalyze this reaction under mild conditions in a biphasic water-butanol system. Remarkably, incorporation of phosphorus in the TiO_2 framework enhances the target product selectivity. This is ascribed to increased surface area, enhanced acidity as well as thermal stability arising from the Ti-O-P bond formation. Under optimal reaction conditions, phosphated TiO_2 was found to be very active resulting in 97 % glucose conversion and 81 % HMF yield after 3 h reaction at 175 °C. More importantly, the catalyst showed good stability and can be reused for several reaction cycles.

5.1 Introduction

Conversion of sugars to platform chemicals is a promising process for achieving sustainable production of value added chemicals. The use of sugars obtained from non-edible biomass resources has attracted considerable attention due to its potential to offset the dependence on fossil fuels.[1-3] Cellulose is an inexpensive and readily available raw material that can undergo hydrolysis to C_6 sugars (hexoses). Subsequent dehydration of these sugars produces 5-hydroxymethylfurfural (HMF), which has been identified as a key bio-refining intermediate for chemicals and fuels.[4]

Hexose conversion to HMF is primarily an acid catalyzed reaction. Traditionally, mineral acids such as H_2SO_4, H_3PO_4 and HCl [5-7] were used as catalysts for this reaction, which constitute significant corrosion and environmental problems. In recent times, a variety of solid acids such as zeolites,[8-10] acidic ion exchange resins,[10-13] oxides, sulfates and phosphates,[14-18] heteropoly acid salts[10, 19] have been investigated in search of a suitable and efficient catalyst for the synthesis of HMF. Production of HMF from fructose is widely studied and significant progress has been achieved. However, glucose is cost effective and readily available in comparison to fructose.[20] Therefore, efficient process for the direct conversion of glucose and its polymers to HMF is desirable for industrial production. Although, the use of homogeneous metal halides with ionic liquid results in high selectivities and yields of HMF from glucose, catalyst handling, separation and reuse remain a concern in scaling up for industrial application.[21-23] Therefore, it is required to develop a heterogeneously catalyzed process that enables high HMF selectivity along with high glucose conversion.

Titania (TiO_2) is known to serve as a cheap, sustainable and eco-friendly metal oxide with a wide variety of applications including photo catalysis,[24, 25] sensors,[26, 27] and electrodes.[28] Owing to its chemical stability and rich surface chemistry, acid-base property of titania can be modified and applied to heterogeneous catalysis.[29, 30] Several authors have reportedly used titania to catalyze the transformation of carbohydrates to HMF. Watanabe et al.[31, 32] studied the dehydration of glucose to HMF in hot compressed water catalyzed with anatase TiO_2. They suggested that the presence of high-density acidic and basic sites influenced the catalytic activity of TiO_2. The basic sites were responsible for glucose isomerization to fructose, whereas the acid sites facilitated the successive dehydration to HMF. The catalytic dehydration of glucose using self-assembled mesoporous titania nanospheres was also described by De and coworkers.[33] They also identified that the surface acidity of the mesoporous titania was responsible for catalyzing the dehydration reaction. Likewise, mesoporous titania nanosphere templated with sodium salicylate was tested for the dehydration of various carbohydrate substrates.[34] The high surface area and Lewis acidity of the nanoparticle played a significant role in the microwave assisted conversion of the carbohydrates to HMF. A later

study by the same group also achieved efficient conversion of biomass and carbohydrates to HMF utilizing titanium phosphate nanoparticles under microwave assisted-heating.[35] Recently, Kuo et al.[36] explored the synthesis of acidic TiO_2 nanoparticle and its application for the catalytic conversion of biomass derived carbohydrates. They observed the nanoparticle was capable of promoting dehydration of carbohydrates to HMF as well as other value added products such as levulinic and HMF-derived esters. Very recently, Nakajima et al.[37] significantly improved the performance of TiO_2 to catalyze the conversion of glucose to HMF by immobilizing TiO_2 with H_3PO_4. As such, TiO_2 nanoparticles have shown great potential in the catalytic transformation of carbohydrates to HMF. A limitation of the TiO_2 catalyst reported so far is that it exhibits only Lewis acid sites. Convincing evidence has shown that catalytic systems with bifunctional Lewis and Brønsted acidity exhibit better performance for HMF formation than catalysts with either Lewis or Brønsted acid only.[19, 38] Therefore, we believe that titania catalyst with Lewis and Brønsted acid functionalities would be more effective in HMF production from glucose.

Design of an optimum catalyst is one of the most crucial roadblocks in HMF synthesis. However, solvent environment can also significantly influence reaction pathways. Therefore, the role of an appropriate reaction medium cannot be overlooked.[39] The synthesis of HMF from hexoses can generally involve isomerization, dehydration, fragmentation, reversion and condensation steps either in an aqueous or non-aqueous reaction media.[40] Reaction in aqueous medium suffers a low HMF yield due to its concomitant rehydration to levulinic acid and its degradation to polymeric humins. Ionic liquids[41, 42] and polar organic solvents such as dimethyl sulfoxide (DMSO),[15] dimethylformamide (DMF)[11, 43] and dimethylacetamide (DMA),[44] are found to be efficient for high yields of HMF due to their capacity to inhibit undesirable reactions. Nevertheless, poor solubility of hexoses/cellulosic biomass and the associated high separation cost of the target product constitute a major setback when using these solvents. A variety of biphasic systems of water-organic reaction medium have been developed to facilitate selective production of HMF and this has proven efficient in overcoming the limitations of either aqueous or non-aqueous reaction media.[5-7]

Here, we report the synthesis of a series of bifunctional phosphated TiO_2 nanoparticles combining both Lewis and Brønsted acid functionalities. The catalysts were extensively characterized using N_2-adsorption, X-ray diffraction (XRD), inductively couple plasma atomic emission spectroscopy (ICPAES), transmission electron microscopy (TEM), Fourier transform infrared spectroscopy of pyridine adsorption (pyridine-IR), temperature-programmed desorption of ammonia (NH_3-TPD) and X-ray spectroscopy (XPS) techniques. The catalytic activity of phosphated TiO_2 for glucose conversion was tested in a water-butanol biphasic system. N-butanol is

a cheap, biorenewable and environmental friendly solvent. In addition, it is a promising medium for upgrading HMF into useful fuels and chemicals, which helps to reduce overall process costs. The effects of reaction time and temperature, catalyst loading and substrate concentration were also investigated to optimize the process.

5.2 Experimental

5.2.1 Materials and catalyst synthesis

Titanium IV butoxide, n-butanol, ammonium phosphate monobasic, ammonium hydroxide solution (28%), glucose, fructose, 5-hydroxymethylfurfural, cellobiose, levoglucosan, furfural, were all purchased from Sigma Aldrich. Levulinic acid was purchased from Merck-Schuchardt and formic acid was supplied by Ajax Finechem. All solutions were prepared using water with a conductivity of 18 MΩ/cm obtained by Elga ultra pure water distillation apparatus.

TiO_2 NPs were prepared by sol-gel neutral amine approach using titanium IV butoxide as the precursor. The sol was prepared by the dropwise addition of the alkoxide precursor into an aqueous solution containing n-butanol under stirring. The pH of the solution was adjusted to 7 by adding ammonium hydroxide solution and the resulting solution was maintained under reflux for 24 h. After gelation, excess solvent removal was carried out using rotary evaporator followed by vacuum drying at 80 °C to obtain the titanium hydroxide hydrate. Phosphated TiO_2 was prepared via impregnation of titanium hydroxide hydrate with an aqueous solution of required amount of ammonium phosphate monobasic ($(NH_4)_3PO_4$) to give 5 to 25 wt% phosphate content. A typical synthesis of 5 wt% phosphate loading is as follows: 0.085 g of the phosphate precursor was dissolved in water. 2 g of dried hydrated titania was added, followed by stirring at room temperature for 4 h. Excess water was evaporated and the resulting solid was dried at 80 °C for 12 h. Finally, the pure and phosphated TiO_2 NPs were obtained after calcination at 600 °C for 4 h.

5.2.2 Catalyst characterisation

Wide angle X-ray diffraction patterns were recorded on a Rigaku Miniflex with monochromatic CoKα radiation (30 kV, 15 mA). The data was collected in a range of 2θ values between 10° and 90° using a step size of 0.02 and 1 s step time. Nitrogen adsorption–desorption isotherm measurement was collected at -196 °C using a Micromeritics TriStar II 3020 surface area and porosity analyzer. Specific surface areas were calculated according to the BET method and the pore size distributions using the BJH model on the desorption branches. Total pore volumes were estimated from the amount of N_2 adsorbed at a relative pressure (p/p_o) of 0.99. Compositional analysis was examined using ICP measurement. The procedure involves sample digestion using a

Milestone Ethos-1 microwave digester and then analyzed using a Varian Vista Pro ICPOES instrument. X-ray photoelectron spectra (XPS) was acquired using a Kratos Axis ULTRA X-ray photoelectron spectrometer equipped with a 165 mm hemispherical electron energy analyser using a monochromatic Al Kα (1486.6 eV) X-ray source. A survey wide scan was collected at an analyzer pass energy of 160 eV and multiplex (narrow) high resolution scans at 20 eV. The binding energies were referenced to the C 1s peak of adventitious carbon at 284.8 eV to account for the charging effects. Data analysis was done using Casa-XPS (v 2.3.12) employing a Shirley-background subtraction prior to fitting the spectra using Gaussian–Lorentzian curves. Temperature-programmed desorption of ammonia (NH_3-TPD) was carried out using Micromeritics AutoChemII Chemisorption Analyzer to determine total acid sites on the catalyst samples. About 70 mg of each sample was loaded in a quartz U-tube and pretreated at 500 °C in a flow of He (50 ml min^{-1}) for 1 h. This was followed by saturating the sample with ammonia (15 vol.% in He) at 100 °C for 30 min. Physisorbed ammonia on the sample surface was removed by purging the system with He stream for 2 h at 100 °C. The sample was then heated linearly at a heating rate of 10 K/min from 100 to 800 °C in a flow of He (25 ml/min) while monitoring the ammonia desorption profile using TCD. Pyridine infrared spectroscopy analysis was used to identify the nature of acid sites. Pyridine was chemisorbed on catalyst surface (50 mg) at 150 °C. Excess gaseous and physisorbed pyridine were removed by holding the temperature for 30 min under N_2 flow. FT-IR spectra were obtained at 128 scans and 4 cm^{-1} resolution using a Nicolet 6700 (Smart Orbit Accessory). Transmission electron microscopy (TEM) micrographs were taken using a JEOL JSM 2100 operated at an acceleration voltage of 200 kV.

5.2.3 Catalytic evaluation

Glucose dehydration to HMF was carried out in a stainless steel Parr reactor. In a typical experimental run, required amount of substrate, solvent and catalyst were charged into a 300 mL reactor, purged and then pressurized to 30 bar with high purity Ar. Biphasic mixture of water and n-butanol (30:70 v/v) was used as the reaction medium. The reactor was heated to its set point temperature, which was measured by a thermocouple inside the reaction mixture. Time zero in the reaction was defined as the time when the reactor reached its set point temperature. Catalytic experiments were repeated to check for reproducibility of data. Typical errors observed were in the range of ±2 %. Product analysis was done by Shimadzu Prominence HPLC equipped with both refractive index (RID-10) and UV-Vis (SPD-M20A) detectors using Bio-Rad Aminex HPX-87H as the analytical column. The column was operated at 50 °C using 5 mM H_2SO_4 as the mobile phase at a flow rate of 0.6 ml/min for the analysis of both the aqueous and organic phases. Product

identification was also done using Shimadzu GCMS-QP2010 Ultra equipped with Rxi-5ms column. The conversion of glucose and product yield were calculated as follows:

$$Conversion(\%) = \left(1 - \frac{n}{n_o}\right) \times 100\%$$

$$Yield(Y_i, \%) = \left(\frac{n_i}{n_o}\right) \times 100\%$$

where n_o and n denotes the moles of glucose in the feed and product, respectively, and n_i is the mole of product i (e.g. HMF, fructose, levulinic acid, levoglucosan).

5.3 Results and Discussion

Phosphated TiO_2 catalyst was prepared by impregnation of freshly prepared hydrated TiO_2 with ammonium phosphate monobasic ($(NH_4)_3PO_4$). After impregnation, the sample was dried and then calcined at 600 °C for 4 h to obtain the phosphated TiO_2 NP. Phosphated TiO_2 catalyst with different phosphate content was obtained by varying the amount of the precursor loaded during the impregnation step. The samples after calcination were denoted as xP-TiO_2 where x represents the theoretical weight percent of phosphorus, P, in the catalyst based on the amount of phosphate precursor added.

5.3.1 Powder X-ray diffraction

The XRD patterns of TiO_2 NPs with 0–25 wt% phosphate content are shown in Figure 5.1. The diffraction patterns of all the samples can be indexed as anatase phase of TiO_2 (JCPDS No. 21-1272). The diffraction pattern of pure TiO_2 appeared sharp and intense, indicating high crystallinity of the nanoparticle. In contrast, crystallinity of TiO_2 particles reduced after phosphate treatment show peak broadening with reduction in the peak intensity. This suggests the incorporation of phosphorus in the framework of TiO_2.[45] All the samples were composed of nano-sized crystals and their mean size obtained by Debye-Scherrer's equation given in Table 5.1 ranges from 5.3 nm to 27.3 nm. Increase in the phosphate content resulted in decrease in the crystallite size of the nanoparticle.

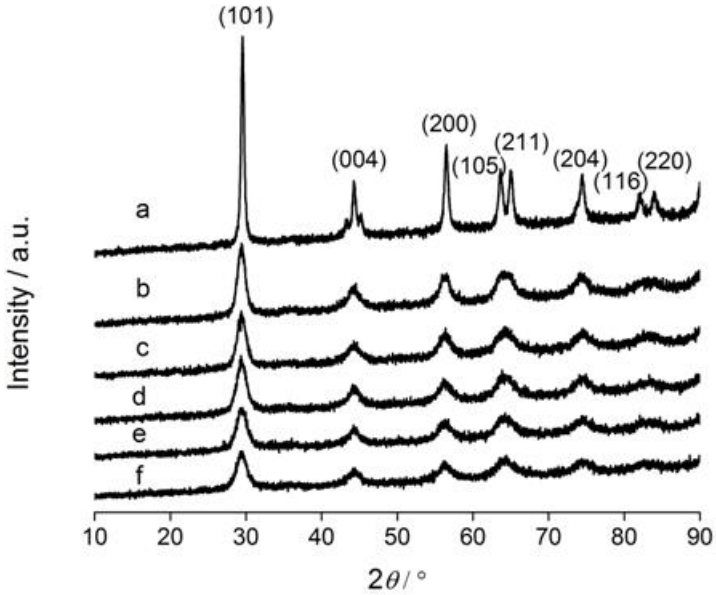

Figure 5.1 XRD patterns of: a) TiO_2, b) 5P-TiO_2, c) 10P-TiO_2, d) 15P-TiO_2, e) 20P-TiO_2, and f) 25P-TiO_2 nanoparticles

Table 5.1 Physical, compositional and acid properties of TiO_2 NPs

Entry	Samples	Ti/P molar ratio	Ti/P molar ratio ICP[a]	S_{BET} (m^2/g)[b]	Pore vol (cm^3/g)	Crystal size (nm)[c]	Total acidity (mmol/g)[d]
1	TiO_2	-	-	54.7	0.22	27.3	0.76
2	5P- TiO_2	31.1	33.5	124.8	0.31	7.34	1.92
3	10P- TiO_2	14.7	15.8	146.8	0.36	6.36	1.96
4	15P- TiO_2	9.3	10.1	151.0	0.43	6.12	2.36
5	20P- TiO_2	6.5	7.1	145.7	0.34	5.55	1.99
6	25P- TiO_2	4.9	5.1	79.4	0.25	5.30	1.40

[a] Determined by ICPAES analysis.
[b] BET surface area.
[c] Measured by XRD using Scherrer's equation for the (101) plane.
[d] Determined by NH_3-TPD.

5.3.2 N_2 adsorption-desorption

As shown in Figure 5.2, the nitrogen adsorption-desorption isotherms of all the samples are of type IV, with a capillary condensation step characteristics of mesoporous materials having narrow pore size distribution. The onset of the mesoporous filling step for phosphated TiO_2 shifts to relatively lower pressure in comparison with pure TiO_2. Likewise, a shift of pore diameter to lower values

indicates a distortion in the mesoporous structure of TiO_2 by phosphorus incorporation. The specific surface area (S_{BET}) of the NPs are summarized in Table 5.1. The surface area of the samples increased from 54.7 m^2/g to 151.8 m^2/g with an increase in phosphate content up to 15 wt%. Further increase in phosphate content led to a decline in surface area to 79.4 m^2/g, which can be attributed to partial pore blockage by excess phosphate.[46] All phosphated TiO_2 samples have higher surface area in comparison to pure TiO_2, which can be related to stabilization effect of the phosphate anions against sintering. This stabilization effect is assumed to be because of phosphate anions replacing some of the hydroxyl bridges originally present in the dried uncalcined TiO_2 during impregnation. After calcination, these impregnated anions result in the formation of Ti-O-P bond linkages. Dalai et al.[47] also reported a similar beneficial role of incorporated sulphate ions in TiO_2 to have retarded sintering through bond strengthening.

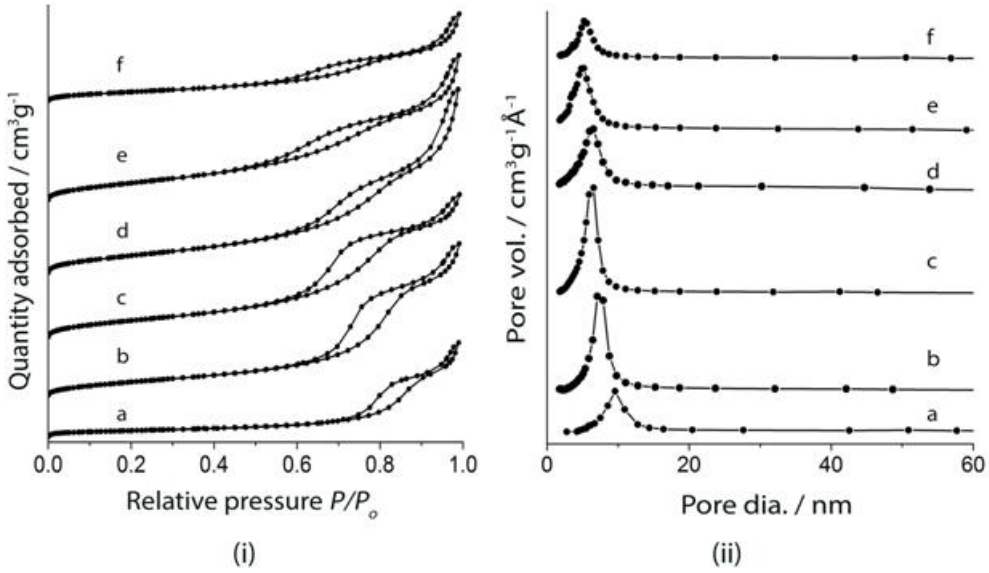

Figure 5.2 (i) BET isotherm and (ii) pore size distribution of: a) TiO_2, b) 5P-TiO_2, c) 10P-TiO_2, d) 15P-TiO_2, e) 20P-TiO_2, and f) 25P-TiO_2 nanoparticles

5.3.3 Compositional and surface analysis

Elemental composition of the catalyst samples was determined by ICPAES. The results summarized in Table 5.1 shows that the theoretical values of Ti/P molar ratio estimated from the loaded phosphate precursor are in good agreement with the measured content by the ICP analysis. XPS measurement was used to identify the oxidation states and bonding characteristics of the elements. Deconvoluted XPS spectrum of the O 1s region of TiO_2 (Figure 5.3(a)) revealed two peaks indicating presence of two oxygen species. The oxygen peak observed at 530.1 eV is ascribed to the lattice oxygen of TiO_2 and the peak centered at 531.7 eV corresponds to the oxygen from the

hydroxyl (OH) group.[48] After phosphate treatment, an additional peak was observed at 531.5 eV which can be assigned to oxygen species of P-O bonding.[49]

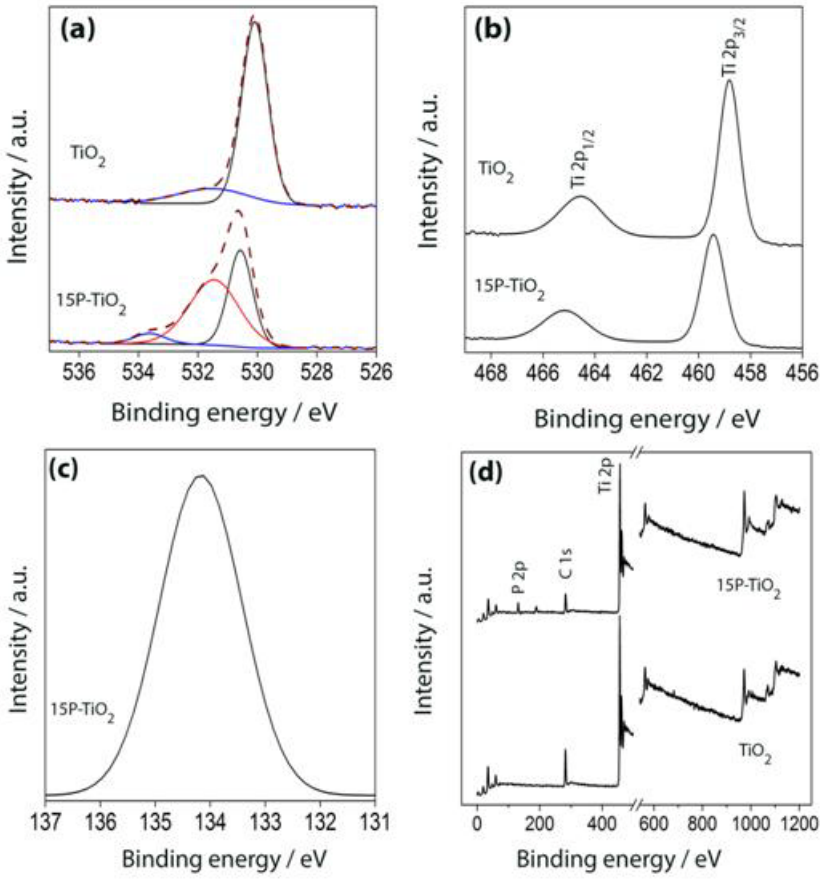

Figure 5.3 High resolution XP spectra of: a) O 1s, b) Ti 2p, c) P 2p, and d) wide scan survey

The oxygen peaks representing Ti-O and OH group shifted to higher binding energies of 530.6 eV and 533.6 eV, respectively. As shown in Figure 5.3(b), the Ti $2p_{3/2}$ peaks of pure and phosphated TiO_2 centered at 458.8 eV and 459.4 eV, respectively can be fitted as a single peak, thus confirming the presence of Ti ions in an octahedral environment. Notably, is the shift to higher binding energy of lattice oxygen in the O 1s region and Ti $2p_{3/2}$ of phosphated sample. This is because of partial electron transfer from Ti to P due to incorporation of phosphorus into the TiO_2 lattice, thereby decreasing the electron density on Ti. This result is consistent with the report of Guo and coworkers.[50] High resolution spectra of P 2p shown in Figure 5.3(c) reveals a single peak at 134.1 eV, indicating the existence of phosphorus in the pentavalent oxidation state (P^{5+}).[50] This peak was not observed in the pure TiO_2 sample as shown in Figure 5.3(d). Hence, the XPS result confirmed the successful incorporation of phosphorus into TiO_2 framework and the existence of Ti-O-P linkage as suggested by both XRD and BET results.

5.3.4 Transmission electron microscopy (TEM)

The TEM micrograph of TiO_2 (Figure 5.4(a)) shows a plate-like morphology. The crystallite size estimated by the particle size distribution shown in Figure S5.1 ranges between 23-38 nm, which is similar to the particle size estimated by the XRD. Figure 5.4(b) shows the High resolution TEM (HRTEM) of TiO_2. This reveals clear crystalline lattice fringes with measured spacing of 0.351 nm, assigned to (101) plane.[51, 52] In contrast to TiO_2, phosphated TiO_2 shows a significant reduction in the particle size, forming clusters of small nano-sized crystals as shown in Figure 5.4(c). The HRTEM of phosphated TiO_2 (Figure 5.4(d)) also shows the presence of lattice fringes, suggesting the TiO_2 structure is retained after phosphate treatment.

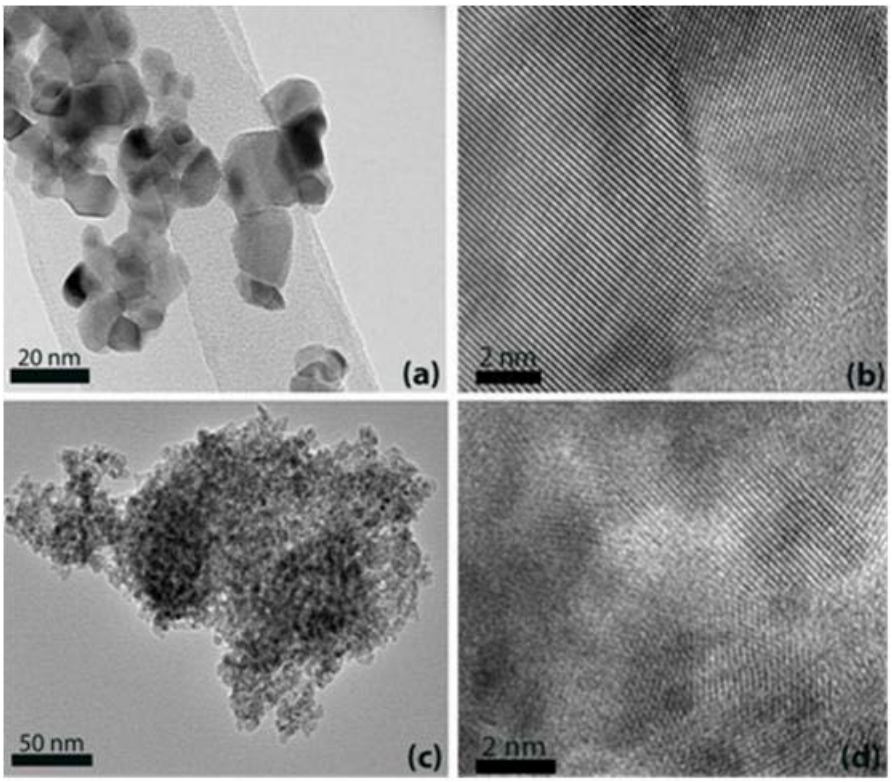

Figure 5.4 TEM images of: TiO_2 (a & b) and 15P-TiO_2 (c & d). Images (b) & (d) represent HRTEM of TiO_2 and 15P-TiO_2 showing lattice fringes of plane (101)

5.3.5 Acidity measurement

The acidity measurement of the TiO_2 NPs was carried out using NH_3-TPD. The total acid amount evaluated by the quantity of desorbed ammonia is summarized in Table 5.1. All phosphated samples exhibited superior acidity compared to pure TiO_2. A progressive increase in total acidity was observed with phosphate loading until 15 wt% thereafter, acidity declined in a similar trend as surface area. Relatively, surface area could be responsible for influencing the total acidity in terms

of accessibility of the probe gas to available acid sites. Depending on the temperature of the desorption peak, acid sites can be categorized into low (< 200 °C), medium (200–400 °C) and high strength (> 400 °C).[53] The desorption spectra of ammonia shown in Figure S4.2 indicates that bulk of the acid sites present are of low to medium strength even after phosphate treatment. Information regarding the nature of the acid sites was examined by pyridine-IR (py-IR). Characteristic absorption bands at 1443 cm^{-1} and 1600 cm^{-1} observed in pure TiO_2 are typical of pyridium ion associated with Lewis acid sites[15, 54, 55] (Figure 5.5(a)). As shown in Figure 5.5(b), phosphate treatment results in the appearance of a peak at 1540 cm^{-1} assigned to pyridinium ion coordinating with Brønsted acid sites, and the disappearance of the peaks at 1565 cm^{-1} and 1600 cm^{-1}. However, the peak at 1443 cm^{-1} was retained but has a weakened intensity. Additionally, an intense peak at 1490 cm^{-1} is assigned to the superimposed signals of pyridine adsorbed on both Lewis and Brønsted acid sites.[56] Therefore, in contrast to pure TiO_2, phosphated TiO_2 is characterized with the two types of acid functionalities i.e. Lewis and Brønsted acidity.

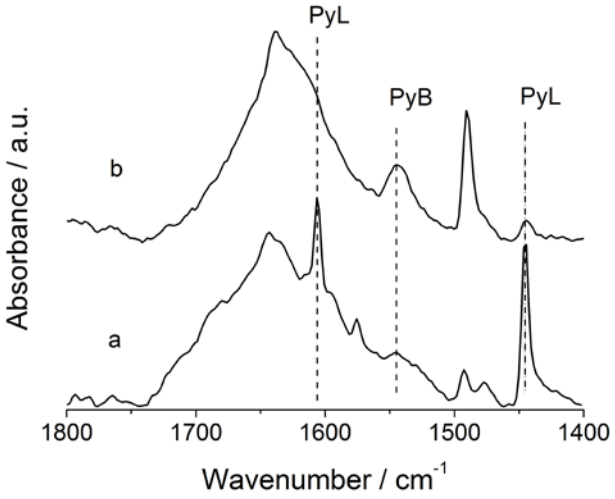

Figure 5.5 Infrared spectra of pyridine adsorbed on: a) TiO_2 and b) 15P-TiO_2 after evacuation at 150 °C

5.3.6 Catalyst activity

Dehydration of glucose to HMF was investigated using pure and phosphated TiO_2 catalyst. Initial tests were performed with 2 wt% glucose concentration in water-butanol biphasic system. The conversion of glucose was only 53.8 % with 27.6 % HMF yield when the reaction was carried out in the presence of pure TiO_2 catalyst. Under similar reaction conditions, phosphated TiO_2 NPs were substantially more active than pure TiO_2 with HMF yield ranging from 60 to 70 %, depending on the phosphate content as shown in Figure 5.6.

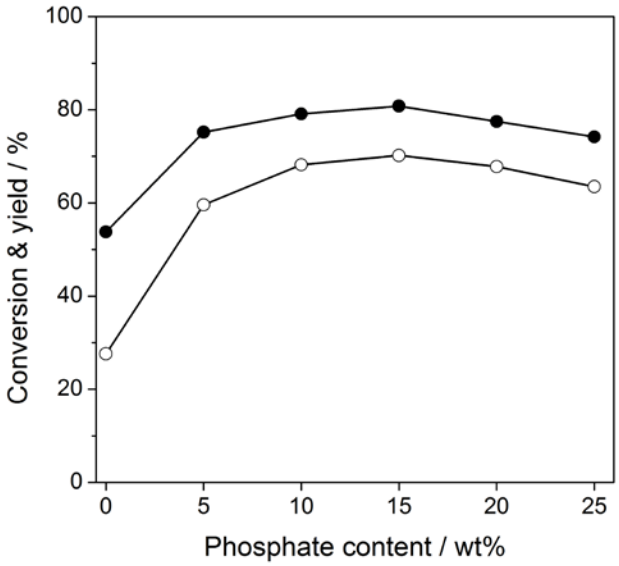

Figure 5.6 Influence of phosphate content on catalytic activity of TiO_2 NP. (●) Glucose conversion and (○) HMF yield. Reaction conditions: 2 g glucose, catalyst wt. = 0.4 g, temperature = 160 °C, time = 5 h, water = 30 mL, n-butanol = 70 mL

Firstly, the enhanced catalytic activity of phosphated-TiO_2 can be ascribed to the presence of Brønsted acid sites (Figure 5.5). This view is clarified by the activity result of Table S5.1, which illustrates the beneficial role of a catalyst system consisting of both Brønsted and Lewis acidity towards HMF formation. With a solid acid catalyst of pure Brønsted acidity (Amberlyst 70), very low HMF yield of 8.3 % at 70 % glucose conversion could be achieved, whereas pure Lewis acid catalyst in form of TiO_2 gave a 27.6 % HMF yield at 53.8 % conversion. Conversion and HMF yield reached 76.6 % and 31.2 %, respectively, for a physical mixture of Amberlyst 70 and pure TiO_2, thus demonstrating the beneficial role of the two acid functionalities in promoting higher glucose conversion and HMF yield.

Notably, both conversion and yield on phosphated-TiO_2 were enhanced as the phosphate loading increased to 15 wt%. Further increase in the phosphorus content caused reduction in the catalytic activity. Optimum catalytic performance of TiO_2 was achieved at 15 wt% phosphate loading corresponding to NP with highest surface area and acidity, indicating that catalytic activity can be correlated with surface acidity. Moreover, it can also be observed that the formation of very small nano-sized particles contributed to the overall higher catalytic performance of TiO_2 after phosphate treatment.

In an attempt to investigate the influence of crystal size and acidity on catalytic activity of the NPs, TiO_2 was calcined at varying temperatures (400 °C to 700 °C), before and after phosphate treatment. Calcination temperature is believed to influence the crystal growth of TiO_2 NP,[57] and this

is evidenced by the XRD result shown in Figure S5.3(a). The variations reflected in the peak intensities represent a range of crystal sizes. The estimated crystal size of the NPs considerably rose from 6.8 nm to 34.1 nm with increasing temperature. Crystallinity also increased with temperature. Transformation of anatase to rutile phase was observed for TiO_2 calcined at 700 °C. Figure 5.7(a) describes the catalytic activity of the TiO_2 NPs calcined at different temperatures. We observed that an increase in temperature corresponds to crystal size increment, and that led to a significant decline in activity. For instance at 400 °C, glucose conversion of 81.8 % and 41.4% HMF yield was attained but reduced to 31.8 % and 19.0 %, respectively after calcination at 700 °C.

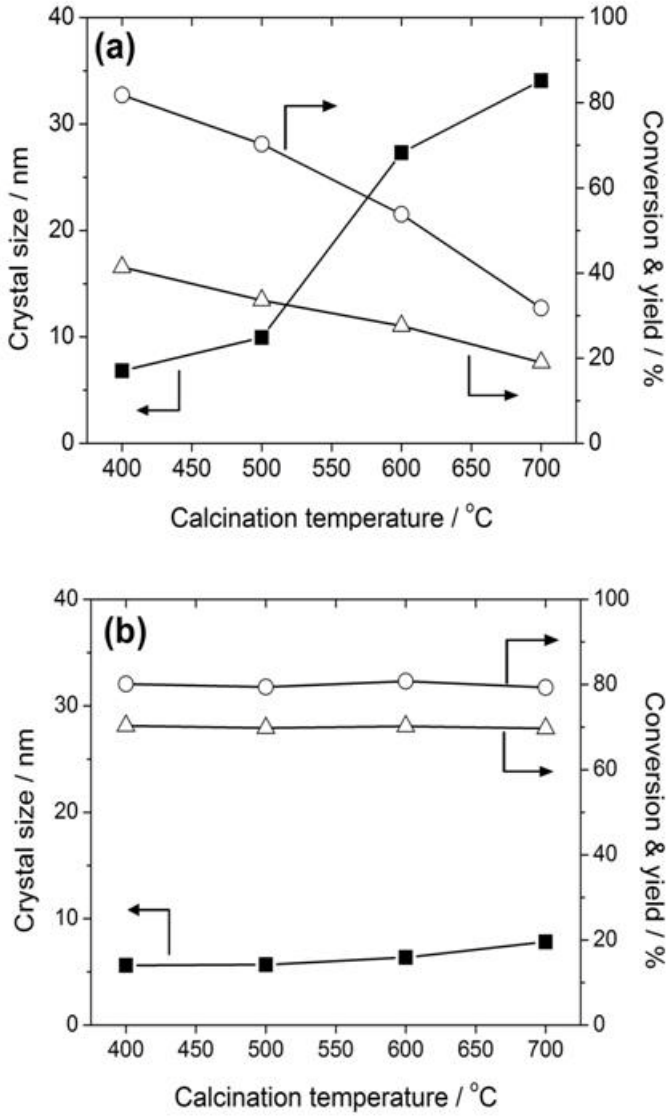

Figure 5.7 Effect of calcination temperature on crystal size and catalytic activity of TiO_2 NP: a) pure and b) phosphated (15 wt%). Reaction conditions: 2 g glucose, catalyst wt. = 0.4 g, temperature = 160 °C, time = 5 h, water = 30 mL, n-butanol = 70 mL. (○) Glucose conversion, (Δ) HMF yield and (■) crystal size

Small nano-sized crystals have been reported to contribute to large surface area that facilitate the adsorption of reactants.[58] Dutta et al.,[35] also reported that smaller nano-sized particles facilitated the mass transport of substrate within the catalytic material. This affords better access to the internal mesoscopic void spaces and ultimately exposing more active sites for surface interaction with reactant for enhanced reactivity. Meanwhile, when TiO_2 was treated with phosphate (15 wt%) prior to calcination at various temperature, no distinct structural changes was observed from the XRD patterns (Figure S5.3(b)) and the calculated crystal size ranges from 5.61 nm at 400 °C to 7.82 nm at 700 °C. More so, anatase-rutile transition was inhibited at 700 °C, which was present in pure TiO_2 calcined at the same temperature. Hence, we can conclude that phosphate treatment significantly inhibited the crystal growth of anatase and its transformation to rutile at temperatures up to 700 °C. This conclusion was supported by the report of Körösi and cowokers[59] who showed that phosphate treatment enhanced thermal stability of TiO_2 NPs. All the phosphated NPs calcined at various temperatures exhibited identical performance for glucose conversion. In all cases, ~80 % glucose conversion with 70 % HMF yield was recorded as shown in Figure 5.7(b). This result indicates that slight change of crystal size has negligible influence on catalytic performance. Hence, we may conclude that similar activity can be achieved with nano-sized TiO_2 crystals of similar dimension and acid content.

In order to explore acid content effect on glucose dehydration to HMF, we examined TiO_2 NPs of similar crystal size but different acid content i.e. pure TiO_2 at 400 °C (6.82 nm crystal size, 136.9 m^2/g S_{BET}, 1.28 mmol/g acidity) and 15P-TiO_2 at 600 °C (6.12 nm crystal size, 151 m^2/g S_{BET}, 2.36 mmol/g acidity). From Figure 5.7, it was found that about 80 % glucose conversion was achieved on both samples. However, remarkable increase in HMF yield was attained on 15P-TiO_2, which may be associated to the increased acid sites. This suggests that both the TiO_2 and 15P-TiO_2 of similar crystal size had comparable activity for glucose conversion. However, modification of the catalyst surface through phosphate treatment was essential to enhance the selectivity of HMF. We conclude that the crystal size reduction achieved by just thermal treatment is insufficient in improving the activity of TiO_2 catalyst for HMF synthesis.

5.3.6.1 Influence of reaction parameters

As shown in the previous section, 15P-TiO_2 was most active for glucose to HMF conversion. This catalyst was used to evaluate the influence of critical reaction parameters. Figure 5.8 shows the influence of loading amount of catalyst on conversion and yield. We observed a progressive increase in both conversion and yield as the amount of catalyst loaded increased up to 0.6 g. The

yield of HMF appeared to plateau after 0.6 g with a slight increase in the conversion. Hence, optimum catalyst loading was at 0.6 g, which corresponds to glucose/catalyst weight ratio of 10:3.

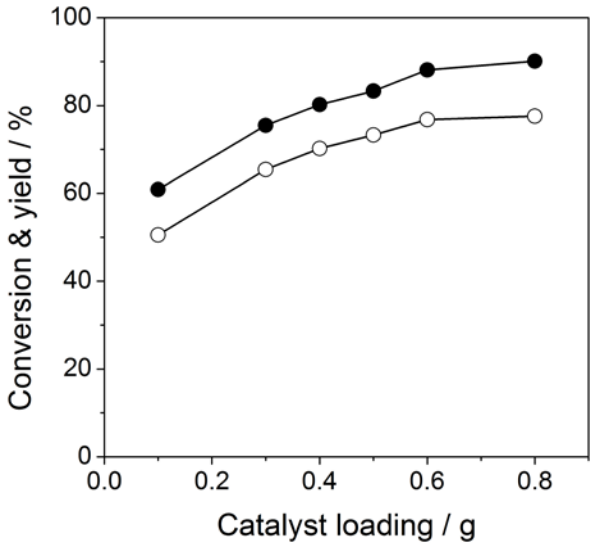

Figure 5.8 Glucose dehydration to HMF as a function of catalyst loading in a water/butanol biphasic solvent using 15P-TiO_2 catalyst. Reaction conditions: 2 g glucose, temperature = 160 °C, time = 5 h, water = 30 mL, n-butanol = 70 mL. (●) Glucose conversion and (○) HMF yield

Furthermore, we examined the influence of both reaction temperature and time at this optimum catalyst loading. Figure 5.9 depicts the effect of both reaction temperature and time on HMF yield. The time analysis shows that the reaction proceeded fast in the first 3 h to produce HMF and thereafter, gradual increase in product yield with time is noticed. Temperature had a significant impact on both the glucose conversion and HMF yield as well. Glucose conversion at 180 °C was 97 % after 4 h of reaction, whereas at 160 °C glucose conversion was 93 % after 8 h reaction. This indicates longer time is needed at lower temperature to reach similar glucose conversion at higher temperature. However, because HMF is more reactive at high temperature,[7] a prolonged reaction time resulted in the decline of HMF yield at 180 °C after 6 h. Based on these results, optimized condition for this reaction was 3 h of reaction time at 175 °C. At these optimized conditions, we investigated the effect of initial glucose concentration.

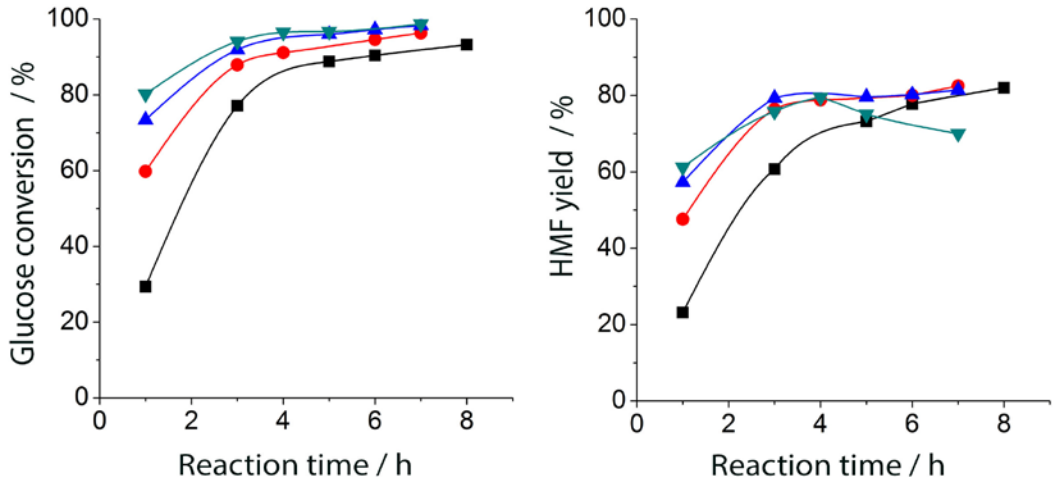

Figure 5.9 Influence of reaction time and temperature on glucose dehydration on 15P-TiO_2 catalyst. (—■—) 160 °C, (—●—) 170 °C, (—▲—) 175 °C and (—▼—) 180 °C. Reaction conditions: 2 g glucose, catalyst wt. = 0.6 g, water = 30 mL, n-butanol = 70 mL

Figure 5.10 represents the influence of glucose concentration on HMF formation rate. Glucose conversion was similar but HMF yield decreased with increased initial glucose concentration. The loss of HMF yield with increasing glucose concentration may be due to the propensity of humin formation via condensation polymerization of HMF with glucose and other reactive intermediates in the aqueous phase.[60-63]

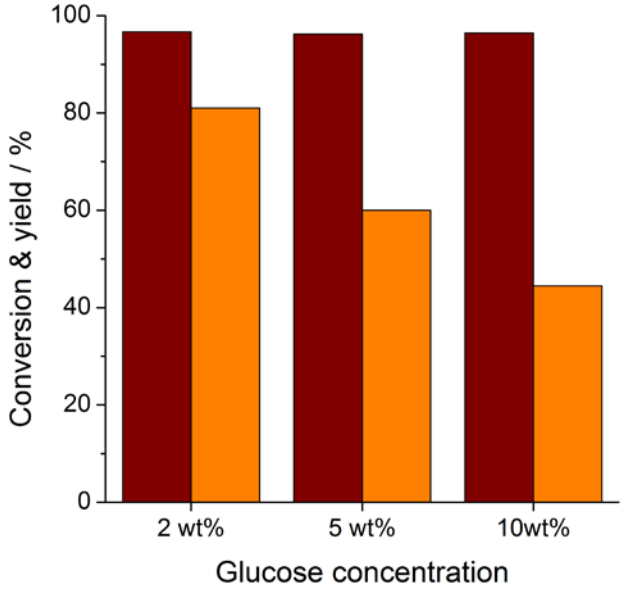

Figure 5.10 Influence of initial glucoe concentration on HMF yield over 15P-TiO_2 catalyst. (■) Glucose conversion and (■) HMF yield. Reaction conditions: glucose/catalyst wt. ratio = 10:3, temperature = 175 °C, time = 3 h, water = 30 mL, n-butanol = 70 mL

5.3.6.2 Plausible reaction pathway

The scope of this study does not entail an in-depth elucidation of the reaction mechanism. This comprises our current work and the results will be the focus of a future publication. However, based on the composition of the products we propose a plausible reaction pathway shown in Scheme 5.1. Major intermediates and by-products formed during the reaction were identified using HPLC and GC-MS (Figure S5.4). Small amounts of levoglucosan, furfural, formaldehyde, formic and levulinic acids were detected along with HMF. Time course of the products are shown in Figure S5.5. The presence of levoglucosan is indicative of the loss of one molecule of water from glucose.[43] Besides the anticipated rehydration products of HMF (levulinic acid and formic acid), the formation of furfural indicates that HMF also decomposed via loss of formaldehyde.[64, 65] In addition, formic acid may also be produced as a result of hydrolytic fission of furfural.[65] Based on these results, we propose that the isomerization of glucose to fructose is accompanied by concurrent dehydration reaction of glucose to form levoglucosan. Following the formation of HMF through dehydration of fructose, HMF undergoes rehydration to produce levulinic and formic acids. Furthermore, decomposition of HMF can also occur via loss of formaldehyde to produce furfural.

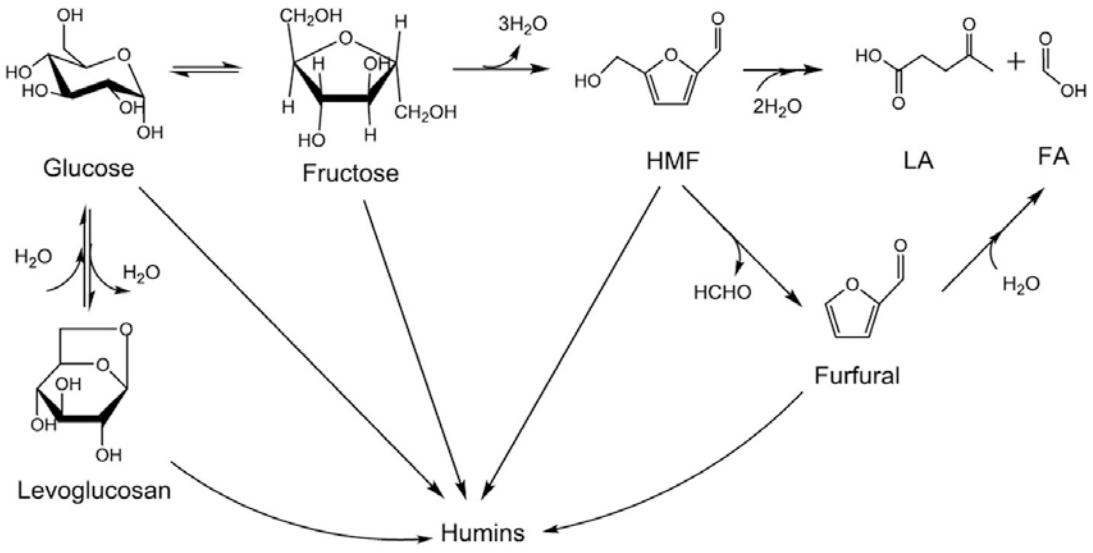

Scheme 5.1 Glucose conversion to HMF in a water-butanol (30:70 v/v) biphasic system on 15P-TiO_2 NP

5.3.6.3 Catalyst reusability

One of the most important factors contributing to catalytic performance is the catalyst stability and reusability during reaction. Reusability test with 15P-TiO_2 catalyst was investigated by performing the glucose dehydration reaction up to six recycles. After completion of each reaction cycle, the

catalyst was recovered by filtration, washed with acetone, dried and then used for the next run. It can be seen from Figure 5.11 that there was no significant change in the conversion of glucose for all the reaction runs. However, HMF yield continuously declined over the first three runs from 81 % to 70 %. We visually observed a change in colour of the catalyst from white to dark brown. The likely cause of this is deposition of humin compounds on the catalyst surface causing deactivation of the active sites. Lewis acid-catalyzed isomerization of glucose to fructose is unaffected on the basis of the minor change in glucose conversion. We hypothesized that the humins deposited on catalyst surface is most likely affecting the dehydration step catalyzed by Brønsted acid. HMF is reported to have stronger adsorption affinity onto Brønsted acid site.[56, 66] Adsorbed HMF on the surface of the recycled catalyst undergoes condensation reaction to humins, consistent with the catalyst colour change. The strongly adsorbed HMF on the Brønsted acid sites can also cause blockage of active sites as well as undergo further rehydration reaction to organic acids.

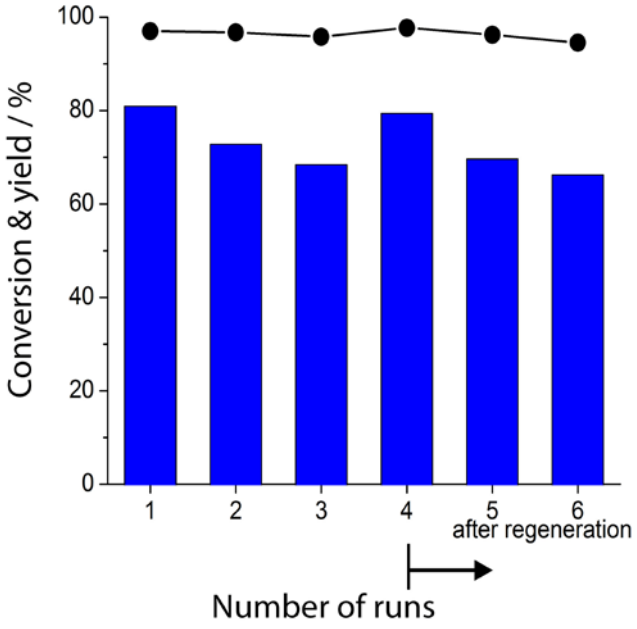

Figure 5.11 Reusability test of 15P-TiO_2 catalyst for the conversion of glucose to HMF. Reaction conditions: 2 g glucose, catalyst wt. = 0.6 g, temperature = 175 °C, time = 3 h, water = 30 mL, n-butanol = 70 mL. (●) Glucose conversion, (■) HMF yield

This is evidenced by the slight increased yields of fructose and levulinic acid as shown in Figure S5.6. To test this hypothesis, we decided to regenerate the catalyst before subsequent reaction runs. A post treatment of the catalyst was carried out by calcination at 600 °C for 4 h. The recovered catalyst after post treatment was about 0.51 g. Catalyst loss was during the decantation and filtration process. Fresh catalyst (15 % of the total catalyst weight) was supplemented to achieve an initial

catalyst weight of 0.6 g for the next reaction. The reaction cycles were then repeated under similar conditions as previously described for the first three runs. A comparable activity was achieved both before and after catalyst regeneration suggesting the catalytic activity can be restored. XRD and HRTEM were used to analyze the structural stability of the spent catalyst. The results of the analyses (Figures S5.7 and S5.8) in comparison with the fresh sample show that no significant changes occurred to the structural framework of the nanoparticle after reaction. Overall, these findings from the reusability test suggest the stability and recyclability of the catalyst. Moreover, catalyst deactivation because of humin deposition is reversible by regeneration.

5.4 Conclusion

We demonstrated the conversion of glucose to HMF in water-butanol biphasic system catalyzed by TiO_2 NP synthesized by sol-gel method. Modification of TiO_2 was achieved via phosphate treatment by impregnation. Phosphorus was successfully incorporated into the structural framework of TiO_2 as confirmed by XPS analysis. Phosphate treatment enhanced the thermal stability of TiO_2 and prevented the phase transformation from anatase to rutile phase at high temperature. N_2 sorption study revealed that the P-TiO_2 has superior surface area compared to unmodified TiO_2. Furthermore, presence of Lewis and Bronsted acid functionalities were confirmed by pyridine-IR. P-TiO_2 was effective for the catalytic conversion of glucose to HMF due to the formation of very small nano-sized crystals with enhanced surface acidity. We studied the effects of temperature, time, catalyst weight and substrate concentration. In general, all these parameters influence catalytic performance and yield of HMF. Under optimized reaction conditions, remarkable high HMF yield of *ca.* 81 % and 97 % glucose conversion was achieved at 2 wt% glucose concentration. Under comparable reaction conditions, HMF yield of 60 % and 45 % was attained at glucose concentrations of 5 wt% and 10 wt%, respectively. Lastly, catalyst stability under the given reaction conditions afforded recycling for multiple reaction runs.

Acknowledgements

The financial support from the NANOMAC Centre at The University of Queensland, Australia is highly appreciated. The authors also acknowledge the facilities, scientific and technical assistance, of the Australian Microscopy and Microanalysis Research Facility at The University of Queensland. The first author would also like to appreciate sponsorship from the International Postgraduate Research Scholarship (IPRS) and UQ Centennial Scholarship (UQ Cent).

References

1. L. T. Fan, M. M. Gharpuray and Y. H. Lee, *Cellulose hydrolysis*, Springer, Berlin [etc.], 1987.
2. G. Centi and R. A. van Santen, in *Catalysis for Renewables*, Wiley-VCH, Weinheim, 2007.
3. T. Wang, M. W. Nolte and B. H. Shanks, *Green Chemistry*, 2014, **16**, 548-572.
4. R.-J. van Putten, J. C. van der Waal, E. de Jong, C. B. Rasrendra, H. J. Heeres and J. G. de Vries, *Chemical Reviews*, 2013, **113**, 1499-1597.
5. Y. Román-Leshkov, J. N. Chheda and J. A. Dumesic, *Science*, 2006, **312**, 1933-1937.
6. Y. Román-Leshkov, C. J. Barrett, Z. Y. Liu and J. A. Dumesic, *Nature*, 2007, **447**, 982-985.
7. J. N. Chheda, Y. Roman-Leshkov and J. A. Dumesic, *Green Chemistry*, 2007, **9**, 342-350.
8. K. Lourvanij and G. L. Rorrer, *Industrial & Engineering Chemistry Research*, 1993, **32**, 11-19.
9. C. Moreau, R. Durand, C. Pourcheron and S. Razigade, *Industrial Crops and Products*, 1994, **3**, 85-90.
10. K.-i. Shimizu, R. Uozumi and A. Satsuma, *Catalysis Communications*, 2009, **10**, 1849-1853.
11. A. Takagaki, M. Ohara, S. Nishimura and K. Ebitani, *Chemical Communications*, 2009, 6276-6278.
12. X. Qi, M. Watanabe, T. M. Aida and R. L. Smith, *Industrial & Engineering Chemistry Research*, 2008, **47**, 9234-9239.
13. X. Qi, M. Watanabe, T. M. Aida and J. R. L. Smith, *Green Chemistry*, 2009, **11**, 1327-1331.
14. X. H. Qi, M. Watanabe, T. M. Aida and R. L. Smith, *Catalysis Communications*, 2009, **10**, 1771-1775.
15. H. Yan, Y. Yang, D. Tong, X. Xiang and C. Hu, *Catalysis Communications*, 2009, **10**, 1558-1563.
16. F. Benvenuti, C. Carlini, P. Patrono, A. M. Raspolli Galletti, G. Sbrana, M. A. Massucci and P. Galli, *Applied Catalysis A: General*, 2000, **193**, 147-153.
17. C. Carlini, P. Patrono, A. M. R. Galletti and G. Sbrana, *Applied Catalysis A: General*, 2004, **275**, 111-118.
18. F. S. Asghari and H. Yoshida, *Carbohydrate Research*, 2006, **341**, 2379-2387.
19. C. Y. Fan, H. Y. Guan, H. Zhang, J. H. Wang, S. T. Wang and X. H. Wang, *Biomass Bioenerg*, 2011, **35**, 2659-2665.

20. A. I. Torres, P. Daoutidis and M. Tsapatsis, *Energy & Environmental Science*, 2010, **3**, 1560-1572.
21. H. Zhao, J. E. Holladay, H. Brown and Z. C. Zhang, *Science*, 2007, **316**, 1597-1600.
22. X. Qi, M. Watanabe, T. M. Aida and R. L. Smith, *ChemSusChem*, 2010, **3**, 1071-1077.
23. C. Li, Z. Zhang and Z. K. Zhao, *Tetrahedron Letters*, 2009, **50**, 5403-5405.
24. T. Peng, D. Zhao, K. Dai, W. Shi and K. Hirao, *The Journal of Physical Chemistry B*, 2005, **109**, 4947-4952.
25. D. Chen, D. Yang, Q. Wang and Z. Jiang, *Industrial & Engineering Chemistry Research*, 2006, **45**, 4110-4116.
26. A. Teleki, S. E. Pratsinis, K. Kalyanasundaram and P. I. Gouma, *Sensor Actuat B-Chem*, 2006, **119**, 683-690.
27. S.-J. Bao, C. M. Li, J.-F. Zang, X.-Q. Cui, Y. Qiao and J. Guo, *Advanced Functional Materials*, 2008, **18**, 591-599.
28. E. S. Kwak, W. Lee, N.-G. Park, J. Kim and H. Lee, *Advanced Functional Materials*, 2009, **19**, 1093-1099.
29. P. V. Kamat, *The Journal of Physical Chemistry C*, 2007, **111**, 2834-2860.
30. D. Chandra, N. Mukherjee, A. Mondal and A. Bhaumik, *The Journal of Physical Chemistry C*, 2008, **112**, 8668-8674.
31. M. Watanabe, Y. Aizawa, T. Iida, R. Nishimura and H. Inomata, *Applied Catalysis A: General*, 2005, **295**, 150-156.
32. X. Qi, M. Watanabe, T. M. Aida and R. L. Smith Jr, *Catalysis Communications*, 2008, **9**, 2244-2249.
33. S. De, S. Dutta, A. K. Patra, A. Bhaumik and B. Saha, *Journal of Materials Chemistry*, 2011, **21**, 17505-17510.
34. S. Dutta, S. De, A. K. Patra, M. Sasidharan, A. Bhaumik and B. Saha, *Applied Catalysis A: General*, 2011, **409–410**, 133-139.
35. A. Dutta, A. K. Patra, S. Dutta, B. Saha and A. Bhaumik, *Journal of Materials Chemistry*, 2012, **22**, 14094-14100.
36. C.-H. Kuo, A. S. Poyraz, L. Jin, Y. Meng, L. Pahalagedara, S.-Y. Chen, D. A. Kriz, C. Guild, A. Gudz and S. L. Suib, *Green Chemistry*, 2014, **16**, 785-791.
37. K. Nakajima, R. Noma, M. Kitano and M. Hara, *Journal of Molecular Catalysis A: Chemical*, 2014, **388–389**, 100-105.
38. E. Nikolla, Y. Román-Leshkov, M. Moliner and M. E. Davis, *ACS Catalysis*, 2011, **1**, 408-410.

39. H. Kimura, M. Nakahara and N. Matubayasi, *The Journal of Physical Chemistry A*, 2013, **117**, 2102-2113.
40. J. Zhang and E. Weitz, *ACS Catalysis*, 2012, **2**, 1211-1218.
41. G. Yong, Y. Zhang and J. Y. Ying, *Angewandte Chemie International Edition*, 2008, **47**, 9345-9348.
42. T. Ståhlberg, W. Fu, J. M. Woodley and A. Riisager, *ChemSusChem*, 2011, **4**, 451-458.
43. M. Ohara, A. Takagaki, S. Nishimura and K. Ebitani, *Applied Catalysis A: General*, 2010, **383**, 149-155.
44. J. B. Binder and R. T. Raines, *Journal of the American Chemical Society*, 2009, **131**, 1979-1985.
45. K. J. A. Raj, R. Shanmugam, R. Mahalakshmi and B. Viswanathan, *Indian J Chem A*, 2010, **49**, 9-17.
46. K. M. Parida, M. Acharya, S. K. Samantaray and T. Mishra, *Journal of Colloid and Interface Science*, 1999, **217**, 388-394.
47. A. K. Dalai, R. Sethuraman, S. P. R. Katikaneni and R. O. Idem, *Industrial & Engineering Chemistry Research*, 1998, **37**, 3869-3878.
48. D. Sethi, A. Pal, R. Sakthivel, S. Pandey, T. Dash, T. Das and R. Kumar, *Journal of Photochemistry and Photobiology B: Biology*, 2014, **130**, 310-317.
49. J. C. Yu, L. Zhang, Z. Zheng and J. Zhao, *Chemistry of Materials*, 2003, **15**, 2280-2286.
50. S. Guo, S. Han, M. Haifeng, C. Zeng, Y. Sun, B. Chi, J. Pu and J. Li, *Materials Research Bulletin*, 2013, **48**, 3032-3036.
51. Y. Mao and S. S. Wong, *Journal of the American Chemical Society*, 2006, **128**, 8217-8226.
52. S. P. Albu, A. Ghicov, S. Aldabergenova, P. Drechsel, D. LeClere, G. E. Thompson, J. M. Macak and P. Schmuki, *Advanced Materials*, 2008, **20**, 4135-4139.
53. M. Paul, N. Pal, P. R. Rajamohanan, B. S. Rana, A. K. Sinha and A. Bhaumik, *Physical Chemistry Chemical Physics*, 2010, **12**, 9389-9394.
54. M. M. Mohamed, W. A. Bayoumy, M. Khairy and M. A. Mousa, *Microporous and Mesoporous Materials*, 2007, **103**, 174-183.
55. S. K. Das, M. K. Bhunia, A. K. Sinha and A. Bhaumik, *ACS Catalysis*, 2011, **1**, 493-501.
56. V. V. Ordomsky, J. van der Schaaf, J. C. Schouten and T. A. Nijhuis, *Journal of Catalysis*, 2012, **287**, 68-75.
57. V. Puddu, H. Choi, D. D. Dionysiou and G. L. Puma, *Applied Catalysis B: Environmental*, 2010, **94**, 211-218.

58. M. Xie, L. Jing, J. Zhou, J. Lin and H. Fu, *Journal of Hazardous Materials*, 2010, **176**, 139-145.
59. L. Körösi, S. Papp, I. Bertóti and I. Dékány, *Chemistry of Materials*, 2007, **19**, 4811-4819.
60. B. F. M. Kuster, *Starch - Stärke*, 1990, **42**, 314-321.
61. S. De, S. Dutta and B. Saha, *Green Chemistry*, 2011, **13**, 2859-2868.
62. S. J. Dee and A. T. Bell, *ChemSusChem*, 2011, **4**, 1166-1173.
63. J. Wang, J. Ren, X. Liu, J. Xi, Q. Xia, Y. Zu, G. Lu and Y. Wang, *Green Chemistry*, 2012, **14**, 2506-2512.
64. F. Tao , H. Song and L. Chou, *ChemSusChem*, 2010, **3**, 1298-1303.
65. R. Weingarten, W. C. Conner and G. W. Huber, *Energy & Environmental Science*, 2012, **5**, 7559-7574.
66. J. S. Kruger, V. Choudhary, V. Nikolakis and D. G. Vlachos, *ACS Catalysis*, 2013, **3**, 1279-1291.

Supplementary Material

Table S5.1 Effect of Lewis and Bronsted acidity on HMF formation[a]

Entry	Catalyst	Conversion (%)	HMF yield
1	TiO_2	53.8	27.6
2	Amberlyst 70	70.1	8.30
3	TiO_2 & Amberlyst 70[b]	76.6	31.2
4	15P-TiO_2	80.2	70.2

[a] Reaction conditions: 2 g glucose, catalyst weight = 0.4 g, temperature = 160 °C, time = 5 h, water = 30 mL, n-butanol = 70 mL.

[b] Physical mixture of Amberlyst 70 and TiO_2. Amberlyst 70 is mixed with TiO_2 in a proportion accounting for 15 wt% of the total catalyst weight as a comparison with 15P-TiO_2.

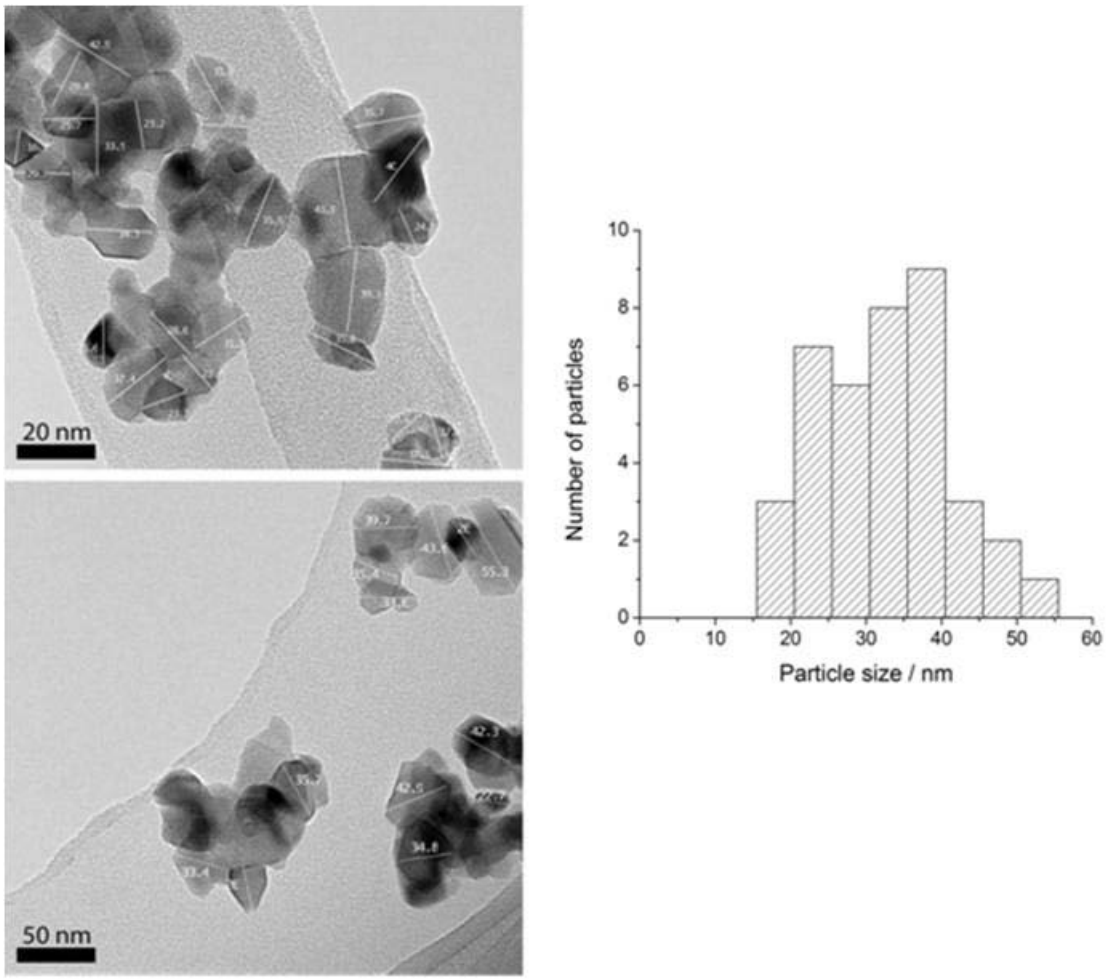

Figure S5.1 TEM images along with particle size distribution of TiO_2 NP

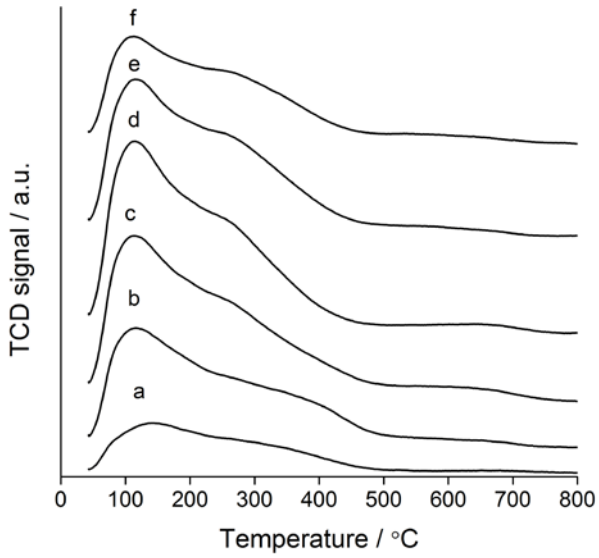

Figure S5.2 NH_3-TPD spectra of: a) TiO_2, b) 5P-TiO_2, c) 10P-TiO_2, d) 15P-TiO_2, e) 20P-TiO_2 and f) 25P-TiO_2

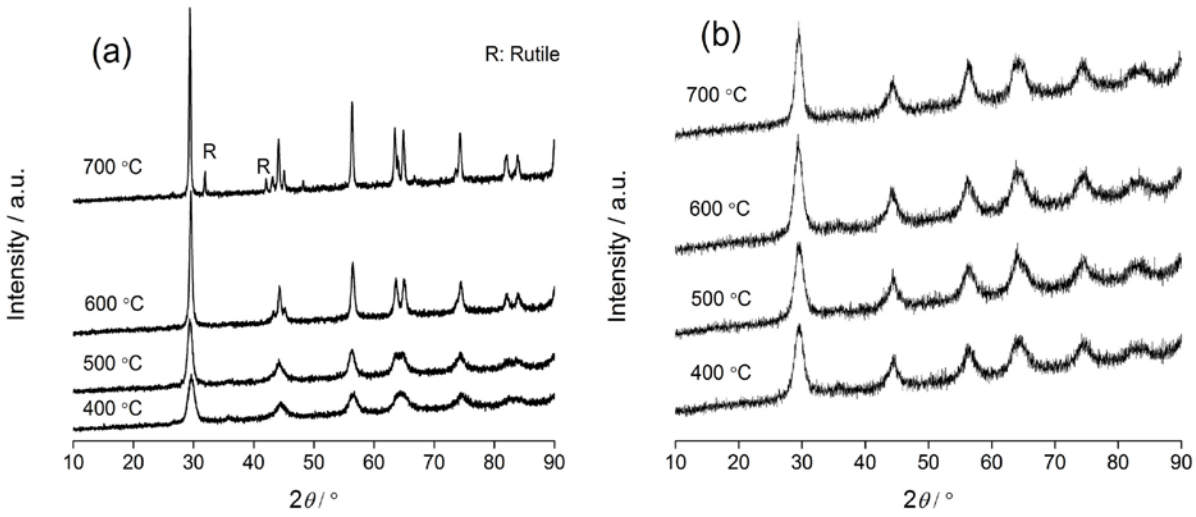

Figure S5.3 X-ray diffraction pattern of: A) pure TiO_2 and B) 15P-TiO_2 calcined at various temperatures

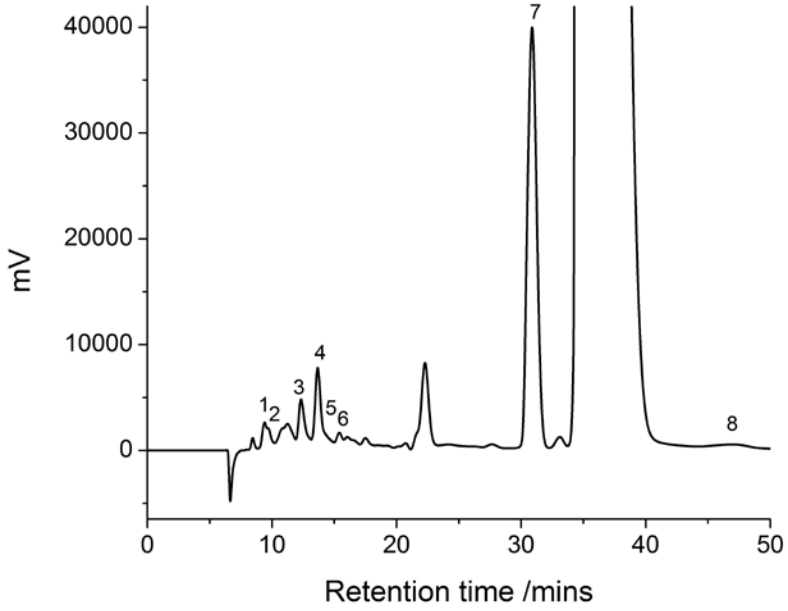

Figure S5.4 HPLC analytical profile measured using RID detector of the organic layer obtained from glucose-to-HMF reaction with 15P-TiO_2 catalyst. Reaction conditions: 2 g glucose, catalyst wt. = 0.6 g, temperature = 175 °C, time = 3 h, water = 30 mL, n-butanol = 70 mL. 1) glucose, 2) fructose, 3) levoglucosan, 4) formaldehyde, 5) formic acid, 6) levulinic acid, 7) 5-hydroxymethylfurfural, 8) furfural

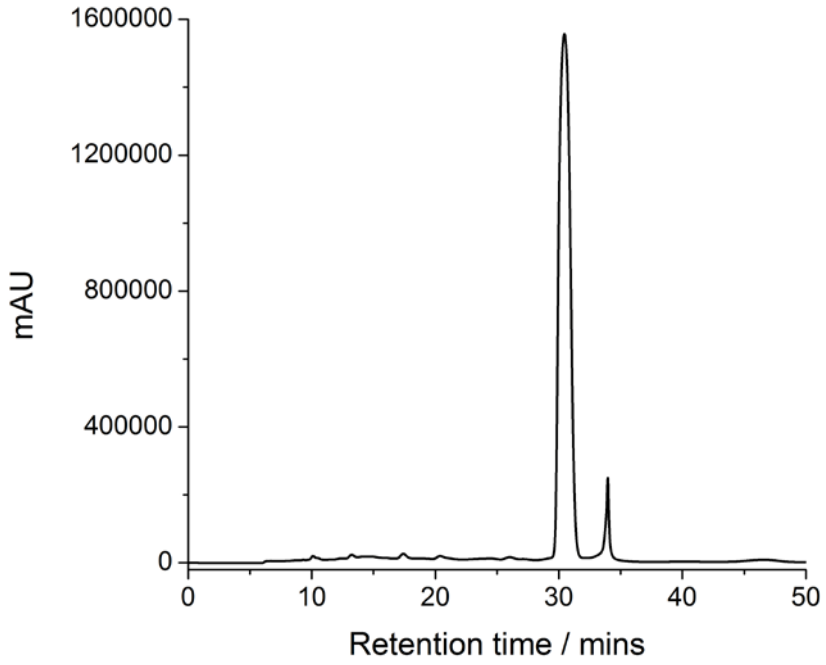

Figure S5.5 Typical representative of HPLC UV analytical profile of HMF in the organic layer. (Same reaction conditions as Figure S5.4)

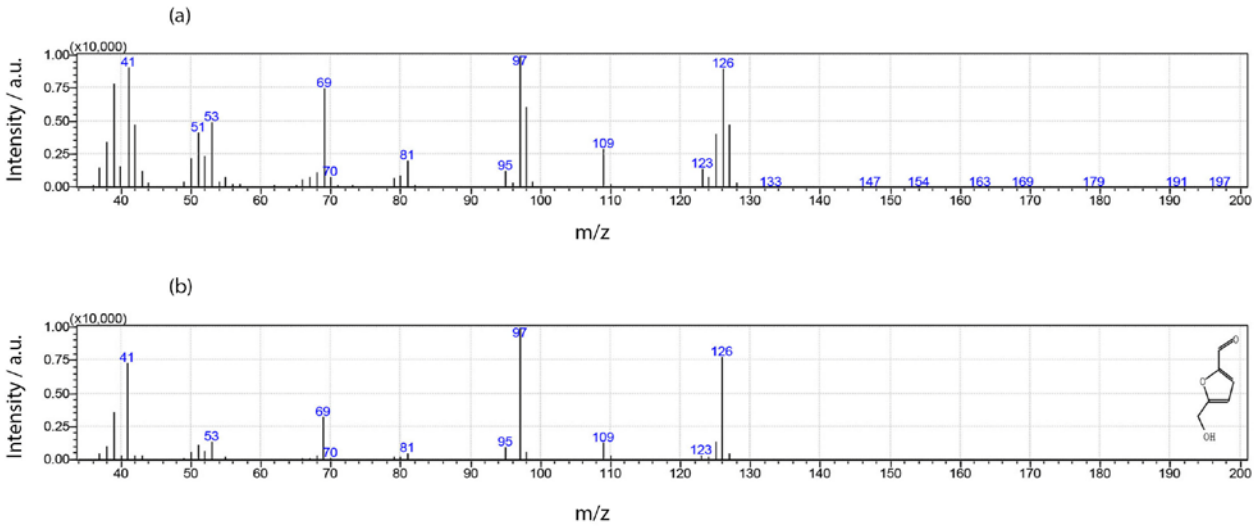

Figure S5.6 Mass spectrum of: a) 5-hydroxymethylfurfural in the reaction product, and b) standard 5-hydroxymethylfurfural

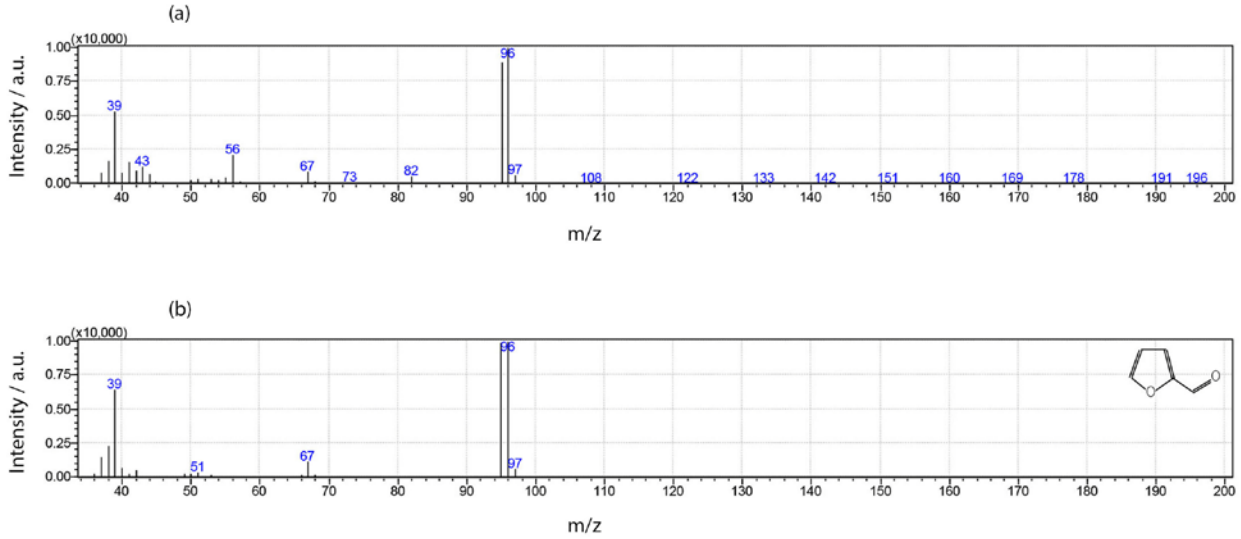

Figure S5.7 Mass spectrum of: a) furfural in the reaction product, and b) standard furfural

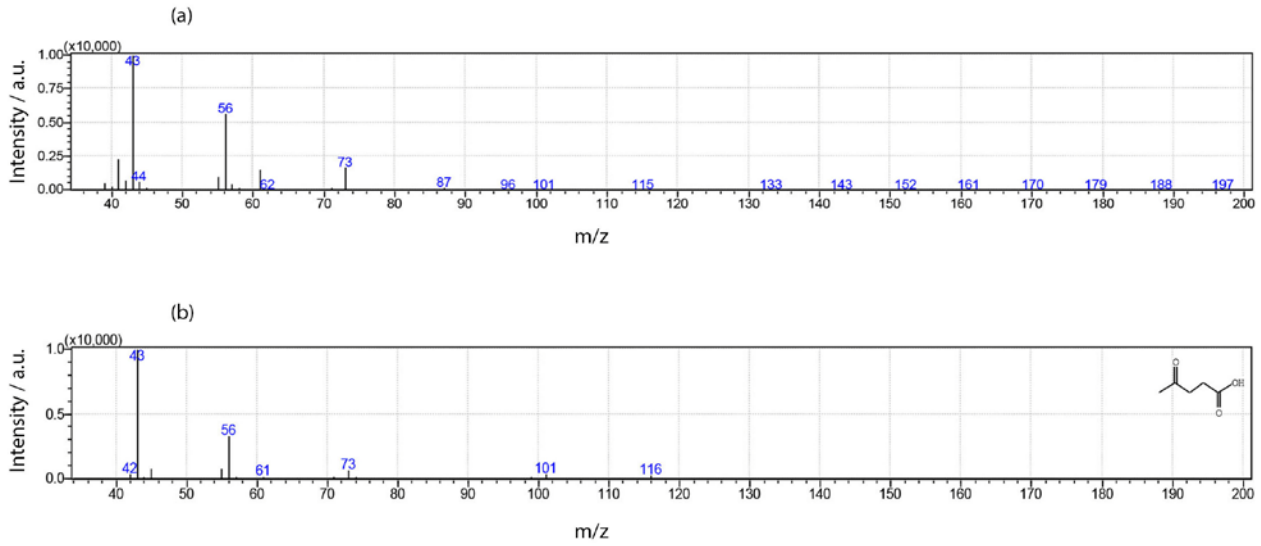

Figure S5.8 Mass spectrum of: a) levulinic acid in the reaction product, and b) standard levulinic acid

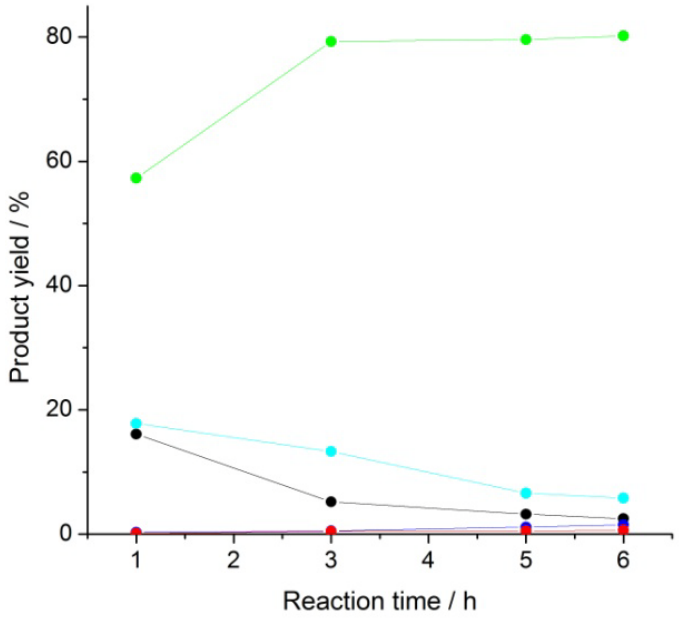

Figure S5.9 Product yield as a function of time in the conversion of glucose to HMF on 15P-TiO_2 catalyst. Reaction conditions: 2 g glucose, catalyst wt. = 0.6 g, temperature = 175 °C, water = 30 mL, n-butanol = 70 mL. (●) HMF, (●) Fructose, (●) Levoglucosan, (●) Levulinic acid, (●) Furfural

.

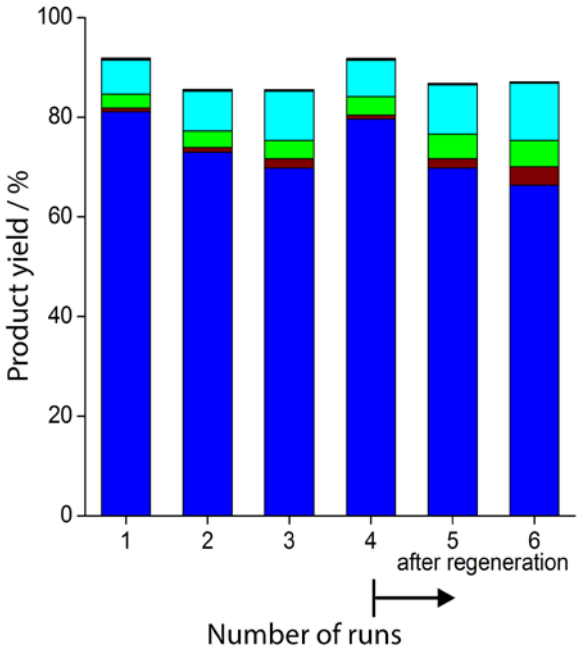

Figure S5.10 Product distribution of glucose conversion over 15P-TiO_2 catalyst. Reaction conditions: 2 g glucose, 0.6 g catalyst wt., temperature = 175 °C, time = 3 h, water = 30 mL, n-butanol = 70 mL. (■) HMF, (■) fructose, (■) levulinic acid, (■) levoglucosan, (■)furfural

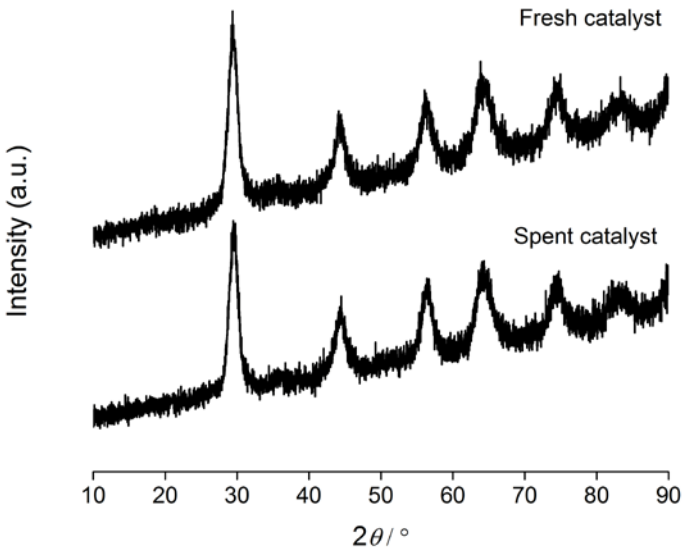

Figure S5.11 X-ray diffraction of fresh and spent 15P-TiO_2 catalyst

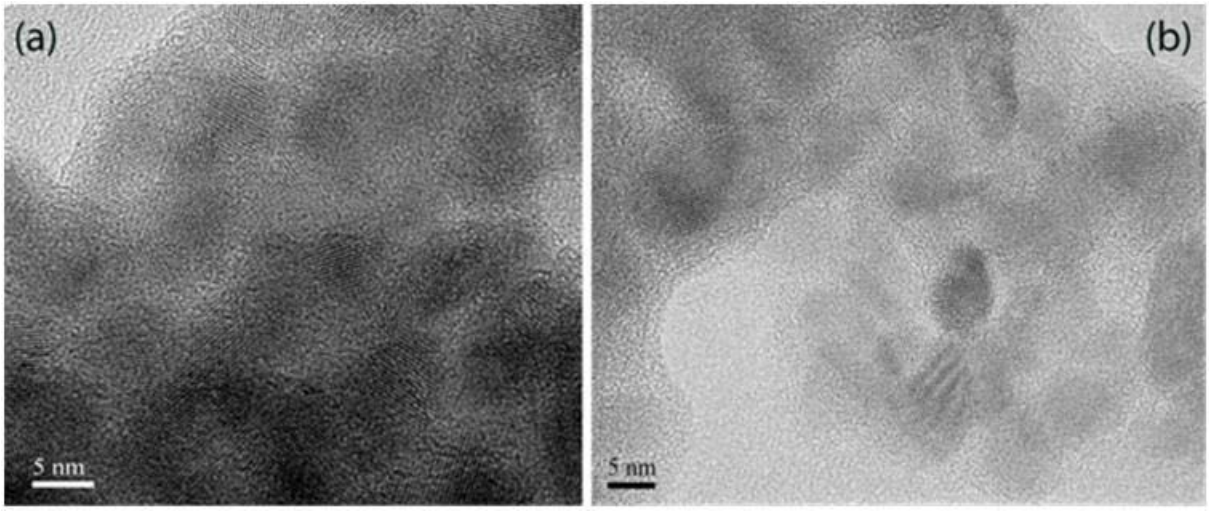

Figure S5.12 HR-TEM image showing lattice fringes of 15P-TiO_2 catalyst: a) fresh and b) spent

Chapter 6

Direct production of 5-Hydroxymethylfurfural via catalytic conversion of simple and complex sugars over phosphated–TiO_2

This chapter was published in ChemSusChem, 2015, 8, 2907-2916

Direct production of 5-Hydroxymethylfurfural via catalytic conversion of simple and complex sugars over phosphated-TiO_2

Luqman Atanda,[a] Abhijit Shrotri,[a,b] Swathi Mukundan,[a] Qing Ma,[a] Muxina Konarova[a] and Jorge Beltramini[a]

[a] *Nanomaterials Centre, Australian Institute for Bioengineering & Nanotechnology and School of Chemical Engineering, The University of Queensland, Brisbane, QLD 4072, Australia*

[b] *Catalysis Research Center, Hokkaido University, Kita 21 Nishi 10, Kita-Ku, Saporro 001-0021, Japan*

Abstract

Water-THF biphasic system containing N-methyl-2-pyrrolidone (NMP) was found to enable the efficient synthesis of 5-hydroxymethylfurfural (HMF) from a variety of sugars: simple to complex, using phosphated TiO_2 as a catalyst. Fructose and glucose were selectively converted to HMF resulting in 98% and 90% yield, respectively at 175 °C. Cellobiose and sucrose also gave high yields of HMF 94% and 98%, respectively at 180 °C. Other sugar variants such as starch (potato and rice) and cellulose were also investigated. The yields of HMF from starch (80-85%) were high, whereas cellulose gave a modest yield of 33%. Direct transformation of cellulose to HMF in significant yield (86%) was assisted by mechanocatalytic depolymerization; a process of ball milling of acid impregnated cellulose. This effectively reduces cellulose crystallinity and particle size to form soluble cello-oligomers, which is responsible for the enhanced substrate-catalytic sites contact rate and subsequent rate of HMF formation. During catalyst recyclability, P-TiO_2 was observed to be reusable for four cycles, without any loss in activity. We also investigated the conversion of the cello-oligomers to HMF in a continuous flow reactor. Good yield of HMF (53%) were achieved using a water-MIBK+NMP biphasic system. This current catalytic process creates a potential opportunity to develop a viable synthetic route for producing HMF from biorenewable sugar sources. Biomass pretreatment process, versatility of the catalytic material and the effectiveness of the reaction system could make affordable HMF production a reality.

6.1 Introduction

5-Hydroxymethylfurfural (HMF) is a vital platform chemical that can revolutionalize the bio-refinery industry. It is a key component in the production of high-value chemicals, polymers and fuels.[1, 2] For example, HMF can be readily oxidized to 2,5-furandicarboxylic acid (FDCA),[3] a potential replacement for petroleum-based terephthalic acid, relevant to the plastic industry for the production of polyethylene terephthalate (PET).[4, 5] Rehydration of HMF gives levulinic acid from which γ- valerolactone can be produced, a useful chemical that serves as a solvent and fuel additive.[6-8] Another important derivative of HMF is 2,5-Dimethylfuran (DMF), a potential biofuel.[9] DMF has energy density comparable to gasoline (31.5 MJ L^{-1} vs 35 MJ L^{-1}) and approximately 40% higher than ethanol (23 MJ L^{-1}),[10] making it suitable as a replacement for ethanol in gasoline-ethanol blends. 2-Methylfuran which is an intermediate of HMF hydrogenolysis, also possesses excellent fuel qualities.[9] Therefore, critical to efficient production of bio-fuels and chemicals, as well as a replacement of petroleum-derived counterparts requires a cost-effective process for selective production of HMF from biorenewable feedstock.[11]

HMF can be obtained by catalytic dehydration of simple sugars, such as fructose and glucose or directly from cellulose, a complex sugar as shown in scheme 6.1.

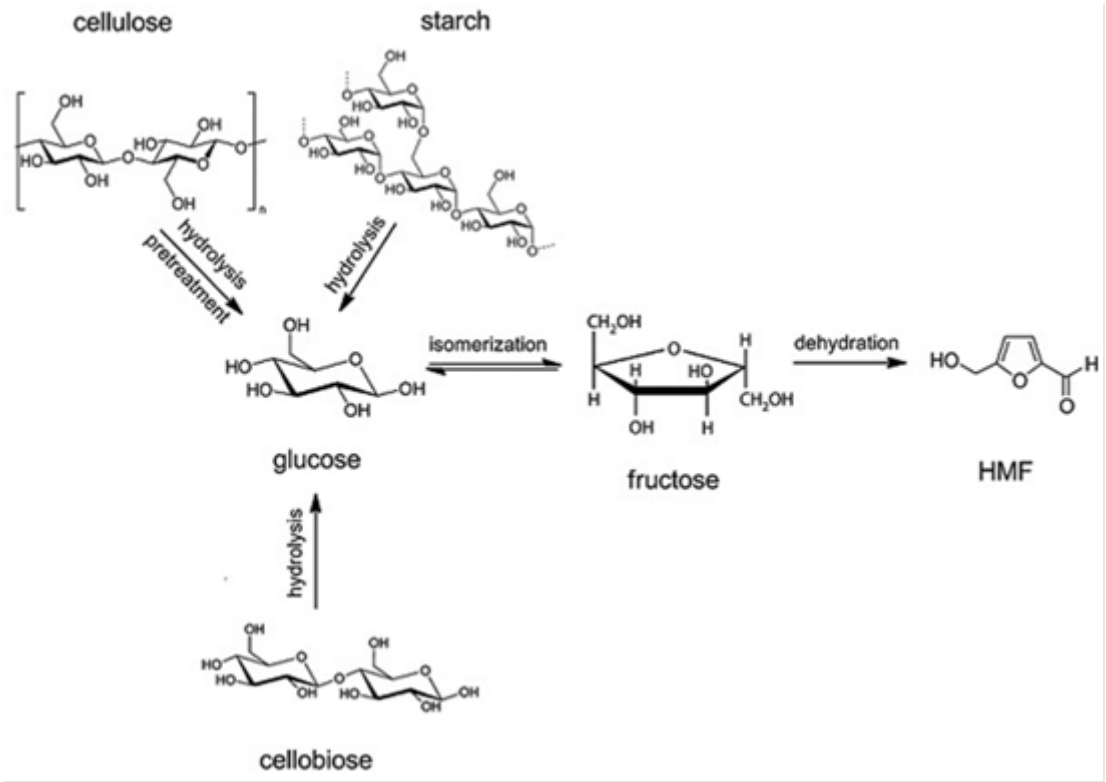

Scheme 6.1 Catalytic reaction pathway for sugar conversion to HMF.

In spite of excellent production of HMF achievable from fructose and glucose,[12-19] it is practically more economical and sustainable to use a biomass-derived sugar that is readily available and accessible. Cellulose is readily obtained in abundance from industry, forestry or agricultural residues.[20, 21] Unlike starch which is consumed by humans, cellulose is inedible, and thus it has the added advantage of not impacting negatively on agricultural food production. Hence, a one-pot chemical transformation of cellulose to HMF is a potential strategy to effective utilization of this enormous biomass reserve to supply next generation of chemicals and fuels. Nonetheless, chemical conversion of cellulose faces a major challenge due to its robust structure.[22-24] Cellulose suffers from high crystallinity, insolubility in water and chemical stability, leading to its poor reactivity. A possible solution to overcome this issue is to solubilize cellulose prior to reaction.

Although, cellulose is known to be insoluble in most conventional solvents, recent advances in the dissolution of cellulose in the presence of ionic liquids[25-31] or subcritical/supercritical fluids[32-38] have been proposed. These techniques depolymerize cellulose into soluble oligosaccharides, thus allowing subsequent production of useful chemical compounds in high yields. Despite the success and viability of these strategies, high costs associated with recycling of ionic liquid[39] or high energy input required to generate sub- or super-critical fluids[40] pose a number of challenges for process economics and sustainability. Alternatively, cellulose can be solubilized via mechanocatalytic depolymerization.[41-47] This technique involves a contact between cellulose and an acid catalyst, followed by a mechanically assisted solid-state depolymerization. This approach of cellulose dissolution is scalable, amenable to multi-feedstock, involves less waste and can be easily integrated into existing biorefineries.[41] Since the pioneering work of Hick et al.,[41] mechanocatalytic depolymerization of cellulose with acid catalysts have become of great interest for the complete dissolution of cellulose. [42, 43]

Due to the realization of cellulose depolymerization into soluble oligomers, it would be highly desirable to develop an efficient heterogeneous catalytic route for HMF production under continuous flow conditions. A plethora of homogeneous and heterogeneous catalytic systems have been described in the literature for the conversion of solubilized cellulose to HMF in a batchwise process.[48-53] For example, cellulose dissolution with 1-butyl-3-methyl-imidazolium chloride ([BMIM]Cl) was demonstrated to facilitate the conversion of cellulose to sugars and further to HMF in high yields (62%) catalyzed by a paired $CrCl_3$/LiCl catalyst system.[50] Shi et al.[51] described the formation of 53% HMF by direct degradation of cellulose in a biphasic system with concentrated $NaHSO_4$ and $ZnSO_4$ as a co-catalyst. Nandiwale et al.[52] reported a catalytic conversion of cellulose using bimodal micro/mesoporous H-ZSM-5 zeolite, in which HMF was formed in 46% yield and 67% cellulose conversion. Mascal and Nikitin[53-55] reported another route of cellulose

deconstruction in an aqueous HCl-LiCl solution to give mainly 5-chloromethylfurfural, which could subsequently be converted to high HMF yield (72%) by simple hydrolytic reaction.[53] To the best of our knowledge, the only existing report of HMF production from cellulose utilizing a flow reactor is by McNeff et al.[56] In their approach, they utilized a fixed-bed porous metal oxide-based catalytic process. Dissolution of cellulose was achieved by introducing a preheated water-organic mixture into a solubilization chamber containing cellulose. The cascade process of a preheater–solubilization chamber–catalytic reactor allows the continuous depolymerization of cellulose, which resulted in 87% conversion of cellulose to produce 35% yield of HMF.

Herein, we report on the catalytic production of HMF from sugars applying phosphated TiO_2 catalysts, under batch as well as continuous flow reaction conditions. The main aim is to selectively transform cellulose to HMF. However, because of the complexity of working with cellulose, parametrical activity study of pure and modified TiO_2 with phosphorus, tungsten, molybdenum and vanadium oxides was investigated for the catalytic conversion of glucose to HMF. In addition, the effect of phase modifiers on the aqueous phase of the biphasic water-organic medium was examined. The flexibility of the batch process conversion of glucose to HMF was checked by testing other sugar variants such as fructose, cellobiose, sucrose, starch and cellulose. Dissolution rate and reactivity of cellulose was enhanced via mechanocatalysis pretreatment using the procedure described by Shrotri et al.[43] Lastly, the viability of converting the water-soluble cello-oligomers to HMF in a biphasic continuous reactor was explored.

6.2 Experimental

6.2.1 Materials and catalyst preparation

The following chemicals were used: glucose (≥99.5%, Sigma-Aldrich), fructose (99%, Sigma-Aldrich), cellobiose (≥98%, Sigma-Aldrich), cellulose (Sigmacell Type 20, 20 μm), starch-rice (Sigma-Aldrich), starch-potato (Sigma-Aldrich), 5-hydroxymethyfurfural (≥99%, Sigma-Aldrich), titanium IV butoxide (97%, Sigma-Aldrich), n-butanol (≥99.4%, Sigma-Aldrich), ammonium phosphate monobasic (≥98%, Sigma-Aldrich), ammonium molybdate tetrahydrate (81-83% MoO_3 basis, Sigma-Aldrich), ammonium metavanadate (≥99%, Sigma-Aldrich), ammonium metatungstate hydrate (99.99%, Sigma-Aldrich), aqueous ammonia solution (28 wt%, Sigma-Aldrich), tetrahydrofuran (99.9%, Merck), methyl isobutyl ketone (99.5%, Sigma-Aldrich), n-methyl-2-pyrrolidone (99.5%, Sigma-Aldrich), acetonitrile (99.9%, Merck), toluene (99.9%, Merck) and acetone (99.9%, Merck). Ultra pure water (18 MΩ/cm) from Elga ultra pure apparatus was used for catalyst synthesis and reaction.

TiO_2 and modified TiO_2 nanoparticles were prepared according to our previously developed method.[57] Typically, titanium hydroxide hydrate was prepared by the neutral amine sol-gel technique using titanium IV butoxide as the TiO_2 precursor. Excess solvent was evaporated and the sample was dried at 80 °C overnight. Phosphating was accomplished by treating the titanium hydroxide hydrate with ammonium phosphate monobasic. Titanium hydroxide was slurred in a minimum amount of ammonium phosphate solution. The mixture was stirred for 4 h before the removal of excess water by evaporation and then followed by drying at 80 °C overnight. TiO_2 containing 15 wt% phosphate loading is employed in this study. Molybdating, vanadating and tungstating of TiO_2 were carried out in a similar procedure outlined above using ammonium molybdate, ammonium metavanadate and ammonium metatungstate, respectively. Samples were then calcined at 600 °C for 4 h. Catalyst samples are designated as x-TiO_2, where x represents P, Mo, V and W heteroatoms.

6.2.2 Catalyst characterisation

Structural analysis of the samples were characterized by X-ray diffraction (XRD) using a Rigaku Miniflex diffractometer with a filtered monochromatic CoKα radiation. The diffraction patterns were collected in the range of $10 \leq 2\ \theta \leq 90°$ with a step size of 0.02. Specific surface area was determined by carrying out N_2 adsorption at -196 °C using a Micromeritics TriStar II 3020 surface area and porosity analyzer. Prior to analysis, the samples were outgassed at 200 °C for at least 8 h under vacuum to remove the surface adsorbed species. The surface area was calculated using the Brunauer-Emmett-Teller (BET) method. Total pore volume was estimated using the volume of N_2 gas adsorbed at a relative pressure (P/P_o) of 0.99. The morphology of the synthesized particles was investigated by transmission electron microscopy (TEM, JEOL JSM 2100), operated at an acceleration voltage of 200 kV. Pyridine infrared spectroscopy analysis was used to identify the nature of surface acid sites. Prior to pyridine adsorption, the catalysts were activated at 200 °C under vacuum for 1 h, and then cooled to 150 °C. Pyridine is then admitted into the system to saturate the exposed catalyst surface (50 mg, 25 mm thickness). Chemisorption of pyridine was maintained at 150 °C for 30 min. Gaseous and physisorbed pyridine were then evacuated under the flow of N_2 gas at 150 °C for another 30 min. FT-IR spectra of the samples were recorded at room temperature with a Nicolet 6700 (Smart Orbit Accessory). The concentration of Brønsted and Lewis acid sites were estimated using the Lambert-Beer Law in the form $C=A/(\varepsilon\rho)$, where C is the concentration of the vibrating species (μmol g^{-1}), A is the intensity of the band (cm^{-1}), ε is the integration extinction coefficient (cm μmol^{-1}) and ρ is the sample thickness (g cm^{-2}).[58] Values of 1.67 cm μmol^{-1} and 2.22 cm μmol^{-1} were used as the integrated molar extinction coefficients for

pyridine bands at 1545 cm^{-1} (PyB) and 1455 cm^{-1} (PyL), respectively.[59] A CHNS-O elemental analyzer (FLASH EA 1112 series, Thermo Electron Corporation) was used to analyze the carbon content of fresh and spent catalyst samples. 2-3 mg of each sample was placed in a tin container, which was combusted in a furnace at 900 °C. The gaseous products were separated chromatographically and analyzed with a thermal conductivity detector (TCD).

6.2.3 Mechanocatalytic depolymerization of cellulose

Water-soluble, cellulose-based oligomers were produced by using methods described elsewhere.[43] In a typical method, H_2SO_4 (2.5 mmol) was diluted to a volume of 40 mL. Sigmacell microcrystalline cellulose (10 g) was then added to this solution, and the solution was stirred for a few minutes. The resulting slurry was dried with a rotary evaporator, followed by overnight air drying at 50 °C. The acidulated cellulose powder thus obtained was then milled in a planetary ball mill using 5 mm stainless steel balls, with a cellulose to ball weight ratio of 1:10. The mill was operated at 300 rpm, with a 20 min pause after every 15 min of continuous milling. The pause allowed dissipation of heat generated during milling, which prevented overheating of reactants. The milling time reported refers only to the active milling time.

6.2.4 Catalytic reactions

Batch transformation reaction of sugars to HMF was carried out in a two-phase reaction system consisting of water-THF (1:4 v/v %). In a typical experimental run, 5 g of substrate, 1.25 g catalyst and 100 mL of solvent were charged into a 300 mL reactor vessel provided by Parr Instrument Company. 4 g NaCl is added to the reaction medium to maintain a biphasic reaction condition as well as improve the efficiency of HMF extraction by the organic layer. The reactor was purged with Ar (99.9 %) and then pressurized to 20 bar. The temperature and stirring were controlled by a 4843 Controller provided by Parr. Temperature in the reactor was monitored by a thermocouple in the solution and a constant stirring rate of 500 rpm was used for the reaction. After the reaction was complete, the product mix was collected, centrifuged and the supernatant was collected for analysis. Catalytic runs were repeated, with an experimental error of ±2%.

Continuous flow reactions were performed on a custom-built fixed-bed reactor system. Two Alltech HPLC pumps were used for feeding the sugar solution and the organic solvent into the fixed-bed reactor. A U-shaped fixed-bed reactor was designed by using 1/4 in. OD SS316 Swagelok tubing and tube fittings. The powdered P-TiO_2 was used as it is without any pelletisation. The catalyst was loaded into the reactor, and a small amount of quartz wool was inserted from both sides of the reactor to hold the catalyst in place. A 7 μm Swagelok inline filter was connected to the

reactor exit, which was followed by a Swagelok back pressure regulator. A steady flow was established through the system until the desired pressure was achieved. The reactor was then dipped slowly into a stirred oil bath set at the reaction temperature, and the reaction time was noted as zero min. Reaction condition is typically 5 g of cello-oligomer dissolved in 100 mL water, 3:1 MIBK:NMP ratio, 1:1 water:MIBK+NMP ratio and 60 bar back pressure while varying the flow rate, reaction temperature and catalyst dosage between 0.2-0.4 mL min^{-1}, 210-230 °C and 350-450 mg, respectively.

Liquid products were analyzed using Shimadzu Prominence HPLC equipped with both refractive index (RID-10) and UV-Vis (SPD-M20A) detectors using a Bio-Rad Aminex HPX-87H as the analytical column. The column was operated at 50 °C using 5 mM H_2SO_4 as the mobile phase at a flow rate of 0.6 ml/min for the analysis of both the aqueous and organic phases. The concentrations of glucose, fructose, HMF and other identifiable products were quantified by HPLC analysis through the external standard method and calibration curves of commercially available standard substrates. Sugar conversion (Conv. mol %) and product yield (mol %) were calculated according to:

$$Conv.(mol\%) = \left(1 - \frac{nC_6}{nC_6^o}\right) \times 100\%$$

$$\text{Product yield}\,(mol\%) = \left(\frac{n_i}{nC_6^o}\right) \times 100\%$$

where nC_6 and nC_6^o denote number of moles of C_6 sugar in the product and feed, respectively, and n_i is the number of moles of identified products (HMF, levulinic acid, levoglucosan etc.).

6.3 Results and Discussion

Neutral amine sol-gel method was used to prepare TiO_2 nanoparticle. A previous report of the material synthesis showed that the TiO_2 nanoparticle exists as anatase phase with a mesoscopic structure.[57] The material possesses Lewis acidity and was found active for glucose dehydration reaction to HMF. In addition, the catalytic performance of TiO_2 was promoted by phosphate treatment due to enhanced surface acidity. Indeed, increasing the surface area and the accessibility of the active sites on TiO_2 has also been reported by other others to improve the catalytic performance of TiO_2 to efficiently catalyze the dehydration of sugars into HMF.[60-66] In this present study, we investigate the role of tungstate, molybdate and vanadate on the properties of TiO_2, especially as it affects the surface acidity in comparison to that of phosphate. For this purpose,

hydrated titanium hydroxide initially prepared via the neutral amine sol gel method was impregnated with ammonium salts of phosphorus, tungsten, molybdenum and vanadium.

6.3.1 Catalyst characterization

Powder x-ray diffractometer (XRD) technique was used to examine the crystalline structure of the asynthesized materials. Figure 6.1 represents the XRD patterns of TiO_2 nanoparticles before and after modification.

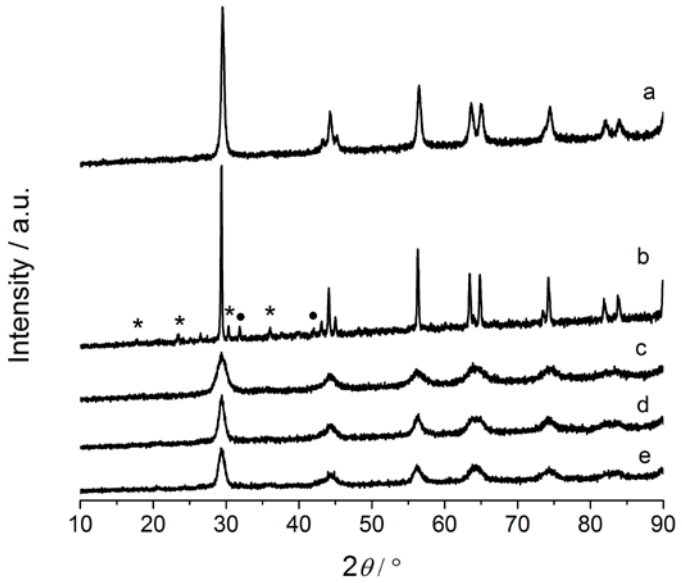

Figure 6.1 XRD measurement of: a) TiO_2, b) V-TiO_2, c) P-TiO_2, d) W-TiO_2 and e) Mo-TiO_2. * vanadium oxide, • rutile-TiO_2

We observed a distinct peak reflection at 2θ value of 29.5 °, which could be matched with the (101) plane of the JCPDS file no. 21-1272. This indicates the formation of anatase TiO_2 polymorph in all the samples. It is also of interest that no evidence of the crystalline phases of the oxides of phosphorus, tungsten and molybdenum were observed in Figure 6.1(c-e). This suggests that these oxides could be present in an amorphous phase or as crystals with very small sizes which are not detectable by XRD. On the contrary, weak reflections of crystalline vanadium oxide and the onset of rutile TiO_2 formation were identified in Figure 6.1(b), which can be correlated with JCPDS file numbers 01-089-0612 and 21-1276, respectively. The anatase-to-rutile transformation has been ascribed to proceed via the surface reaction of vanadium oxide with titanium sites, governed by a mechanism of grain growth.[67] This fact is supported by the estimated crystal size determined by applying Scherrer equation applied to plane (101). It is noted that the average crystal size of TiO_2 increased by approximately 2 fold from 27.3 to 53 nm, indicating crystal growth (Table 6.1). On the

other hand, from the XRD line broadening analysis of other modified TiO_2 samples, crystal size of TiO_2 is reduced and estimated to be between 6 and 10 nm.

The result of the N_2 adsorption-desorption isotherm of the TiO_2 samples is also presented in Table 6.1. The isotherm of pure TiO_2 shown in Figure S6.1(a) exhibits a sharp increase in the adsorbed N_2 volume at relative pressure of 0.65, characteristic for capillary condensation of a material with uniform mesopore structures. The isotherms of the modified TiO_2 samples (Figure S6.1(b-d)) are similar to the parent material, and onset of the condensation step shifts to lower values (P/P_o ~ 0.6), with the exception of V-TiO_2 (Figure S6.1(e)). The isotherm of V-TiO_2 resembles a typical material with low surface area. The reason for this can be ascribed to a phase transition of anatase to rutile,[68] which causes a drastic reduction in the surface area and a corresponding crystal growth.

Table 6.1 Physical and acid properties of pure and modified TiO_2 nanoparticles

Entry	Sample	S_{BET} (m^2/g)[a]	Pore vol. (cm^3/g)[b]	Crystal size (nm)[c]	Acidity (μmol/g)[d]	
					PyL	PyB
1	TiO_2	54.7	0.22	27.3	3.68	-
2	P-TiO_2	151.0	0.43	6.12	0.72	3.81
3	W-TiO_2	112.5	0.32	9.54	1.73	5.35
4	Mo-TiO_2	115.2	0.33	9.36	-	18.2
5	V-TiO_2	9.34	0.02	53.0	0.20	0.97

[a] BET surface area.
[b] Determined by BJH measurement at P/P_o = 0.99.
[c] Measured by XRD using Debye-Scherrer equation for the (101) plane
[d] Determined using the Lambert Beer Law.

TEM micrographs of the samples are shown in Figure 6.2. The morphological feature of TiO_2 is influenced by the presence of other oxides. We clearly observed that the particle size of TiO_2 (Figure 6.2(a)) is far larger than those of P-TiO_2, W-TiO_2 and Mo-TiO_2 (Figures 6.2(b-d)), which can be used to explain the low specific surface area of TiO_2 in comparison with these three samples. The phosphate, tungstate and molybdate ions in TiO_2 are believed to stabilize the TiO_2 structure and prevented sintering during thermal treatment, which could have led to grain growth.[57, 69] Contrarily, a remarkable increment of crystal size is observed with V-TiO_2, suggesting crystal growth (Figure 6.2(e)). Combining together with the result from XRD, a mechanism of crystal growth can be described by lattice strain relaxation phenomenon, which involves reconfiguration of

the TiO_2 crystal geometry and the reduction of the induced strain arising from lattice distortion due to the presence of vanadium ion.[70] This behavior is facilitated by thermal treatment that cause mobility and segregation of vanadium oxide, and transformation of the TiO_2 structure to a thermodynamically more stable rutile phase.[70]

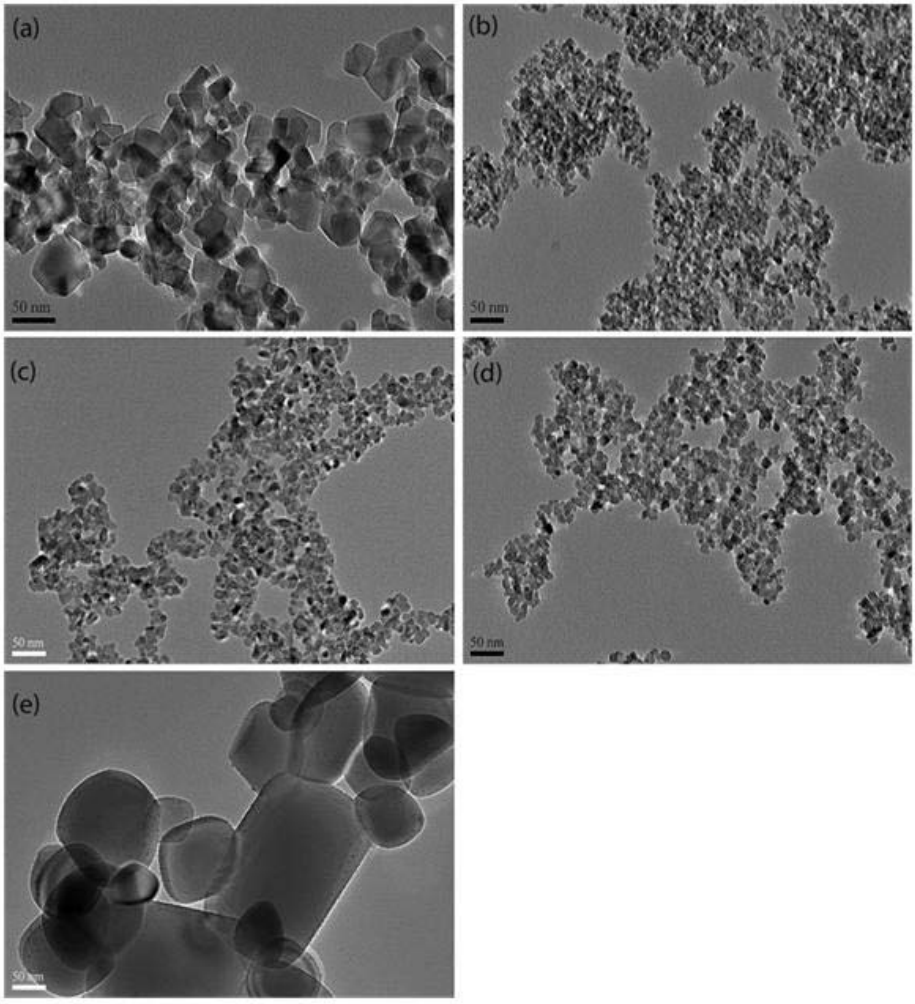

Figure 6.2 TEM micrographs of: a) TiO_2, b) P-TiO_2, c) W-TiO_2, d) Mo-TiO_2 and e) V-TiO_2

At the same time, pyridine adsorption experiments on the pure and modified TiO_2 nanoparticles were conducted to probe the presence of Lewis or Brønsted surface acid sites. As shown in Figure 6.3(a), the pyridine infrared (py-IR) spectrum of TiO_2 is dominated by absorption bands in the regions of 1400-1450 cm^{-1} and 1570-1620 cm^{-1}, typical of pyridine molecule coordinated with Lewis acid sites. Therefore, TiO_2 nanoparticle is defined here as a pure Lewis acid catalyst. The surface interaction of TiO_2 with the oxides of phosphorus, tungsten, molybdenum and vanadium leads to considerable modification of the nature of its surface acid sites. The detection of a band in the region of 1500-1560 cm^{-1} on TiO_2 after oxides modification (Figure 6.3(b-e)), allows

us to identify the presence of Brønsted acid sites. The variation of the intensity of this band indicates a change in concentration of the available Brønsted acid sites. The estimated concentrations of Brønsted (PyB) and Lewis (PyL) acid sites are presented in Table 6.1. The result shows that Brønsted acidity decreases in the order: Mo-TiO_2 > W-TiO_2 > P-TiO_2 > V-TiO_2. More so, Mo-TiO_2 appears to be a pure Brønsted acid catalyst because of the disappearance of all the bands associated with Lewis acid sites. Similarly, Damyanova et al.[71] observed that pyridine adsorbed on titania supported 12-molybdophosphate existed predominantly as protonated form (Brønsted acidity) when the sample was pretreated at 250 °C, but Lewis acidity appears on the sample pretreated at 350 °C due to isolated Mo^{6+} cations of molybdenum oxide phase(s). Hence, a plausible reason for the acidity change of TiO_2 from Lewis to Brønsted in Mo-TiO_2 may be as a result of strong interaction between the surface of titanium hydroxide and molybdenum oxide. In the case of the other modified TiO_2 samples, the presence of weak band intensity at 1450 cm^{-1} implies that a relatively small amount of Lewis acid sites are still retained.

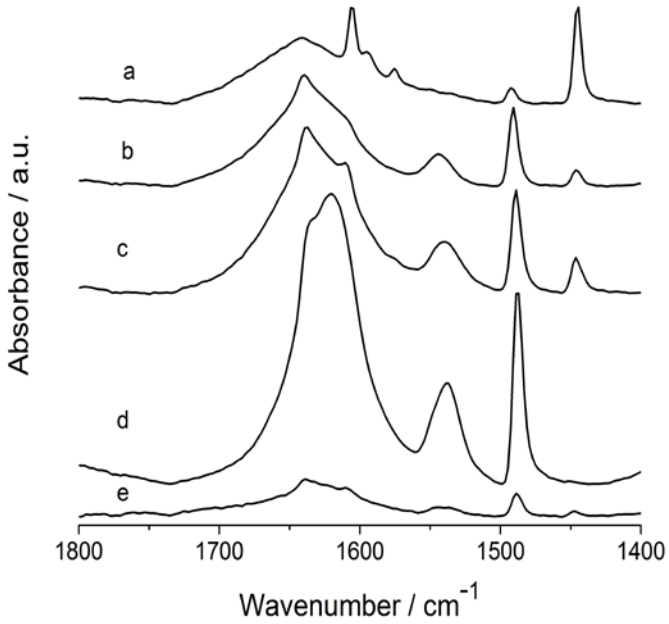

Figure 6.3 FT-IR spectra of adsorbed pyridine on: a) TiO_2, b) P-TiO_2, c) W-TiO_2, d) Mo-TiO_2 and e) V-TiO_2

6.3.2 Catalyst evaluation

6.3.2.1 Simple sugars to HMF

Previously, we reported that P-TiO_2 has better catalytic performance than TiO_2 in the transformation of glucose to HMF in a water-butanol reaction medium.[57] Herein, glucose dehydration reaction is carried out in a water-THF biphase system, and the catalytic performance of

TiO_2 and P-TiO_2 is compared. Preliminary experiments using 2 wt% glucose concentrations as the reaction feed were conducted and the results presented in Table 6.2. The outcome of the experiment confirmed the superior activity of P-TiO_2 over TiO_2. A conversion of 90.4% and 72.8% yield of HMF was achieved with TiO_2, given in Entry 1. Meanwhile, HMF yield improved to 83.4% at 93.6% conversion when P-TiO_2 was used as catalyst (Entry 2). Other identifiable products are fructose, levoglucosan, levulinic acid, formic acid and acetic acid, and their corresponding yields are listed in Table S6.1.

Table 6.2 Catalytic conversion of glucose to HMF using TiO_2 and modified TiO_2 nanoparticles[a]

Entry	Sample	Glucose conc. (wt %)	Glucose conv. (%)	HMF yield (%)
1	TiO_2	2	90.4	72.8
2	P-TiO_2	2	93.6	83.4
3	P-TiO_2	5	96.5	62.8
4	V-TiO_2	5	99.9	35.5
5	W-TiO_2	5	98.5	27.5
6	Mo-TiO_2	5	99.9	17.0

[a] Reaction conditions: 4:1 glucose/cat. wt. ratio, 100 mL solvent (water:THF = 1:4 v/v), 4 g NaCl, 105 mins reaction time, 175 °C reaction temperature, 20 bar Ar gas

However, from practical industrial point of view, it is of much interest to work at relatively higher glucose concentration in order to achieve a more economical and sustainable process. Then conducting the reaction with 5 wt% glucose concentration on P-TiO_2 under similar reaction conditions, HMF yield dropped to 62.8% (Table 6.2, Entry 3). This phenomena can be explained that at high concentration, glucose forms oligosaccharides which contain reactive hydroxy groups that lead to higher rates of cross-polymerizations with reactive intermediates and HMF.[72] This hypothesis is supported by observing a colour change of the catalyst from yellowish-white to dark brown at the end of the reaction (Figure S6.2). The colour change can be ascribed to the deposition and coverage of the catalyst surface with humin compounds. Therefore, seeking a catalyst system that is resistant to humins or a reaction medium that impedes the formation of humins is essential to effectively convert high glucose concentration feedstocks into HMF with good selectivity and high conversion. Hence, TiO_2 was modified with the introduction of oxides of molybdenum, vanadium and tungsten in a similar procedure as that for phosphorus oxide.[57] This attempt was unsuccessful as lesser yields of HMF were achievable (Table 6.2, Entries 4-6). The catalytic performance of these materials can be understood with respect to their surface acidity. On the basis of the py-IR result,

Mo-TiO_2 is characterized mainly by Brønsted acidity and very low HMF yield could be achieved. This is because isomerization of glucose to fructose is crucial to HMF formation which is catalyzed by Lewis acidity. On the other hand, W-TiO_2 and V-TiO_2 have both Brønsted and Lewis acid functionalities just like P-TiO_2. The band intensities of W-TiO_2 suggest the presence of more concentration of acid sites than P-TiO_2. Lesser yield of HMF on W-TiO_2 may then be ascribed to the presence of excess acid sites, which could be responsible for favoring unwanted reactions. There is a general consensus that interaction of bulk vanadium oxide with the surface of TiO_2 form a thin monolayer film.[73] We reasoned that the segregated vanadium oxide led to partial surface monolayer coverage of TiO_2. As a result, Brønsted acidity which is contributed by the vanadium oxide comes readily in contact with the glucose substrate and just few Lewis acid sites are available to play a relevant role during the isomerization of glucose to fructose. However, V-TiO_2 has superior HMF yield in comparison to W-TiO_2 (35.5% vs 27.5%), which can be ascribed to the acid sites concentration. W-TiO_2 has more concentration of acid sites especially, Brønsted, which can easily promote rapid degradation of HMF.

The other approach was to modify the reaction medium in order to minimize HMF degradation. Undesired side reactions can be suppressed through the addition of phase modifiers.[74] In this study, organic solvents such as: acetone, acetonitrile (AN), N-methyl-2-pyrrolidone (NMP) and toluene were examined. Figure 6.4(a) shows that selectivity to HMF was significantly improved with the addition of NMP.

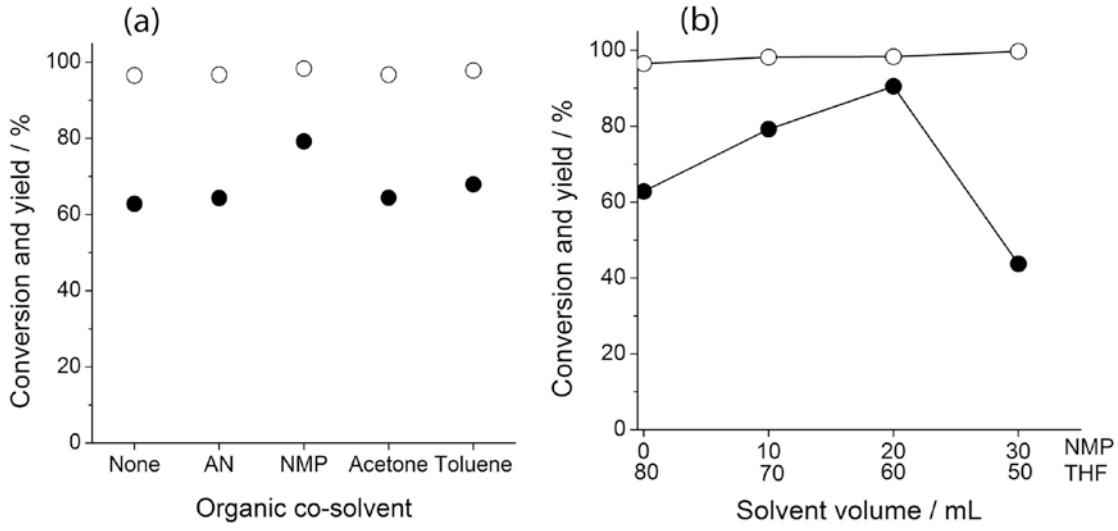

Figure 6.4 a) Influence of organic co-solvents on the selective conversion of glucose to HMF; 10 mL organic co-solvent, 70 mL THF. b) Volume ratio effect of THF/NMP on glucose-to-HMF reaction. Reaction conditions: 4:1 glucose/cat. wt. ratio, 1.25 g P-TiO_2 catalyst, 100 mL solvent (water:organic = 1:4 v/v), 4 g NaCl, 105 mins reaction time, 175 °C reaction temperature, 20 bar Ar gas. (o) Glucose conversion and (●) HMF yield

For example, addition of 10 mL of NMP to the water-THF medium enabled about 80% yield of HMF. According to a report from Román-Leshkov et al.,[74] NMP acts as an aqueous phase modifier that can suppress humin formation in water, and simultaneously enhance partitioning of HMF into the organic layer. Horvat et al.[75, 76] explained the mechansim of HMF transformation in aqueous medium. The authors stated that addition of water to the 2,3-carbon positions on HMF is responsible for the undesired polymerization reactions to humin, whereas water added to 4,5-carbon positions gave way to levulinic acid formation via decarboxylation to produce formic acid. Therefore, we can say that the beneficial role of NMP on HMF formation is related to its ability to minimize ring opening of these carbon atoms. The less intense colour change of the catalyst after reaction also supports the fact that NMP helps to reduce humins formation and deposition on the catalyst (Figure S6.3) in comparison to reaction without NMP.

Furthermore, we attempted to favor the formation of HMF by increasing the volume of NMP added to the water-THF reaction medium. We observed from the result shown in Figure 6.4(b) that HMF yield increased to a maximum value of 90.5% at 60/20 THF/NMP volume ratio. Further increment in NMP volume caused a drastic reduction in HMF yield. This is because a single phase reaction system was formed at the end of the reaction. Since there is a lack of partitioning, the already formed HMF undergoes further reaction. Thus, the optimal reaction medium for subsequent experimental design is 20:60:20 water/THF/NMP volume ratio.

Using this reaction condition, glucose was replaced with fructose as the feed in the production of HMF. The result is presented in Table 6.3 and shows that conversion of fructose into HMF proceeds significantly faster than with glucose, achieving 98.6% HMF yield within 30 mins of reaction time (Entry 2). This suggests that the mechanism of glucose transformation to HMF occurs via the rate determining step of intermediate fructose formation. Other simple sugars that were also investigated for the production of HMF are cellobiose and sucrose. Cellobiose and sucrose are dimers of monomeric unit of glucose-glucose and glucose-fructose, respectively. It is expected that the presence of additional functional groups in each of these dimers will increase the multistep reactions, beginning with hydrolytic reaction to produce their constituent monomer units, followed by isomerization and dehydration reaction steps. Therefore, we carried out the reaction with the dimers at a higher temperature, to facilitate the hydrolysis step. Identical results of HMF formation were obtained for both cellobiose and sucrose (Table 6.3, Entries 3 and 4). However, higher HMF yield obtainable from sucrose in comparison with cellobiose (98.2% vs 94.2%) is attributed to the presence of fructose in the dimer structure, which can undergo dehydration faster than glucose.

Table 6.3 Catalytic conversion of a variant of sugars to HMF over P-TiO_2 catalyst[a]

Entry	Substrate	Temp. (°C)	Conversion (%)	HMF yield (%)
1	Fructose[b]	175	99.9	98.6
2	Glucose	175	98.2	90.5
3	Cellobiose	180	99.7	94.2
4	Sucrose	180	99.8	98.2
5	Starch-rice	180	99.7	80.7
6	Starch-potato	180	99.8	84.6
7	Cellulose	180	56.7	33.0
8	Pre-treated cellulose	180	99.9	86.2

[a] Reaction conditions: 4:1 substrate/cat. wt. ratio, 100 mL solvent (water:THF+NMP = 1:4 v/v), 4 g NaCl, 105 mins reaction time, 20 bar Ar gas.
[b] 30 mins reaction time.

6.3.2.2 Complex sugars to HMF

Considering the successful production of HMF in high selectivity from simple sugars, we investigated a much more practical and sustainable production of HMF from complex sugars. Thus, we explore the reactivity of starch and cellulose towards HMF formation. The conversion of starch into HMF proceeds significantly faster and with higher selectivity than cellulose (Table 6.3, Entries 5-7). Starch from rice and potato, gave good yields of HMF (80-85%), whereas modest yield (33%) of HMF was obtained from cellulose. The reason for the disparity in the reactivity of starch and cellulose can be attributed to the structural difference of the two polymers. Starch is a polymer of glucose units linked together through α-1,4 or α-1,6 linkages whereas cellulose is a polymer of glucose linked together in an unbranched β-1,4 fashion, and are densely packed via strong inter-chain hydrogen bonds.[21] Due to the presence of strong glycosidic bonding between the sugar moieties of cellulose, it is more crystalline and less soluble than starch. On this basis, reactivity is low due to poor interaction between cellulose and the catalyst which are both present in solid state. However, cellulose is more ideal as a starting material for HMF production, being the most abundant naturally occurring feedstock. Conversion of cellulose to HMF in significant yield can be achieved via a mechanocatalytic depolymerization of cellulose, with the objective of reducing cellulose crystallinity and simultaneously facilitating the cleavage of β-1,4-glycosidic bond linkages.[41-45] With acid impregnation of cellulose, formation of soluble cello-oligomers during ball milling is facilitated. Entry 8 of Table 6.3 shows that conversion rate of cellulose was significantly promoted after the pretreatment process, producing 86.2% yield of HMF. We have previously

shown through x-ray diffraction and scanning electron microsopy analyses that the structure of the pretreated cellulose is amorphous and has a reduced particle size.[43] Furthermore, liquid state nuclear magnetic resonance result suggests the formation of oligomers comprising mainly C_1-C_6 carbons. These factors altogether are responsible for the enhanced solubility and reactivity of the pre-treated cellulose. In this way, good yield of HMF can be effectively produced from cellulose.

6.3.3 Catalyst recyclability

To minimize cost and environmental impact of catalytic industrial processes, it is desirable that the catalyst is stable and can be easily recycled once the reaction is over. Recycling efficiency of P-TiO_2 catalyst was investigated using glucose conversion to HMF as a representative reaction. The reaction was performed in a water/(THF+NMP) medium, at 175 °C for 105 mins. After each reaction, the catalyst was recovered by filtration, and the spent catalyst was washed with acetone and kept for drying. The recovered catalyst was reused without any post treatment. This procedure was followed for four subsequent cycles and the result is shown in Figure 6.5.

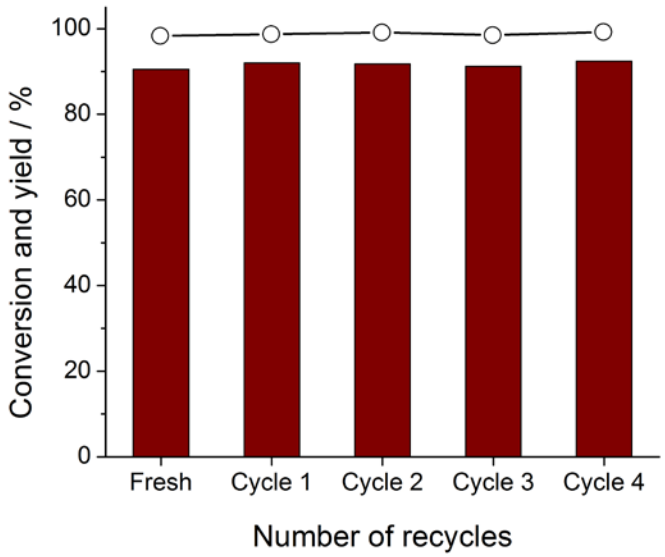

Figure 6.5 Catalyst recyclability test. Reaction conditions: 4:1 glucose/cat. wt.ratio, 100 mL solvent (water:THF+NMP = 1:4 v/v), 4 g NaCl, 105 mins reaction time, 175 °C reaction temperature, 20 bar Ar gas. (○) Glucose conversion and (■) HMF yield.

The activity of the catalyst was found to give > 90% yield of HMF and remains fairly the same even after its repeated use for four times. As reported previously, catalyst regeneration was performed because of deactivation resulting from catalyst surface coverage by deposited humins, albeit structural stability of the catalyst was maintained.[57] With NMP serving as an aqueous phase

modifier, unwanted reaction to humins was greatly inhibited. This was further supported through a quantitative analysis of deposited humins on the catalyst. The spent catalysts after the reaction, with and without NMP in the reaction system, were recovered, washed with deionized water, filtered and kept under vacuum at 80 °C overnight for drying. A known weight of the samples were measured and the carbon content analyzed by CHNS-O elemental analyzer. The carbon content of the fresh catalyst sample was also analyzed as a reference. The result shows that < 0.4% carbon was present on the fresh sample. For the reaction system with NMP, 4.1% carbon was found on the spent catalyst and this value rose to 21.2% carbon content on the spent catalyst from the reaction system without NMP. The measured carbon content can be related to the amount of humins deposited on the catalyst surface, which is reasonable high in the reaction system without NMP. Thus, we can deduce that the inhibitory effect of NMP on humins deposition on the catalyst surface seems to explain the observed stability of the catalyst activity.

6.3.4 HMF production under a continuous flow condition

To further improve the attractiveness of HMF production and simulate an industrial scenario, we progressed to investigate the catalytic performance of phosphated TiO_2 for the conversion of cellulose in a biphasic continuous flow reactor. The reactor system consists of a U-shaped stainless steel tubular reactor, two HPLC pumps (Alltech 426), heating oil bath, back pressure regulator and a reservoir to collect the reaction product. The schematic diagram of the reactor set-up is shown in Figure 6.6.

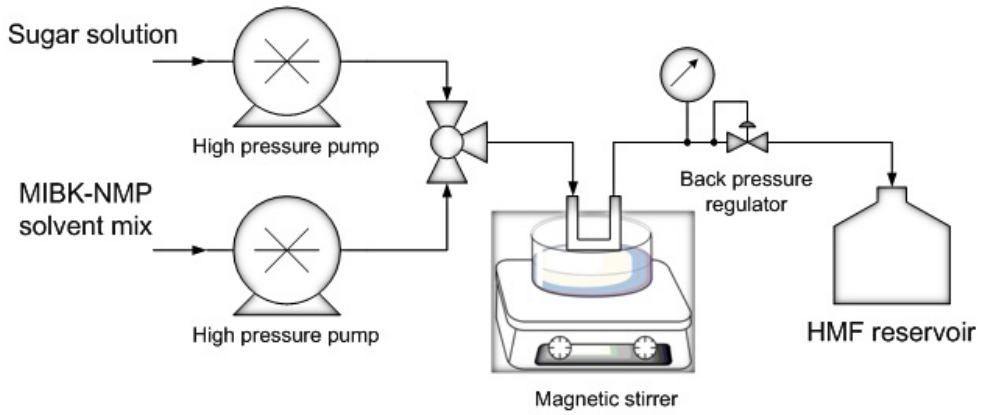

Figure 6.6 Schematic diagram of the flow reactor set-up for the conversion of cello-oligomers to HMF.

The biphasic system consists of a sugar solution (aqueous solution of the soluble cello-oligomers obtained from treated cellulose) and an organic solvent mix (MIBK:NMP 3:1 v/v), where MIBK is

defined as methyl-isobutyl-ketone. The choice of MIBK in replacing THF as the organic extracting solvent is due to its very low miscibility with water even at high reaction temperature.[56] The two feed streams were delivered by the HPLC pumps, and then connected by a 'T' connection to form a single pre-mixed stream prior to entering the flow reactor. A back pressure regulator was connected to the reactor outlet to control the pressure of the reaction system. Under a steady flow rate at 60 bars (back pressure), the pre-loaded reactor with P-TiO_2 catalyst (400 mg) was immersed in the heating oil bath maintained at the reaction temperature. A short induction period was noticed which may be due to back mixing of liquid in the pressure regulator. A factor used to measure the efficiency of the reactor is liquid hourly space velocity (LHSV). Herein, it is defined as the ratio of the volumetric flow rate of the feed solution (in mL h^{-1}) to the heated reactor volume (in mL).

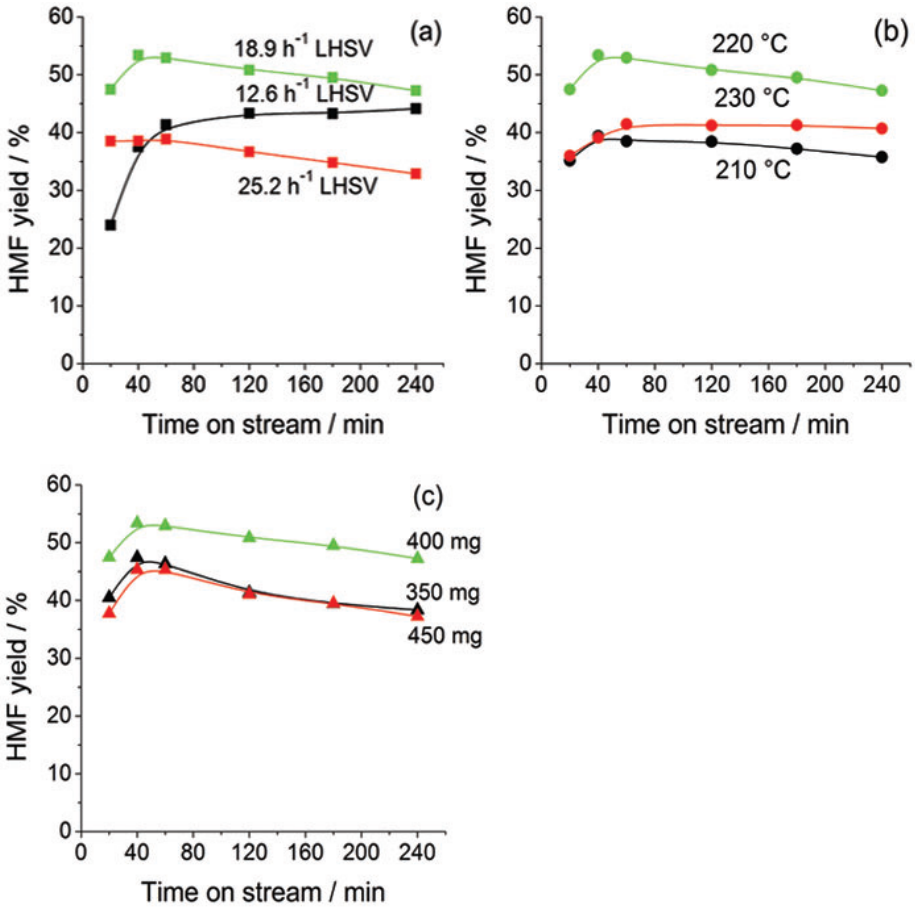

Figure 6.7 Effect of reaction parameters: a) LHSV, b) reaction temperature, c) catalyst loading amount; on the production of HMF in a flow reactor using P-TiO_2 catalyst. Reaction conditions: 5 g cello-oligomer in 100 mL water, 3:1 MIBK:NMP ratio, 1:1 water:MIBK+NMP ratio, and 60 bar back pressure.

The role of LHSV on the catalytic transformation of the cello-oligomers was investigated. The different LHSV were obtained by changing the total flow rates of the feed streams between 0.2 and 0.4 mL min^{-1}, which corresponds to a LHSV of 12.6 – 25.2 h^{-1}. The flow rate of the two feed streams was kept at a ratio 1:1. As shown in Figure 6.7(a), initial experiment at 220 °C showed that a maximum HMF yield of 53% could be reached at a total flow rate of 0.3 mL min^{-1}, corresponding to LHSV of 18.6 h^{-1}. At higher LHSV, the yield of HMF starts to decline which is attributable to lower residence time within the reactor and hence, reduced contact time of the sugar substrate with the catalyst.

The effect of reaction temperature was also investigated, and the experiments were carried out between 210 – 230 °C at a fixed LHSV of 18.9 h^{-1}. In Figure 6.7(b), we observed that temperature has a significant effect on the HMF yield. When the temperature rose from 210 to 220 °C, there was a significant increase in the HMF yield from about 40% to 53% within 60 minutes time on stream. This suggests that higher temperature accelerates glycosidic bond cleavage of the cello-oligomers, and thus reactivity is enhanced. However, a further increment of the reaction temperature to 230 °C was detrimental for HMF yield as shown in Figure 6.7(b). This may be due to unwanted reaction producing humins. Another factor that may enhance reaction performance is catalyst loading. Under a fixed LHSV of 18.9 h^{-1} and reaction temperature of 220 °C, we studied the effect of catalyst loading amount between the range from 350 to 450 mg. From the result illustrated in Figure 6.7(c), we observed HMF yield to be increasing with the increase in catalyst loading from 350 to 400 mg. The enhanced productivity can be ascribed to availability of more active sites accessible by the reactant. With further increment in catalyst loading, the yield of HMF declined. We can deduce that catalyst loading of 400 mg provides the required active acid sites for the multi-step reactions in the conversion of the cello-oligomers to HMF. Above 400 mg, the excessive acidic sites can promote degradation of HMF, resulting in the decline of HMF yield. In spite of considerable activity decay as the reaction progressed beyond 40 minutes time on stream, which may be due to glucose fractions of the cello-oligomers turning into char or humins, we have been able to demonstrate the feasibility of the continuous production of HMF from cellulose in a relatively good yield. Further optimization of reactor configuration and process conditions may effectively enhance the application of this biphasic continuous reactor for the production of HMF, and this study will be reported in a future publication.

6.4 Conclusion

We described a batch and continuous process of catalytic conversion of sugars to HMF in a biphasic system. The effectiveness of the catalytic process to selective formation of HMF was enhanced by

adding NMP to the reaction medium. This effect was the consequence of the suppression of undesired polymerization of HMF to humins. Phosphated TiO_2 was found to be an efficient and versatile solid acid catalyst in the selective conversion of a variety of sugars towards HMF formation. The reaction system of water-THF+NMP medium and P-TiO_2 catalyst operated as a batch reaction process, affords fructose and glucose conversion efficiencies up to 98% and 90% yields of HMF, respectively. Furthermore, cellobiose and sucrose conversions achieved 94% and 98% HMF, respectively. The minor difference in their reactivity is ascribed to difference in the dehydration rate of the monomeric units of the dimers. Sucrose contains fructose which is more reactive than glucose. Similarly, high HMF product (80-85%) from starch (rice, potato) than from cellulose (33%) was observed, which is mainly attributed to the hydrolysis rate as glucose units of cellulose are strongly linked by β-1,4-glycosidic bond. Mechanocatalytic depolymerization of cellulose was used as an efficient pretreatment process for the production of soluble cello-oligomers that can be easily hydrolyzed to glucose units, and subsequently achieving 86% HMF yield. Catalyst recyclability study shows that the P-TiO_2 catalyst is easily recoverable and reproducible activity is achieved.

A flow reactor system was also used to demonstrate the capability of a continuous production of HMF. Utilizing the soluble oligomers obtained from pre-treated cellulose in a water-MIBK+NMP biphasic system and P-TiO_2 catalyst, a reasonably good yield of HMF (53%) is obtainable. Thus, the pre-treatment of cellulose to give soluble oligomers appears to be advantageous and applicable for the continuous production of HMF using a flow reactor. Hence, this approach is amenable to direct transformation of real biomass for production of HMF in scalable quantities.

Acknowledgements

The authors gratefully acknowledge the financial support of the Nanomaterials Center at The University of Queensland, Australia. The authors also acknowledge the facilities, scientific and technical assistance, of the Australian Microscopy and Microanalysis Research Facility at The University of Queensland. The first author sincerely appreciates the sponsorship from the International Postgraduate Research Scholarship (IPRS) and UQ Centennial Scholarship (UQ Cent).

References

1. J. N. Chheda, G. W. Huber and J. A. Dumesic, *Angewandte Chemie International Edition*, 2007, **46**, 7164-7183.
2. J. J. Bozell and G. R. Petersen, *Green Chemistry*, 2010, **12**, 539-554.
3. O. Casanova, S. Iborra and A. Corma, *ChemSusChem*, 2009, **2**, 1138-1144.
4. C. Moreau, M. Belgacem and A. Gandini, *Top Catal*, 2004, **27**, 11-30.
5. A. Gandini, A. J. D. Silvestre, C. P. Neto, A. F. Sousa and M. Gomes, *Journal of Polymer Science Part A: Polymer Chemistry*, 2009, **47**, 295-298.
6. D. M. Alonso, S. G. Wettstein and J. A. Dumesic, *Green Chemistry*, 2013, **15**, 584-595.
7. I. T. Horvath, H. Mehdi, V. Fabos, L. Boda and L. T. Mika, *Green Chemistry*, 2008, **10**, 238-242.
8. Á. Bereczky, K. Lukács, M. Farkas and S. Dóbé, *Natural Resources*, 2014, **2014**.
9. Y. Román-Leshkov, C. J. Barrett, Z. Y. Liu and J. A. Dumesic, *Nature*, 2007, **447**, 982-985.
10. J. B. Binder and R. T. Raines, *Journal of the American Chemical Society*, 2009, **131**, 1979-1985.
11. X. Tong, Y. Ma and Y. Li, *Applied Catalysis A: General*, 2010, **385**, 1-13.
12. G. Yong, Y. Zhang and J. Y. Ying, *Angewandte Chemie International Edition*, 2008, **47**, 9345-9348.
13. R. Huang, W. Qi, R. Su and Z. He, *Chemical Communications*, 2010, **46**, 1115-1117.
14. J. N. Chheda, Y. Roman-Leshkov and J. A. Dumesic, *Green Chemistry*, 2007, **9**, 342-350.
15. H. Zhao, J. E. Holladay, H. Brown and Z. C. Zhang, *Science*, 2007, **316**, 1597-1600.
16. Y. Román-Leshkov and J. Dumesic, *Top Catal*, 2009, **52**, 297-303.
17. J. Wang, W. Xu, J. Ren, X. Liu, G. Lu and Y. Wang, *Green Chemistry*, 2011, **13**, 2678-2681.
18. Z. Zhang, Q. Wang, H. Xie, W. Liu and Z. Zhao, *ChemSusChem*, 2011, **4**, 131-138.
19. X. Qi, M. Watanabe, T. M. Aida and J. R. L. Smith, *Green Chemistry*, 2008, **10**, 799-805.
20. M. Stöcker, *Angewandte Chemie International Edition*, 2008, **47**, 9200-9211.
21. P. L. Dhepe and A. Fukuoka, *ChemSusChem*, 2008, **1**, 969-975.
22. Y. Nishiyama, P. Langan and H. Chanzy, *Journal of the American Chemical Society*, 2002, **124**, 9074-9082.
23. Y. Nishiyama, J. Sugiyama, H. Chanzy and P. Langan, *Journal of the American Chemical Society*, 2003, **125**, 14300-14306.

24. D. Klemm, B. Heublein, H.-P. Fink and A. Bohn, *Angewandte Chemie International Edition*, 2005, **44**, 3358-3393.
25. Y. Su, H. M. Brown, G. Li, X.-d. Zhou, J. E. Amonette, J. L. Fulton, D. M. Camaioni and Z. C. Zhang, *Applied Catalysis A: General*, 2011, **391**, 436-442.
26. Y. Zhang, H. Du, X. Qian and E. Y. X. Chen, *Energy & Fuels*, 2010, **24**, 2410-2417.
27. E. Ohno and H. Miyafuji, *J Wood Sci*, 2014, **60**, 428-437.
28. M. P. Foley, L. M. Haverhals, D. K. Klein, W. B. McIlvain, W. M. Reichert, D. W. O'Sullivan, H. C. De Long and P. C. Trulove, *American Journal of Biomass and Bioenergy*, 2014, **3**, 68-82.
29. R. P. Swatloski, S. K. Spear, J. D. Holbrey and R. D. Rogers, *Journal of the American Chemical Society*, 2002, **124**, 4974-4975.
30. Y. Cao, J. Wu, J. Zhang, H. Li, Y. Zhang and J. He, *Chemical Engineering Journal*, 2009, **147**, 13-21.
31. O. A. El Seoud, A. Koschella, L. C. Fidale, S. Dorn and T. Heinze, *Biomacromolecules*, 2007, **8**, 2629-2647.
32. Z. Fang and J. A. Koziński, *Proceedings of the Combustion Institute*, 2000, **28**, 2717-2725.
33. L. K. Tolonen, M. Juvonen, K. Niemelä, A. Mikkelson, M. Tenkanen and H. Sixta, *Carbohydrate Research*, 2015, **401**, 16-23.
34. S. Kumar and R. B. Gupta, *Industrial & Engineering Chemistry Research*, 2008, **47**, 9321-9329.
35. M. Sasaki, Z. Fang, Y. Fukushima, T. Adschiri and K. Arai, *Industrial & Engineering Chemistry Research*, 2000, **39**, 2883-2890.
36. Y. Ishikawa and S. Saka, *Cellulose*, 2001, **8**, 189-195.
37. A. Koriakin, H. Van Nguyen, D. W. Kim and C.-H. Lee, *The Journal of Supercritical Fluids*, 2014, **95**, 175-186.
38. F. S. Asghari and H. Yoshida, *Carbohydrate Research*, 2010, **345**, 124-131.
39. D. Klein-Marcuschamer, B. A. Simmons and H. W. Blanch, *Biofuels, Bioproducts and Biorefining*, 2011, **5**, 562-569.
40. K. T. Tan and K. T. Lee, *Renewable and Sustainable Energy Reviews*, 2011, **15**, 2452-2456.
41. S. M. Hick, C. Griebel, D. T. Restrepo, J. H. Truitt, E. J. Buker, C. Bylda and R. G. Blair, *Green Chemistry*, 2010, **12**, 468-474.
42. N. Meine, R. Rinaldi and F. Schüth, *ChemSusChem*, 2012, **5**, 1449-1454.
43. A. Shrotri, L. K. Lambert, A. Tanksale and J. Beltramini, *Green Chemistry*, 2013, **15**, 2761-2768.

44. R. Carrasquillo-Flores, M. Käldström, F. Schüth, J. A. Dumesic and R. Rinaldi, *ACS Catalysis*, 2013, **3**, 993-997.
45. J. Hilgert, N. Meine, R. Rinaldi and F. Schuth, *Energy & Environmental Science*, 2013, **6**, 92-96.
46. M. Kaldstrom, N. Meine, C. Fares, F. Schuth and R. Rinaldi, *Green Chemistry*, 2014, **16**, 3528-3538.
47. P. Dornath, H. J. Cho, A. Paulsen, P. Dauenhauer and W. Fan, *Green Chemistry*, 2015, **17**, 769-775.
48. W.-H. Peng, Y.-Y. Lee, C. Wu and K. C. W. Wu, *Journal of Materials Chemistry*, 2012, **22**, 23181-23185.
49. Y. Su, H. M. Brown, X. Huang, X.-d. Zhou, J. E. Amonette and Z. C. Zhang, *Applied Catalysis A: General*, 2009, **361**, 117-122.
50. P. Wang, H. Yu, S. Zhan and S. Wang, *Bioresource Technology*, 2011, **102**, 4179-4183.
51. N. Shi, Q. Liu, Q. Zhang, T. Wang and L. Ma, *Green Chemistry*, 2013, **15**, 1967-1974.
52. K. Y. Nandiwale, N. D. Galande, P. Thakur, S. D. Sawant, V. P. Zambre and V. V. Bokade, *ACS Sustainable Chemistry & Engineering*, 2014, **2**, 1928-1932.
53. M. Mascal and E. B. Nikitin, *Green Chemistry*, 2010, **12**, 370-373.
54. M. Mascal and E. B. Nikitin, *Angewandte Chemie International Edition*, 2008, **47**, 7924-7926.
55. M. Mascal and E. B. Nikitin, *ChemSusChem*, 2009, **2**, 859-861.
56. C. V. McNeff, D. T. Nowlan, L. C. McNeff, B. Yan and R. L. Fedie, *Applied Catalysis A: General*, 2010, **384**, 65-69.
57. L. Atanda, S. Mukundan, A. Shrotri, Q. Ma and J. Beltramini, *ChemCatChem*, 2015, **7**, 781-790.
58. A. A. Budneva, E. A. Paukshtis and A. A. Davydov, *React Kinet Catal Lett*, 1987, **34**, 63-67.
59. C. A. Emeis, *Journal of Catalysis*, 1993, **141**, 347-354.
60. A. Chareonlimkun, V. Champreda, A. Shotipruk and N. Laosiripojana, *Fuel*, 2010, **89**, 2873-2880.
61. S. De, S. Dutta, A. K. Patra, A. Bhaumik and B. Saha, *Journal of Materials Chemistry*, 2011, **21**, 17505-17510.
62. S. De, S. Dutta, A. K. Patra, B. S. Rana, A. K. Sinha, B. Saha and A. Bhaumik, *Applied Catalysis A: General*, 2012, **435–436**, 197-203.

63. S. Dutta, S. De, A. K. Patra, M. Sasidharan, A. Bhaumik and B. Saha, *Applied Catalysis A: General*, 2011, **409–410**, 133-139.
64. A. Dutta, A. K. Patra, S. Dutta, B. Saha and A. Bhaumik, *Journal of Materials Chemistry*, 2012, **22**, 14094-14100.
65. C.-H. Kuo, A. S. Poyraz, L. Jin, Y. Meng, L. Pahalagedara, S.-Y. Chen, D. A. Kriz, C. Guild, A. Gudz and S. L. Suib, *Green Chemistry*, 2014, **16**, 785-791.
66. K. Nakajima, R. Noma, M. Kitano and M. Hara, *Journal of Molecular Catalysis A: Chemical*, 2014, **388–389**, 100-105.
67. M. A. Bañares, L. Alemany, amp, x, J. s, M. C. Jiménez, M. A. Larrubia, F. Delgado, M. L. Granados, Martı, amp, x, A. nez-Arias, J. M. Blasco, J. L. Fierro, amp, x and G. s, *Journal of Solid State Chemistry*, 1996, **124**, 69-76.
68. E. C. Bucharsky, G. Schell, R. Oberacker and M. J. Hoffmann, *Journal of the European Ceramic Society*, 2009, **29**, 1955-1961.
69. A. K. Dalai, R. Sethuraman, S. P. R. Katikaneni and R. O. Idem, *Industrial & Engineering Chemistry Research*, 1998, **37**, 3869-3878.
70. L. E. Depero, P. Bonzi, M. Musci and C. Casale, *Journal of Solid State Chemistry*, 1994, **111**, 247-252.
71. S. Damyanova, M. L. Cubeiro and J. L. G. Fierro, *Journal of Molecular Catalysis A: Chemical*, 1999, **142**, 85-100.
72. B. F. M. Kuster, *Starch - Stärke*, 1990, **42**, 314-321.
73. G. Centi, *Applied Catalysis A: General*, 1996, **147**, 267-298.
74. Y. Román-Leshkov, J. N. Chheda and J. A. Dumesic, *Science*, 2006, **312**, 1933-1937.
75. J. Horvat, B. Klaić, B. Metelko and V. Šunjić, *Tetrahedron Letters*, 1985, **26**, 2111-2114.
76. J. Horvat, B. Klaic, B. Metelko and V. Sunjic, *Croatica Chemica Acta*, 1986, **59**, 429-438.

Supplementary Material

Table S6.1 Catalytic conversion of glucose to HMF using TiO_2 and modified TiO_2 nanoparticles[a]

Entry	Sample	Glucose conc. (wt %)	Glucose conv. (%)	Product yield (%)					
				HMF	Fructose	LA	FA[b]	AA	Levoglucosan
1	TiO_2	2	90.4	72.8	10.3	0.83	3.07	0.12	2.06
2	P-TiO_2	2	93.6	83.4	1.78	1.14	3.46	0.56	1.13
3	P-TiO_2	5	96.5	62.8	0.25	4.94	10.7	2.01	0.67
4	V-TiO_2	5	99.9	35.5	0.00	1.65	5.23	0.86	7.33
5	W-TiO_2	5	98.5	27.5	4.13	0.32	5.56	4.66	5.13
6	Mo-TiO_2	5	99.9	17.0	3.17	1.53	6.22	5.79	4.97

[a] Reaction conditions: 4:1 glucose/cat. wt. ratio, 100 mL solvent (water:THF = 1:4 v/v), 4 g NaCl, 105 mins reaction time, 175 °C reaction temperature, 20 bar Ar gas. LA – Levulinic acid, FA – Formic acid, AA – Acetic acid

[b] Rehydration of HMF induces ring cleavage to give levulinic acid along with an equivalent amount of formic acid. Higher yield of formic acid more than the expected equivalent yield may be ascribed to hydrolytic fission of furfural,[1] which was detected as one of the products by HPLC but at low concentration beyond quantifiable limit.

References

1. R. Weingarten, W. C. Conner and G. W. Huber, *Energy & Environmental Science*, 2012, **5**, 7559-7574.

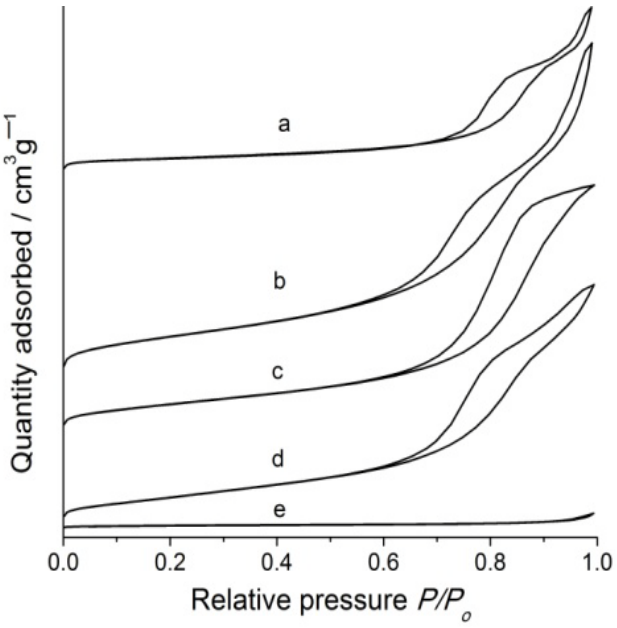

Figure S6.1 Nitrogen adsorption-desorption isotherms for: a) TiO_2, b) P-TiO_2, c) W-TiO_2, d) Mo-TiO_2 and e) V-TiO_2

Figure S6.2 Colour change of P-TiO_2 catalyst: a) before reaction and after reaction. Reaction conditions: 4:1 glucose/cat. wt. ratio, 100 mL solvent (water:THF = 1:4 v/v), 4 g NaCl, 105 mins reaction time, 175 °C reaction temperature, 20 bar Ar gas

Figure S6.3 Colour change of P-TiO_2 catalyst after reaction: a) without NMP and b) with NMP. Reaction conditions: 4:1 glucose/cat. wt. ratio, 100 mL solvent (water:organic = 1:4 v/v), 4 g NaCl, 105 mins reaction time, 175 °C reaction temperature, 20 bar Ar gas

Chapter 7

High yield conversion of cellulosic biomass into 5-Hydroxymethylfurfural and a study of the reaction kinetics of cellulose to HMF conversion in a biphasic system

This chapter was published in Catalysis Science & Technology, DOI: 10.1039/c6cy00820h

High yield conversion of cellulosic biomass into 5-Hydroxymethylfurfural and a study of the reaction kinetics of cellulose to HMF conversion in a biphasic system

Luqman Atanda,[a] Muxina Konarova,[a] Qing Ma,[a] Swathi Mukundan,[a] Abhijit Shrotri[b] and Jorge Beltramini[a]

[a] *Nanomaterials Centre, Australian Institute for Bioengineering & Nanotechnology and School of Chemical Engineering, The University of Queensland, Brisbane, QLD 4072, Australia*

[b] *Institute for Catalysis, Hokkaido University, Kita 21 Nishi 10, Kita-Ku, Sapporo, 001-0021, Japan*

Abstract

Catalytic technology for cellulosic biomass conversion has been proven as a promising approach for valuable chemical feedstock production. However, its recalcitrant nature is a major limitation to unlocking the carbohydrate biopolymer content and their subsequent conversion into 5-hydroxymethylfural (5-HMF). This paper investigates the production of 5-HMF using glucose, cellulose, sugarcane bagasse and rice husk as the feedstocks. Acid dehydration of the carbohydrate sources was conducted in a biphasic system of water–MeTHF modified with N-methyl-2-pyrrolidone (NMP) over a phosphated-TiO_2 catalyst. The catalyst displayed a very good catalytic performance for the conversion of glucose into HMF (91% yield). More so, it is suitable for the selective conversion of mechanocatalytic depolymerized cellulose to 74.7% yield of HMF. Cellulosic biomass could also be directly converted into HMF and furfural in reasonable yields. Efficiency of biomass–to–HMF production was further advanced after biomass fractionation treatment. Remarkable yields of 72% and 65% HMF were produced from sugarcane bagasse and rice husk, respectively. Finally, reaction kinetics of solubilized cellulose–to–HMF was investigated and a simplified kinetic model comprising of two reaction steps was developed: (1) hydrolysis of cello-oligomers to glucose; and (2) glucose dehydration to HMF.

7.1 Introduction

Alternatives to non-renewable source of chemical and energy production have gained a lot of interest in recent years to meet the increasing global demand for these commodities. Transition from fossil-fuel driven to greener economy may be achieved through the utilization of lignocellulosic biomass, which is acknowledged as the world's most abundant renewable carbon resources.[1] As a result, considerable research is on-going to advance catalytic technologies through novel catalyst design and innovative reaction engineering to realize sustainable bio-refinery processes for production of chemicals and fuels.[2-4] A key step in this direction is the transformation of the biopolymer carbohydrate components, especially cellulose, which constitutes a major percentage (up to 50%) of biomass composition, to produce valuable platform chemicals like 5-hydroxymethylfurfural (HMF).

HMF is a vital building block compound whose derivatives can be applied in the production of solvents, polymers and fuels.[5-7] The main route extensively reported for obtaining HMF is by acid catalyzed dehydration of monosaccharides, such as glucose and fructose.[5, 7, 8] Currently, efficient production of HMF from cellulose or directly from lignocellulosic biomass using ionic liquid has recorded significant progress.[9-16] However, commercial viability of this approach is faced with challenges owing mainly to high cost of ILs and the prohibitive cost of separation.[17] Adopting biphasic solution of water–organic system is favoured as a highly effective and economically acceptable route of selectively producing HMF on an industrial scale. [17-21] The continuous partitioning of HMF into the organic phase prevents its re-polymerization or decomposition and thus, improves recovery efficiency of high purity product. More importantly, realizing a low boiling point biomass-derived solvent with high partitioning coefficient will minimize intensive requirement for product recovery, thereby facilitating overall industrial viability of carbohydrate dehydration in biphasic systems.

The design of an effective, easily separable and reusable catalyst is also crucial for HMF synthesis. Metal chlorides in tandem with mineral acids constitute the dominant catalyst system (homogeneous catalysis) used for acid dehydration of carbohydrates in biphasic media.[19, 22-25] Despite their effectiveness to produce high yields of HMF, they are still faced with the challenge of safe handling and corrosion hazards for large scale processing. Meanwhile, solid acids may potentially overcome the above mentioned limitations, though they present additional challenges of low product yield compared to homogeneous catalysts and sometimes require frequent regeneration due to deactivation arising from partial/complete active site blockage by deposited humin compounds. Consequently, emphasis is to design an effective single catalyst system that is recalcitrant to humin formation. Zeolites,[26, 27] heteropoly acids,[28, 29] sulfonated polymer,[30]

phosphates,[31] metal oxides[32] and mesoporous metal phosphates[33, 34] are some of the solid acids reported to have good catalytic performance for biphasic dehydration of carbohydrates. Recently, we reported the development of phosphated-TiO_2 by a two-step synthesis method as a highly active and selective catalyst for the conversion of carbohydrates to HMF.[35, 36] The excellent catalytic behavior of phosphated-TiO_2 was rationalized in terms of its Ti–O–P bonding, resulting in an acid bifunctional nanoparticle with high surface acidity.[35] Reaction medium was found to play a complementary role in favouring the formation of the desired product. By using a biphasic water–THF system modified with NMP, catalytic performance of the catalyst was remarkably enhanced.[36]

In this present work, we attempted a more facile catalyst preparation technique by synthesizing phosphated–TiO_2 via a one-pot route. The structure and porosity characteristics of the above material were verified by employing XRD and N_2 porosimetry analyses. Microscopic analysis including field emission scanning electron microscopy (FE-SEM) and high resolution transmission electron microscopy (HR-TEM) were applied to examine the morphology of the material. XPS and EDS analyses were used to examine the chemical composition of the resulting material. The nanoparticle was tested for the catalytic conversion of carbohydrates to HMF in a water–MeTHF biphasic medium. Reaction pathway towards HMF formation was examined, which was monitored through time analysis of cellulose, cellobiose and glucose conversion reactions. Based on the observed data, we developed a simplified reaction model, and performed kinetic studies to obtain important reaction parameters. Direct utilization of raw biomass feedstock such as sugarcane bagasse and rice husk was also examined for the production of HMF.

7.2 Experimental

7.2.1 Chemicals and materials

Glucose, fructose, cellobiose, sigmacell 20 μm micro-crystalline cellulose (MCC), oxalic acid, 5-hydroxymethylfurfural (HMF), furfural, titanium IV butoxide, *n*-butanol, ammonium hydroxide solution (28 wt%), ammonium phosphate monobasic, n-methyl-2-pyrrolidone, sodium hydroxide and barium hydroxide were obtained from Sigma-Aldrich. 2-Methyltetrahydrofuran was purchased from Merck Millipore. De-pithed sugarcane bagasse was provided by Sugar Research Institute, Queensland University of Technology, and rice husk was obtained from local suppliers. All the chemicals were used without further purification. Ultrapure water (18.2 MΩ cm^{-1}) from Elga distillation system was used for all the experiment.

7.2.2 Catalyst preparation

Neutral amine sol-gel technique was used to prepare phosphated–TiO_2 nanoparticle using titanium IV butoxide as the TiO_2 precursor. The sol was prepared by the dropwise addition of the alkoxide precursor into an aqueous solution of ammonium phosphate monobasic containing *n*-butanol under stirring. The mole ratio of butanol/alkoxide/ammonium phosphate/water in the initial mixture is 1/0.125/0.0124/2. Finally, the pH of the solution was controlled and maintained at 7 by adding ammonium hydroxide solution and the mixture was maintained under reflux at 353 K for another 24 h. After gelation, excess solvent was evaporated under reduced pressure and the sample was dried at 353 K overnight. Then, the resultant solid was calcined at 873 K for 4 h.

7.2.3 Catalyst characterization

XRD patterns were obtained using a Rigaku Miniflex equipped with a monochromatic CoKα radiation (30 kV, 15 mA). Analyses were performed at a scan speed of 5°/min with a step of 0.02°, in the 2θ range of 10°–90°. N_2 adsorption-desorption isotherms were obtained at 77 K on a Micromeritics Tristar II 3020 analyzer surface area and porosity analyzer. The sample was outgassed overnight at 473 K before measurement. SEM and TEM micrographs were obtained with a JEOL 7100 and JEOL 2100, respectively. Field emission-scanning electron microscopy (FE-SEM) and high resolution transmission electron microscopy (HR-TEM) studies were conducted on a JEOL JSM-7100 at 20 kV and a JEOL JEM 2010 microscope at 200 kV, respectively. EDS is used as a chemical microanalysis technique to characterize the elemental composition of the nanomaterial.

7.2.4 Two-stage biomass fractionation

Two-stage fractionation of rice husk and sugarcane bagasse was carried out by alkali pulping followed by organocat process. Alkali treatment of biomass was carried out with 2.5% NaOH at 353 K for 2 h in a solid/liquid ratio of 1:10 for rice husk and 1:15 for sugarcane bagasse. Subsequently, the alkali-treated materials were subjected to the organocat process in a Parr reactor vessel following the procedure reported by Grande et al.[37] 10 g rice husk was suspended in a solution of 100 mL of water (150 mL of water is used in the case of sugarcane bagasse) and oxalic acid (0.1 M), and 50 mL MeTHF was added into the vessel. Thereafter, temperature was ramped to and held at 413 K for 3 h under 10 bar Ar pressure with vigorous stirring.

7.2.5 Mechanocatalytic depolymerization

Mechanocatalytic depolymerization of cellulose/biomass was conducted by ball milling of acidulated substrate sample, and the procedure has been described elsewhere.[38] In a typical method,

H_2SO_4 (2.5 mmol) was diluted to a volume of 40 mL. Sigmacell microcrystalline cellulose/biomass (10 g) was then added to this solution, and the solution was stirred for a few minutes. The resulting slurry was dried under a reduced pressure, followed by overnight air drying at 323 K. The acidulated cellulose/biomass thus obtained was then milled in a planetary ball mill using 5 mm stainless steel balls, with a substrate to ball weight ratio of 1:10. The mill was operated at 400 rpm, with a 15 min pause after every 30 min of continuous milling for a total milling time of 10 h. The milling time reported refers only to the active milling time. The pause allowed dissipation of heat generated during milling, which prevented overheating of reactants.

7.2.6 Catalytic test and product analysis

Catalytic test: Carbohydrate conversion reaction was carried out in a stainless steel reaction vessel (Parr Instrument). The mixture of the carbohydrate substrate, water, MeTHF, NMP and catalyst were charged into the reactor vessel and sealed. The system was purged with high purity (99.9%) Ar gas and then pressurized to 20 bar. The reactor was raised to the desired temperature, kept under vigorous stirring and held at the set temperature for a predetermined reaction time. Each experimental run was repeated three times with a typical error in the range of ±2%.

Product analysis: The products were analyzed by a Shimadzu Prominence HPLC equipped with an analytical column (Bio-Rad Aminex HPX-87H) and both RID–10 (refractive index) and SPD–M20A (UV–Vis) as detectors. The HPLC was operated under the following conditions: oven temperature, 323 K, mobile phase, 5 mM H_2SO_4; flow rate, 0.6 ml/min; injection volume, 10 µL. Using external standard method and calibration curves of commercially available standard substrates, conversion (Conv. mol %) and products yield (mol %) were calculated according to:

$$Conv.(mol\%) = \left(1 - \frac{nC_6}{nC_6^o}\right) \times 100\%$$

$$Product\ yield\ (mol\%) = \left(\frac{n_i}{nC_6^o}\right) \times 100\%$$

where nC_6 and nC_6^o denote number of moles of C_6 sugar in the product and feed, respectively, and n_i is the number of moles of identified products (HMF, furfural etc.)

7.3 Results and Discussion

7.3.1 Catalyst characterization

XRD pattern of the material is shown in Figure 7.1(a). The presence of anatase phase of titania is confirmed by observing 2θ diffraction peaks at 28, 45, 57 and 74, which corresponds to (101), (004), (200) and (204) planes, respectively. The position and intensity of these peaks are in agreement with JCPDS File No. 21-1272. The broadening of the diffraction peaks indicates small-sized nanocrystals and by using Scherrer's equation, the average crystallite size is calculated as 7.7 nm from diffraction plane (101). The nitrogen adsorption-desorption isotherm shown in Figure 7.1(b) is a representative of type IV isotherm with onset capillary condensation at P/P_o = 0.6, typical of mesoporous particle. The specific surface area of the particle is 125 m^2/g while the pore diameter is estimated to be 6.04 nm.

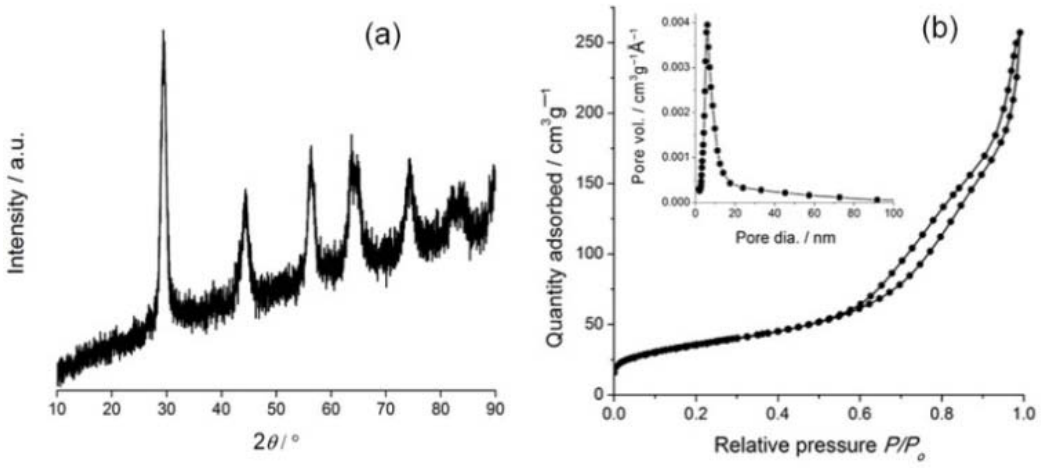

Figure 7.1 Structural and textural properties of phosphated–TiO_2 nanoparticle: a) XRD pattern and b) N_2 adsorption-desorption isotherm

XPS analysis was carried out to analyse the chemical composition and elucidate the chemical state of the nanomaterial as shown in Figure 7.2(a). The high resolution Ti 2p spectrum exhibits two peaks at 459 and 465, which are characteristic of Ti^{4+}. P 2p spectra could be observed at a binding energy of 134.1 eV, which indicates phosphorus exits in the pentavalent oxidation state (P^{5+}). Deconvolution of the O 1s region by peak fitting revealed the presence of three species of oxygen at 530.2, 531.1 and 533.4 eV corresponding to Ti–O, P–O and O–H bonding, respectively.[35, 39]

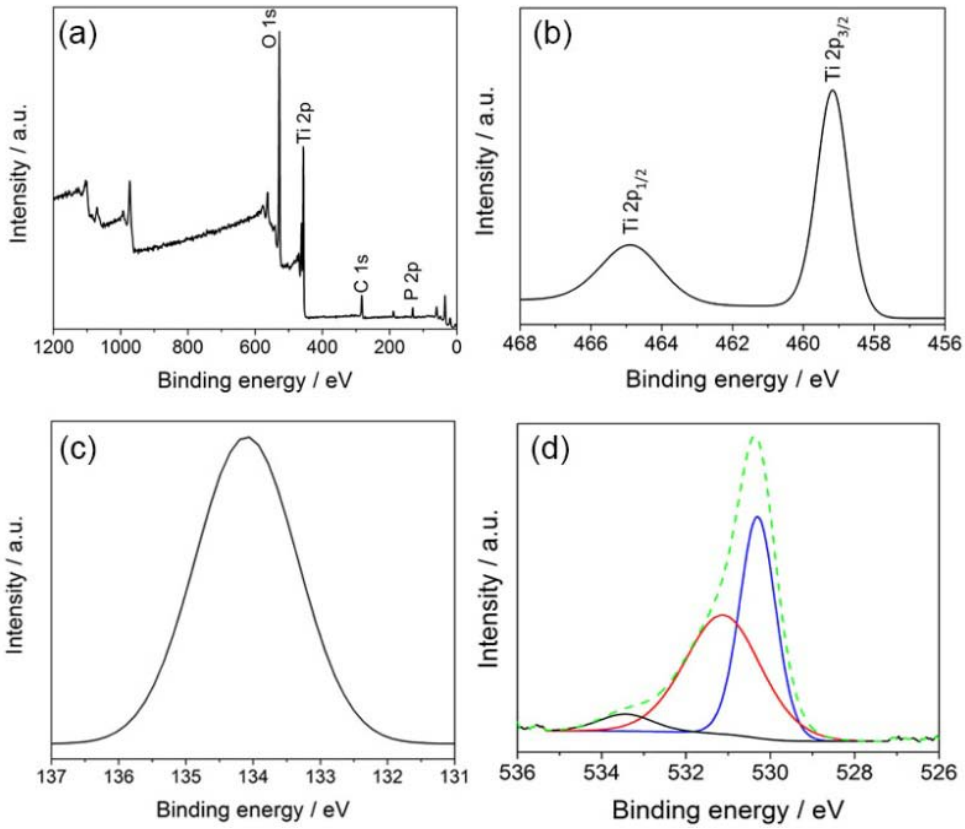

Figure 7.2 XPS analysis of phosphated–TiO_2 nanoparticle. a) wide survey scan and high resolution spectra of: b) Ti 2p, c) P 2p, d) O 1s

SEM micrograph (Figure 7.3(a)) shows that the sample consisted of plate-like clusters of size 20-40 μm and based on HRTEM data (Figure 7.3(b)), these particles consist of anatase-TiO_2 nanocrystals having a mean size of 8.8 nm and this agrees well with the result obtained from XRD. In addition, EDS spectrum (Figure S7.1) confirmed that the nanoparticle is elementally composed of Ti, O and P, with the C peak originating from carbon sputtering prior to SEM analysis. Based on these data, we can conclude that the as-prepared material is of anatase polymorph with successful incorporation of phosphorus in the titania framework. Therefore, the work-up procedure involved in the synthesis of phosphated–TiO_2 we reported previously[35] can be reduced by employing this simple one-pot route.

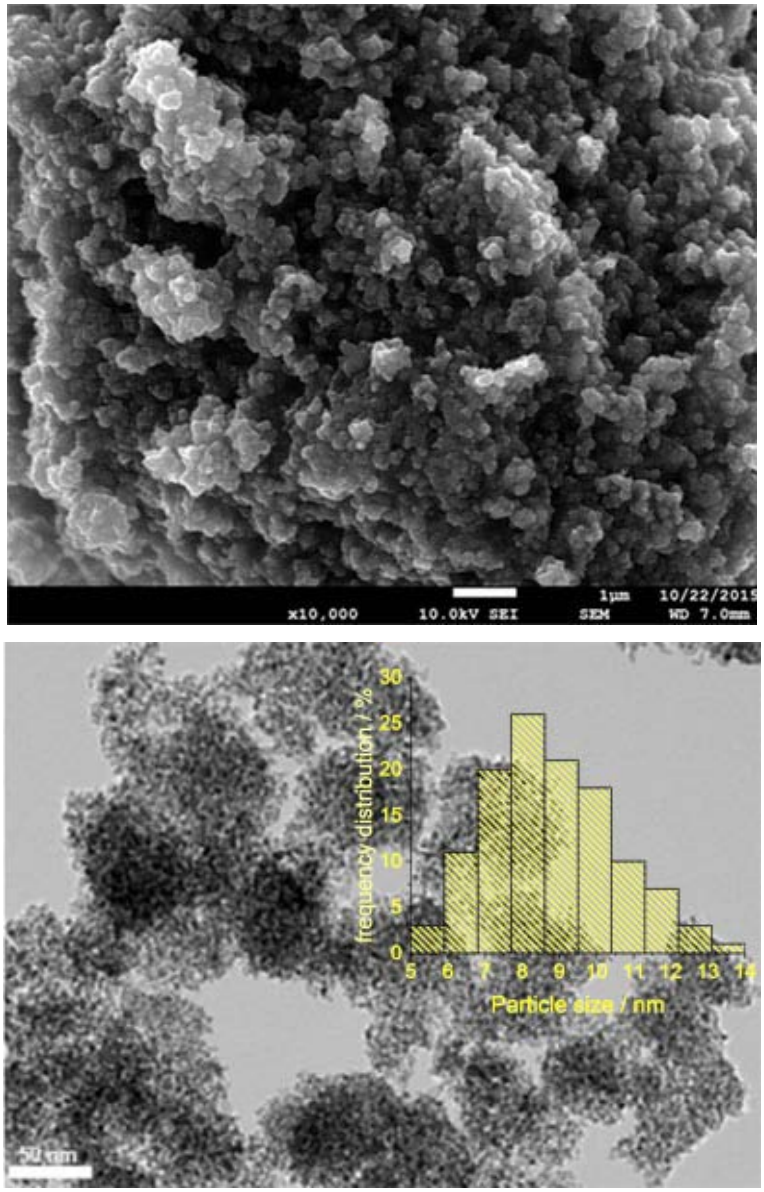

Figure 7.3 Microscopic analysis of phosphated–TiO_2 showing micrographs obtained by: a) FE-SEM and b) HR-TEM

7.3.2 Activity tests

In a preliminary study, catalytic activity of the as-prepared phosphated–TiO_2 nanoparticle was evaluated for glucose conversion into HMF in a water–MeTHF biphasic reaction medium. Glucose conversion and HMF yield were 89.4% and 58.8%, respectively, as shown in Figure 7.4. Selective production of HMF was further enhanced to a yield of 91% by modifying the biphasic medium with N-methyl-pyrrolidone (NMP). NMP serves as an aqueous phase modifier and its role is to: a) suppress humin formation and b) prevent rehydration of HMF.[36] This is confirmed by the high concentration of HMF in the reactive phase of the water–MeTHF system modified with NMP as compared to that of the unmodified system (Figure 7.4).

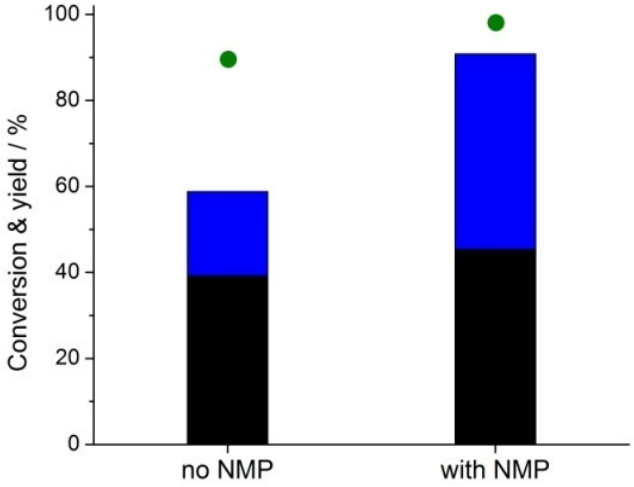

Figure 7.4 Glucose conversion to HMF in unmodified and modified water–MeTHF biphasic system. Reaction conditions: 10 g glucose, 1.25 g catalyst, 175 °C, 80 min, 100 mL solvent volume (water–organic solvent 3:7 v/v). MeTHF:NMP 6:1 v/v for the modified reaction system. Glucose conversion (●) and HMF yield in: organic phase (■) and aqueous phase (■)

Furthermore, product distribution shown in Figure S7.2 confirmed that HMF undergoes rehydration to a greater extent in the unmodified reaction system, producing significantly higher concentrations of levulinic acid and formic acid as compared to NMP modified system. Although, other products identified were in minor concentrations, we deduced that the product balance is mainly humins, which was remarkably high in the unmodified system and justified by the colour change of the spent catalyst from white to intense dark brown.

Next, we examined the reactivity of cellulose, a cheap and readily available glucose polymer. Although, conversion of cellulose is a challenge because of its chemical inertness and structural rigidity, structural deconstruction of cellulose is reported to improve its reactivity.[40] As a control, conversion of raw cellulose without any treatment was carried out and as expected, a poor conversion and low yield of HMF was observed (Table 7.1, entry 1). For this reason, cellulose was subjected to ball milling prior to reaction. Conversion of cellulose increased from 6.08% (raw cellulose; MCC) to 28.8% (ball-milled cellulose; BMC). This may be explained as a result of decrystallization of MCC to amorphous state (Figure S7.3), thus possessing fewer hydrogen bonds per repeating monomer.[40, 41] Consequently, MCC became sparingly soluble in water after milling, thereby enhancing substrate-catalyst contact. Nevertheless, solubility of milled cellulose in water is low and as a result, milling alone was insufficient to achieve excellent cellulose reactivity as the yield of HMF does not exceed 20% (Table 7.1, entry 2). By acidulating cellulose before milling (mechanocatalytic depolymerized cellulose; MDC) and then reacting the resultant substrate, 74.7%

HMF (Table 7.1, entry 3) was produced at a near-complete conversion. This observation could be explained based on complete dissolution of cellulose in aqueous solution as a result of decrystallization (Figure S7.3) but most importantly, depolymerization to oligomers whose degree of polymerization (DP) is less than 10.[38]

Table 7.1 Influence of cellulose depolymerization on HMF production[a]

Entry	Substrate	Conversion (%)	Yield (%)	
			Glucose	HMF
1	Cellulose (MCC)	6.08	0.09	3.92
2	Ball-milled cellulose (BMC)	28.8	0.88	20.8
3	Mechanocatalytic depolymerized cellulose (MDC)	99.8	0.16	74.7

[a] Reaction conditions: 10 g substrate, 1.25 g catalyst, 180 °C, 80 min, 100 mL solvent volume (water–MeTHF/NMP 3:7 v/v)

Our result also indicates that reaction rate is dependent on degree of cellulose crystallinity but strongly on cleavage of the β-1,4-glycosidic bond, which is considered to be rate determining.[42] Noteworthy to mention is the fact that the presence of residual acid in the acidulated cellulose may promote HMF degradation. Shrotri et al.[38] reported that the presence of residual acid was responsible for the reduced yield of sorbitol due to anhydro sorbitan formation as a result of acid dehydration. To investigate this, aqueous solution of cello-oligomer was neutralized with barium hydroxide ($Ba(OH)_2$) prior to reaction. As shown in Figure 7.5, HMF yield improved to 80.5%. Furthermore, when substrate concentration was changed from 10 to 5% loading, which corresponds to pH variation from 0.87 to 1.25, HMF yield rose from 74.7% to 83.5%. This result suggests that reducing the available residual acid by lowering substrate concentration can also minimize HMF degradation. Further reduction of substrate concentration to 1% (pH value of 1.80) resulted in HMF yield of 93.5% and after neutralization, similar yield (92.3%) of HMF was produced. Therefore, it seems that the most effective way to inhibit HMF degradation is through neutralization, especially at high initial substrate concentration considering that superior HMF yield was obtained after neutralization at 5% (88.7 vs 83.5%) and 10% (80.5 vs 74.7%) substrate concentrations, respectively. More so, irrespective of residual acid, substrate concentration is another factor observed to affect the yield of HMF, which is in agreement with previous studies.[43] A steady loss in yield of HMF as substrate concentration increased may be attributed to higher rate of cross polymerization of HMF with reactive intermediate compounds, thus forming undesired by-products.

For example in Figure 7.5, at 1% substrate concentration 93.5% yield of HMF declined through 83.5% until 74.7% when substrate concentration rose to 5% and 10%.

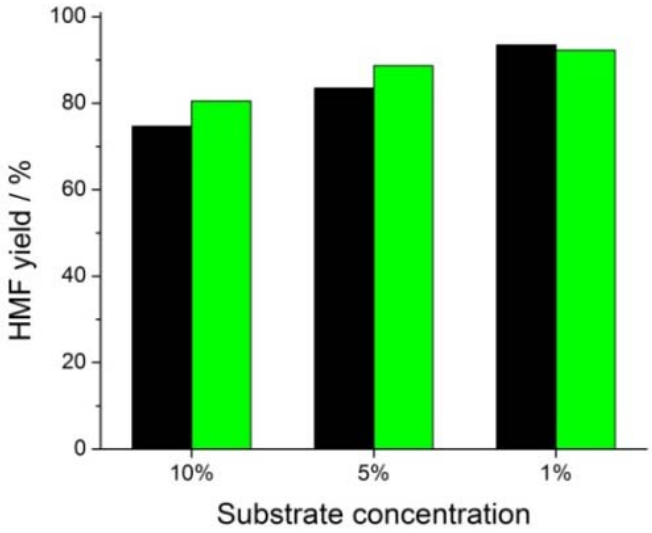

Figure 7.5 Effect of residual acid on the conversion of cello-oligomers into HMF. Reaction conditions: 10 g substrate, 1.25 g catalyst, 175 °C, 80 min, 100 mL solvent volume (water–MeTHF/NMP 3:7 v/v). ■ before neutralization, ■ after neutralization

As we have shown that the phosphated–TiO_2 catalyst in combination with the water–MeTHF/NMP biphasic system was effective for the conversion of cellulose into high yield of HMF, our strategy was then to seek a more economical process for practical implementation by utilizing real biomass as they serve as naturally occurring renewable carbohydrate sources. Hence, non-edible and inexpensive agricultural residues such as sugarcane bagasse and rice husk were considered in the present study. Prior to reaction, the biomass sources were washed with hot water, oven-dried at 50° C and then milled in a Culatti Micro Hammer with 1.5 mm screen size. From the method established by Sluiter et al.,[44] the carbohydrate component of bagasse is determined as 41.5% cellulose and 24.1% xylan whereas that of rice husk is 35.2% cellulose and 18.7% xylan. An integrated conversion of the biomass feedstocks to HMF and furfural, respectively, was realized as shown in Figure 7.6. For example, when bagasse was subjected to the transformation reaction, yields for HMF and furfural were 49.1% and 27.5%, respectively. We also found that 51.9% and 23.1% yields for HMF and furfural, respectively, could be produced from rice husk. To enhance the attractiveness of bio-refinery processes, it is important to fractionate biomass into its major components: cellulose, hemicellulose and lignin, for effective valorization into a variety of chemical compounds. This was achieved by a two-stage fractionation process using alkali pulping then organocat process. Alkali treatment affords partial removal of lignin, xylan and other impurities like

pectin and wax.[45, 46] Another advantage of this step is the weakening of the lignin-carbohydrate bond linkage by esterification and swelling of the biomass fibres.[45, 47] Subsequently, the alkali-treated biomass is subjected to organocat process wherein xylan is hydrolysed into xylose and as a result, lignin disentangles and gets separated into the organic phase to obtain a solid pulp rich in cellulose. As expected, cellulose continuously increased upon chemical treatment. XRD data of the biomass pulps (Figure S7.4) shows increased peak intensity of cellulose after each stage of treatment, suggesting the removal of xylan and lignin that are both of amorphous nature.

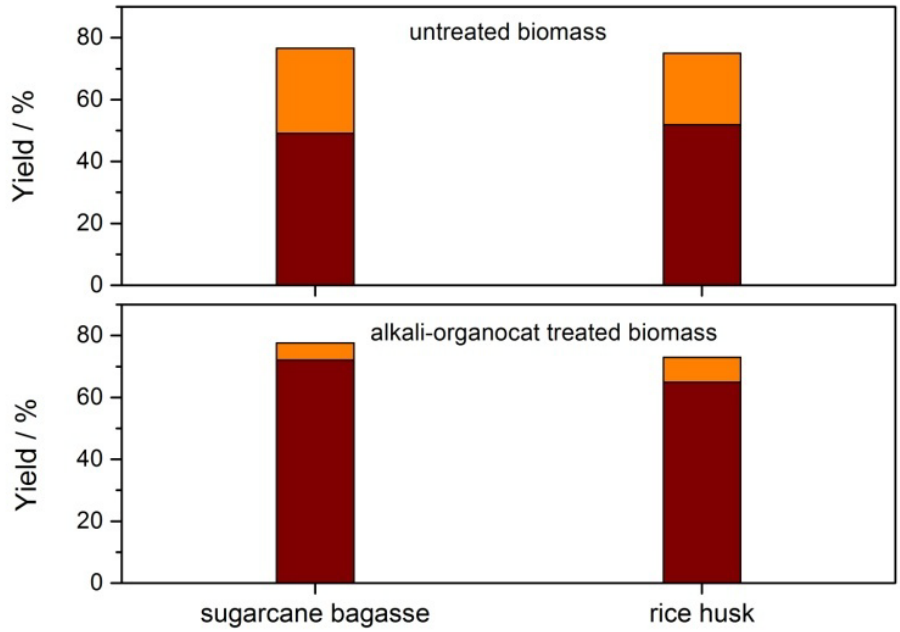

Figure 7.6 Cellulosic biomass conversion to furans on phosphated–TiO_2 catalyst in water–MeTHF/NMP biphasic system. Reaction conditions: 7.5 g substrate, 1.25 g catalyst, 180 °C, 80 min, 100 mL solvent volume (water–MeTHF/NMP 3:7 v/v). HMF, furfural

The recovered carbohydrate content of bagasse and husk after the alkali-organocat treatment is 90.96% (84.4% cellulose, 6.56% xylan) and 83.94% (78% cellulose, 5.94% xylan), respectively. Catalytic activity result for the conversion of the resultant pulp after the alkali-organocat treatment is shown in Figure 7.6. Chemical delignification of biomass appears to have negligible influence in terms of total yield of furans based on carbohydrate content, as comparable results to that of untreated biomass were obtained. This suggests that lignin did not interfere substantially on the conversion of carbohydrates. Nonetheless, we anticipated that fractionating lignin will facilitate the ease of biomass deconstruction as lignin content is reported to contribute to biomass recalcitrance arising from the lignin-carbohydrate interactions.48 Composition of HMF in the furan mix produced after biomass treatment is much higher, which evidently supports fractionation of the

biomass substrates to give cellulose-rich pulp. Consequently, a gram of HMF produced per gram of biomass consumed was effectively enhanced almost two-fold as shown in Figure S7.5. Therefore, a possible approach to sustainable HMF production is to adapt this catalytic process to other agro-industrial residues as alternative feedstock. As such, integration of this process to existing agro-allied industry can potentially generate extra returns on investment as well as simultaneously abate environmental concern and cost associated with waste disposal.

7.3.3 Reaction pathway and kinetics of cellulose to HMF reaction

The reaction pathway of cellulose to HMF in water is considered to be initiated by hydrolysis due to protonation of the β-1,4-glycosidic bonding followed by its dissociation to glucose. Conversion of cellulose as a function of reaction time was depicted by HPLC analysis and shown in Figure S7.6(a). Monitoring the evolution of products as the reaction proceeds, we noticed peaks identified as glucose and cellobiose in the first few minutes of the reaction. Additionally, the HPLC chromatograph revealed extra peaks (1 and 3) which are unidentified but are likely to be glucose oligomers. This is because cleavage of the β-1,4-glycosidic bond is generally accepted to produce water soluble oligomers prior to glucose formation. [49] The observance of peak 3 as well as cellobiose during glucose conversion reaction (Figure S7.6(c)) suggests reversion of glucose due to self condensation.[50, 51] Likewise, peak 3 was also observed during cellobiose reaction, which further supports the assumption that the unknown peak may be a glucose oligomer. Additional peaks, 6 and 7, noticeable in glucose and cellobiose but vaguely present in cellulose, may be regarded as glucose decomposition products. This assumption was based on the fact that when fructose was reacted as shown in Figure S7.6(d), these peaks were not present.

However, no attempts were made to elucidate on neither the pathway of glucose decomposition nor that of subsequent HMF degradation. Hence, a plausible reaction pathway for the phosphated–TiO_2 catalyzed cellulose to HMF in water–MeTHF biphasic system is shown in scheme 7.1. Hydrolysis of cellulose is assumed to proceed mainly with the formation of oligosaccahrides. Further hydrolysis of the oligosaccharides eventually yields glucose. Meanwhile, self condensation of glucose as a result of its reversion reaction gives glucose oligomers. In addition, glucose isomerizes to fructose and subsequent elimination of three molecules of water from the fructose molecule would then readily occur to form HMF. Fructose conversion rate to HMF rapidly takes place and occurs much faster than glucose isomerization to fructose, thus high yield of fructose was not obtained at any time during the course of the reaction. As levulinic acid, formic acid, levoglucosan, acetic acid were all observed in minor quantities, they were not considered as part of main reactions of the proposed reaction scheme.

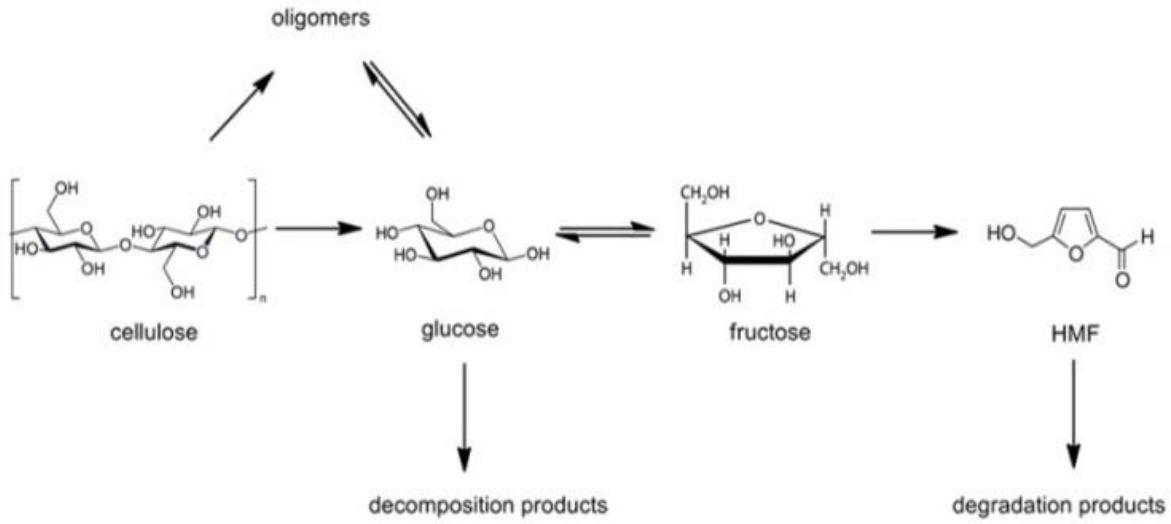

Scheme 7.1 Proposed reaction scheme of cellulose conversion to HMF catalyzed by phosphated–TiO_2

Understanding the kinetics of HMF formation is essential to realizing effective catalytic technologies for the conversion of carbohydrates. To the best of our knowledge, kinetics of HMF formation in a biphasic system over a solid acid catalyst has never been reported. To this end, we studied the kinetics of phosphated–TiO_2 catalyzed conversion of cello-oligomers in a water–MeTHF biphasic system. Cello-oligomers (i.e. depolymerized cellulose) was chosen as a model to represent cellulose because it is soluble and has better reactivity as earlier observed (Table 7.1). Based on our result, the main products detected are glucose and HMF. Hence, cello-oligomer hydrolysis to glucose and glucose dehydration to HMF is considered as a consecutive first order reaction in accordance with the widely accepted model reported by many authors.[52-54] Rate constants for glucose isomerization to fructose and the reversible reaction are both neglected. We assumed that fructose is dehydrated much rapidly to HMF as it is formed, and as a result only trace concentration of fructose is present in the product mix. Glucose oligomers are also detected in trace amount under this biphasic reaction condition, therefore, oligomerization of glucose is neglected. Likewise, other products such as levulinic acid, formic acid, levoglucosan, did not exceed 2% yield, hence, they are not accounted for. Thus, we simplify the cello-oligomer conversion reaction in our reaction system as:

$$cello-oligomers \xrightarrow{k_1} glucose \xrightarrow{k_2} HMF$$

in which k_1 and k_2 are reaction rate constants for hydrolysis and dehydration steps, respectively.

To estimate the kinetic parameters, we employ a kinetic model that consists of two reaction steps: i) cello-oligomer hydrolytic step and ii) glucose dehydration step. As a starting point, glucose dehydration experiments were carried out over reaction temperature range of 428–448 K with an initial glucose concentration of 10% (w/v) and sampling interval of 15 min from 0–60 min. The reaction rate equations of the glucose–to–HMF step are:

$$\frac{dC_g}{dt} = -k_2 C_g \qquad (1)$$

$$\frac{dC_H}{dt} = k_2 C_g \qquad (2)$$

Similar reaction conditions were used for the cello-oligomers–to–HMF reaction, and the following are the derived reaction rate equations:

$$\frac{dC_c}{dt} = -k_1 C_c \qquad (3)$$

$$\frac{dC_g}{dt} = k_1 C_c - k_2 C_g \qquad (4)$$

$$\frac{dC_H}{dt} = k_2 C_g \qquad (5)$$

where C_g, C_H and C_c are the concentrations for glucose, HMF and cello-oligomers.

The resulting set of ordinary differential equations (ODE) was simultaneously solved by a MATLAB program. A least square algorithm was adopted to minimize the error between experimental and predicted data, then subsequent evaluation of reaction rate constants through curve fitting. Activation energies were calculated using the Arrhenius equation given as:

$$k = A\exp\left(-\frac{E_a}{RT}\right) \qquad (6)$$

Arrhenius rate data plot is shown in Figure 7.7(a). As a measure of good approximation of the mathematical model to fit experimental data, R-squared value for both sets of reaction steps is greater than 0.9. The result of the kinetic study is presented in Table 7.2 for which activation energies of 110.9 kJ/mol and 122.4 kJ/mol were calculated for both the dehydration and hydrolysis steps, respectively. The order of magnitude of these energies are similar and this was also reported by Dee et al.[55] According to the authors, these energy barriers are insensitive to temperature and their difference is within 7-11 kJ/mol.

Furthermore, the simplicity of the reaction model remarkably predicts the experimentally observed data as shown by the parity plot of Figure 7.7(b).

Table 7.2 Estimated kinetic parameters for cello-oligomers and glucose conversion to HMF in water–MeTHF/NMP biphasic system

Rate constant (min^{-1})	Temperature K		
	428	438	448
k_1	0.0206	0.0352	0.0961
k_2	0.0117	0.0225	0.0471
Activation energy (kJ/mol)			
E_1		122.4	
E_2		110.9	

Therefore, the estimated kinetic data for cello-oligomers conversion to HMF in a biphasic reaction system provide a reasonable estimation that is in fair agreement with those reported in literature. For instance, Girisuta et al.[56] reported that cellulose and glucose undergo hydrolysis and degradation reaction, respectively, with similar activation energies of approximately 152 kJ/mol from a detailed kinetic study of acid-catalyzed hydrolysis reaction of cellulose in the presence of sulphuric acid. Jiang et al.[57] obtained activation energies of 114 and 95 kJ/mol corresponding to cellulose hydrolysis and glucose dehydration steps, respectively, using acidic ionic liquid catalyst in 1-Butyl-3-methylimidazolium chloride ([Bmim]Cl) solvent. Using cellobiose as a model compound for cellulose, Vanoye et al.[54] determined the activation energies of cellobiose hydrolysis and glucose dehydration in [C_2mim]Cl IL as 111 kJ/mol and 102 kJ/mol, respectively.

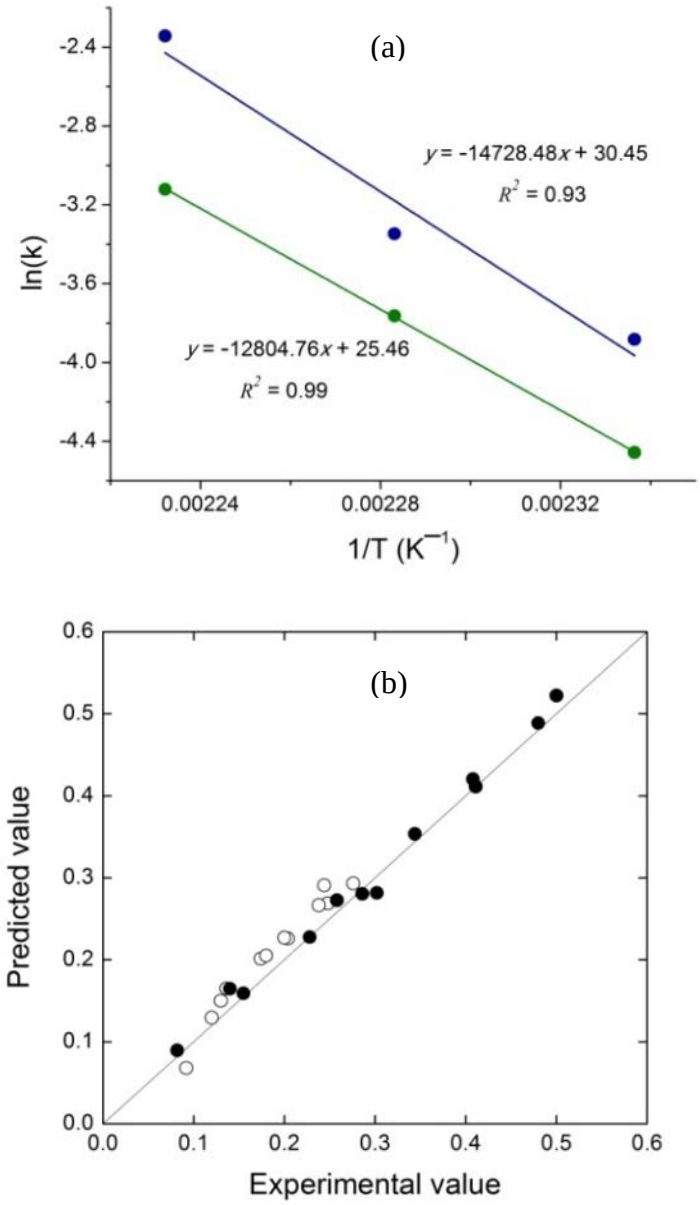

Figure 7.7 a) Arrhenius plot of cello-oligomers conversion to HMF: cello-oligomers hydrolysis to glucose (blue), glucose dehydration to HMF (olive green). b) parity plot of experimental data and model prediction ○ glucose yield ● HMF yield. Reaction conditions: 428 – 448 K, 10% (w/v) initial substrate concentration, 8:1 substrate/cat wt. ratio, 100 mL solvent (water–MeTHF/NMP 3:7 v/v)

7.4 Conclusions

We have described a simple and efficient process suited for the conversion of biomass-derived carbohydrates into HMF. The preparation of phosphated-TiO_2 was achieved by a one-pot synthesis with anatase as the main phase of TiO_2 but modified by the formation of a Ti–O–P bonding. At 10% (w/v) substrate loading, HMF yields of 91% and 74.7% from glucose and solubilized cellulose, respectively, were achieved in a NMP modified water–

MeTHF biphasic medium. Reaction kinetics for the formation of HMF was studied. By analyzing experimental data, a simple kinetic model was developed to estimate kinetic parameters for the tandem hydrolysis-dehydration reaction. Activation energy of cello-oligomer hydrolysis is 122.4 kJ/mol and the energy required for the subsequent dehydration of glucose to HMF is 110.9 kJ/mol. Another desirable attribute of our process is the significant conversion of real biomass to both HMF and furfural. A combined furan yield of about 76% (49-52% HMF and 23-28% furfural) is achievable. Catalytic conversion of the cellulose rich pulp after biomass fractionation led to an increased production in HMF to about 72% (bagasse) and 65% (husk). Overall, the method described herein serves as a means of finding a feasible economical and environmentally-friendly industrial process for the production of HMF.

Acknowledgements

The authors gratefully acknowledge the financial support of the Nanomaterials Centre at The University of Queensland, Australia. The authors also acknowledge the facilities, scientific and technical assistance of the Australian Microscopy & Microanalysis Research Facility at The University of Queensland. The first author sincerely appreciates the sponsorship from the International Postgraduate Research Scholarship (IPRS) and UQ Centennial Scholarship (UQ Cent).

References

1. G. W. Huber, S. Iborra and A. Corma, *Chemical reviews*, 2006, **106**, 4044-4098.
2. J. C. Serrano-Ruiz and J. A. Dumesic, *Energy & Environmental Science*, 2011, **4**, 83-99.
3. P. Gallezot, *Chemical Society Reviews*, 2012, **41**, 1538-1558.
4. L. Faba, E. Díaz and S. Ordóñez, *Renewable and Sustainable Energy Reviews*, 2015, **51**, 273-287.
5. A. A. Rosatella, S. P. Simeonov, R. F. M. Frade and C. A. M. Afonso, *Green Chemistry*, 2011, **13**, 754-793.
6. S. Dutta, S. De and B. Saha, *ChemPlusChem*, 2012, **77**, 259-272.
7. T. Wang, M. W. Nolte and B. H. Shanks, *Green Chemistry*, 2014, **16**, 548-572.
8. R. L. de Souza, H. Yu, F. Rataboul and N. Essayem, *Challenges*, 2012, **3**, 212-232.
9. Y. Zhang, J. Pan, Y. Shen, W. Shi, C. Liu and L. Yu, *ACS Sustainable Chemistry & Engineering*, 2015, **3**, 871-879.
10. Y. Zhang, H. Du, X. Qian and E. Y.-X. Chen, *Energy & Fuels*, 2010, **24**, 2410-2417.
11. Z. Zhang and Z. K. Zhao, *Bioresource technology*, 2010, **101**, 1111-1114.
12. A. M. da Costa Lopes and R. Bogel-Łukasik, *ChemSusChem*, 2015, **8**, 947-965.
13. J. B. Binder and R. T. Raines, *Journal of the American Chemical Society*, 2009, **131**, 1979-1985.
14. A. Takagaki, M. Ohara, S. Nishimura and K. Ebitani, *Chem. Commun.*, 2009, 6276-6278.
15. B. Kim, J. Jeong, D. Lee, S. Kim, H.-J. Yoon, Y.-S. Lee and J. K. Cho, *Green Chemistry*, 2011, **13**, 1503-1506.
16. P. Wang, H. Yu, S. Zhan and S. Wang, *Bioresource technology*, 2011, **102**, 4179-4183.
17. S. P. Teong, G. Yi and Y. Zhang, *Green Chemistry*, 2014, **16**, 2015-2026.
18. Y. Román-Leshkov, J. N. Chheda and J. A. Dumesic, *Science*, 2006, **312**, 1933-1937.
19. Y. Yang, C.-w. Hu and M. M. Abu-Omar, *Green Chemistry*, 2012, **14**, 509-513.
20. N. Shi, Q. Liu, Q. Zhang, T. Wang and L. Ma, *Green Chemistry*, 2013, **15**, 1967-1974.
21. B. Saha and M. M. Abu-Omar, *Green Chemistry*, 2014, **16**, 24-38.
22. Y. J. Pagan-Torres, T. Wang, J. M. R. Gallo, B. H. Shanks and J. A. Dumesic, *Acs Catalysis*, 2012, **2**, 930-934.
23. T. Wang, Y. J. Pagán-Torres, E. J. Combs, J. A. Dumesic and B. H. Shanks, *Topics in Catalysis*, 2012, **55**, 657-662.
24. T. Dallas Swift, H. Nguyen, A. Anderko, V. Nikolakis and D. G. Vlachos, *Green Chemistry*, 2015, **17**, 4725-4735.

25. R. Carrasquillo-Flores, M. Käldström, F. Schüth, J. A. Dumesic and R. Rinaldi, *Acs Catalysis*, 2013, **3**, 993-997.
26. R. Otomo, T. Yokoi, J. N. Kondo and T. Tatsumi, *Applied Catalysis A: General*, 2014, **470**, 318-326.
27. E. Nikolla, Y. Román-Leshkov, M. Moliner and M. E. Davis, *Acs Catalysis*, 2011, **1**, 408-410.
28. C. Fan, H. Guan, H. Zhang, J. Wang, S. Wang and X. Wang, *biomass and bioenergy*, 2011, **35**, 2659-2665.
29. Q. Zhao, L. Wang, S. Zhao, X. Wang and S. Wang, *Fuel*, 2011, **90**, 2289-2293.
30. S. Mondal, J. Mondal and A. Bhaumik, *ChemCatChem*, 2015, **7**, 3570-3578.
31. V. V. Ordomsky, J. van der Schaaf, J. C. Schouten and T. A. Nijhuis, *ChemSusChem*, 2013, **6**, 1697-1707.
32. S. Dutta, S. De, A. K. Patra, M. Sasidharan, A. Bhaumik and B. Saha, *Applied Catalysis A: General*, 2011, **409–410**, 133-139.
33. A. Dutta, A. K. Patra, S. Dutta, B. Saha and A. Bhaumik, *Journal of Materials Chemistry*, 2012, **22**, 14094-14100.
34. A. Dutta, D. Gupta, A. K. Patra, B. Saha and A. Bhaumik, *ChemSusChem*, 2014, **7**, 925-933.
35. L. Atanda, S. Mukundan, A. Shrotri, Q. Ma and J. Beltramini, *ChemCatChem*, 2015, **7**, 781-790.
36. L. Atanda, A. Shrotri, S. Mukundan, Q. Ma, M. Konarova and J. Beltramini, *ChemSusChem*, 2015, **8**, 2907-2916.
37. P. M. Grande, J. Viell, N. Theyssen, W. Marquardt, P. Dominguez de Maria and W. Leitner, *Green Chemistry*, 2015, **17**, 3533-3539.
38. A. Shrotri, L. K. Lambert, A. Tanksale and J. Beltramini, *Green Chemistry*, 2013, **15**, 2761-2768.
39. J. C. Yu, L. Zhang, Z. Zheng and J. Zhao, *Chemistry of Materials*, 2003, **15**, 2280-2286.
40. P. L. Dhepe and A. Fukuoka, *ChemSusChem*, 2008, **1**, 969-975.
41. K. Mazeau and L. Heux, *The Journal of Physical Chemistry B*, 2003, **107**, 2394-2403.
42. A. Cabiac, E. Guillon, F. Chambon, C. Pinel, F. Rataboul and N. Essayem, *Applied Catalysis A: General*, 2011, **402**, 1-10.
43. B. Kuster, *Starch-Stärke*, 1990, **42**, 314-321.
44. A. Sluiter, B. Hames, R. Ruiz, C. Scarlata, J. Sluiter, D. Templeton and D. Crocker, *Report N. TP-510-42618*, 2011, 17.

45. X. Zhao, F. Peng, K. Cheng and D. Liu, *Enzyme and Microbial technology*, 2009, **44**, 17-23.
46. N. Johar, I. Ahmad and A. Dufresne, *Industrial Crops and Products*, 2012, **37**, 93-99.
47. M. M. Ibrahim, W. K. El-Zawawy, Y. R. Abdel-Fattah, N. A. Soliman and F. A. Agblevor, *Carbohydrate Polymers*, 2011, **83**, 720-726.
48. M. E. Himmel, S.-Y. Ding, D. K. Johnson, W. S. Adney, M. R. Nimlos, J. W. Brady and T. D. Foust, *Science*, 2007, **315**, 804-807.
49. S. Van de Vyver, J. Thomas, J. Geboers, S. Keyzer, M. Smet, W. Dehaen, P. A. Jacobs and B. F. Sels, *Energy & Environmental Science*, 2011, **4**, 3601-3610.
50. Q. Xiang, Y. Y. Lee and R. W. Torget, in *Proceedings of the Twenty-Fifth Symposium on Biotechnology for Fuels and Chemicals Held May 4–7, 2003, in Breckenridge, CO*, eds. M. Finkelstein, J. D. McMillan, B. H. Davison and B. Evans, Humana Press, Totowa, NJ, 2004, pp. 1127-1138.
51. H. M. Pilath, M. R. Nimlos, A. Mittal, M. E. Himmel and D. K. Johnson, *Journal of Agricultural and Food Chemistry*, 2010, **58**, 6131-6140.
52. J. F. Saeman, *Industrial & Engineering Chemistry*, 1945, **37**, 43-52.
53. N. S. Mosier, A. Sarikaya, C. M. Ladisch and M. R. Ladisch, *Biotechnology progress*, 2001, **17**, 474-480.
54. L. Vanoye, M. Fanselow, J. D. Holbrey, M. P. Atkins and K. R. Seddon, *Green Chemistry*, 2009, **11**, 390-396.
55. S. J. Dee and A. T. Bell, *ChemSusChem*, 2011, **4**, 1166-1173.
56. B. Girisuta, L. Janssen and H. Heeres, *Industrial & engineering chemistry research*, 2007, **46**, 1696-1708.
57. F. Jiang, Q. Zhu, D. Ma, X. Liu and X. Han, *Journal of Molecular Catalysis A: Chemical*, 2011, **334**, 8-12.

Supplementary Material

mass of feed stock = 7.5 g

Table S7.1 Furan yield calculation from biomass feedstock

	untreated		alkali-organocat treated	
		Sugarcane bagasse		
	%	g	%	g
cellulose	41.5	3.11	84.4	6.33
xylan	24.1	1.81	6.56	0.49
		Rice husk		
	%	g	%	g
cellulose	35.2	2.64	82.0	6.15
xylan	18.7	1.40	5.47	0.41

$$mole\,of\ glucose = \frac{mass\,of\ cellulose}{162.14}$$

$$mole\,of\ xylose = \frac{mass\,of\ xylan}{132.12}$$

$$total\ moles = mole\,of\ glucose + mole\,of\ xylose$$

$$HMF\ yield = \frac{moles\,of\ HMF\ produced}{total\ moles}$$

$$furfural\ yield = \frac{moles\,of\ furfural\ produced}{total\ moles}$$

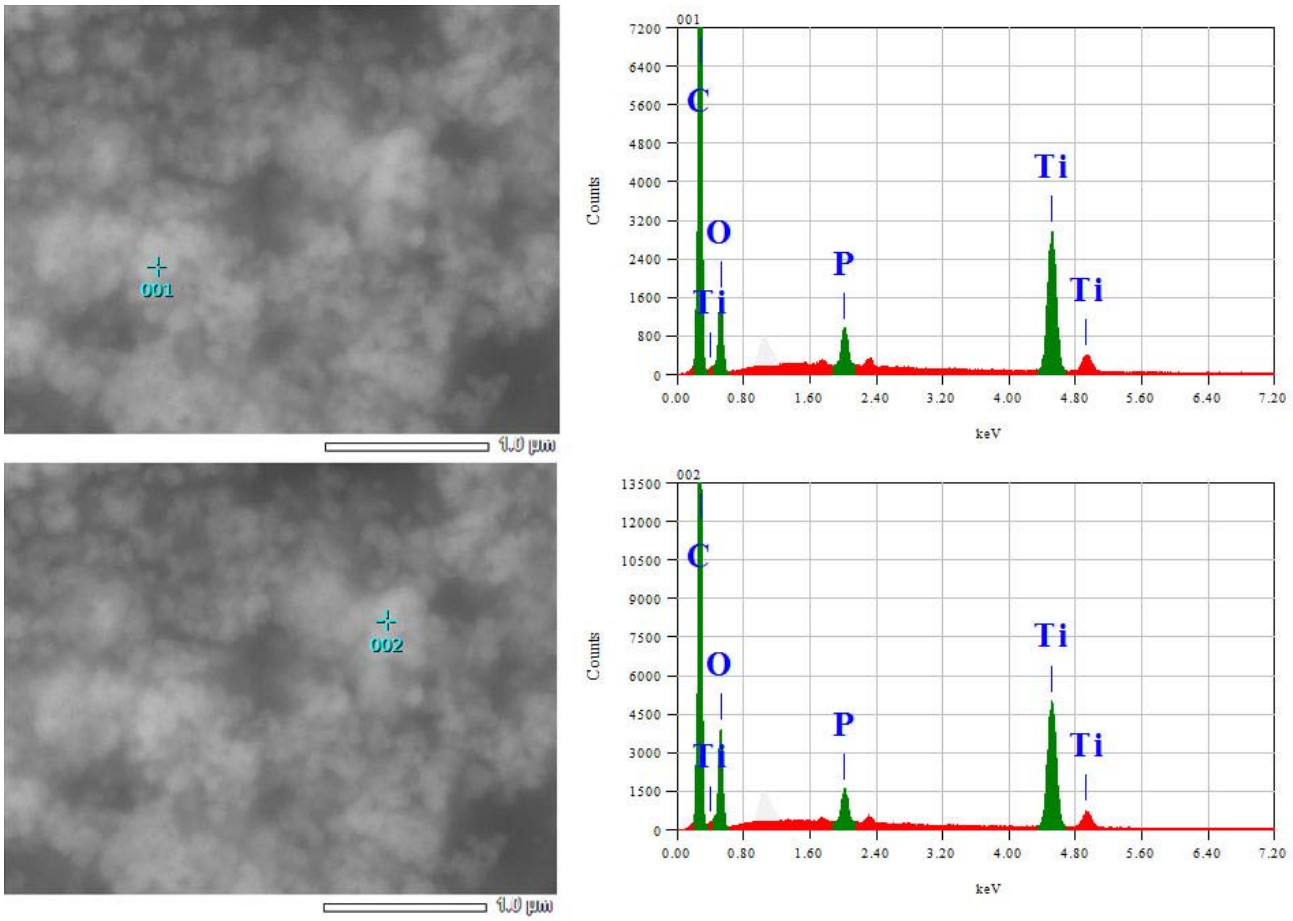

Figure S7.1 EDS analysis of phosphated–TiO_2 nanoparticle

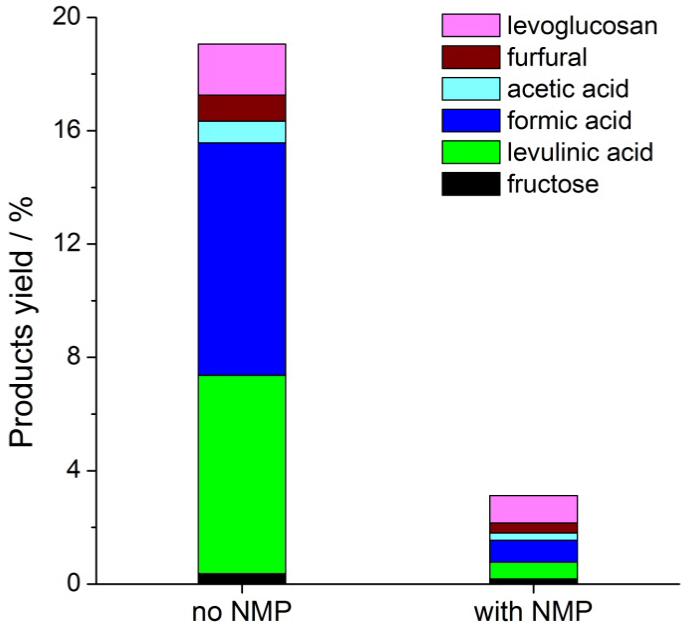

Figure S7.2 Product distribution of glucose conversion on phosphated-TiO_2 catalyst. Reaction conditions: 10 g glucose, 1.25 g catalyst, 175 °C, 80 min, 100 mL solvent volume (water–organic solvent 3:7 v/v). MeTHF:NMP 6:1 v/v for the modified reaction system

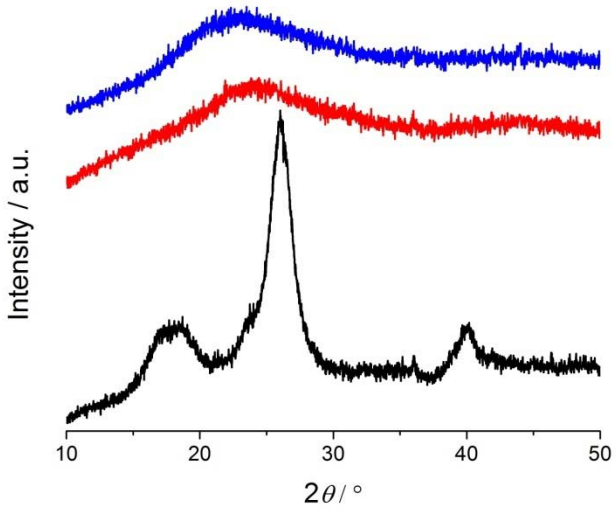

Figure S7.3 XRD pattern of microcrystalline cellulose (black), ball-milled cellulose (red), mechanocatalytically depolymerized cellulose (blue)

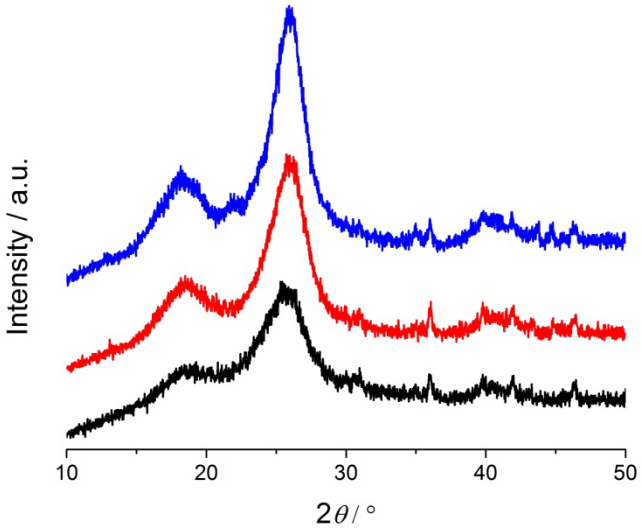

a) sugarcane bagasse

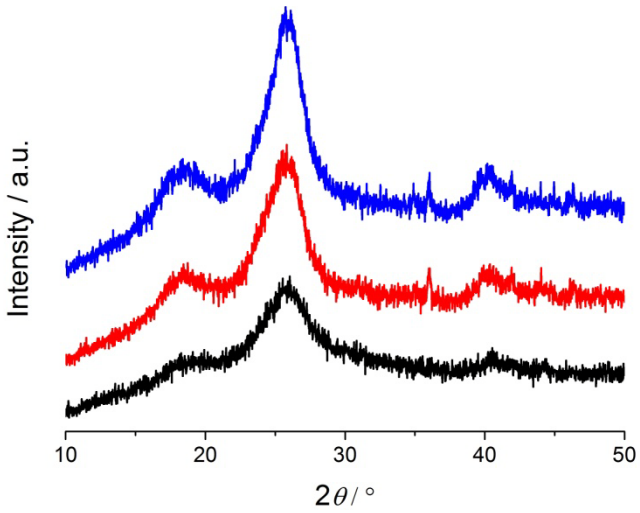

b) rice husk

Figure S7.4 XRD pattern of biomass substrates: a) sugarcane bagasse and b) rice husk. untreated (black), alkali-treated (red), organocat-alkali treated (blue)

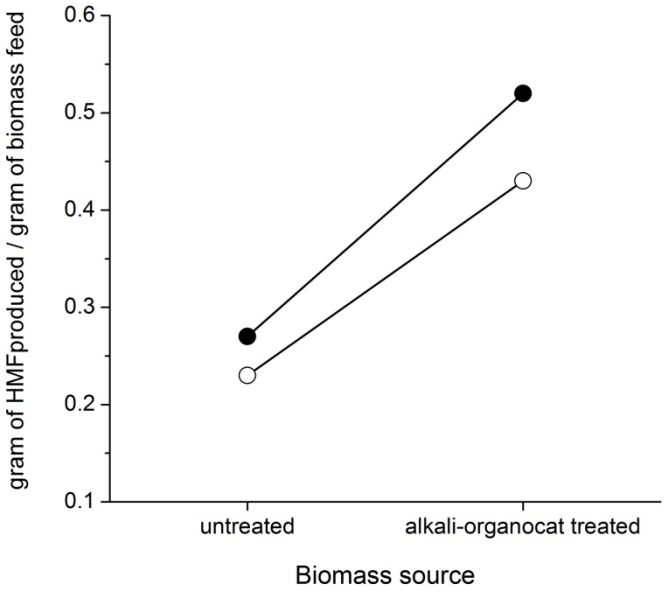

Figure S7.5 HMF production per quantity of biomass source

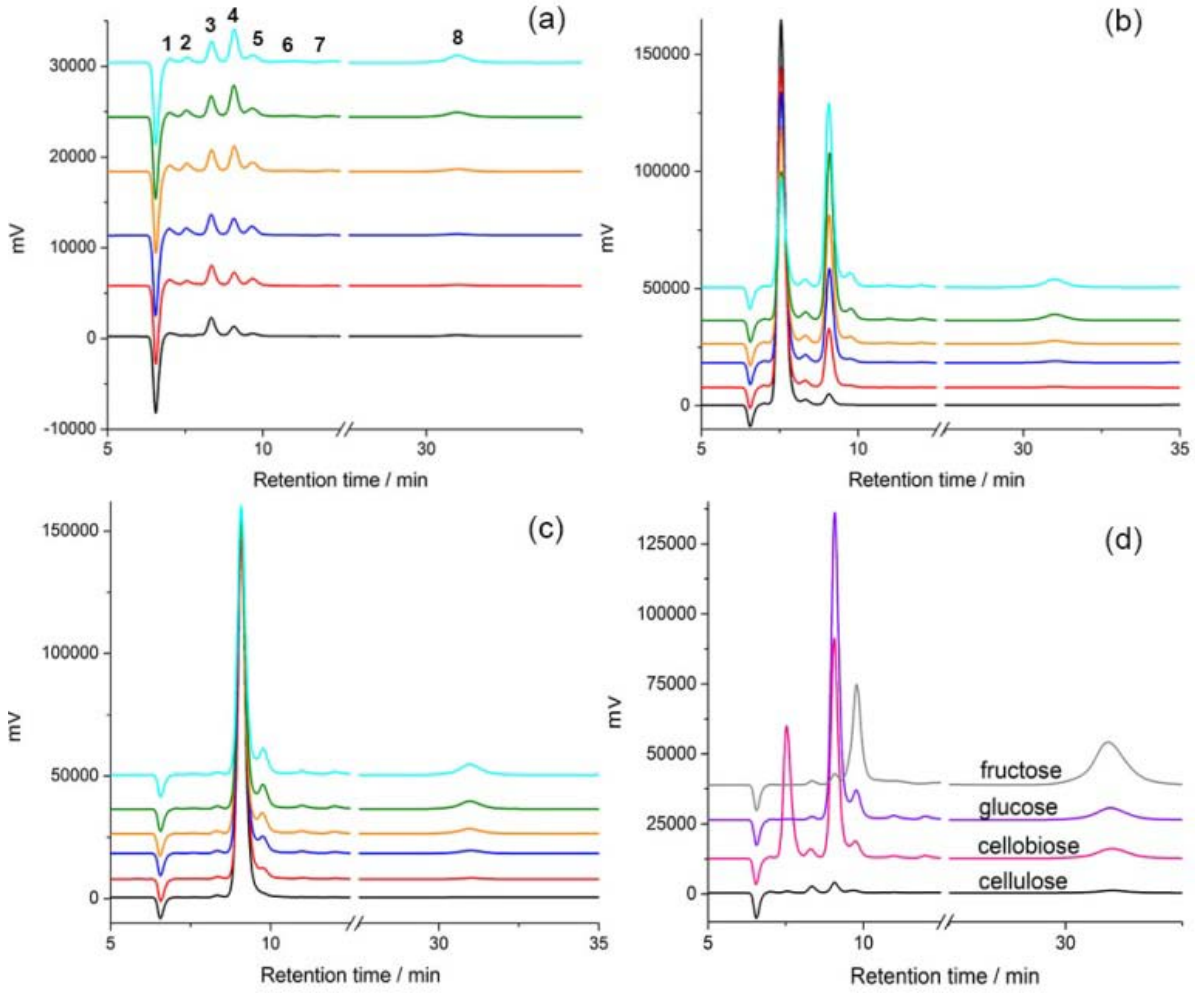

Figure S7.6 HPLC analytical profile of carbohydrates conversion measured using RID detector. a) cellulose, b) cellobiose, c) glucose.[a] Reaction conditions: 1 g substrate, 0.4 g cat. wt. (0.2 g)[a], 180 °C (160 °C)[a], 100 mL water. d) comparison of carbohydrates conversion at 60 min reaction time. Reaction time: 0 min (black), 10 min (red), 20 min (blue), 30 min (orange), 45 min (green) and 60 min (cyan). Products: cellobiose – 2, glucose – 4, fructose – 5, HMF – 8, unknowns – 1, 3, 6 and 7.

Chapter 8

Conclusions and Recommendations

8.1 Conclusions

This thesis has contributed to the understanding and advancement of the current scientific knowledge of 5-hydroxymethylfurfural (HMF) production from biomass-derived carbohydrates in a biphasic reaction system over a bifunctional solid catalyst. The following conclusions can be drawn based on the research outcome of the thesis:

a) A TiO_2 based catalyst was successfully developed using a simple, non-hazardous and scalable sol-gel technique, and then applied for the conversion of a wide range of carbohydrate sources into HMF. Owing to the rich surface chemistry and acid-base property of TiO_2, we modified its catalytic performance by introducing a second metal oxide, zirconia, to form binary oxides of TiO_2 and ZrO_2 (Chapter 4). We carefully tuned the molar ratio of TiO_2:ZrO_2 to achieve optimum balance of acid-base sites which facilitated the consecutive base isomerization of glucose to fructose on ZrO_2 then fructose dehydration to HMF on TiO_2. Although, the binary oxides were effective for the dehydration reaction giving 74% HMF from glucose, a solid Brønsted acid co-catalyst was still required to further promote the formation of HMF as the acidity of the TiO_2–ZrO_2 binary oxides is derived from Lewis acid sites. An improved yield of 86% HMF was achieved when Amberlyst 70 was used as the solid Brønsted co-catalyst. However, the preparation of single catalyst with Lewis and Brønsted acidity is more desirable. In chapters 5 and 6, surface modification of TiO_2 was achieved with ammonium salt precursors of molybdate, phosphate, vanadate and tungstate to prepare Lewis-Brønsted bifunctional solid acids. Phosphate treatment gave optimum Lewis/Brønsted acid ratio suitable for the selective conversion of carbohydrates to HMF in high yield. At optimized catalyst synthesis condition (phosphate loading and calcination temperature) and reaction condition (temperature, catalyst loading, aqueous:organic volume ratio, choice of aqueous modifier), more than 80% yield of HMF was obtainable from different sugar moieties such as fructose, glucose, cellobiose, sucrose, and starch (Chapter 6).

b) Solvent effect was also very crucial in the dehydration reaction of carbohydrates. Despite the advantages of aqueous system in terms of greenness and environmental friendliness, production of HMF is non-selective over the TiO_2 based catalyst (Chapter 4). Selective production of HMF was significantly enhanced when an organic solvent was introduced to form a water-organic biphasic system. Careful selection of the organic phase promoted the reaction preferentially towards the target product due to suppression of unwanted side reactions. Efficiency of the water-organic biphase system was further enhanced by introducing an aqueous modifier which helped to: a) suppress humin formation and b) prevent rehydration of HMF (Chapters 6 and 7).

Both factors were responsible for the enhanced production of HMF even at moderately high feed concentration (10 wt%).

c) In chapter 6, recalcitrance of cellulose led to poor reactivity. While excellent yields of HMF could be produced from other carbohydrate sources, poor yield of HMF (33%) was obtainable from cellulose. Mechanocatalysis, i.e. solid state acid-catalyzed depolymerization of cellulose, was used to overcome the problem of limited reactivity of cellulose. Driven by mechanical forces, ball-milling of acidulated cellulose produced water-soluble oligosaccharides, which display higher reactivity than cellulose to give 86% yield of HMF. This approach also enabled successful reactor re-configuration from batch to flow operation. As a result, water soluble oligosaccharides from cellulose could be dehydrated in a biphasic flow reactor while moderate yields of HMF (up to 53%) was achieved at 5% (w/v) saccharide solution.

d) Furthermore, Chapter 7 shows the applicability of the mechanocatalytic depolymerization on real biomass samples. A combined furan yield of about 76% (49-52% HMF and 23-28% furfural) could be produced from sugarcane bagasse and rice husk. Efficiency of the reaction process to produce HMF directly from biomass was further enhanced by fractionating biomass to obtain rich cellulose pulp and separate streams of lignin and xylose, wherein both can be subsequently transformed into other valuable compounds. Remarkable yields of 72% and 65% HMF were produced from sugarcane bagasse and rice husk, respectively after solid state depolymerisation of the resultant cellulose-rich pulp after fractionation.

e) Finally, kinetic study of solubilized cellulose conversion into HMF was investigated (Chapter 7). The reaction kinetics of the reaction was analyzed based on a simplified model that consists of two main consecutive reaction steps: i) hydrolytic step of the water soluble cello-oligomers to glucose and ii) dehydration of glucose to HMF. The energy requirements for the consecutive hydrolytic and dehydration steps are approximately 122 kJ/mol and 111 kJ/mol, respectively. Since no kinetic data of cellulose dehydration to HMF over solid acids in a biphasic reaction is available yet, the obtained rate parameters could potentially aid the development of more comprehensive models for subsequent kinetics studies.

8.2 Recommendations

Our results suggest that biphasic dehydration of cellulosic biomass can be a viable route to efficiently utilize agricultural wastes and a sustainable way of producing HMF. Nevertheless, further works are required in order to move a step closer towards achieving cost-effective technologies for large scale HMF production.

a) Microwave-assisted conversion of carbohydrates to HMF under this biphasic reaction can be explored. High energy efficiency of microwave irradiation may dramatically enhance product selectivity by reducing reaction time and associated undesirable side reactions. Also, a wide range of biomass sources should be examined under either conventional/microwave irradiation heating to evaluate the robustness of the phosphated-TiO_2 catalyst under biphasic condition for the production of HMF.
b) Further optimization of the mechanocatalysis treatment may be carried out so as to avoid neutralization requirement. For this reason, easily recyclable solid acid that may be ball milled together with cellulose/biomass substrates should be developed.
c) Given that reaction mechanisms are closely dependent on the catalyst and reaction conditions, a detailed mechanistic study of carbohydrates dehydration over phosphated–TiO_2 in water-organic biphasic system should be performed to understand the underlying mechanism of the reaction. Techniques such as nuclear magnetic resonance (NMR) and isotopic labelling may be used to decipher the surface reaction chemistry on the solid catalyst. Consequently, a more comprehensive kinetics study based on the mechanistic study can then be embarked upon to improve the accuracy and validity of the kinetic parameters.
d) Although, the potential of biphasic fixed-bed reaction process to continuously produce HMF was demonstrated, more work is still required to be done. As flow process is much more desirable for industrial application than batch process, detailed reactor design and configuration taking into consideration parameters such as mass transfer, reaction mechanism and kinetics, residence time, catalyst regeneration and solvent recyclability are very important in order to effectively scale-up a continuous flow process. Significant improvement of the flow process could also be achieved by employing biomass derived solvents with high partition coefficients, for example lactones and alkylphenols.
e) Conversion of biomass into HMF requires pre-treatment and in this thesis, we utilized a two-step fractionation process which requires separation stages and different chemicals for pre-treatment, ultimately contributing to overall process cost and energy requirement. Since biomass fractionation represents the most challenging step to unlocking its components for subsequent transformation, future research is needed for an optimized facile approach. Moreover, catalytic strategies that can directly convert raw biomass to liquid fuels or high value chemicals via intermediate HMF formation are desirable. Since HMF is a building block chemical and not the end product, more research effort is required to advance integrated catalytic pathways that involve one-pot dehydration of carbohydrates coupled with other reactions such as

hydrogenation, oxidation, aldol condensation etc., which is a vital strategy to achieve economically viable processes of biomass utilization.